The Numerical Modelling of Rockbolts in Geomechanics by Finite Element Methods

A Thesis submitted for the Degree of Doctor of Philosophy

by

Tung-yo Chao

Department of Mathematics and Statistics,
Brunel University, Middlesex, Uxbridge, UK

October, 1998

Acknowledgements

I would like to express my most sincere thanks and gratitude to Dr. Martin Reed for introducing me to the field of finite elements and its application in geomechanics, and for the huge amount of freedom I was allowed to conduct this research. His continuous and tireless supervision for this work, and his suggestion for improvement and assessment are most valuable in the preparation of this thesis.

I also wish to thank Prof. Edward Twizell for his valuable help and support during my studies at Brunel University, especially during the absence of Dr. Reed from Brunel University.

Special thanks to Dr. Mike Warby for his permission to use his graph-plotting algorithms incorporated in the programs **PREFEL** and **FELVUE** which are the pre- and the post-processor of the main program written according to the theories proposed in this thesis. His continuous technical support and the many fruitful discussions with Dr. Simon Shaw are also much appreciated.

I am grateful to Mr. Robert Campbell for his continuous assistance and moral support, and for his occasional light-hearted attitude to enlighten the atmosphere. Many thanks to all my friends in Brunel University for their support throughout.

I would also like to thank the Department of Mathematics at Brunel University for providing me with a ideal working environment and computing facilities in which I can undertake my research.

Finally, my deep gratitude to my wife, Yuet-ming for her patience, understanding, and support all the time, and my parents for their continuous encouragement, without which this work could not have been done.

Abstract

In tunnel excavation, the use of rockbolts has long been a popular means of reinforcement in rock masses to prevent the rock opening from caving in. The idea has evolved from the earliest form of rockbolt made of wood to the more up-to-date form of pre-tensioned or grouted steel rockbolts.

A major breakthrough in the design of rockbolt models was made by Aydan (1989). This rockbolt element was modelled in coupled form, with one sub-element representing the steel bolt, and the other sub-element the grout. This representation was necessary to model the complex action in the continuous rock mass near the joint.

In elasticity problems, the large displacement formulation of a beam element is derived from the fundamental theory, and the bending phenomenon of a thin rod is analysed by the finite element discretizations of the bar elements and the beam elements. Experiments show that the deformation characteristics of the latter representation resemble a more realistic life behaviour. Based on this finding, this thesis proposes a modification to Aydan's two-dimensional rockbolt element, with the beam elements discretising the steel bolt.

The different mechanical responses of a perfectly elastic rockbolt are considered, and the large displacement formulation of the new rockbolt element is derived by combining those of Aydan's rockbolt element and the beam element.

The mechanics of the Aydan element and the new rockbolt element are described, and their performances are compared in an identical situation. It is found that in the two two-dimensional examples used in this thesis, the modified element ensures the continuity of curvature of the rockbolt, and in general, can act as support across a discontinuity or joint between rock masses well.

In conjunction with the displacement method in the finite element procedures, a conventional iteration solution procedure is first described to solve the nonlinear incremental stiffness equation. However, it is found that this procedure is cumbersome, and requires a large amount of comptutations. Some limited storage quasi-Newton minimization algorithms are considered as an alternative.

Contents

Chapter 1

Introduction

All structures, whether houses, hospitals, bridges, or tunnels, have at least one thing in common: they are expected to be safe from collapse when used for the purpose for which they are intended. To ensure this structural safety together with the economical use of materials of construction and effectiveness of design, the designer has first to investigate the effect of imposed forces.

A force may be defined as an external agency which changes or tends to change the state of equilibrium or uniform motion of a body. That is, a force is associated with the acceleration of a body.

A structure has to be designed so that when realistic forces are acting upon it, it is always in equilibrium, or at rest. One task of a structural engineer is therefore to estimate all the external forces and reactions acting on the structure, and to ensure that these forces will be in equilibrium. The designer has then to choose suitable materials of adequate dimensions to withstand the tensions, compressions, bending, deformations, etc. which are the results of the external forces and reactions, and to improve the efficiency of the design.

This chapter will introduce the ideas of geometric and material linearity and nonlinearity of structures, and it will survey the areas of tunnels and tunnel support mechanisms, with particular reference to rockbolts. Rockbolts will be classified according to their purposes and functions. A brief history and the excavation scheme of the New Austrian Tunnel Driving Method will also be included.

The survey carried out in this chapter is based on the following sources: Beaver (1972), Bowen (1975), Hobst & Zajíc (1983), Jaeger & Cook (1979), Lampe (1963), Meek (1971), Ross (1990), and West (1988).

1.1 Material properties of structures

All materials alter slightly in shape when they are under stress. A member which is subject to tension stress increases in length and its cross-section becomes slightly smaller. Similarly, a compression member becomes shorter and slightly larger in cross-section.

1.1.1 Linear behaviour

The materials used in structural work are frequently assumed to be linearly elastic within the range of stresses caused by working loads and, although a small amount of nonlinear inelastic behaviour may occur as a result of high stresses at joints, a metal structure as a whole may be considered to be both linear and elastic when working loads are not exceeded.

On the other hand, concrete is usually a non-linear inelastic material throughout the whole stress range, and methods of analysis which recognize these characteristics are to be preferred for concrete structures. Even with concrete, however, the early stages of the stress-strain curve may be approximated by a straight line, and linear elastic analysis which has been used with success for so many years may continue to be acceptable in certain circumstances.

1.1.2 Nonlinear behaviour

In structural analysis, nonlinear behaviour may occur because the material of which the structure is made possesses a nonlinear stress-strain law. It may also arise because changes of geometry are significant so that an analysis based on the geometry of the deformed structure yields results which are appreciably different from those based on the original structure geometry. Of course, both of these effects may be present together. Nonlinear behaviour can be classified into the following three groups:

1. **Material nonlinearity**

   In Figure 1.1, strain-stress graphs are used to illustrate some examples of nonlinear material behaviour. The curve in Figure 1.1(a) is that generally assumed for mild steel, with a perfectly elastic portion followed by a perfectly plastic plateau which is

terminated when strain hardening commences. In Figure 1.1(b), the curve given has a perfectly elastic zone followed by a plastic zone in which linear strain hardening takes place. The curves A and B in Figure 1.1(c) illustrates a rigid plastic material. The material A exhibits nonlinear strain hardening, whearas B is perfectly plastic. It should be noted that the rigid-plastic curve is that assumed in the limit theorems and their use for calculation of plastic-collapse loads of structures. The material of the type in Figure 1.1(d) has nonlinear behaviour in both the elastic and plastic states. Other common types of nonlinear material behaviour are elastoplasticity, viscoplasticity and viscoelasticity.

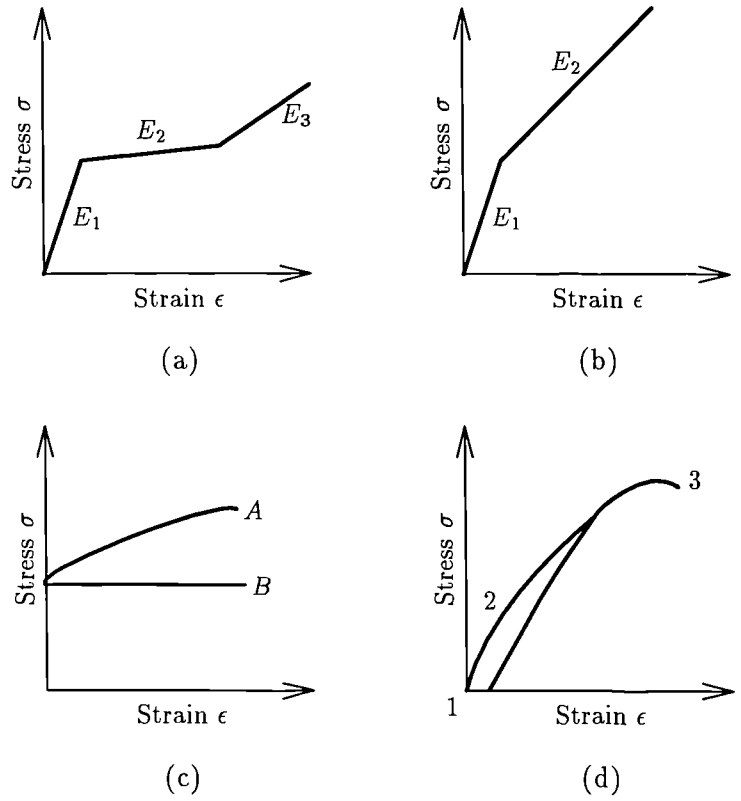

Figure 1.1: Material stress-strain curves (after Meek (1971)

2. Geometric nonlinearity

In some structures, results based on the geometry of the deformed structure will differ appreciably from those based on the initial geometry. The change of geometry, even though small, must be taken into account for realistic modelling. Even though the material may remain linearly elastic throughout, it will result in a nonlinear relation between load and displacement. It is not always easy to see intuitively whether small changes of geometry will be negligible or whether they will profoundly affect the results, but the influence of this nonlinear behaviour must be considered.

Examples of nonlinear geometrical behaviour are shown in Figures 1.2 and 1.3. Figure 1.2(b) shows the load-deflection curve for the tightly stretched cable of Figure 1.2(a). It can be seen that the greater the deflection, the more efficiently the cable can carry the transverse load and hence the load-deflection curve shows a continually increasing slope.

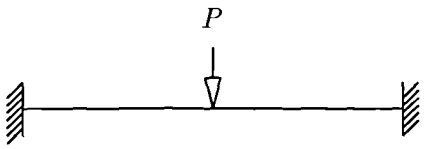

(a) Transverse load on tightly stretched cable

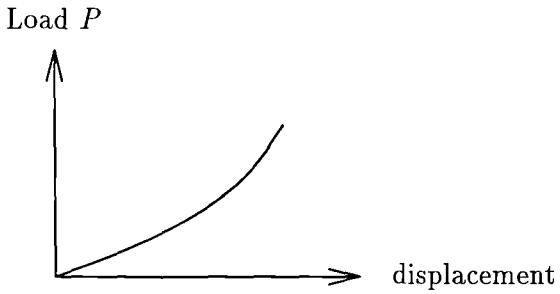

(b) Load-deflection curve

Figure 1.2: Example of geometrical nonlinearity - tight cable

Deflections of a transversely loaded beam are shown in Figure 1.3. If an axial load is applied as shown in Figure 1.3(b), the moments $P\Delta_Q$ will occur and it will produce additional deflections as shown. If linear analyses are assumed for all structures, it is clear that these results cannot be attained, as some errors are present when both axial and bending actions occur. The additional moments $P\Delta_Q$ and displacement are *second-order* effects and a method of analysis which incorporates these effects is a second-order or nonlinear method. The linear stiffness and flexibility procedure is called a *first-order* method.

With the help of a load-deflection graph in the analysis of geometric nonlinearity, it is possible to predict the maximum load, or critical load, that a structure can

withstand before total collapse occurs. Both linear and nonlinear analyses and the numerical prediction of the critical load will be described in full in later chapters.

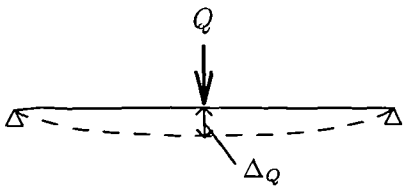

(a) Transverse load on beam

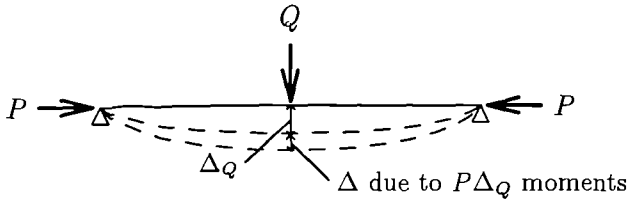

(b) Beam with axial load

Figure 1.3: Example of geometrical nonlinearity - beam

3. Combined material and geometric nonlinearity

The inelastic instability of struts is a typical case of combined material and geometric nonlinearity. This problem can be analysed by the Rankine-Gordon formula, where initial imperfections are important. There are many structures which should theoretically fail through elastic instability but, becasue of initial imperfections, fail at a much lower load than the predictions based on elastic theory. Such structures are said to suffer *elastic knockdown.* This combined nonlinear behaviour of material is more involved and difficult to deal with. Suggestions to solve the problem of combined nonlinear behaviour of structure by finite element analysis can be found in Desai & Phan (1980).

In this thesis, problems with only geometric nonlinear behaviour, in a two-dimensional analysis of a linear elastic body will be dealt with. Other types of nonlinearity are beyond its scope and will not be included here. However, it is hoped that the next stage of development of the algorithm proposed in this thesis will be to adapt it to these material or combined nonlinear behaviours and to three-dimensional problems.

In principle, the inclusion of mild material nonlinearity, for example, strain-hardening plasticity, should be straightforward and could be accommodated within the iterative solution algorithm developed for the geometric nonlinearity. More problematic, and more important, would be the modelling of post-failure behaviour, for example, when the steel bolt of a rockbolt breaks, or a rock joint debonds and shears.

1.2 Tunnels

Tunnels have existed for many years, the earliest having been constructed in order to mine precious metals with manual methods being used to dislodge the minerals. In the eighteenth century, explosives were first utilized for excavating, blasting being used to alter the form of the material in order to facilitate removal. In 1872, the first dynamite was successfully employed in driving the Musconneteong tunnel on the Lehigh Valley Railroad in the USA. Using the same method, an aqueduct tunnel was driven from Ceoton to New York City, and after that, blasting was considered to be both safe and rational as a tool for constructing tunnels. For a full account on the history of tunnelling see Beaver (1972).

1.2.1 Tunnel support mechanisms

The equilibrium stress state of the rock mass can be disturbed by an underground excavation, and as a consequence, lumps of rock become loosened and fall from the exposed rock face, the rock is forced towards the excavated space, and the support system that is constructed experiences an additional stress load. These effects can generally be described as manifestations of rock pressure. The source of this pressure is principally the force of gravity, although sometimes the residual stresses of orogenic activity within the earth's crust, including forces responsible for the formation of the surface relief, are also operative. Usually only the weight of the overlying rock above the excavation is considered in the vertical in situ stress, and a lateral stress ratio used to derive the horizontal stress state.

In general, the tunnelling engineer is faced with two basic problems: to support the roof, face and sides of the heading between the operations of excavating and lining it; and to carry out the various operations of tunnelling - for example, excavating, timbering, mucking and lining - in the necessarily confined working space that the tunnel offers. As a general rule, it may be said that driving through very soft ground is the most difficult form of tunnelling. The excavation must be supported in some manner as soon as it is

completed, otherwise the walls will tend to fall and the bottom may even bulge upwards. These sliding movements may exert enormous pressure upon timbering and can even crush it completely.

Most types of support can be divided into *active support* which imposes deliberate loads on the rock surface and *passive support* which generates loads as a result of its compression by convergence across an excavation. Examples of active supports are hydraulic props used in mining and long rockbolts anchored into the solid elastic rock beyond the zones of failed rock and tensioned around an excavation. Arches, linings, and packs are examples of passive support which generate load only as a result of their compression, as are rockbolts which are anchored in the completely failed rock and form a lining of bolted aggregate.

A variety of methods are used to support the tunnel, and some of the most common ones are described below.

1. **Arches**

   Arches are applicable to all types of compact and fissured rocks, to soft rocks, and even to soils. The arch corresponds to a zone of increased stress which exists within the rock mass and is unaffected directly by excavation. The pressure of the overburden is supported by this arch and transferred on to the sides of the opening and hence into the substrata. The weight of the loosened rock underneath the arch may load the support of the opening.

2. **New primary linings**

   In the construction of soft ground tunnels the erection of the permanent lining takes place as soon as the tunnel has been excavated, usually by the erection of a prefabricated segmental lining in the tailskin of the shield. In the construction of hard rock tunnels, the construction of the permanent lining is often left until the whole tunnel has been excavated. After the tunnel has been driven, a lining train passes through the tunnel, consisting of a travelling shutter and concreteing plant, and the permanent concrete lining is placed. However, if the rock will not stand unsupported, because of being broken up by closely spaced joints for example, then some temporary support, often called primary lining, is installed to keep the rock in place until the permanent lining is placed. If a primary lining has been used, the permanent

lining is sometimes called the secondary lining.

3. **Pipe jacking**

In conventional soft ground tunnelling, the lining for the tunnel is erected close behind the shield, near to the point where the ground is being currently excavated. By contrast, in pipe jacking, although the ground is excavated from within a shield, the lining is formed by adding new sections at the rear end of the tunnel and then jacking the whole tunnel lining forward. (see Figure 1.4). As the name suggests, pipe jacking was originally used for installing small pipes for water, sewage and other services, but the method was soon found applicable to large-diameter pipes and for tunnels. It has been especially used for placing short tunnels, subways, culverts and services beneath existing trunk roads and railways, particularly when these are on embankments.

The great advantage of pipe jacking is that because it is being formed from complete sections of pipe, the complete tunnel has no longitudinal joints; it is therefore far easier to make watertight than a segmental lining and is also structurally stronger. The disadvantages are that only straight or reasonably straight lengths of drive are possible and that there is a limitation on the length of drive which is determined when the frictional resistance of the ground on the pipe exceeds the thrust force available from the jacks.

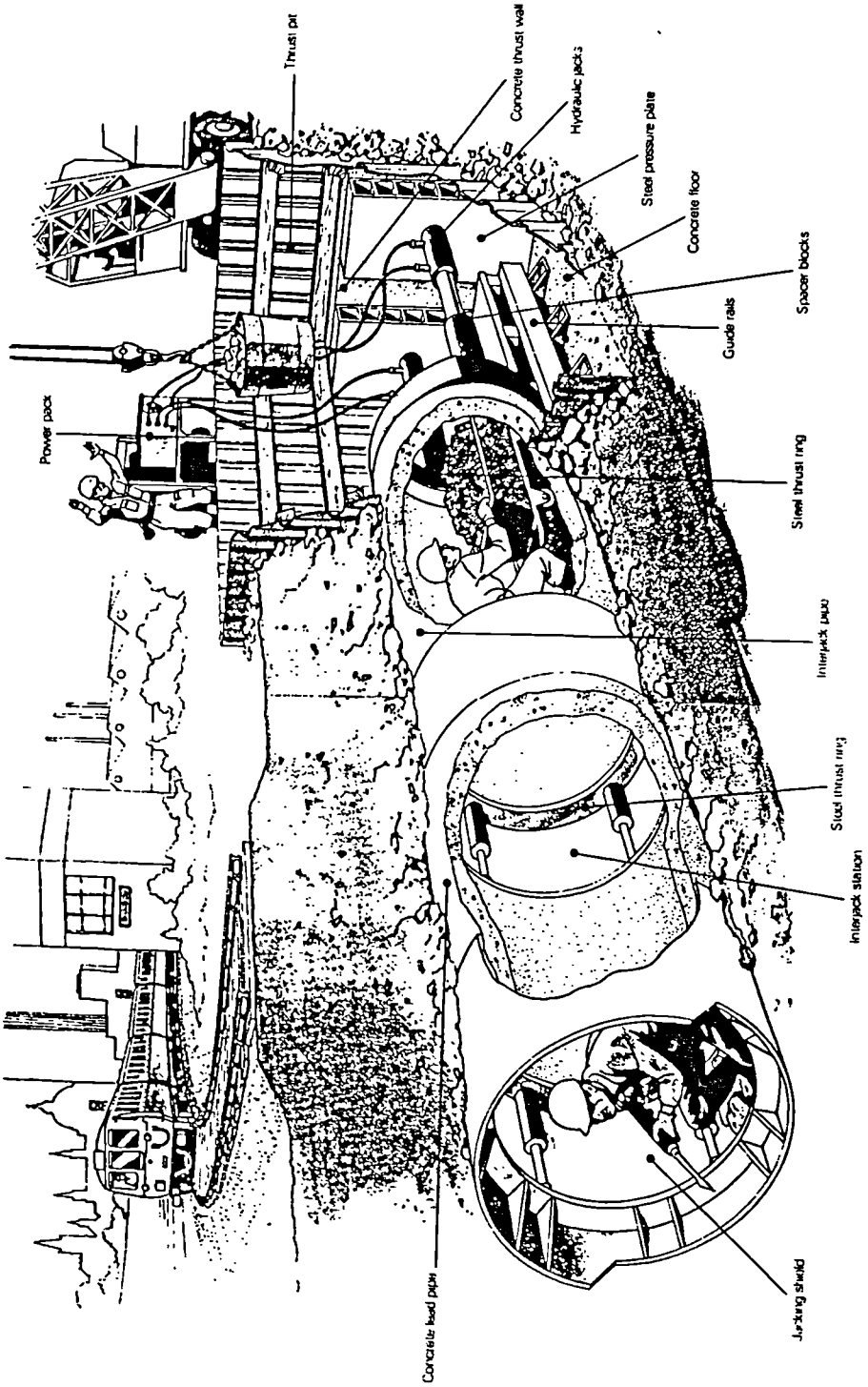

Figure 1.4: Pipe jacking (1980) (from West 1988)

4. Rockbolts

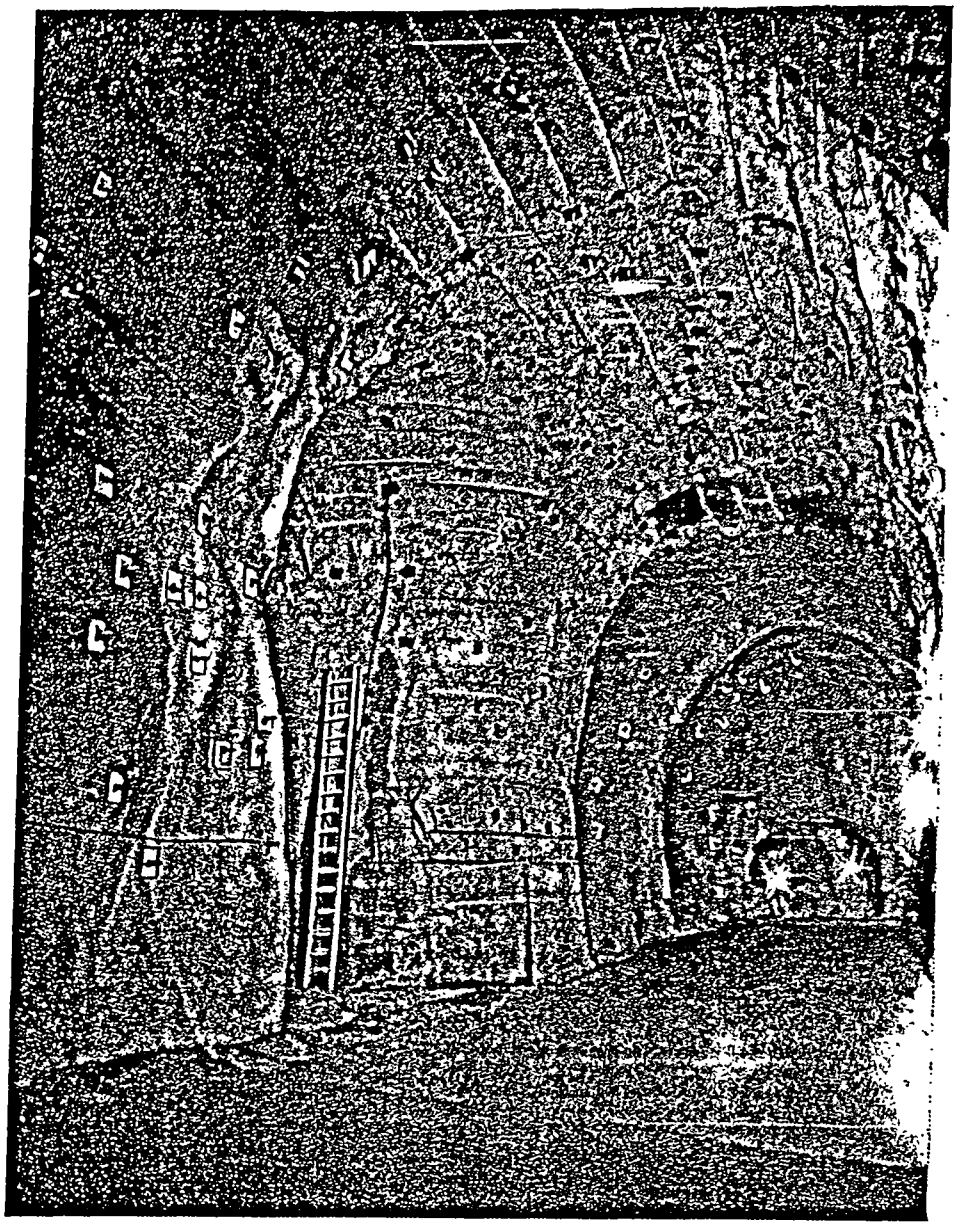

Figure 1.5: The Norad Expansion Project (from Hobst & Zajíc (1983))

Rockbolts were used as early as 1872 in a slate quarry in North Wales. A loose, or potentially loose, block of rock in the tunnel roof or wall is fastened via the rockbolt to the main mass of intact rock. If a fan-shaped array of rockbolts is installed in the tunnel roof, say, then a whole zone of loosened rock can be made stable. Rockbolts are made of steel rods and are of varying sizes. There are different methods of securely attaching the furthermost end into the intact rock mass; mechanical expansion or resin grouting are the most common methods of attachment. A metal plate is placed on the thread end that projects into the tunnel and this is tightly bolted up. Figure 1.5 shows prestressed grouted rockbolts which were installed in a

regular pattern to provide permanent support in the Norad Expansion Project near Colorado Springs in the USA.

5. **Wire mesh**

Sheets of wire mesh are placed around the tunnel wall and held in place either with steel arches or rockbolts. Wire mesh provides little structural support but it does prevent small pieces of rock falling out from the space between rockbolts or arches and can assist in preventing progressive spalling away of the rock, termed 'ravelling', from occurring on the tunnel walls. (See Figure 1.6).

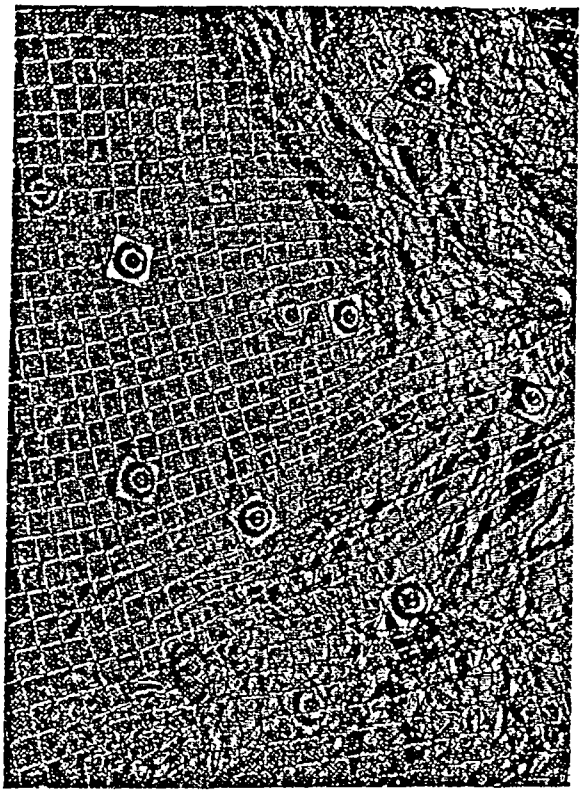

Figure 1.6: Wire mesh on the surface of an excavation secured with rockbolts (from Hobst & Zajíc (1983))

6. **Sprayed concrete**

Sprayed concrete has been used in civil engineering since 1909, and was used underground in Pittsburgh, USA, in 1914. It consists of spraying a mixture of aggregate, sand, cement and water under pressure from a gun onto the surface to which it is desired to apply a layer of concrete. Because of its method of application, sprayed

concrete is often referred to as 'shotcrete' or 'gunite'. As used in tunnels, sprayed concrete is applied to the tunnel walls as soon as possible after excavation. It is often used in conjunction with arches or rockbolts and wire mesh.

1.3 Types of tunnels

Tunnels may be defined as conveyance systems open at both ends, and they may be excavated in soft or hard ground using various mining operational methods. Obviously the nature of the rock and the water table are two of the most critical factors in the structural design of tunnels. Based upon these considerations, Bowen (1975) classified them into the following two types of tunnel, and a brief discussion is provided below.

1.3.1 Hard rock tunnels

In general, tunnels in hard rock are built by blasting. In the full-face method, the entire area of the tunnel cross-section is blasted out at each round. The heading and bench method is rather different, the heading being carried on ahead of the bench, the latter acting as a working platform. Both are shot at one round, the bench charges being detonated first.

Whatever the excavation method, the space between the rock surface and the supports should be packed with stone or concrete and wedged. In many cases, concrete linings are installed and, after their construction, all possible back packing voids ought to be cement mortar grouted. Sometimes different components are utilized. For example, in the Pennsylvannia Turnpike tunnels, voids were filled by blowing in powdered slag, chemicals being subsequently pumped in to form a hard mass after reaction. Here, however, the exacavations were made in solid rock.

1.3.2 Soft rock tunnels

Tunnelling in soft rock is rather different because of the lower tensile and shearing strength encountered. Unlike the sudden, sporadic and violent influx of water sometimes encountered in hard rock tunnels, combating water may be a more or less continuous process. Therefore water table is an important factor. One remedial approach is to lower the water table which may be achieved by sinking well points. Load-bearing supports for the tunnel may not be neccessary if excavation is being carried out in firm soft ground, e.g. a ce-

mented sand. In flowing ground where water may be present, poling boards are employed to support roof and sides, the work progressing by shifting these as required. Blasting is used to facilitate work in cohesive running ground.

One of the most common methods of excavation is that involving the shield. This is a circular steel box or ring usually possessing a transverse diaphragm. The front end is a cutting edge and the rear end juts back over the finished lining, often consisting of cast iron rings. The shield is advanced by means of hydraulic jacks that react against the finished lining to the rear. In firm beds, the work progresses in a series of steps. In soft materials, the shield is pushed against the facing soil and some of these flow into the tunnel through openings in the diaphragm, the balance of the soil material being displaced upwards. The shield is larger than the tunnel lining so that an annular space is created and must be grouted, usually with a dense suspension of cement and sand in equal proportions. Some early examples of shield tunnels are the Holland tunnel in New York City, some parts of the Paris Metro and, most famous of all, the Tower subway under the River Thames at Tower Hill in London, which was constructed using the Greathead shield in 1870.

1.4 Purpose of tunnels

Tunnels may be considered as conveying people or materials, and they can be roughly classified as follows:

1.4.1 People tunnels - pedestrian subways

Subway construction under railways has been greatly facilitated by the introduction of the 'pipe jacking' technique. Previously, they were made by cut and cover or by timbered excavation methods. The 'pipe jacking' approach has the advantage that it can be used without interrupting the traffic. They can have large diameters, from 3 to 3.8m, and are circular in cross-section when constituting pedestrian subways.

1.4.2 People tunnels - vehicle traffic

The original Blackwall tunnel beneath the Thames in London was completed in 1897. At one time, it was the main traffic crossing point. The Mersey road tunnel in the UK was constructed to carry cars and it joins Liverpool and Birkenhead; the main tunnel is about 11m wide. It was drilled through sandstone underlying the mud bed of the Mersey river.

Deep shafts were sunk and lined to the sandstone on each bank of the river and, from their bottoms, two pilot headings were driven, one a top, one a bottom heading. To deal with the water problem, the shafts were drilled much lower than the tunnel depth, and a drainage tunnel was drilled below the two main headings and parallel to them.

1.4.3 Gas tunnels

A very drastic grouting operation has been used in constructing the East River gas tunnel in New York City, a good example of this category built before the First World War. The operation involved two drillings which were located well below the river in order to avoid water problems. However flooding and leaking still persisted. Cement was forced in to fill the whole space between the two underground bulkheads. After much delay, the tunnel was finally completed in 1916.

1.4.4 Water tunnels

A good example of this type of tunnel is in the Tecolote tunnel conveying water from the Cachuma reservior to a conduit in Glen Annie Canyon, California. The work commenced in 1950. After a violent gas methane explosion in 1951, the heading was quickly filled with sand and water, and massive bulkheads were installed to restrain floods. High pressure grouting was employed to seal the leakages.

1.4.5 Some observations

Great advances in tunnelling have occured since the nineteenth century and these have obviated older techniques such as timbering which are rapidly becoming lost arts. Machinery has enormously reduced risks and improved working conditions. All rock removal is now mechanized, blasting in hard rock tunnels, for instance, being followed by mechanical shovel collection of debris which is later loaded on to conveyor belts. Similarly, slurry-pumping plant is used for disposal and, in gravelly soil, sifting may be accomplished by machine, the smallest fragments of the product being utilisable in association with grouting. Such tiny pieces are compressed air-injected into the space between the rock wall and the tunnel lining through holes in the latter. The quantity of cement needed for subsequent grouting is thereby reduced so that the costs diminish. There can be no doubt that tunnelling machinery will become increasingly elegant and it may well be that grouting may eventually become part of a continuous, automated process that also involve excavation, mucking and if necessary, lining.

1.5 Excavation systems

Nowadays, all major tunnelling operations through soft ground are carried out using the shield method which does not require timbering. But it was not always so. A variety of excavation methods were evolved during the last century, most of them taking their name from the country in which they were originated. The most famous ones are the Belgium method, the German method, modified German method, the English method, the Austrian method, the Italian method, radial method, and the upraise method. These methods have been described in detail by Beaver (1972).

1.6 The New Austrian Tunnel Driving Method

Although it is based mostly on empirical knowledge, the New Austrian Tunnel Driving Method has been in use all over the world during the last three decades or so. One of the main innovations of the method is to consider the effects of using rockbolts to stabilize the excavation.

1.6.1 The classic method

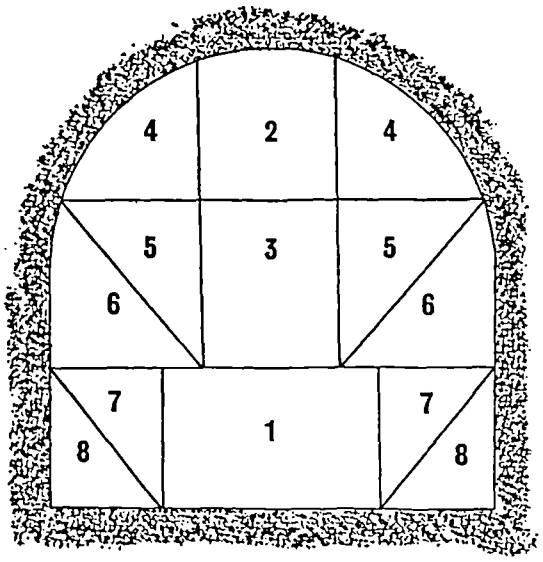

Figure 1.7: Classic Austrian tunnelling method with corresponding support construction sequences (from Beaver (1972))

The classic Austrian tunnelling method was one of methods of tunnelling in the nineteenth-century with timber supports. It was first used in the construction of the Oberau tunnel on the Leipzig and Dresden Railway in 1837. Figure 1.7 shows the order of excavation of this tunnelling method. The main disadvantage was that the strut was liable to distort or gave way under unsymmetrical pressure, and was soon superceded by the New Austrian tunnelling drive method.

1.6.2 The modern method

The modern New Austrian Tunnel Driving method was described by Hobst & Zajíc (1983) as follows.

The rock in the surroundings of the opening, which may be damaged or loosened by excavation work, is strengthened by a regular system of steel bolts to form a self-bearing, but yielding, roof arch. The bolt system is complemented at the rock surface by a layer of gunite or shotcrete of varying thickness, reinforced by wire mesh or steel ribs, if necessary. This reinforcement can be adapted for either temporary or permanent stabilization of underground excavations with a variety of cross-sections; it can be used in full face tunnel sections or in parts, while explosives, tunnelling machines or shields are being used nearby. The extent of the strengthened zone around the excavation varies according to the quality of the rock and the outline of the opening. This zone can easily be strengthened with further rockbolts or layers of gunite, if it seems necessary on the basis of the amount and shape of the deformation of the rock and rock reinforcement registered by instruments set up in the course of excavation. The reinforcement is quickly installed with a high degree of mechanization, made possible by the fact that the opening remains free all the time. The full opening usually has a circular or horseshoe shape.

The design of the rockbolts and the complementary strengthening is usually carried out according to a standard scheme corresponding to particular qualities of the rock or soil. In Europe, the classification of standard schemes for the New Austrian tunnelling driving method compiled by the Austrian experts Rabcewicz (1964, 1965), Lauffer (1958) and Pacher (1973) is well known. There are six classes with corresponding construction sequences and reinforcement ranging from *class 1* for massive, unjointed, or slightly jointed dry rocks to *class 6* for loose soils, detritus and crushed rocks, as shown in Figure 1.8.

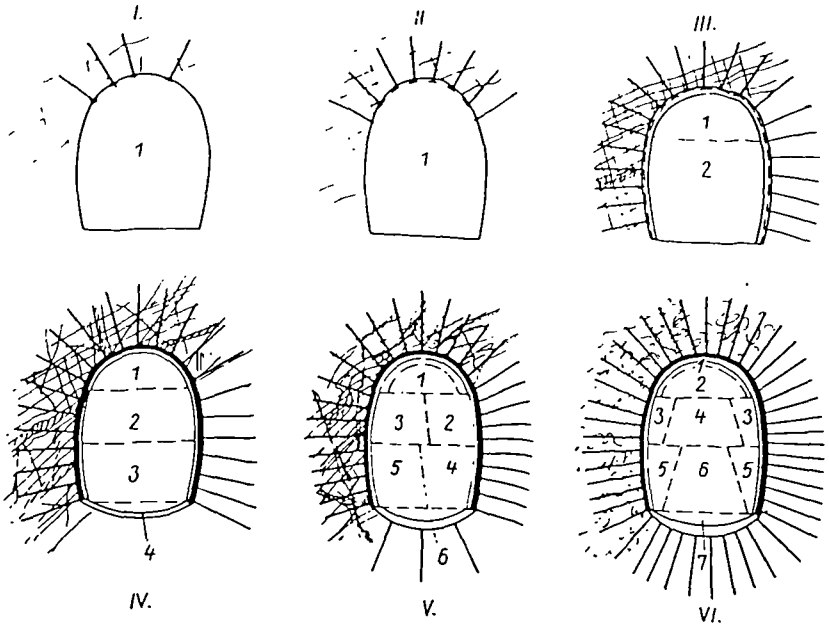

Figure 1.8: New Austrian tunnelling scheme - Six classes of tunnel excavation scheme, with corresponding support construction sequences (from Hobst & Zajíc (1983))

The Austrian tunnel driving method has proved its worth not only in strong rocks, but also in squeezing and loose ground where astonishingly good results have been obtained. For instance, during the construction of the Massenberg tunnel in Austria in slope detritus and weathered shales, initially caving-in occurred even with the use of strong concrete reinforcement of 80cm thick; and the rock was eventually stabilized by the use of rockbolts.

This method is very adaptable to new conditions of the rock mass encountered during the course of excavation, and the reinforcement can be strengthened almost arbitrarily and instantaneously, if necessary. For example, when sections of the Taurus motorway tunnel in the Austrian Alps were driven at a depth of 800 to 1,000m into highly compressed phyllites, the reinforcement turned out to be inadequate. Large deformations rapidly developed during excavation of the roof section as a result of large lateral pressures. To overcome this problem, further non-prestressed grouted rockbolts of 6m in length (and later 9m) were installed, and ultimately two rows of 13m long rockbolts, prestressed to 600kN has to be added. Subsequently the section was stabilized by the additional supports.

Most of the communication tunnels all over the world are driven by this method nowadays.

1.7 Classification of rockbolts

The selection of a suitable type of rockbolts for securing a particular structure to the ground depends on the requirement of the load-bearing capacity, the length and number of rockbolts needed, and the available facilities for placing, fixing and stressing the rockbolts at the site.

As far as purpose is concerned, four of the most common types of rockbolts are classified below by Bowen (1975) and Hobst & Zajíc (1983).

1.7.1 Short rockbolts

Short rockbolts are useful where small tensile forces up to 100kN are to be distributed among a large number of short rockbolts, for example, in the stabilization of a rock face. With regards to manipulation, short rockbolts are the simplest in terms of preparation, placing and prestressing. Bars of low quality steel are normally suitable only for short rockbolts with a short service life, such as those used in securing rock surfaces in small underground excavations, or in situations where no prestressing is required.

1.7.2 Long rockbolts

Long rockbolts of up to 15m can be rapidly installed for taking up larger forces of up to 400kN where sufficient boring capacity and space for manipulation are available, for example, in foundation pits.

1.7.3 Prestressed rockbolts

The purpose of prestressing rockbolts is to create an elastic tension in the free section of the steel bolt tendon with the aid of suitable stressing equipment. In this way, the tendon section exerts a predetermined force on the bolted structure.

The methods of prestressing, testing, and checking rockbolts are now fixed by Standards and Codes in many countries. The recomendations differ in details, but the basic procedures must take account of the characteristics of the materials used and the safety

demands of the bolted structure, and are therefore standard everywhere.

Functionally, prestressed high quality steel rockbolts are the most suitable for anchoring structures into rock and soil. They reduce expenditure on steel and minimize the boring and prestressing requirements. Moreover, reductions in prestressing caused by rock creep, and more especially by soil creep, will be diminished. The prestressing of high quality steel up to the yield point, produces an elongation several times greater than that created by a similar stress in a steel bar of standard quality.

1.7.4 Grouted rockbolts

The fixing of rockbolts by grouting is one of the most highly developed techniques. The ideal of every grouting system is to drill the borehole as quickly as possible, insert the assembled bolt tendon into the borehole with ease, and then prefectly grout the borehole and the immediate rock or soil to create a load-bearing root and reliable anti-corrosive protection of the tendon throughout the service life of the bolt. The appropriate procedure is selected according to the type of soil involved, and the design of the bolt. In general the weaker the rock or soil and the smaller the assumed cohesion between the ground and the bolt root, the more exacting are the requirements placed on the rockbolt technology, if reliability and economy of installation are to be ensured.

Short steel bars, usually shaped with threaded ends, are fitted into prepared boreholes in rock which are then filled partly or completely with grout or mortar. If they are fixed only at the remote end of the borehole, they can also be prestressed. If, however, the entire length is embedded in grout, the bolt remains unstressed and reinforces only the rock mass in the vicinity of the excavation. Compared with mechanically fixed bolts, those embedded in grout are much cheaper and can be used with success in softer rock types; however, the fixing of grouted bolts into boreholes is more complicated and it takes longer for these bolts to be brought into use, since the strength develops with the hardening of the grout or mortar.

In the case when an accelerator is added, the mortar may start to harden after a few minutes and a sufficient strength is reached in two or three hours.

Anchoring bolts or rebars, fixing the borehole length throughout by grout, which is

injected through a special tube inserted down to the borehole at the remote end and pulled out step-by-step with the progress of grouting, are called *SN-bolts* in Europe, named after Store-Norfors, a place in Sweden where they were used for the first time. Bolts, enveloped by grout along their entire length, are more effectively protected against corrosion. Correct positioning in the centre of the borehole must be established by means of suitable spacers attached to the bolt. The bottom part of the borehole must often be de-aerated to ensure its perfect filling by grout. This is achieved by a plastic tube of small diameter, inserted together with the anchor bar down to the bottom of the borehole, or by the bar itself, which is hollow in this case.

So-called *dry* bolts without prestress are short steel bars fully fixed in soft rock only by the grip of the rock without cement. They are driven mechanically into the borehole whose diameter is slightly smaller than that of the bar. This type of anchorage was successful, for example, in the anchoring of the faces of excavations in clayey shales for the Prague Underground railway, and in the excavation of a gallery in much saturated shales under the Rhine bed in Germany.

1.8 Mathematical modelling of tunnelling

Rock structures can generally be divided into two broad categories: constructions realised on the ground surface (such as slopes, embankments) and underground excavations (such as tunnels). The choice of an appropriate method of analysis depends on the geometry and the type of structure.

For underground works in soils, excavations can often be modelled as two-dimensional plane strain, or axisymmetric problems. In particular, tunnels are frequently considered to be of circular cross-section, and the *in situ* stress field in the rock is assumed to be isotropic. Fenner (1938) and Hoek & Brown (1980) provided analytic solutions for the stresses in the axisymmetric tunnel problem for an elastic brittle-plastic material using the Mohr-Coulomb and Hoek-Brown yield criteria respectively, and strains and displacements in the elastic region are obtained from these by elasticity theory. Wilson (1980), Kaiser (1980) and Brown *et al* (1983) proposed methods to predict the displacements in the yielded rock surrounding the tunnel using simplifying assumptions such as the proportionality of major and minor principal strains, and constant or zero elastic strains in the plastic region. An analytic solution for the Mohr-Coulomb problem using the full theory of incremental

plasticity for the case of an elastic ideal-plastic rock model and an associated flow rule was proposed by Florence & Schwer (1978). Reed (1986) suggested an analytic solution for an elastic brittle-plastic rock with Mohr-Coulomb dilation flow rule, using the standard boundary condition.

1.8.1 Finite element solutions

The two-dimensional finite element method has been used by many researchers to analyse plane strain problems in soil mechanics. This technique has been well documented by, for example, Zienkiewicz & Taylor (1989, 1991), Davis (1980). In this technique, the displacement vector is the primary unknown, and the stress vector derived from it is the secondary variable. There are a lot of computer software packages available for both commerical and educational use. This thesis will use the finite element technique to examine deformation along the openning of a tunnel, and it will propose a new finite element to model individual rockbolts as a tunnel supporting mechanism.

1.8.2 Finite element modelling of rockbolts

The first attempt at numerical modelling of simulated pull-out tests of anchored bolts was carried out by Coates & Yu (1970). Egger (1973) was one of the first to propose a method of calculation, taking into account the influence of systematic bolting on the stability of a circular excavation. In the study of the behaviour of any construction, it is necessary to assume certain simplificaions for representation of bolt elements and their interfaces. In the first attempts at finite element modelling of reinforced structures, Heuze & Goodman (1973) used a one-dimensional element with axial stiffness to represent the bolts. The empirical formulae for the *Dowel effect*, which is significant when the bolt is set a perpendicular angle through the joint or discontinuities between rock mass, is considered by Bjurström (1974). Taking into account the tangential stiffness of the bolt and the grout, St. John & van Dillen (1983) elaborated a three-dimensional rockbolt element. Brady & Lorig (1988) suggested an element with two springs, one parallel to the local axis and one to its transverse direction. Aydan (1989) developed a three-dimensional element with eight nodal points - six nodes connected to the rock mass and two representing the steel bolt. Since then, many researchers have modified and improved this type of rockbolt in coupled form. Details of this rockbolt element and some of its modifications can be found in Chapter 8. Egger & Pellet (1992) defined an interface element whose thickness corresponds to the distance between two plastic hinges in the bolt. Based on the stiffness

matrix of an interface element representing the rock joint introduced by Ghaboussi *et al* (1973), Swoboda & Marenče (1991, 1992, 1995) introduced the *Bolt Crossing Joint* (BCJ) element by assigning different coordinates for the bolt nodes and the nodes of rock-grout interfaces, thus resulting in different displacements for the bolt and the rock at the bolt-joint intersection.

The discrete element method and the hybrid finite element - discrete element method (See Chapter 2) have also been used by some researchers to model rock mass, tunnel supporting mechanisms and rockbolts. Lorig (1985), Pan (1988) and Harts (1991) are some of the contributors.

1.9 Purpose and structure of the thesis

When using grouted rockbolts as a medium to prevent caving-in excavating tunnels, the relevant properties of soil and rock strata as well as the rhelogical character of the grouted rockbolts must be examined.

1.9.1 Purpose of the thesis

The stability analysis and rockbolt design for an underground excavation must take into account the geometry of the excavation, the geological structure in the wider surroundings of the excavation, the physical and mechanical characteristics of the rock mass including its initial state of stress, and the excavation method. These starting conditions may vary from the simple to the very complex, and from situations which are well understood at the outset to those that can only be more accurately understood as the excavation proceeds. The rockbolt design is decided by these starting conditions, which are known empirically or from the results of analysis; thus the design may be complemented, if necessary, by the results of observations and measurements carried out in the course of excavation.

The design must in every case be based on up-to-date geological information concerning the location of joints and other major features of the geological structure, and there must be a careful appraisal of the information obtained from behaviour measurements in areas that are already opened up.

A very important part of this appraisal is the observation of the effect of deformation

on the loading of the excavation. Immediately after excavation of the cavity an elastic displacement of the rock into the free space takes place together with a marked drop in radial pressure. This is the most suitable time for setting up the support and reinforcement of the rock, because, according to Rabcewicz et.el. (1972), a relatively weak reinforcement then suffices for its stabilization. Delay in placing the reinforcement leads to a gradual loosening of the rock in the surroundings of the excavation and a further decrease in pressure.

Grouting is a process of injecting appropriate material into certain parts of the earth's crust so as to reduce permeability and/or increase strength. Thus this grouting process appears to be a very good way of partnering rockbolts as a means of stabilising rock strata in underground excavation and should be included in any rockbolt model. Based on the analysis of large displacement theory in elasticity, the aim of this thesis is to propose a new rockbolt element which can effectively and economically model such a reinforcement. As underground excavation is often modelled as a plane strain problem, where the in-plane cross-section of the tunnel is taken as the domain, and further, it is assumed that the surrounding rock is made of isotropic linear elastic material, it is intended to carry out the investigation as a two-dimensional plane strain problem as a first approximation to the reality.

1.9.2 Structure of the thesis

There are eleven chapters in this thesis. Chapter 1 is the introductory chapter which describes linearity and nonlinearity problems in structural engineering. It also gives a brief classification of different types of tunnels and their use. Some common tunnel excavation methods and tunnel stabilizing techniques are discussed. In particular, the ideas and advantages of using rockbolts as a supporting mechanism are assessed.

Chapter 2 surveys some of the most commonly used numerical methods in engineering. Their basic principles, brief history, the current state of development, the application and limitations are assessed and compared.

Chapter 3 covers the basic fundamentals of the finite element analysis of elasticity problems and establishes the stiffness matrix by minimization method. The continuous linear elastic two-dimensional structure is discretised by a mesh of eight-noded isopara-

metric elements, and a linear strain-displacement relationship is assumed. This technique has been widely adopted, and two examples are included to validate the principles.

Chapter 4 introduces the idea of large displacement which arises when geometric non-linearity is considered. The theory again focuses on the use of eight-noded isoparametric elements to discretise the linear elastic structure. Loads are applied in incremental steps, and iterations are introduced to deal with the nonlinear change of the geometry. A buckling problem is used as an example to validate the theory.

In Chapter 5, the theory established in the last chapter is adapted to two- and three-noded bar elements, where each node assumes translational degrees of freedom only. Because of the absence of rotational degrees of freedom, this adaptation gives unsatisfactory bending results and does not reflect the general bending phenomenon of a rod. Several examples are used to illustrate the main drawback of this algorithm.

To give a more realistic representation, rotational degrees are introduced to the end-nodes of the beam elements. Simple small displacement analysis for two-noded beam elements can be found in some standard text, but in Chapter 6, new formulations for large displacement for two- and three-noded beam elements are proposed, together with an iteration algorithm to refine the overall results due to geometrical nonlinearity. The examples used in the last chapter are re-tried to show improvements of the new algorithm.

Based on some established results on joint elements, Chapter 7 develops a suitable model of a joint element which will be implemented in later chapters. Validations of this algorithm are described by the use of some examples.

Chapter 8 proposes a new algorithm for grouted rockbolt element. This algorithm combines the exisiting rockbolt model proposed by Aydan (1989) and the formulations established for beam element in Chapter 6. Formulations for both small and large displacements have been derived, and they are used to compare results with other established algorithms with the use of some examples. This chapter also proposes to combine new iterative solution techniques to deal with the convergence of large displacements.

In Chapter 8, the solution procedure for the stiffness equation in the large displacement

analysis of rockbolt is provided by iterations based on residuals. Although this method works, it is very inefficient and time consuming, Therefore, as an alternative, Chapter 9 proposes the use of limited-storage Quasi-Newton algorithms. Unfotunately, the use of this method in this research is still in its early stage, so no concrete conclusion can be drawn. But the signs are good, and it will be interesting to see how this method progress in the future.

By using a set of parameter as closely as possible to the one used by other researchers in the University of Innsbruck, Austria, a wedge stability problem is presented in Chapter 10. To make it more interesting, different sets of parameter are used in the same problem for direct comparsion.

Chapter 11 concludes this research, and discusses its strengths and weaknesses. It also sets out suggestions for possible further development.

1.10 Conclusions

It is hoped that the new algorithm for grouted rockbolt proposed in this thesis can improve the accuracy of similar finite element models that are currently under investigation, and it may offer a slightly different angle on the way this problem can be tackled. From the foundamental theories of elasticity and tehniques of finite element methods, both linear and geometric nonlinear models will be discussed in full and compared. While this algorithm may offer some advantages over other methods, some established powerful numerical algorithms may complement this proposal and make the whole package a more efficient one. However, due to the limitation of the scope of this research, only a few possible improvements have been investigated.

The pre and post processors of this programming package were written in FORTRAN 77 jointly by Dr. Martin Reed and Dr. Mike Warby, both are lecturers at Brunel University, Uxbridge, UK. The main program itself is also coded in FORTRAN and has been compiled and run using the DOS version of FTN77 (Salford FORTRAN).

Chapter 2

Survey of some common numerical methods used in engineering

When a structural member is subject to an applied load, and if it is cut theoretically at any section so that two or more separate free bodies are formed, then for the whole member and for each part, the conditions of equilibrium state that equal and opposite internal and external forces act on each side of the cut section. One of the most fundamental aspects of a structural engineer's work is to give consideration to and evaluate the magnitude and distribution of stresses in the materials of construction.

All engineering materials deform under stress, and the amount and shape of the deformation of the member depends on the resulting strains of each element of the material. The compatibility of finite elements, which enables them to fit together in the deformed state, is a necessary condition of the displacements and strains, just as equilibrium is a necessary condition of force and stress systems.

The requirements of equilibrium and compatibility for each element must extend to and across the boundaries of the member and indeed of the structure. Thus, at any boundary, the external and internal forces and stresses must balance exactly. Further, it is essential that any solution of the problem must comply with all boundary conditions. Any problem that involves boundary conditions is called a *boundary value problem.*

There are many practical engineering problems which may be classified as boundary value problems. A typical boundary value problem consists of one or more differential

or integral equations within a specified domain, together with some conditions over the boundary of the domain. There are some situations where it may be possible to find an analytical or a closed-form solution for a given boundary value problem, but in other cases, there may be no other choice but to employ a numerical procedure to approximate the solution of the given problem. With the arrival and the advancement of high-speed digital computers, approximate numerical procedures have become very accurate and reliable for the solution of initial and boundary value problems. Currently, the most frequently used numerical techniques in engineering analysis are the **finite difference method** (**FDM**), the **finite element method** (**FEM**), the **boundary element method** (**BEM**), the **distinct** (or **discrete**) **element method** (**DEM**), and the **structural element method**. These methods are briefly described below.

The survey casrried out in this chapter is based on the following sources:

1. Brebbia C.A., Venturini W.S. (ed.) (1987) *Boundary Element Techniques: Application in Stress analysis and Heat transfer.* Computational Mechanics Publications, Southampton.

2. Brown E.T. (ed.) (1987) *Analytical and Computational Methods in Engineering Rock Mechanics).* Allen & Unwin, London.

3. Cookson, R.A. (1987) State of the art review of the boundary element method. *Advances in the use of the Boundary Element Method for Stress analysis.* Mechanical Engineering Publications, London.

4. Pan, X.D. (1988) *Numerical modelling of rock movements around mine openings.* PhD Thesis, University of London (Imperial College).

2.1 The finite difference method

The **finite difference method** is a straightforward and well-tested numerical algorithm for the solution of ordinary and partial differential equations on domains of simple geometry. The domain of the given problem is discretised point-wise into a rectangular grid of mesh points and the unknown parameters are considered to be the values of the field functions at those mesh points. Using the forward difference formula, or the five-point formula, or otherwise, derivatives of the field function can be approximated by the difference or other combination of values of the field function at neighbouring mesh points.

Hence, the differential equation can be reduced to a system of algebraic equations of the unknown field values, which may be solved directly or iteratively by standard numerical methods.

While the finite difference method is a reliable technique for the solution of fluid mechanics and transient analysis problems, some measures should be taken into consideration to maintain the numerical stability of finite difference algorithms. A scheme is said to be stable if local errors remain bounded as the method proceeds from one step to the next. There is a great deal of literature on the stability of finite difference schemes, e.g. Smith (1978).

In this technique, every derivative in the original equation is substitued by a formula which involves differences of several field values at neighbouring mesh points. Therefore accuracy of this method depends heavily on the accuracy of these substitutions. There are a host of formulae where these substitutions can be chosen from, but in general, an accurate formula involves many terms, which in turn will complicate the use of boundary values, or cause complexity in forming the corresponding system of equations that follows.

Further, there are some difficulties encountered with complex domains and/or generalised boundary conditions. In general, the finite difference method requires many mesh points to fit a finite difference mesh to the given irregular domain with good accuracy, and for this reason, the finite difference mesh is often chosen in such a way that the mesh points do not actually lie on the boundary at all. To approximate the given boundary conditions, difference operators with unequal arms are used. This may consequently reduce the overall accuracy of the method and cause inefficiency and difficulties from a programming point of view. Therefore in the finite difference method, the application of the boundary conditions may become a very complicated process. This drawback is particularly serious for the modelling of tunnelling and other geotechnical problems.

Another difficulty associated with the finite difference approach concerns the effect of a mixed boundary condition on the system of equations. It may cause the overall system of equations to lose symmetry. This is not the case in the finite element method in most applications.

2.2 The finite element method

Like the finite difference method, the fundamental idea of the **finite element method** is the discretization of the domain into several subdomains, or finite elements. But these elements can be irregular and possess different material properties, so that they can be used to discretise complex structures which are made up of different materials. The governing continuous functions can be replaced by piecewise approximations, which are usually polynomials.

An integral formulation for the governing equation of a boundary value problem may be obtained by using variational or weighted residual methods. A variational method is based upon the determination of a function which gives rise to a stationary point of a functional of this function and the field function. It may be solved directly by means of the Rayleigh-Ritz method. Alternatively the solution of the governing differential equation can be approximated by a linear combination of a set of chosen basis functions, and it can be substituted into the governing differential equation to give a weighted error. A weighted-residual expression is based upon the minimization over the whole domain, of the weighted error, and the determination of the unknown coefficients in the approximated solution at the minimum point. Numerical solutions to weighted-residual expressions may be obtained directly by means of point-collocation, least squares, Galerkin methods, etc. These methods have been described in detail by Davies (1980) and Zienkiewicz & Taylor (1989 and 1991). The finite element method is based upon the piecewise discretization of the variational or weighted-residual approaches. Discretising the problem domain piecewise into a number of subdomains, or finite elements, the governing equations for each element can be obtained by means of variational or weighted-residual approaches. Assembling together the equations for the subdomains, a global system of algebraic equations can be obtained and then solved.

In the case of elasticity analyses, the element stiffness matrix is obtained by minimizing the potential energy function with respect to the nodal parameters for each element, and by assemblying element stiffness matrices for all elements, the global stiffness matrix for the structure is obtained.

There is a wide range of applications of the finite element method for which realistic boundary conditions can be stated. As each element is dealt with individually before

assembling for the whole stucture, this method has the distinct advantage of being able to deal with a structure with complex properties. However, its main drawback is that as it is based on a whole body discretization scheme, this may lead to a very large number of elements, or the use of higher-order elements with many degrees of freedom, and hence result in a large system of equations. This is especially true when dealing with complex three-dimensional structures. Typical three-dimensional problems may require thousands of equations and, of course, a very powerful computer to solve them. For surface engineering problems, such as those encountered with linear elastic fracture mechanics, there is no escape from the tedious calculation of superfluous results inside the domain interior.

Structures or domains, where the shape or internal geometry is complicated, are best modelled by the finite element method. From a practical point of view, simple elements, such as quadrilateral or triangular elements for two-dimensional problems and eight-noded brick elements for three-dimensional continuum problems, are commonly employed. The use of higher order elements is attractive from an accuracy point of view. However, it should be noted that, while, for the same number of elements, the number of degrees of freedom is increased which makes the resulting global stiffness matrix more complex, the expectation is that a smaller number of elements will be needed for the same accuracy.

The modern use of finite elements really started in the field of structural engineering. Probably the first attempts were by Hrennikoff (1941) and McHenry (1943) who developed analogies between actual discrete elements, like bars and beams, and the corresponding portions of a continuous solid. A major breakthrough was made by Turner *et al* (1956) with numerical methods in structural mechanics, when they presented the element stiffness matrix, based on displacement assumptions, for a triangular element, together with the direct stiffness method for assembling the elements.

Workers in the early 1960s soon turned their attention towards the solution of nonlinear problems. Turner *et al* (1960) showed how to implement an incremental technique to solve geometrically nonlinear problems, that is, problems in which the strains remain small but displacements are large. Stability analysis also came into consideration and was discussed by Martin (1965). Plasticity problems involving nonlinear material behaviour were modelled at this time by Gallagher *et al* (1962), and the method was also applied to the solution of problems in visco-elasticity.

In 1965, Melosh showed that the finite element method could be extended to field problems by variational methods, while Ziekiewicz & Cheung (1965) applied it to a large number of steady-state and transient field problems.

The scale of computational power and its accessessibility have recently increased at an astonishing rate. This has contributed to the acceleration of the use and development of the finite element method. The method has now become an important technique from both a practical and theoretical point of view, and the number of published papers began to increase at a tremendous rate from 1970 onwards.

It must be stated here that there is still some work to be done in some nonlinear areas, e.g. the coupled diffusion-convection problem involved in solving the Navier-Stokes equations is still, from a finite element point of view, far from satisfactory. The types of problems currently being attempted using finite elements cover the whole range of the physical sciences, including both steady and unsteady phenomena. The method is also finding applications in the field of biomedical engineering, where the problems exhibit all the difficulties associated with geometric and material nonlinearity.

A further area which has recieved much attention involves the development of suitable numerical algorithms for the calculation of element matrices, and efficient solution of the resulting overall system of equations for the whole system, e.g. multigrid methods. Despite the continuous progress made in other numerical techniques, the finite element method offers greater flexibility in the treatment of nonlinearities, inhomogeneities and anisotropy.

Finally, it may be said that the theory and application of finite element method offers much in the way of interesting problems for engineers, physicists, applied mathematicans, and numerical analysts. All of these groups have made important contributions, and undoubtedly will continue to contribute to its development.

2.3 The boundary element method

The following description of the *boundary element method* is based on the article by Cookson *et al* (1987).

Using some mathematical techniques, such as potential theory (as demonstrated by Kellogg (1929)), a partial differential equation over a domain can be transformed into a boundary integral equation over the boundary of the domain. The boundary integral equation may be solved numerically by means of piecewise discretization, whereby the boundary of the domain is divided into sub-boundaries, or boundary elements. The equations on the sub-boundaries, or elements, are assembled to form a system of algebraic equations in terms of the values of the field function parameters over the boundary. Solving such equations, the value of the field function at any point inside the domain can be obtained by means of a simple equation which involves the evaluation of some boundary integrals. This approach, which is known as the **boundary element method**, has the following advantages, compared with other numerical techniques:

- It reduces the dimension of the problem by one, resulting in a smaller system of equations and a considerable reduction in the amount of data required for the analysis.
- The boundary element method offers continuous interior modelling within the solution domain, and the values of the solution variables can be calculated at any selected interior point.
- Boundary conditions at infinity are properly accounted for in the formula represented by the integral, and hence there is no need to resort to truncated domains. Therefore the method is well suited to problems of infinite domain, such as soil mechanics, hydraulics, stress analysis, for which the classical domain methods are unsuitable.

Since the 1960's, boundary element researchers have managed to apply the method to a large range of applications.

Cruse (1969) provided formulations of the boundary element method, followed by Watson (1979), Brady (1979) and many others. Crotty & Wardle (1985) extended the application of the method to analyse heterogeneous media with continuous planes of weakness.

The developments made in the finite element method started to find their ways into the formulations and solutions of boundary integral equations, and the first textbook on the boundary element method was written by Brebbia in 1978. International conferences on topics of boundary elements were regularly held, and proceedings of these meetings were edited by Brebbia, and also by Banerjee *et al.* Cruse (1969) applied the boundary

integral equation method to three-dimensional stress analysis and improved the algorithm in 1974.

His work was followed by Lachat & Watson (1976). Jaswon & Maiti (1968) investigated an integral equation method to solve the plate-bending problem. Bezine & Gamby (1978), and Tottenham (1979) proposed different algorithms for the same problem. Elastoplastic analysis of axisymmetric bodies was introduced by Dobare *et al* (1982), and the large deflection problem of viscoplasticity was considereded by Chandra & Mukherjee (1983). An advanced algorithm for the boundary element analysis of two- and three-dimensional problems in elastoplasticity was proposed by Banerjee & Raveendra (1986).

Despite the increasing interest in the boundary element method, there are still some difficulties encountered with the use of the method, thus preventing its popularity in engineering disciplines. Primarily, these difficulties arise in modelling inhomogeneity, and material nonlinearity problems.

2.4 The discrete element method

The **discrete element** or **distinct element method** is one of the most powerful and versatile methods for simulating discontinuum behaviour. This method was originally developed by Cundall (1971) as a means of modelling the progressive failure of rock slopes. In this method, the region of interest is a discontinuous medium, with real joints intersecting the body to form a system of differently shaped individual 'blocks'. The stresses and displacements are continuous within each block, but are generally discontinuous between these blocks. Therefore the general partial differential equations for the static equilibrium problem are usually not satisfied for the whole region, because overlaps and cavitation often occur. Other equations governing the constitutive relations between the joints have to be introduced. This also means that unlike other methods, the compatibility condition is no longer satisfied in the governing equations of the distinct element method so that more assumptions are usually involved in the solution procedure.

In the original and basic form of the distinct element method, the blocks are taken to be rigid, and deformations are associated with the surface of contact between blocks. Physically this means that the deformability of the surface material, such as asperities of the joints, is far greater than that of the solid rock. A universal law, Newton's second

law of motion, is then applied as the primary governing equation for the problem, and the behaviour of contacts between blocks is simulated using other assumptions concerning the geometry, the contact points and the force - displacement relations at the contacts.

The solution procedure is by use of a modification of the dynamic relaxation technique of the finite difference method (Southwell 1940, 1946, Otter *et al* 1967), so that in the procedure one block is equivalent to a nodal point of this classical dynamic relaxation. Like other explicit methods, it is not necessary to solve global simultaneous equations, and the numerical iteration is stable only if the time step is taken as very small.

2.5 The structural element method

The **structural element method**, discussed in detail by Lorig (1984), and Lorig & Brady (1984), is more general in its treatment of rock support mechanics, and rock support interaction.

The essence of the structural element method of analysis of support systems is the formulation of a stiffness matrix defining the generalized load-displacement behaviour of the support structure. The method forms part of the well established engineering procedures for matrix analysis of linear structural systems. The usual displacement formulation of the method is presented in many texts on structural mechanics, such as that by Ghali and Neville (1978). A structure is resolved into discrete structural elements, assumed to deform in a linearly elastic way under applied load. The stiffness matrix of each element may be established from its simple deformation mechanics, and the stiffness matrix for the structure is constructed by satisfying the conditions for equilibrium and continuity at each node of the structure.

2.6 Hybrid methods

Pan (1988) surveyed some of the following hybrid methods. They are briefly described below with their development history.

The advantages and limitations of the various numerical methods of analysis in engineering rock mechanics have been briefly discussed in the preceding sections. In the application of these numerical methods, it has been found that none of the methods is

ideally suitable for all practical problems because of the limitations involved in each of the methods. A hybrid method is a combined or coupled computational scheme in which two or three different methods are used to combine the advantages of each numerical procedure and to minimize disadvantages. The existing hybrid methods used in rock mechanics include the finite element - boundary element method, the boundary element - distinct element method and the finite element - distinct element method.

2.6.1 The finite element - boundary element method

The procedures of coupling the finite element method with boundary integral solutions were first introduced by Zienkiewicz *et al* (1977). Georgiou (1981) and Brebbia *et al* (1984) suggested the conversion of boundary element equations to equivalent stiffness matrix equations compatible with the finite element equations. This idea has since been further developed and widely applied by Sivakumar (1985), Vallabhan & Sivakumar (1986). The latter developed a static condensation procedure, which is similar to substructuring in the finite element method, to reduce the boundary element equations to the order of the displacements of the boundary. This technique is very efficient on the computer and helps the user to prepare data easily.

Investigations in the three-dimensional excavation problems (Beer *et al* 1987) was carried out. Asymptotic error estimates for Galerkin methods and for certain cases of collocation were investigated by Wendland (1988), and Eberhardsteiner *et al* (1991) applied this technique to stress analysis in elastoplasticity. Brink (1991) compared this coupled method with finite element-infinite element method in two-dimensional problems in linear elastostatics.

2.6.2 The discrete element - boundary element method

In order to analyse the stress distribution and displacement in a jointed and fractured region of a rock mass, a hybrid distinct element - boundary element model has been developed (Lorig and Brady 1982, 1984; Lemos and Brady 1983). When representing the rock which constitutes the near field of an excavation with distinct elements, and the far field with boundary elements, the problem has generally to be solved in an iterative way. This is unlike the linkage of the finite element and the boundary element method, because the distinct element method is a specially developed explicit technique while the boundary element solution is an implicit procedure. The calculation proceeds by considering

the satisfaction of the displacement continuity and equilibrium conditions at the interface between the two solution domains (Brady 1985). In other words, it was assumed that no slip or separation could occur at the interface.

Verification of the performance of this hybrid method appears very difficult, particularly for the occurrence of large movement of distinct elements. Practical applications of the method have not been found.

2.6.3 The finite element - discrete element method

Dowding *et al* (1983) presented a coupled finite element - rigid block (distinct element) model to analyse lined openings in a jointed rock mass. In their model, an explicit finite element formulation (dynamic analysis) was used to coincide with the relaxation algorithm of discrete element analysis. Finite element nodes at the interface were assumed to be fixed on the neighbouring rigid blocks, and only linear elastic analysis examples were given. No existing program of this type was found in the literature (Plishke 1988; Coulthard & Perkings 1987). Pan (1988) combined the finite element package COAL with the discrete element package BLOCK and used this coupled method to analyse the non-linear modelling of rock mass behaviour around mine excavation.

As has been described, the hybrid scheme is usually implemented by coupling the different codes to model different parts of the region. One variation is the deformable block model of a jointed rock mass developed by Maini *et al* (1978) and Vargas (1982) in which finite differences and finite elements were used to represent the deformable rocks within the distinct elements. This technique has been used in the development of updated discrete element programs (Lemos *et al*, 1985).

2.6.4 The structural element method with discrete element - boundary element method

The structural element may be readily coupled with the discrete element - boundary element method. In this procedure, contact at various points between the rock and support is represented by springs orientated normal and parallel to the surface. The springs are taken to have stiffness. Their contribution to the performance of the support structure is taken into account by the inclusion of appropriate terms in the support stiffness matrix.

Computationally, linkage is achieved by imposing continuity and equilibrium conditions at the points where the rock mass bears upon the support contact springs. The forces imposed by the support at the discrete element contacts are introduced in the computational cycle for the discrete element domain. Thus, the support forces mobilized by rock displacements can be updated in each computational cycle, in the same way as the interface forces between the infinite domain and the discrete element domain.

The coupling of these hybrid methods have proved to be very effective and successful, and clearly it has great potential for future investigation. At present, many researchers are proposing different algorithms to analytically combine these hydrid methods, and finding their applications in rock mechanics, engineering and other scientific problems, it would be interesting to monitor its development in future.

2.7 Conclusions

Various exisiting numerical methods in rocks mechanics have been briefly discussed and assessed. It would be impossible to pin down one single method that would provide the best solution for all types of problems in rock mechanics. In fact, each method has its own strengths and weaknesses, and the choice must, therefore, depend on how well the strength of one particular method can be utilized as much as possible without incurring much compromise.

The finite element method is one of the most frequently used techniques for analysing stability in underground excavations. It takes into account, with minimum difficulty, many of the factors which affect stability.

Analysis by the finite element method is based on the assumption that the surroundings of an underground excavation can be considered as a large number of small geometric elements with two, three or four apices, increasing in size with distance from the opening or narrow boundary as the effect on stress diminishes (see Figure 2.1). The calculation considers a unit displacement of one apex of the element and the force which can be said to have induced the deformation of the element is sought. This force must be equal to the resultant of all forces actually acting on the rock element. Physical and mechanical characteristics of the rock mass, found as a result of investigation, are substituted into the deformation equations for one element. Similar equations are obtained for the other

elements of the mesh. The entire program comprises a system of large number of equations depending on the number of nodes used in the mesh and degree of freedom of each node. The computation gives the magnitude of the stress at different points in the excavation surroundings. By studying these points, any zone in which the strength of the rock might be exceeded can be identified.

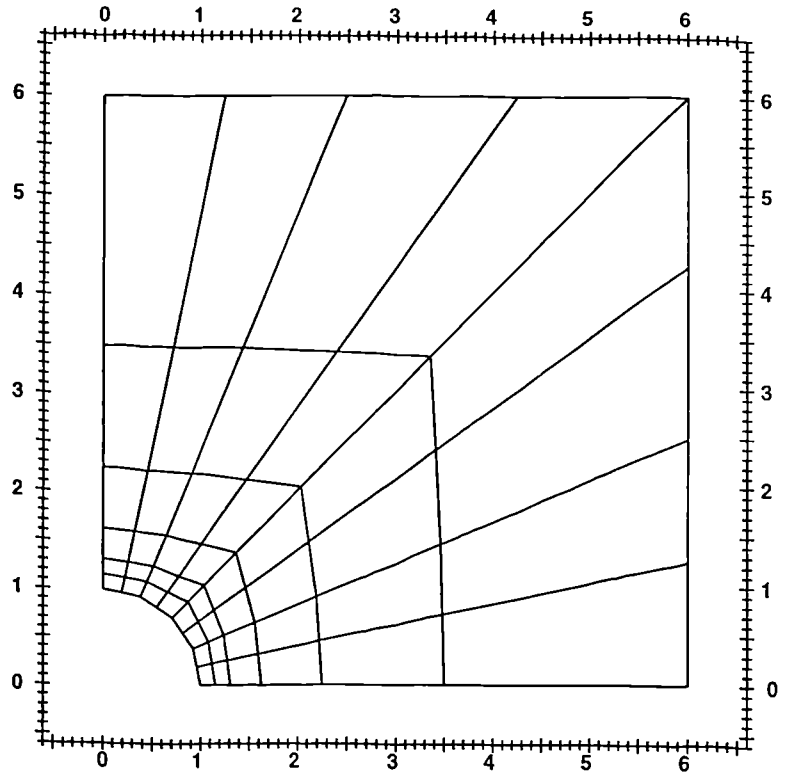

Figure 2.1: Example of a finite element mesh

In the study of the effect of using grouted rockbolts as a stablizing technique in underground excavation in a two-dimensional plane strain problem, the whole structure consists of many different media, namely the rock, the joints, the rockbolts, and the grouting. These media are of different shapes, and are made of different material which have different material properties and behaviour. Even the material in the same medium may exhibit different characteristics. For example, the rock in the surroundings of the tunnel opening may be softer at one end, or rockbolts may be made of different steel bolts to maximize the effect. Therefore it is essential that all these different materials can be analysed simultaneously under one scheme with minimum effort and minimum loss of information and continuity.

One of the fundamentals of the finite element method is to consider the mesh of the structure under investigation as an integration of a large number of small geometric elements, and each of these elements is analysed and formulated individually according to its own characteristic and shape before they are assembled to form a formulation for the complete system. Therefore the finite element method appears to be the ideal tool to perform this inhomogeneous analysis. Further, because of the popularity of the finite element method in geomechanics, there are many good and readily available finite element packages which can be used as a starting point, and they can be used as a platform to extend to the new theory.

This research is based on the computer package FESTA (**F***inite* **E***lement* **S***imulation for* **T***unnelling* **A***pplications*). It was orginally developed on an SERC/British Coal co-funded research project at the Oxford University Computing Laboratory between 1985 and 1986. Since then, it has been subject to continuous development at the Department of Mathematics and Statistics at Brunel University under the support of SERC (until 1992) and British Coal (until 1988). The program structure is based on the linear elastic finite element package FINEPACK develped at the Department of Civil Engineering University College of Swansea (Naylor 1977, Hinton & Owen 1977).

FESTA has been developed to model the deformation and stresses in rock masses in two dimensions. It uses elasto-viscoplastic theory for the nonlinear analysis. The detailed theory and features, as well as a user's guide, can be found in Reed & Lavender (1988), Reed & Pan (1990), and later updated by Qu (1992a, 1992b). The present research deals with the deformation of the elasticity problem. It is based on the large displacement theory incorporated in FESTA, and it is extended to develop a new element to model grouted rockbolts in two-dimensional plane strain analyses of underground excavations. This element incorporates the features of beam elements and joint elements which are used to model the steel bolt and grouting respectively, together with special formulations for large displacements and the bolt axisymmetry. The different materials used in this thesis are assumed to be isotropic and linearly elastic throughout.

Chapter 3

Basic theory of Finite Element Method in Elasticity

Finite elements take many and varied forms, depending on the shape of the object they are supposed to represent. For example, to represent flat plates, the choice of finite elements will usually be of triangular or quadrilateral shape, whilst for solids, the finite elements will usually appear in the form of tetrahedrons or cubes. In the two-dimensional analysis of elasticity of materials, the choice of eight-noded quadrilateral elements ('serendipity' elements) is frequently adopted.

The main advantage of using isoparametric elements with quadratic shape functions is that, in a mesh, curved boundaries can be represented. Linear shape functions also impose restrictions on the stress contours - for example, the linear triangular elements which were introduced by Turner *et al* (1956) assume the stress and the strain in any given direction for any particular element are constant, and they are therefore not sufficiently accurate to use in the mathematical modelling of stress distributions in areas of steep stress gradient, without a very dense mesh of elements in such regions.

One of the problems that occurs with these elements is that the determination of stiffness matrix for each element involves the integration of a matrix over the element, and therefore each entry in this matrix requires, in general, to be determined numerically. Despite the efficiency of today's many numerical integration schemes, the computational time required to generate these element matrices is much larger than that required for the constant strain triangle elements.

Another problem with these elements is that even if the domain is covered with a mesh of the same number of elements, an increase in the number of nodes in each element will result in a corresponding increase in size of the bandwidth of the resulting global stiffness matrix (this will be discussed in full in the latter part of this chapter). This will result in a substantial increase of computer storage space and computational time. However, these drawbacks are compensated by the superior stress and strain predictions and also in the improved modelling of the structure, particular if it has curved boundaries.

To investigate the theory of elasticity solution by finite element method, consider a perfectly elastic isotropic body which is constrained to deform linearly in plane strain under a prescribed load. To deal with a more realistic real life situation, it can be formulated so that the body can be modelled by a combination of different materials with different properties. The theory of this finite element discretization is well documented by many textbooks, such as Hinton & Owen (1977), Cheung & Yeo (1979), Zienkiewicz & Taylor (1989, 1991).

3.1 Stresses and Strains

It has been mentioned in the introductory chapter that for a more realistic representation, consideration must often be given to nonlinear effects on the deformation of the body. However, as a first step, this chapter concentrates on the simple linear problem when both the geometrical and material properties are taken to behave linearly throughout. Further, the domain of the body Ω, with loaded boundary Γ, is assumed to be discretised by a mesh of eight-noded isoparametric quadrilateral elements. Based on these assumptions, the theory of linear elasticity will be used to establish the small displacement formulations, and these algorithms will then be extended to deal with nonlinear behaviour and adapted to other types of element in later chapters.

Let the stresses and strains at a point in the body in plane strain, omitting the out-of-plane direction, be given by the vectors

$$\sigma = (\sigma_x \quad \sigma_y \quad \tau_{xy})^T$$

and

$$\epsilon = (\epsilon_x \quad \epsilon_y \quad \gamma_{xy})^T$$

respectively.

In a two-dimensional problem, let $\mathbf{u} = (u\ v)^T$ be a vector representing the displacement functions at a point $(x\ y)^T$ in the body.

With displacements known at all points within an element in a continuous body, the linear strain at a point is determined by the rate of change of displacement with distance, i.e. the direct strains in the x and y directions are given by

$$\epsilon_x = \frac{\partial u}{\partial x} \qquad \text{and} \qquad \epsilon_y = \frac{\partial v}{\partial y} \tag{3.1}$$

with shear strain

$$\gamma_{xy} = \frac{\partial u}{\partial y} + \frac{\partial v}{\partial x}. \tag{3.2}$$

In matrix form, these linear relationships may be expressed as

$$\epsilon = \mathbf{A}\mathbf{u} \tag{3.3}$$

where $\mathbf{A}$ is the strain-displacement operator

$$\mathbf{A} = \begin{bmatrix} \frac{\partial}{\partial x} & 0 \\ 0 & \frac{\partial}{\partial y} \\ \frac{\partial}{\partial y} & \frac{\partial}{\partial x} \end{bmatrix}. \tag{3.4}$$

According to the linear elastic constitutive law when the structure is assumed to exhibit linear elastic behaviour, stresses and strains are related linearly by

$$\sigma = \mathbf{D}\epsilon \tag{3.5}$$

where $\mathbf{D}$ is the elasticity matrix. In plane strain of an isotropic material where there is no movement in the out-of-plane direction, this matrix takes the form

$$\mathbf{D} = \frac{E(1-\nu)}{(1+\nu)(1-2\nu)} \begin{bmatrix} 1 & \frac{\nu}{1-\nu} & 0 \\ \frac{\nu}{1-\nu} & 1 & 0 \\ 0 & 0 & \frac{1-2\nu}{2(1-\nu)} \end{bmatrix}, \tag{3.6}$$

whereas in plane stress, this matrix becomes

$$\mathbf{D} = \frac{E}{1-\nu^2}\begin{bmatrix} 1 & \nu & 0 \\ \nu & 1 & 0 \\ 0 & 0 & \frac{1-\nu}{2} \end{bmatrix},$$

where E is Young's modulus and ν is Poisson's ratio.

As the mesh is made up of a number of eight-noded isoparametric quadrilateral elements, the nodal displacement vector $\mathbf{u}^e$ for any element e within the mesh is

$$\mathbf{u}^e = (u_1 \quad v_1 \quad u_2 \quad v_2 \quad u_3 \quad v_3 \cdots u_8 \quad v_8)^T$$

The shape functions, or basis functions, N_i, with $i = 1, 2, \cdots, 8$, in terms of the curvilinear coordinates ξ, η, and the nodal displacement parameters u_i, v_i, are used to represent the displacement variations at a point within the element.

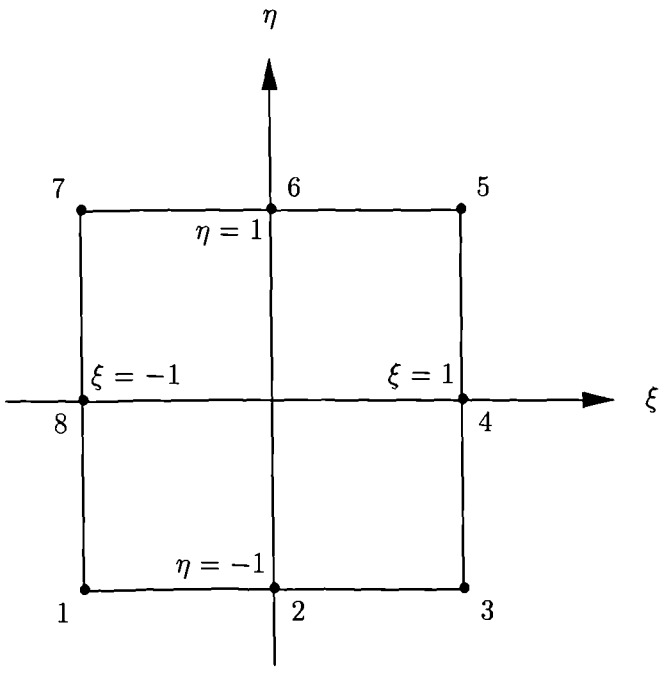

Figure 3.1: Eight-noded isoparametric element

To satisfy compatibility, shape functions should be parabolic. In general, the shape function N_i for the corner nodes (ξ_i, η_i), where $\xi_i = \pm 1, \eta_i = \pm 1$, is given by

$$N_i = \frac{1}{4}(1 + \xi\xi_i)(1 + \eta\eta_i)(\xi\xi_i + \eta\eta_i - 1),$$

and for mid-side nodes with $\xi_i = 0$,

$$N_i = \frac{1}{2}(1-\xi^2)(1+\eta\eta_i),$$

and with $\eta_i = 0$,

$$N_i = \frac{1}{2}(1+\xi\xi_i)(1-\eta^2).$$

Hence, the displacement functions over the whole element can be expressed in the form

$$u(x,y) = \sum_{i=1}^{8} N_i(\xi,\eta)u_i \qquad \text{and} \qquad v(x,y) = \sum_{i=1}^{8} N_i(\xi,\eta)v_i, \tag{3.7}$$

and from equation (3.3), it follows that the strain vector ϵ at a point (x,y) inside the element e is given by

$$\epsilon = \mathbf{B}^e\ \mathbf{u}^e \tag{3.8}$$

with

$$\begin{aligned} \mathbf{B}^e &= \begin{bmatrix} \frac{\partial N_1}{\partial x} & 0 & \frac{\partial N_2}{\partial x} & 0 & \cdots & \frac{\partial N_8}{\partial x} & 0 \\ 0 & \frac{\partial N_1}{\partial y} & 0 & \frac{\partial N_2}{\partial y} & \cdots & 0 & \frac{\partial N_8}{\partial y} \\ \frac{\partial N_1}{\partial y} & \frac{\partial N_1}{\partial x} & \frac{\partial N_2}{\partial y} & \frac{\partial N_2}{\partial x} & \cdots & \frac{\partial N_8}{\partial y} & \frac{\partial N_8}{\partial x} \end{bmatrix} \\ &= \mathbf{AN} \end{aligned} \tag{3.9}$$

where

$$\mathbf{N} = \begin{bmatrix} N_1 & \cdots & N_8 \\ N_1 & \cdots & N_8 \\ N_1 & \cdots & N_8 \end{bmatrix} \tag{3.10}$$

Combining equations (3.5) and (3.8) gives

$$\sigma = \mathbf{D}\mathbf{B}^e\mathbf{u}^e \tag{3.11}$$

3.2 Principle of Minimum Total Potential Energy

The principle of minimum total potential energy states that, in order to satisfy the equations of elasticity and equilibrium, the potential energy of the system must be at a local minimum, i.e. when the change of potential with respect to the displacement must be stationary.

It is shown in standard texts that the principle of minimum potential energy is equivalent to the principle of virtual work. However, it is important to note that the principle of virtual work is the more general concept since it is independent of the stress-strain relationship, and indeed can be used even if a potential energy function does not exist. However, for the purposes of extending the ideas outside the structural analysis, the principle of minimum potential energy is extremely useful, and may be used directly for the purpose here.

The total potential energy of a system is given by

$$\Phi = U + W \tag{3.12}$$

where W is the potential energy of the external forces in the deformed configuration, and is defined by

$$W = -\iint_{\Omega} \mathbf{u}^T \mathbf{b}\, dV - \int_{\Gamma} \mathbf{u}^T \mathbf{p}\, dS, \tag{3.13}$$

and where U is the strain energy of the deformed structure, which is given by

$$U = \frac{1}{2} \iint_{\Omega} \epsilon^T \sigma\, dV \tag{3.14}$$

In finite element discretization, substituting equations (3.8) and (3.11) into equation (3.14), it can be seen that

$$U = \frac{1}{2} \sum_{e} \iint_{\Omega} \mathbf{u}^{eT} \mathbf{B}^{eT} \mathbf{D} \mathbf{B}^{e} \mathbf{u}^{e}\, dV \tag{3.15}$$

The potential energy of the external forces may be simplified if the surface and the body forces can be approximated by a set of equivalent nodal forces $\mathbf{q}$. Thus, the force at any point in an element would be given by $\sum_{i=1}^{8} N_i q_i$, which can be written as $\mathbf{N}^T \mathbf{q}$, where

$$\mathbf{N} = \begin{bmatrix} N_1 & N_2 & \cdots & N_8 \\ N_1 & N_2 & \cdots & N_8 \end{bmatrix}$$

With this approximation, the potential energy can be written as

$$W = -\sum_{e} \iint_{\Omega} \mathbf{u}^{eT} \mathbf{N}^T \mathbf{q}\, dV, \tag{3.16}$$

so that the total potential energy of the system becomes

$$\Phi = \frac{1}{2}\sum_e \iint_\Omega \mathbf{u}^{eT}\mathbf{B}^{eT}\mathbf{D}\mathbf{B}^e\mathbf{u}^e \, dV - \sum_e \iint_\Omega \mathbf{u}^{eT}\mathbf{N}^T\mathbf{q} \, dV \tag{3.17}$$

By variational principles, this is minimized when

$$\frac{\partial \Phi}{\partial \mathbf{u}} = 0,$$

where $\mathbf{u}$ is the global vector of nodal displacements. When this is applied to the global system form of (3.17),

$$\frac{\partial \Phi}{\partial \mathbf{u}} = \iint_\Omega \mathbf{B}^T\mathbf{D}\mathbf{B}\mathbf{u} \, dV - \iint_\Omega \mathbf{N}^T\mathbf{q} \, dV = 0.$$

In matrix form, this system of equations can be written as

$$\mathbf{K}\mathbf{u} = \mathbf{f} \tag{3.18}$$

where $\mathbf{K}$, the global stiffness matrix, is given by

$$\mathbf{K} = \iint_\Omega \mathbf{B}^T\mathbf{D}\mathbf{B} \, dV \tag{3.19}$$

and $\mathbf{f}$, the global consistent load vector, is given by

$$\mathbf{f} = \iint_\Omega \mathbf{N}^T\mathbf{q} \, dV. \tag{3.20}$$

These formulae can also be obtained from the virtual work approach. Details of the theory and procedure of this approach can be found in Zienkiewicz & Taylor (1989).

In this analysis, equation (3.18) is a linear matrix equation, and it can be solved numerically by many well-proven methods for the displacement vector $\mathbf{u}$. In the finite element method, however, the body of the structure is discretised in a mesh, and the stiffness matrix for each individual element must be found first before they can be assembled to form the global stiffness matrix for the whole system.

3.3 Element Stiffness Matrix

For the purpose of finding the stiffness matrix for an arbitrary element e lying inside the mesh, the global stiffness matrix can be written

$$\mathbf{K} = \sum_{e=1}^{n} \mathcal{L}^e\mathbf{K}^e\mathcal{L}^{eT} \tag{3.21}$$

with

$$\mathbf{K}^e = \iint_{\Omega^e} \mathbf{B}^{eT}\mathbf{D}\mathbf{B}^e \, dV$$

and the $\mathcal{L}^e$ are Boolean matrices representing the assembly procedure.

The element strain matrix $\mathbf{B}^e$ has earlier been established in equation (3.9), and from this formulation, it can be observed that the shape functions for an eight-noded isoparametric element are defined with respect to the curvilinear coordinates ξ and η, and therefore cannot be differentiated directly with respect to the global x and y axes. To overcome this difficulty, it is necessary to obtain a relationship between the derivatives of these two sets of coordinates.

For a two-dimensional problem, the normal chain rule of partial differentiation gives

$$\frac{\partial N_i}{\partial \xi} = \frac{\partial N_i}{\partial x}\frac{\partial x}{\partial \xi} + \frac{\partial N_i}{\partial y}\frac{\partial y}{\partial \xi}$$

and

$$\frac{\partial N_i}{\partial \eta} = \frac{\partial N_i}{\partial x}\frac{\partial x}{\partial \eta} + \frac{\partial N_i}{\partial y}\frac{\partial y}{\partial \eta},$$

which, in matrix form, can be written as

$$\begin{bmatrix} \frac{\partial N_i}{\partial \xi} \\ \frac{\partial N_i}{\partial \eta} \end{bmatrix} = \mathbf{J} \begin{bmatrix} \frac{\partial N_i}{\partial x} \\ \frac{\partial N_i}{\partial y} \end{bmatrix} \tag{3.22}$$

The 2×2 matrix $\mathbf{J}$ relating the derivatives of the two system is called the *Jacobian matrix* and it takes the form

$$\mathbf{J} = \begin{bmatrix} \frac{\partial x}{\partial \xi} & \frac{\partial y}{\partial \xi} \\ \frac{\partial x}{\partial \eta} & \frac{\partial y}{\partial \eta} \end{bmatrix} \tag{3.23}$$

For an eight-noded isoparametric element, the coordinates at a point, in terms of the nodal coordinates, can be expressed by

$$x = \sum_{i=1}^{8} N_i x_i, \qquad y = \sum_{i=1}^{8} N_i y_i$$

in the same way as for the displacements, where (x_i, y_i) are the global coordinates of node i.

Thus, from

$$\frac{\partial x}{\partial \xi} = \sum_{i=1}^{8} \frac{\partial N_i}{\partial \xi} x_i, \qquad \text{etc.,} \tag{3.24}$$

equation (3.22) can be rearranged as

$$\begin{bmatrix} \frac{\partial N_i}{\partial x} \\ \frac{\partial N_i}{\partial y} \end{bmatrix} = \mathbf{J}^{-1} \begin{bmatrix} \frac{\partial N_i}{\partial \xi} \\ \frac{\partial N_i}{\partial \eta} \end{bmatrix} \tag{3.25}$$

so that the 2×2 Jacobian matrix $\mathbf{J}$ will have to be inverted in order to find the equivalent Cartesian derivatives.

Further, to work out this element stiffness matrix, it is necessary to tranform the double integral into the $\xi\eta$-coordinate system. To achieve this, it can be observed that, for any function $F(x, y)$,

$$\iint_{\Omega^e} F dx\, dy = \int_{-1}^{1}\int_{-1}^{1} F\,(\det \mathbf{J}) \cdot d\xi\, d\eta \tag{3.26}$$

where $\det \mathbf{J}$ is the determinant of the Jacobian matrix.

Hence the element stiffness matrix becomes

$$\mathbf{K}^e = \int_{-1}^{1}\int_{-1}^{1} \mathbf{B}^{eT}\mathbf{D}\mathbf{B}^e\,(\det \mathbf{J})\, d\xi\, d\eta. \tag{3.27}$$

Each entry in this matrix involves integration over the ξ and η axes, and in general, the evaluation of this integral cannot be carried out explicitly, especially when some complex functions are involved in the integrand. For this purpose, a standard numerical integration technique can be used.

Recall that the shape functions for an isoparametric element are quadratic polynomials, and that terms in the $\mathbf{B}$ matrix involve the first partial derivatives of the shape functions. Therefore, the simplest accurate numerical integration scheme for this purpose is the following 2×2 Gaussian rule : if a function $f(\xi, \eta)$ is defined for the variables ξ and η, then the double integral can be approximated by the sum

$$\int_{-1}^{1}\int_{-1}^{1} f(\xi, \eta) d\xi\, d\eta \simeq \sum_{i=1}^{4} w_i f_i \tag{3.28}$$

where the Gauss weights $w_1 = w_2 = w_3 = w_4 = 1$, and f_i are the values of f at the four Gauss-points $(\pm\frac{1}{\sqrt{3}}, \pm\frac{1}{\sqrt{3}})$.

With this numerical integration scheme, entries in the matrix product $\mathbf{B}^{eT}\mathbf{D}\mathbf{B}^{e}$ can be integrated term by term to form the element stiffness matrix.

When the stiffness matrix for each element is found, they can then be assembled to form the global stiffness matrix for the whole system. Procedures for assembling this matrix will be discussed in full later in this chapter.

3.4 The Load Vector

To initiate deformations, loadings must be applied to the structure. The types of mechanical loading that can be applied to a two-dimensional element are divided into two main groups: surface traction, such as pressure and nodal points loads; and body forces, such as those due to gravity and centrifugal loads; the latter is being omitted in this project.

All loads in a triangular element can be assigned to nodes intuitively or by statics, but in the case of an eight-noded isoparametric element, the nodal loads due to distributed loads must be computed in accordance with the consistent load vector for each element, which is given in equation (3.20) as

$$\mathbf{f}^{e} = \iint_{\Omega^{e}} \mathbf{N}^{T}\mathbf{q}\, dV$$

where N is a matrix containing the shape functions, and

$$\mathbf{f}^{e} = (F_{x1} \quad F_{y1} \quad F_{x2} \quad F_{y2} \cdots F_{x8} \quad F_{y8})^{T},$$

where F_{xi}, F_{y_i} etc. are the x and y components in the global x and y directions of the equivalent loads at each node i of the element e.

The equivalent nodal forces are added, element by element, into the global load vector $\mathbf{f}$ before it is used in the solution procedure. The treatment of the different types of load discussed in detail below.

3.4.1 Point loads

It is common to assume that point loads will always be applied at nodes and not at an arbitrary point on the element boundary. This can always be achieved by arranging the element mesh with nodes where the concentrated loads are acting. The point loads are

resolved into their x and y components, and they are then added directly to the appropriate entries in the load vector $\mathbf{f}$.

3.4.2 Surface tractions

If a series of forces are applied along one edge of an element, it is usual to approximate the actual surface traction variation along the edge by a parabolic distribution defined by the point values at each of the three nodes along that edge, and all intermediate pressure values can be calculated using the shape functions.

For convenience in coding, all nodes of the element are used in the computation so that there is no need to sort out the appropriate shape functions for the three nodes with given pressure values, which can include an input value of zero. Thus

$$P = \sum_{k=1}^{8} N_k P_k.$$

Consider a pressure P, which is specified in force per unit length, applied along the $\eta = 1$ edge of an element with nodes 5, 6 and 7, as shown in Figure 3.2(b).

P may vary along the edge, i.e. $P = P(\xi)$. As the local coordinate system will not be the same as the global coordinates, there will usually be both x and y components of pressure.

The task here is find the components of the equivalent nodal forces on the nodes along the loaded side

$$P_{x5},\ P_{y5},\ P_{x6},\ P_{y6},\ P_{x7},\ P_{y7}.$$

Referring to Figure 3.2(c), consider a small element $d\xi$ along the loaded side. The force applied to this element is $P\ d\xi$.

The x and y components of this force are

$$P_x = P\,\frac{\partial y}{\partial \xi}\,d\xi \qquad \text{and} \qquad P_y = -P\,\frac{\partial x}{\partial \xi}\,d\xi \tag{3.29}$$

and hence the equivalent nodal forces are given by

$$P_{x5} = \int_{-1}^{1} P\ N_5\,\frac{\partial y}{\partial \xi}\,d\xi$$

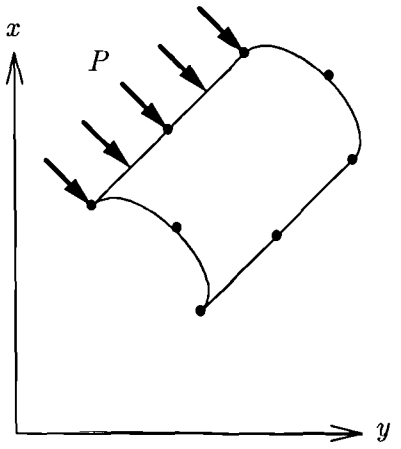

(a) Global element

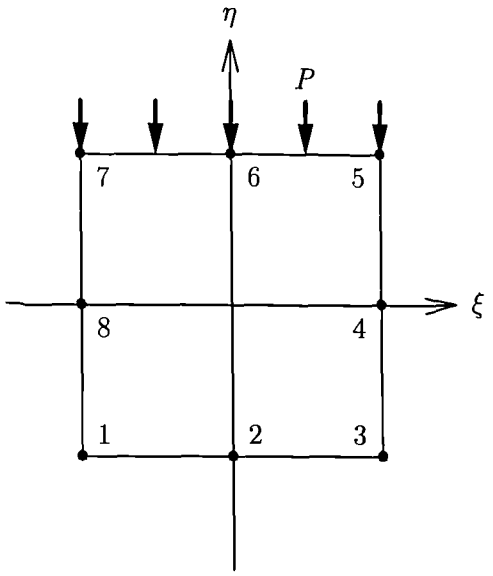

(b) Local element

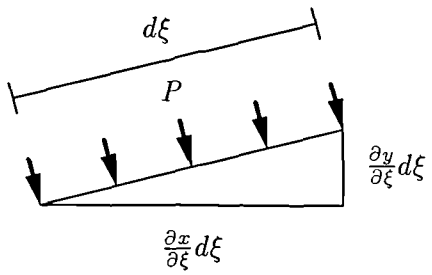

(c) Surface traction

Figure 3.2: Surface traction

and

$$P_{y_5} = \int_{-1}^{1} P\, N_5\, (-\frac{\partial x}{\partial \xi})\, d\xi \tag{3.30}$$

and similarly for nodes 6 and 7 respectively, using N_6 and N_7. In general, the element load vector $\mathbf{P}^e$ can be represented by the matrix equation

$$\mathbf{P}^e = \int_{-1}^{1} P\, \mathbf{N}^T \begin{bmatrix} \frac{\partial y}{\partial \xi} \\ -\frac{\partial x}{\partial \xi} \end{bmatrix} d\xi \tag{3.31}$$

where

$$\mathbf{N} = \begin{bmatrix} N_1 & 0 & N_2 & 0 & \cdots & 0 \\ 0 & N_1 & 0 & N_2 & \cdots & N_8 \end{bmatrix} \tag{3.32}$$

The above integrals can be evaulated accurately by numerical methods. In accordance with the Gaussian rule (3.28) employed to approximate the integral in (3.27), a corresponding two-point Gaussian rule is generally used:

$$\mathbf{P}^e \simeq \sum_{k=1}^{2} w_k P_k \, \mathbf{N}_k^T \begin{bmatrix} \frac{\partial y}{\partial \xi} \\ -\frac{\partial x}{\partial \xi} \end{bmatrix}_k \tag{3.33}$$

where $\mathbf{N}_k$ is the value of $\mathbf{N}$ as defined in (3.32) at the Gauss-point k, and w_k is the Gauss weight. This numerical method should be sufficiently accurate as the shape functions involved in (3.33) are all quadratic polynomials.

3.4.3 Body forces

The usual types of body force are those due to gravity g_y and those due to earthquake loading g_y. The formulation is given by

$$\begin{aligned} \mathbf{P}^e &= \int_{-1}^{1}\int_{-1}^{1} m\mathbf{N}^T \begin{bmatrix} g_x \\ g_y \end{bmatrix} \det \mathbf{J} \, d\xi \, d\eta \\ &= \sum_{i=1}^{n}\sum_{j=1}^{n} w_i w_j m\mathbf{N}^T \begin{bmatrix} g_x \\ g_y \end{bmatrix} \det \mathbf{J} \end{aligned} \tag{3.34}$$

where m is the mass per unit area and g_x and g_y are accelerations in the x and y directions respectively.

3.5 Global stiffness matrix

In the last section, methods of calculating the element stiffness matrix $\mathbf{K}^e$ and element load vector $\mathbf{f}^e$ for an element inside the mesh have been described.

When all element matrices are found, the next step is to assemble them into the global system

$$\mathbf{K}\mathbf{u} = \mathbf{f},$$

where the global matrices consist of entries from all corresponding element matrices. With this matrix equation, the solution vector $\mathbf{u}$ for the complete system can then be solved to give the displacement vector of the deformed body.

3.5.1 The assembly

To assemble the global matrices **K** and **f**, it is always best to construct a global 'destination vector' **w** first. This vector **w** consists of the x- and y-displacements of all nodes inside the mesh, and thus it would be more convenient to use **w** as a reference to assign entries in each element stiffness matrix and element load vector into their corresponding position in the global matrices.

This procedure can of course be done automatically by a computer under a certain prescribed algorithm. As a general rule, the element stiffness entry $k^e{}_{ij}$ will go to entry k_{lm} in the global stiffness matrix, where l is the global node number of the i'th node in element e, and m is the global node number of the j'th node. $(i, j = 1, 2, ..., 8)$. It is useful to note the following two properties of the global stiffness matrix:

1. In most applications, **K** will be symmetric, as indeed is each of the element stiffness matrices.

2. If the structure is made up of a large number of elements, the global stiffness matrix **K** will have a large dimension, but if the nodes of the elements in the mesh are numbered sensibly (the reason for this will be given in the next section), **K** will be sparse and banded about the leading diagonal for most structural problems. In this case, there are some special algorithms that can be employed to reduce the storage of **K** without losing any of its details in order to increase the efficiency of the solution procedure of the global matrix system.

3.5.2 Condensed rectangular matrix

There are various choices of methods for solving a linear matrix equation, and these vary in computational efficiency and accuracy. One of the most simple and frequently used methods is Guassian elimination. However, as the number of elements increases, so does the dimension of the global stiffness matrix, which makes these methods most inefficient in terms of core requirement and the number of numerical operations in achieving a solution. A more efficient algorithm will be discussed in full in later chapters.

To take advantage of the two properties mentioned in the last section, Cheung & Yeo (1979) suggested a more efficient and space-saving band matrix solution routine, in which only the upper half, or the lower half, together with the leading diagonal of the band

matrix is stored as a rectangular matrix as shown in Figure 3.3. The number of entries in any one row is called the *half band width* of the matrix.

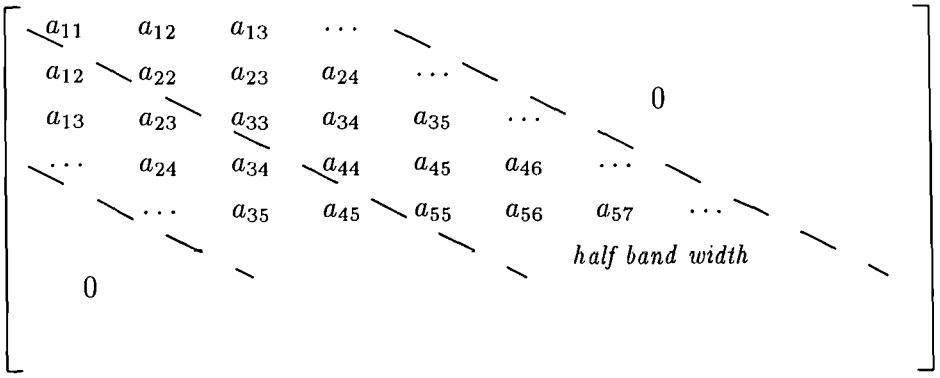

(a) Original sparse banded matrix

$$\begin{bmatrix} a_{11} & a_{12} & a_{13} & \cdots \\ a_{22} & a_{23} & a_{24} & \cdots \\ a_{33} & a_{34} & a_{35} & \cdots \\ \vdots & \vdots & \vdots & \\ & & & a_{n-3,n} \\ & & a_{n-2,n} & 0 \\ & a_{n-1,n} & 0 & 0 \\ a_{nn} & 0 & 0 & 0 \end{bmatrix}$$

(b) Condensed rectangular matrix

Figure 3.3: Space saving technique for global stiffness matrix

It can be seen from the figure that the width of the condensed rectangular matrix depends on the half band width of the original matrix, and it can be calculated from the relationship

$$h_{bw} = n_{dof} \times (m_{diff} + 1), \tag{3.35}$$

where n_{dof} is the number of degree of freedom at each node (in the case of an eight-noded isoparametric element, it is two), and m_{diff} is the overall maximum difference in global node numbers in all elements. Therefore in order to maximize the efficiency of this storage-saving scheme, great care must be exercised in the numbering of the nodes so that the difference between connecting nodes can be minimized.

3.6 Nodal fixity

One further important property of all element stiffness matrices, and hence the subsequent global stiffness matrix, is that they are always singular. To remove this singularity, the structure must be fixed against rigid-body motions. In practice, the problem of nodal fixity arises when some constraints are necessary to prescribe displacements which very often are zero displacements at rigid supports. Non-zero displacements are prescribed for support settlements and also for boundary points of local fine mesh analysis in which the displacements were first obtained through a coarse mesh of a much larger domain. Without this nodal fixity, the body will slide or move infinitely along a frictionless surface when a load is applied upon it. The nodal fixity can be applied at any node in the mesh in either the u or the v direction or both.

One very simple method that deals with nodal fixity was suggested by Cheung & Yeo (1979). This method has been adapted throughout this project because of its simplicity in its theory and its implementation into a computer program.

Suppose that there is a rigid support at a node with known prescribed direction. The method suggests the adding of a very large arbitrary number, say 10^{50}, to the matching diagonal coefficients of the node which physically corresponds to 'earthing' the structure with a very stiff spring. The sudden increase of this large number in the global stiffness matrix will give rise to a very small, but not absolute zero, displacement in the corresponding node, which satisfies the requirement of nodal fixity for a rigid support.

Hence, the reaction for that support can be obtained by the formula

$$\text{reaction} = -\ (\text{big spring stiffness}) \times (\text{very small displacement})$$

This method will fail if the arbitrary number, or the stiffness of the spring, is not significantly big enough. However, with a suggested value of 10^{50}, it is unlikely to occur in practice.

3.7 Some practical everyday examples

In the following simple example, a structure is assembled by four identically sized isotropic and perfectly elastic blocks, as shown in Figure 3.4. Each elastic block is modelled by four

equal eight-noded isoparametric elements. The structure is secured on a horizontal floor, where its bottom end is rigidly supported, so that this edge cannot slide or move in both the x and the y directions when the rest of the body is free to deform under loadings.

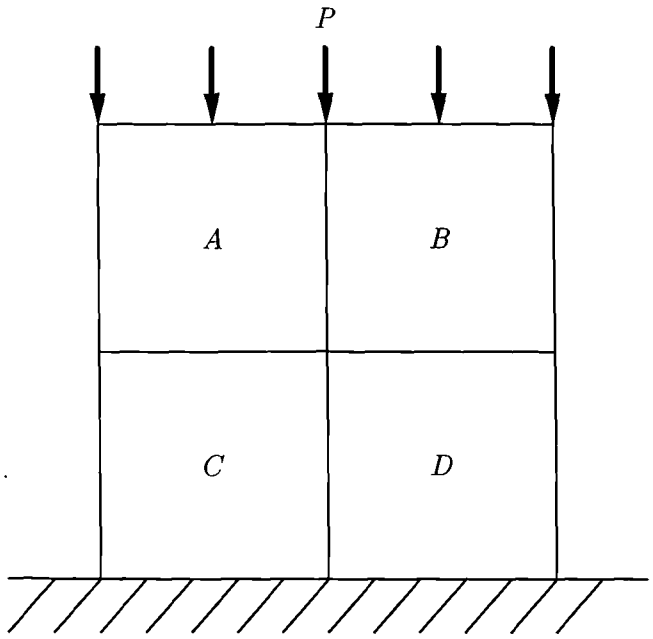

Figure 3.4: Structure made up of four identically sized elastic blocks

To initiate deformations of the structure, surface traction is applied uniformly, vertically downwards along the top side of the structure. To investigate the effect of using different materials in a non-homogeneous structure, two problems are run. In Problem 1, all four elastic blocks have the same material properties, with Young's modulus and Poisson ratio of 0.4×10^6 N/m^2 and 0.3 respectively. In Problem 2, Young's moduli for block A, B, C, and D are of 0.1×10^6, 0.2×10^6, 0.8×10^6, and 0.4×10^6 N/m^2 respectively, while Poisson ratios of 0.3 are used throughout.

Using finite element method, the theory for eight-noded isoparametric elements is applied to the system. Figures 3.5 and 3.6 show details of deformation of the whole body when an exaggeration factor of 50 is used to magnify the magnitude of the deformation.

In Problem 1, although the structure is modelled by four different blocks, it behaves like one unit, as the four blocks have the same material properties, as shown in Figure 3.5. The whole body is squashed downwards, while the middle section slightly bulges out. The deformation is symmetrical about the vertical centre of the structure.

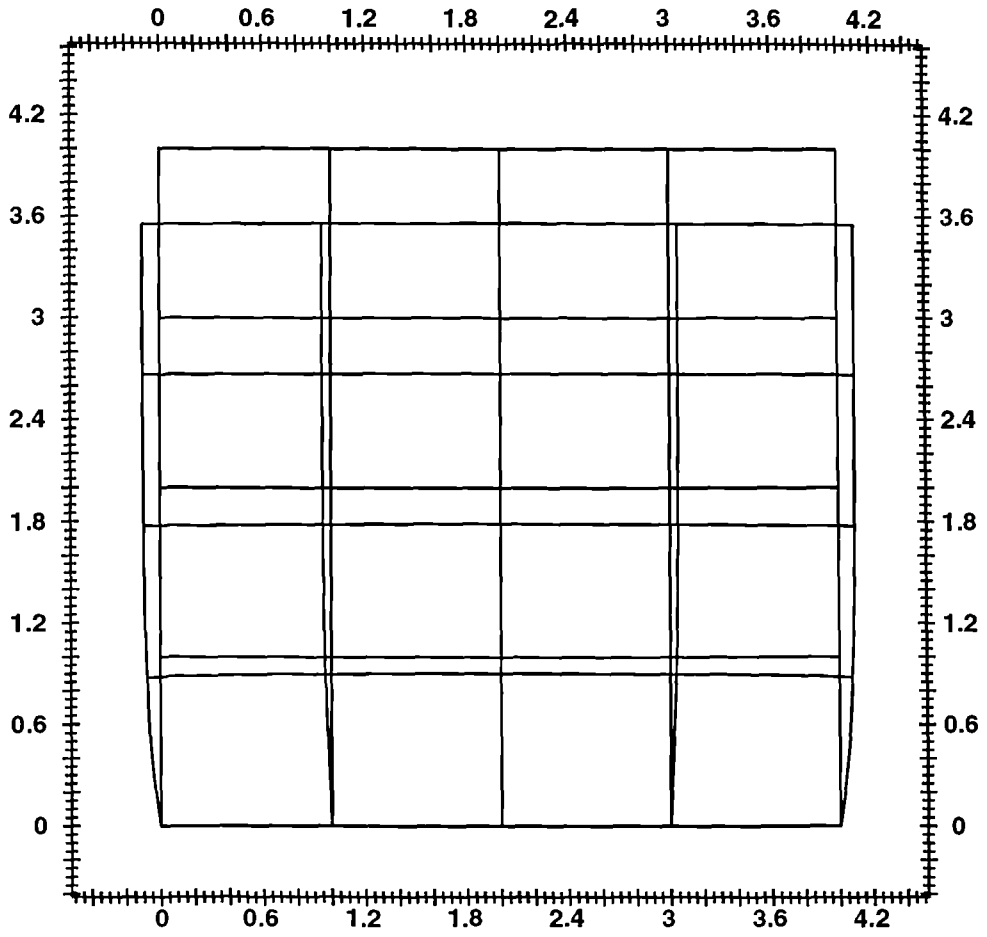

Figure 3.5: Problem 1 - deformation of structure with equal material property

Figure 3.6 shows the deformation of the structure in Problem 2 when the four blocks have different material properties. As the Poisson ratio is constant throughout, the deformation depends heavily on the stiffness of the material, or the value of the Young's moduli of the blocks. Block A has the smallest Young's modulus, and it deforms most, while Block C has the highest Young's modulus, and it deforms least.

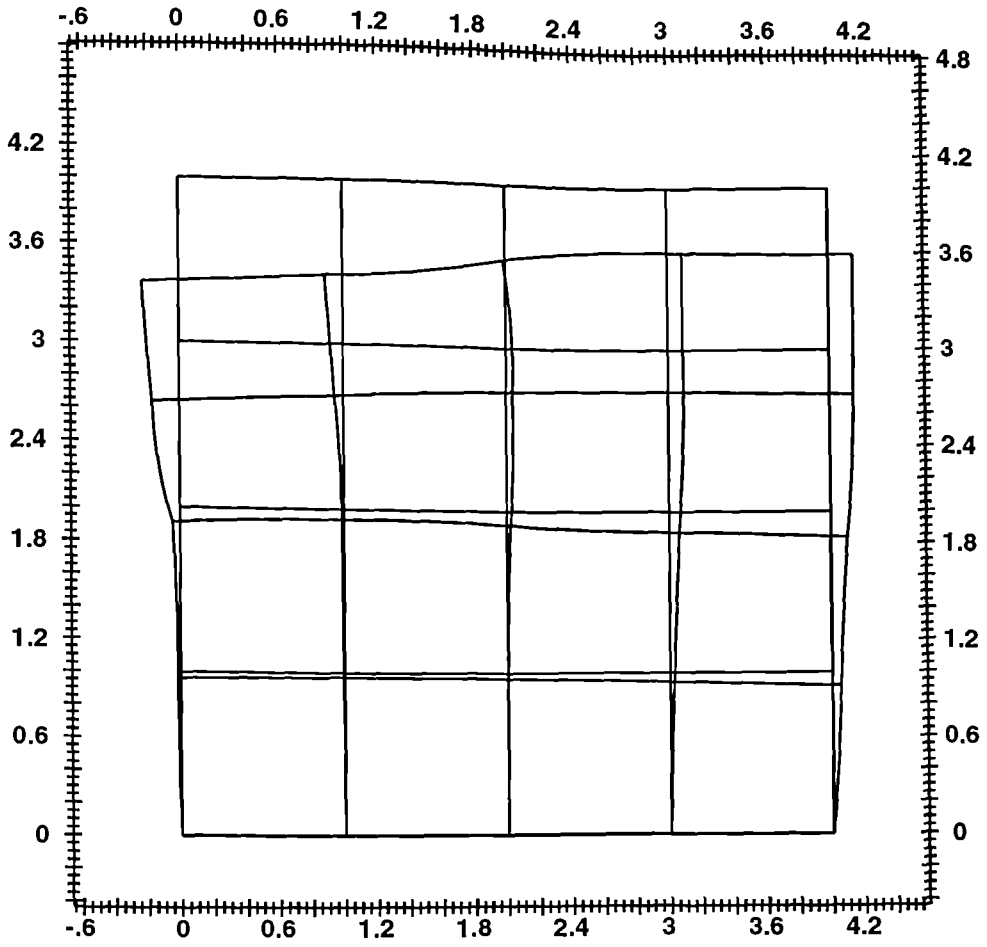

Figure 3.6: Problem 2 - deformation of structure with different material properties

3.8 Summary

The standard finite element method for analysing two-dimensional linear elasticity problems for eight-noded isoparametric elements has been presented and discussed. Improvements on the efficiency of this method, and ways to save computer storage space and computation times during execution of the program are summarized. It can be concluded that, as long as the elasticity problem remains linear throughout, and that the rock mass can be discretised in a mesh of eight-noded isoparametric elements, this small displacement formulation can be used to carry out stress analysis and accurate calculation of the deformation of rock mass in linear elasticity problems.

Chapter 4

Large Displacement Analysis

4.1 Introduction

In the last chapter, simple two-dimensional elasticity problems have been solved by the finite element method for eight-noded isoparametric elements. This analysis has been considered accurate when certain approximations for the stress and displacements of the structure are made.

The strain-displacement relationships defined in equations (3.1) and (3.2) have been taken as linear, thus ignoring second and higher order terms in the partial derivatives of the displacement functions. This linear relationship gives rise to the small displacement analysis of structures. If higher order terms in these relationships are taken into consideration in the analysis, the finite element method can also be extended to cover some problems in nonlinear structural mechanics.

Nonlinear behaviour of a structure may be due to the inherent nonlinear stress-strain relationship of the material, or due to nonlinear changes in the geometry in dimensions and configuration caused by the loads. If the material has a linear stress-strain relationship, then as long as the displacements caused by the loads are small compared to the dimensions of the structure, the structure will behave linearly for all practical purposes. This linearity case has been dealt with in the small displacement analysis discusssed in the last chapter for eight-noded isoparametric elements. However, as the displacements increase, the linearity assumption of the original stiffness matrix can no longer adequately represent the behaviour of the structure. A large displacement analysis is therefore required.

4.2 Material and Geometric Nonlinearity

The linear elastic theory of structures assumes that the material is within its elastic limit, and that it follows a simple linear stress-strain curve. Material nonlinear behaviour of structures may be due to the inherent nonlinear stress-strain relationship of the material - for example, when the material undergoes plastic deformation.

In large displacement problems, care has to be taken with the applied loading as the geometry changes, because a nodal load will not generally rotate around the node, while surface tractions will follow the model as it moves. Body forces continue to act in their original directions.

If a structure undergoes a large displacement due to an applied load, then, since its geometry changes, its stiffness matrix needs to be adjusted accordingly. There are two ways in which this can be achieved. The first approximate method assumes that the size of the individual elements is constant, so that a re-orientation of the element stiffness matrices due to the elements' rotation and translation is all that is required. The second method is more accurate, and recalculates the stiffness matrices of the elements after adjusting the nodal coordinates with the calculated displacements. In both cases, an incremental solution is required. If the spatial motions are not large, then it is possible to apply the load in a single step with several iterations, but for large motions, the load is best applied in smaller incremental steps.

Problems requiring both material and geometric nonlinearities are probably the most demanding type of quasi-static analyses that can be undertaken by the finite element method. The difficulty in applying the stiffness analysis to problems involving instability is that any compressive axial load on a structural member will tend to decrease its bending stiffness and vice versa for a tensile axial load. Thus, if a structural member is subjected to compressive axial loading, buckling will occur when the bending stiffness is so decreased, that any small bending caused by the offset of the load will be larger than the bending resistance of the structure. Such analysis is further complicated by the effects of material nonlinearity where the stresses in certain parts of the structure have exceeded the limit of proportionality.

4.2.1 Previous works

Investigation of structures involving material and geometric nonlinear behaviour has been a subject of study for a long time. Derivation of a new class of stiffness matrix and the conception of incremental step for large displacement analysis were described by Turner *et al* (1960), and further work was done by Argyris (1964), Turner *et al* (1964), and Oden (1969). Davidson & Chen (1974), Carter *et al* (1977) investigated large deformation response to elastoplastic materials. Desai & Phan (1980) extended the theories of material and geometric nonlinearities to general three-dimensional problems.

In dealing with geometric nonlinear behaviour, all the kinematic and static variables are referred to the previous configuration of the continuum. If they are referred to the original undeformed configuration, the approach is called Total Lagrangian. Works by Zienkiewicz & Nayak (1971) and Bathe *el al* (1975) were based on this approach. If the variables are based on the recently computed configuration, the approach is called Updated Lagrangian or Approximate Eulerian. Yamada (1972) and many researchers universally adopted this approach. In fact, the Updated Lagrangian approach is found to be more general and efficient during computation, hence all large displacement formulations derived and used throughout this thesis are based on this approach.

In this chaper, only large displacement due to geometric nonlinearity will be considered.

4.3 Nonlinear strain matrix for isoparametric element

According to Newton's law, a particle or body can have no acceleration if there is no resultant force acting on it. Such a body is said to be in a state of *equilibrium.* Zero acceleration may of course imply constant velocity, but in the context of civil engineering structures, the state most frequently dealt with is that of zero velocity.

A body is in a state of equilibrium if the resultant of all forces acting on it is zero. There are two kinds of forces, external forces and internal forces. The internal forces represent the interactions between different particles or elements in the body. Since actions and reactions are equal and opposite, the internal reactions may be represented by equal and opposite vectors having the same line of action.

By applying the virtual work principle, or by minimising the total energy of the structure of a body, the equilibrium equation of a body can be derived as

$$\int_{\Omega} \mathbf{B}^T \sigma d\Omega + \mathbf{f} = 0 \tag{4.1}$$

where $\mathbf{B}$ is the nonlinear strain matrix and $\mathbf{f}$ is the vector of equivalent nodal loads, and the integration is performed over the region Ω.

If a body is in equilibrium, then every element of the body must also be in equilibrium. Thus the idea of 'removing' an element of the complete body can be conceived, and it will be in equilibrium under the action of any applied external forces. This means that it is possible to extract any element from a larger structure and examine it in detail under the action of all forces acting on it. On extending this idea, the whole body may be considered as an assembly of these elements. In conjunction with the last chapter, eight-noded isoparametric elements are used to model the body throughout this chapter.

Consider an arbitrary element e, the element strain matrix $\mathbf{B}^e$ can be written in the augmented form

$$\mathbf{B}^e = [\mathbf{B}_1 \ \mathbf{B}_2 \ \cdots \ \mathbf{B}_8],$$

where $\mathbf{B}_i$ is the $\mathbf{B}$ matrix for node i in element e.

In large displacement analysis, these matrices $\mathbf{B}_i$ must be nonlinear. The first step here is to derive $\mathbf{B}^e$ in its explicit form.

4.3.1 Derivation of nonlinear strain matrix

Figure 4.1 shows a body lying in a Cartesian coordinate system. The coordinates of a particle in the body in vector notation are given by

$$x = (x_0, y_0)^T.$$

Suppose some loadings are applied to the body in incremental form. In the n-th increment, if the body undergoes some changes of configuration and moves to a new location under certain conditions, the displacements of the particle can be defined in vector form as $u_n = u(x)$, where

$$u_n = (u_n, v_n)^T,$$

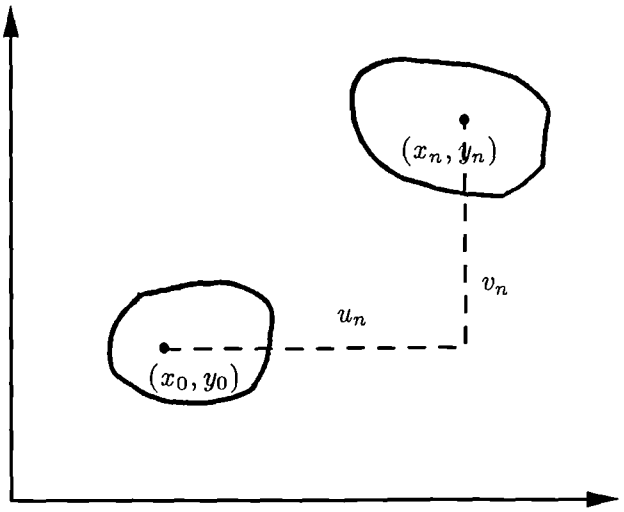

Figure 4.1: Body deformation and displacement notation

and so the new coordinates of the particle become

$$x_n = (x_n, y_n)^T = (x_0 + u_n, y_0 + v_n)^T.$$

Using these definitions, Bathe (1996) and Pan (1988) explicitly defined the nonlinear strain-displacement relation as

$$\epsilon = \begin{bmatrix} \epsilon_x \\ \epsilon_y \\ \gamma_{xy} \end{bmatrix} = \begin{bmatrix} \frac{\partial u_n}{\partial x} + \frac{1}{2}\left(\frac{\partial u_n}{\partial x}\right)^2 + \frac{1}{2}\left(\frac{\partial v_n}{\partial x}\right)^2 \\ \frac{\partial v_n}{\partial y} + \frac{1}{2}\left(\frac{\partial u_n}{\partial y}\right)^2 + \frac{1}{2}\left(\frac{\partial v_n}{\partial y}\right)^2 \\ \frac{\partial u_n}{\partial x} + \frac{\partial v_n}{\partial y} + \frac{\partial u_n}{\partial x}\frac{\partial u_n}{\partial y} + \frac{\partial v_n}{\partial x}\frac{\partial v_n}{\partial y} \end{bmatrix} \tag{4.2}$$

where ϵ_x, ϵ_y and γ_{xy} are the shear components in the x, y plane.

For convenience, the strain vector in equation (4.2) is split into two components, namely the linear and the nonlinear parts:

$$\epsilon = \epsilon_L + \epsilon_{NL} \tag{4.3}$$

where

$$\epsilon_L = \begin{bmatrix} \frac{\partial u_n}{\partial x} \\ \frac{\partial v_n}{\partial y} \\ \frac{\partial u_n}{\partial x} + \frac{\partial v_n}{\partial y} \end{bmatrix}$$

and

$$\begin{aligned}
\epsilon_{NL} &= \begin{bmatrix} \frac{1}{2}\left(\frac{\partial u_n}{\partial x}\right)^2 + \frac{1}{2}\left(\frac{\partial v_n}{\partial x}\right)^2 \\ \frac{1}{2}\left(\frac{\partial u_n}{\partial y}\right)^2 + \frac{1}{2}\left(\frac{\partial v_n}{\partial y}\right)^2 \\ \frac{\partial u_n}{\partial x}\frac{\partial u_n}{\partial y} + \frac{\partial v_n}{\partial x}\frac{\partial v_n}{\partial y} \end{bmatrix} \\
&= \frac{1}{2}\begin{bmatrix} \frac{\partial u_n}{\partial x} & \frac{\partial v_n}{\partial x} & 0 & 0 \\ 0 & 0 & \frac{\partial u_n}{\partial y} & \frac{\partial v_n}{\partial y} \\ \frac{\partial u_n}{\partial y} & \frac{\partial v_n}{\partial y} & \frac{\partial u_n}{\partial x} & \frac{\partial v_n}{\partial y} \end{bmatrix} \begin{bmatrix} \frac{\partial u_n}{\partial x} \\ \frac{\partial v_n}{\partial x} \\ \frac{\partial u_n}{\partial y} \\ \frac{\partial v_n}{\partial y} \end{bmatrix} \\
&= \frac{1}{2}\mathbf{A}\theta
\end{aligned} \tag{4.4}$$

For isoparametric elements, the displacement vector can be written as

$$u = \mathbf{N}\mathbf{u}^e \tag{4.5}$$

where $\mathbf{N}$ is the matrix of element shape functions as defined in (3.10) for an eight-noded isoparametric element, and $\mathbf{u}^e$ is the nodal displacement vector.

In most constitutive laws in elasticity, the incremental strain $d\epsilon$ is assumed to be small. From this assumption and equation (4.3), $d\epsilon$ can be decomposed into linear strain $d\epsilon_L$ and nonlinear strain $d\epsilon_{NL}$ as

$$d\epsilon = d\epsilon_L + d\epsilon_{NL} \tag{4.6}$$

where the linear part

$$\begin{aligned}
d\epsilon_L &= d\begin{bmatrix} \frac{\partial u_n}{\partial x} \\ \frac{\partial v_n}{\partial y} \\ \frac{\partial u_n}{\partial y} + \frac{\partial v_n}{\partial x} \end{bmatrix} = \begin{bmatrix} \frac{\partial du_n}{\partial x} \\ \frac{\partial dv_n}{\partial y} \\ \frac{\partial du_n}{\partial y} + \frac{\partial dv_n}{\partial x} \end{bmatrix} \\
&= \mathbf{B}_L\, d\begin{bmatrix} u_n \\ v_n \end{bmatrix} = \mathbf{B}_L\, d\mathbf{u}^e
\end{aligned} \tag{4.7}$$

and the nonlinear part can be obtained from the relationship in equation (4.4) as

$$d\epsilon_{NL} = \frac{1}{2}d\mathbf{A}\cdot\theta + \frac{1}{2}\mathbf{A}\cdot d\theta \tag{4.8}$$

From the properties of $\mathbf{A}$ and θ,

$$
\begin{aligned}
d\mathbf{A}\cdot\theta &= \begin{bmatrix} d\frac{\partial u_n}{\partial x} & d\frac{\partial v_n}{\partial x} & 0 & 0 \\ 0 & 0 & d\frac{\partial u_n}{\partial y} & d\frac{\partial v_n}{\partial y} \\ d\frac{\partial u_n}{\partial y} & d\frac{\partial v_n}{\partial y} & d\frac{\partial u_n}{\partial x} & d\frac{\partial v_n}{\partial x} \end{bmatrix} \begin{bmatrix} \frac{\partial u_n}{\partial x} \\ \frac{\partial v_n}{\partial x} \\ \frac{\partial u_n}{\partial y} \\ \frac{\partial v_n}{\partial y} \end{bmatrix} \\
&= \begin{bmatrix} \frac{\partial u_n}{\partial x} & \frac{\partial v_n}{\partial x} & 0 & 0 \\ 0 & 0 & \frac{\partial u_n}{\partial y} & \frac{\partial v_n}{\partial y} \\ \frac{\partial u_n}{\partial y} & \frac{\partial v_n}{\partial y} & \frac{\partial u_n}{\partial x} & \frac{\partial v_n}{\partial x} \end{bmatrix} \begin{bmatrix} d\frac{\partial u_n}{\partial x} \\ d\frac{\partial v_n}{\partial x} \\ d\frac{\partial u_n}{\partial y} \\ d\frac{\partial v_n}{\partial y} \end{bmatrix} \\
&= \mathbf{A}\cdot d\theta
\end{aligned} \tag{4.9}
$$

and hence the nonlinear part can be simply written as

$$d\epsilon_{NL} = \mathbf{A}\cdot d\theta \tag{4.10}$$

Further, by (4.5), the vector θ as defined in (4.4) can be expressed in the form

$$\theta = \begin{bmatrix} \frac{\partial u_n}{\partial x} \\ \frac{\partial v_n}{\partial x} \\ \frac{\partial u_n}{\partial y} \\ \frac{\partial v_n}{\partial y} \end{bmatrix} = \mathbf{G}\mathbf{u}^e \tag{4.11}$$

where for each node i,

$$\mathbf{G}_i = \begin{bmatrix} \frac{\partial N_i}{\partial x} & 0 \\ 0 & \frac{\partial N_i}{\partial x} \\ \frac{\partial N_i}{\partial y} & 0 \\ 0 & \frac{\partial N_i}{\partial y} \end{bmatrix} \tag{4.12}$$

Substituting (4.11) into (4.10), it can be seen that

$$d\epsilon_{NL} = \mathbf{A}\cdot d\theta = \mathbf{A}\cdot d[\mathbf{G}\mathbf{u}^e] = \mathbf{A}\mathbf{G}\cdot d\mathbf{u}^e = \mathbf{B}_{NL}\, d\mathbf{u}^e, \tag{4.13}$$

and together with (4.7), equation (4.6) becomes

$$d\epsilon = (\mathbf{B}_L + \mathbf{B}_{NL})\, d\mathbf{u}^e = \mathbf{B}\, d\mathbf{u}^e \tag{4.14}$$

where

$$\begin{aligned}\mathbf{B} &= \mathbf{B}_L + \mathbf{B}_{NL} \\ &= \mathbf{B}_L + \mathbf{AG}\end{aligned}$$

Therefore, for each node i, the matrix $\mathbf{B}_i$ can be expressed in the explicit form

$$\begin{aligned}[\mathbf{B}_i] &= [\mathbf{B}_L]_i + \mathbf{A}_i\mathbf{G}_i \\ &= \begin{bmatrix} \frac{\partial N_i}{\partial x} & 0 \\ 0 & \frac{\partial N_i}{\partial y} \\ \frac{\partial N_i}{\partial y} & \frac{\partial N_i}{\partial x} \end{bmatrix} + \begin{bmatrix} \frac{\partial u_n}{\partial x}\frac{\partial N_i}{\partial x} & \frac{\partial v_n}{\partial x}\frac{\partial N_i}{\partial x} \\ \frac{\partial u_n}{\partial y}\frac{\partial N_i}{\partial y} & \frac{\partial v_n}{\partial y}\frac{\partial N_i}{\partial y} \\ \frac{\partial u_n}{\partial y}\frac{\partial N_i}{\partial x} + \frac{\partial u_n}{\partial x}\frac{\partial N_i}{\partial y} & \frac{\partial v_n}{\partial y}\frac{\partial N_i}{\partial x} + \frac{\partial v_n}{\partial x}\frac{\partial N_i}{\partial y} \end{bmatrix}\end{aligned} \tag{4.15}$$

4.3.2 Factorization of strain matrix

The nonlinear element strain matrix $\mathbf{B}_i$ for node i has now been expressed as the sum of a linear part, which is now written as $[\mathbf{B}_L]_i$, and a nonlinear part $[\mathbf{B}_{NL}]_i$, and it can be written as

$$[\mathbf{B}]_i = [\mathbf{B}_L]_i + [\mathbf{B}_{NL}]_i \tag{4.16}$$

Referring to Figure 4.1, the relationships between the coordinates and the displacements of the body before and after deformation are

$$u_n = x_n - x_0, \qquad v_n = y_n - y_0$$

and

$$\frac{\partial x_0}{\partial x} = \frac{\partial y_0}{\partial y} = 1, \qquad \frac{\partial x_0}{\partial y} = \frac{\partial y_0}{\partial x} = 0 \tag{4.17}$$

where u_n and x_n are respectively the x-displacement and the new x-coordinate of a particle after deformation in the body at the nth incremental load, *etc.*

With these relationships, entries in $[\mathbf{B}]_i$ can be simplified, *viz*

$$\begin{aligned}\frac{\partial N_i}{\partial x} + \frac{\partial u_n}{\partial x}\frac{\partial N_i}{\partial x} = \frac{\partial N_i}{\partial x} + \left(\frac{\partial x_n}{\partial x} - \frac{\partial x_0}{\partial x}\right)\frac{\partial N_i}{\partial x} = \frac{\partial N_i}{\partial x}\frac{\partial x_n}{\partial x} \\ \frac{\partial u_n}{\partial y}\frac{\partial N_i}{\partial y} = \left(\frac{\partial x_n}{\partial y} - \frac{\partial x_0}{\partial y}\right)\frac{\partial N_i}{\partial y} = \frac{\partial N_i}{\partial y}\frac{\partial x_n}{\partial y}\end{aligned} \tag{4.18}$$

$$\begin{aligned}\frac{\partial N_i}{\partial y} + \frac{\partial u_n}{\partial y}\frac{\partial N_i}{\partial x} + \frac{\partial u_n}{\partial x}\frac{\partial N_i}{\partial y} &= \frac{\partial N_i}{\partial y} + \left(\frac{\partial x_n}{\partial y} - \frac{\partial x_0}{\partial y}\right)\frac{\partial N_i}{\partial x} + \left(\frac{\partial x_n}{\partial x} - \frac{\partial x_0}{\partial x}\right)\frac{\partial N_i}{\partial y} \\ &= \frac{\partial N_i}{\partial y}\frac{\partial x_n}{\partial x} + \frac{\partial N_i}{\partial x}\frac{\partial x_n}{\partial y}\end{aligned}$$

Likewise, the following can be obtained:

$$\frac{\partial v_n}{\partial x}\frac{\partial N_i}{\partial x} = \frac{\partial N_i}{\partial x}\frac{\partial y_n}{\partial x}$$

$$\frac{\partial N_i}{\partial y} + \frac{\partial v_n}{\partial y}\frac{\partial N_i}{\partial y} = \frac{\partial N_i}{\partial y}\frac{\partial y_n}{\partial y} \tag{4.19}$$

and

$$\frac{\partial N_i}{\partial x} + \frac{\partial v_n}{\partial y}\frac{\partial N_i}{\partial x} + \frac{\partial v_n}{\partial x}\frac{\partial N_i}{\partial y} = \frac{\partial N_i}{\partial x}\frac{\partial y_n}{\partial y} + \frac{\partial N_i}{\partial y}\frac{\partial y_n}{\partial x}$$

With these simplifications, $[\mathbf{B}]_i$ in (4.15) can be reduced to the compact form

$$\begin{aligned}
[\mathbf{B}]_i &= \begin{bmatrix} \frac{\partial N_i}{\partial x}\frac{\partial x_n}{\partial x} & \frac{\partial N_i}{\partial x}\frac{\partial y_n}{\partial x} \\ \frac{\partial N_i}{\partial y}\frac{\partial x_n}{\partial y} & \frac{\partial N_i}{\partial y}\frac{\partial y_n}{\partial y} \\ \frac{\partial N_i}{\partial y}\frac{\partial x_n}{\partial x} + \frac{\partial N_i}{\partial x}\frac{\partial x_n}{\partial y} & \frac{\partial N_i}{\partial x}\frac{\partial y_n}{\partial y} + \frac{\partial N_i}{\partial y}\frac{\partial y_n}{\partial x} \end{bmatrix} \\
&= \begin{bmatrix} \frac{\partial N_i}{\partial x} & 0 \\ 0 & \frac{\partial N_i}{\partial y} \\ \frac{\partial N_i}{\partial y} & \frac{\partial N_i}{\partial x} \end{bmatrix} \begin{bmatrix} \frac{\partial x_n}{\partial x} & \frac{\partial y_n}{\partial x} \\ \frac{\partial x_n}{\partial y} & \frac{\partial y_n}{\partial y} \end{bmatrix} \\
&= [\mathbf{B}_L]_i \mathbf{J}_D
\end{aligned} \tag{4.20}$$

where $\mathbf{J}_D$ is called the Deformation Jacobian matrix, and is given by

$$\mathbf{J}_D = \begin{bmatrix} \frac{\partial x_n}{\partial x} & \frac{\partial y_n}{\partial x} \\ \frac{\partial x_n}{\partial y} & \frac{\partial y_n}{\partial y} \end{bmatrix}.$$

This particular form of $[\mathbf{B}]_i$ is very useful in practice, because it is expressed as a product of two simple matrices, and so it can be conveniently used in further analyses.

4.4 Nonlinear Instability Analysis

To give a more realistic simulation in the study of nonlinear instability behaviour of a structure by the finite element method, the deformation of the structure under loading has to be calculated in incremental form. This process has been under investigation since 1970 by Zienkiewicz & Nayak (1973), Carter *et al* (1977), Yamada & Wifi (1977), Desai & Phan (1980), Kiousis *et al* (1986). Pan (1988) investigated this process using time increments. Most of these works focused on geometric nonlinearity, while significantly less work has been done on material nonlinearity.

4.4.1 Incremental equilibrium equation

The idea of incremental approach for nonlinear problems was first investigated by Turner *et al* (1960).

In the incremental approach to matrix analysis for nonlinear instability and large displacement problems, the single solution of the nonlinear set is replaced by the repetitive solution of the linearized set, and the loads (or in some cases the specified displacements) are applied in a series of increments. At each increment step, the displacements are accumulated due to large deformation, and hence the element stiffness matrix and the resulting global stiffness matrix are constantly changing. So they have to be recalculated at each incremental step.

For the purpose of analysing nonlinear instability behaviour of a linear elastic material, it is necessary to first of all deduce an incremental equilibrium equation due to incremental loading.

Suppose an incremental load $\delta\mathbf{f}$ is applied to the system, which is previously in equilibrium under load $\mathbf{f}$ and stress σ. Denoting

$$\begin{aligned} \delta\mathbf{f} &= \mathbf{f}^n - \mathbf{f} \\ \delta\sigma &= \sigma^n - \sigma \\ \delta\mathbf{B} &= \delta\mathbf{B}_{NL} = \mathbf{B}^n - \mathbf{B} \end{aligned} \tag{4.21}$$

where $\delta\mathbf{B}_{NL}$ is a nonlinear function of incremental displacements δu_n and δv_n.

With these relationships, the equilibrium equation (4.1) for the new load $\mathbf{f}^n$ and stress σ^n becomes

$$\int_\Omega \left\{(\mathbf{B} + \delta\mathbf{B}_{NL})^T (\sigma + \delta\sigma)\right\} d\Omega + \mathbf{f} + \delta\mathbf{f} = 0. \tag{4.22}$$

Expanding (4.22),

$$\int_\Omega \left\{\mathbf{B}^T\sigma + [\delta\mathbf{B}_{NL}]^T\sigma + [\delta\mathbf{B}_{NL}]^T\delta\sigma + \mathbf{B}^T\delta\sigma\right\} d\Omega + \mathbf{f} + \delta\mathbf{f} = 0 \tag{4.23}$$

Using the original equilibrium equation (4.1), equation (4.23) can be simplified to the form

$$\int_\Omega [\delta \mathbf{B}_{NL}]^T \sigma d\Omega + \int_\Omega \mathbf{B}^T \delta\sigma d\Omega + \int_\Omega [\delta \mathbf{B}_{NL}]^T \delta\sigma d\Omega + \delta\mathbf{f} = 0 \tag{4.24}$$

which is now the incremental equilibrium equation for the incremental load $\delta\mathbf{f}$.

Equation (4.24) is nonlinear. To solve it for $\delta\sigma$ and hence $\delta\mathbf{u}$, there are many readily available numerical methods, such as Newton's method, Quasi-Newton method, conjugate gradient method etc. For simplicity, (4.24) is replaced by an approximate linear equation, and the solution of this linear equation is used as an initial approximation in a simple iteration scheme based on the idea of residual load.

4.4.2 Method of solution

The third term in equation (4.24) involves the product of two increment terms, and hence it is infinitesimal when compared to the other terms. Therefore, it can be neglected to give the approximate incremental equilibrium equation

$$\int_\Omega \mathbf{B}^T \delta\sigma d\Omega + \int_\Omega [\delta \mathbf{B}_{NL}]^T \sigma d\Omega + \delta\mathbf{f} = 0. \tag{4.25}$$

From (4.15), it has been deduced that, for each node i in element e,

$$[\mathbf{B}]_i = [\mathbf{B}_L]_i + [\mathbf{B}_{NL}]_i,$$

where

$$[\mathbf{B}_L]_i = \begin{bmatrix} \frac{\partial N_i}{\partial x} & 0 \\ 0 & \frac{\partial N_i}{\partial y} \\ \frac{\partial N_i}{\partial y} & \frac{\partial N_i}{\partial x} \end{bmatrix}$$

and

$$[\mathbf{B}_{NL}]_i = \begin{bmatrix} \frac{\partial u_n}{\partial x}\frac{\partial N_i}{\partial x} & \frac{\partial v_n}{\partial x}\frac{\partial N_i}{\partial x} \\ \frac{\partial u_n}{\partial y}\frac{\partial N_i}{\partial y} & \frac{\partial v_n}{\partial y}\frac{\partial N_i}{\partial y} \\ \frac{\partial u_n}{\partial y}\frac{\partial N_i}{\partial x} + \frac{\partial u_n}{\partial x}\frac{\partial N_i}{\partial y} & \frac{\partial v_n}{\partial y}\frac{\partial N_i}{\partial x} + \frac{\partial v_n}{\partial x}\frac{\partial N_i}{\partial y} \end{bmatrix},$$

and where the matrix $[\mathbf{B}_{NL}]_i$ can be factorized in the form

$$[\mathbf{B}_{NL}]_i = [\mathbf{A}]_i[\mathbf{G}]_i \tag{4.26}$$

with

$$[\mathbf{A}]_i = \begin{bmatrix} \frac{\partial u_n}{\partial x} & \frac{\partial v_n}{\partial x} & 0 & 0 \\ 0 & 0 & \frac{\partial u_n}{\partial y} & \frac{\partial v_n}{\partial y} \\ \frac{\partial u_n}{\partial y} & \frac{\partial v_n}{\partial y} & \frac{\partial u_n}{\partial x} & \frac{\partial v_n}{\partial x} \end{bmatrix} \quad \text{and} \quad [\mathbf{G}]_i = \begin{bmatrix} \frac{\partial N_i}{\partial x} & 0 \\ 0 & \frac{\partial N_i}{\partial x} \\ \frac{\partial N_i}{\partial y} & 0 \\ 0 & \frac{\partial N_i}{\partial y} \end{bmatrix}.$$

When compared to the nonlinear strain matrix $\mathbf{B}_{NL}$ in equation (4.15), the incremental nonlinear strain matrix $\delta\mathbf{B}_{NL}$ at node i can be similarly expressed as

$$[\delta\mathbf{B}_{NL}]_i = \begin{bmatrix} \frac{\partial \delta u_n}{\partial x}\frac{\partial N_i}{\partial x} & \frac{\partial \delta v_n}{\partial x}\frac{\partial N_i}{\partial x} \\ \frac{\partial \delta u_n}{\partial y}\frac{\partial N_i}{\partial y} & \frac{\partial \delta v_n}{\partial y}\frac{\partial N_i}{\partial y} \\ \frac{\partial \delta u_n}{\partial y}\frac{\partial N_i}{\partial x} + \frac{\partial \delta u_n}{\partial x}\frac{\partial N_i}{\partial y} & \frac{\partial \delta v_n}{\partial y}\frac{\partial N_i}{\partial x} + \frac{\partial \delta v_n}{\partial x}\frac{\partial N_i}{\partial y} \end{bmatrix} \tag{4.27}$$

Following (4.26), (4.27) can be written as

$$\begin{aligned} [\delta\mathbf{B}_{NL}]_i^T &= \begin{bmatrix} \frac{\partial N_i}{\partial x} & 0 & \frac{\partial N_i}{\partial y} & 0 \\ 0 & \frac{\partial N_i}{\partial x} & 0 & \frac{\partial N_i}{\partial y} \end{bmatrix} \begin{bmatrix} \frac{\partial \delta u_n}{\partial x} & 0 & \frac{\partial \delta u_n}{\partial y} \\ \frac{\partial \delta v_n}{\partial x} & 0 & \frac{\partial \delta v_n}{\partial y} \\ 0 & \frac{\partial \delta u_n}{\partial y} & \frac{\partial \delta u_n}{\partial x} \\ 0 & \frac{\partial \delta v_n}{\partial y} & \frac{\partial \delta v_n}{\partial y} \end{bmatrix} \\ &= [\mathbf{G}]_i^T [\delta\mathbf{A}]_i^T \end{aligned} \tag{4.28}$$

To express equation (4.25) in terms of the unknown vector $\delta\mathbf{u}$, it can be seen that, for each node i,

$$[\mathbf{B}]_i^T \delta\sigma_i = [\mathbf{B}]_i^T [\mathbf{D}]_i \delta\epsilon_i = [\mathbf{B}]_i^T [\mathbf{D}]_i [\mathbf{B}]_i \delta u_i \tag{4.29}$$

where δu_i is the subsequent incremental displacement, and by using (4.28),

$$\begin{aligned} [\delta\mathbf{B}_{NL}]_i^T \sigma &= [\mathbf{G}]_i^T [\delta\mathbf{A}_i]^T \sigma \\ &= [\mathbf{G}]_i^T \begin{bmatrix} \frac{\partial \delta u_n}{\partial x}\sigma_x + \frac{\partial \delta u_n}{\partial y}\tau_{xy} \\ \frac{\partial \delta v_n}{\partial x}\sigma_x + \frac{\partial \delta v_n}{\partial y}\tau_{xy} \\ \frac{\partial \delta u_n}{\partial y}\sigma_y + \frac{\partial \delta u_n}{\partial x}\tau_{xy} \\ \frac{\partial \delta v_n}{\partial y}\sigma_y + \frac{\partial \delta v_n}{\partial x}\tau_{xy} \end{bmatrix} \end{aligned}$$

$$= [\mathbf{G}]_i^T \begin{bmatrix} \sigma_x \mathbf{I} & \tau_{xy}\mathbf{I} \\ \tau_{xy}\mathbf{I} & \sigma_y \mathbf{I} \end{bmatrix} [\mathbf{G}]_i \delta u_i$$

$$= [\mathbf{G}]_i^T \mathbf{M} [\mathbf{G}]_i \delta u_i \tag{4.30}$$

where

$$\mathbf{M} = \begin{bmatrix} \sigma_x \mathbf{I} & \tau_{xy}\mathbf{I} \\ \tau_{xy}\mathbf{I} & \sigma_y \mathbf{I} \end{bmatrix} \tag{4.31}$$

and

$$\mathbf{I} = \begin{bmatrix} 1 & 0 \\ 0 & 1 \end{bmatrix}$$

$\mathbf{G}_i$ is defined in (4.12), and it has to be recalculated for each node i in element e. To assemble them for the element, augmentation must be used. For example, if an eight-node isoparametric element is used, $[\mathbf{G}^e]$ for element e is the augumented 4×16 matrix

$$[\mathbf{G}^e] = [\mathbf{G}_1 \, \mathbf{G}_2 \cdots \mathbf{G}_8]. \tag{4.32}$$

Hence, the 16×16 matrix in the second term in (4.25) becomes

$$[\mathbf{K}^e]_{NL} = \int_{\Omega^e} [\mathbf{G}^e]^T \mathbf{M} [\mathbf{G}^e] \, d\Omega. \tag{4.33}$$

Assembling equations (4.29) and (4.30) for each node i, and then for each element e, the resultant element matrices can then be substituted into (4.25) to obtain the global stiffness matrix $\mathbf{K}$ with

$$\mathbf{K}\delta u = -\delta \mathbf{f} \tag{4.34}$$

which is now the approximate equilibrium equation for the incremental load $\delta \mathbf{f}$ in matrix form, where

$$\mathbf{K} = \mathbf{K}_I + \mathbf{K}_{II},$$

with

$$\mathbf{K}_I = \int_\Omega \mathbf{B}^T \mathbf{D} \mathbf{B} \, d\Omega, \tag{4.35}$$

and

$$\mathbf{K}_{II} = \int_\Omega \mathbf{G}^T \mathbf{M} \mathbf{G} \, d\Omega, \tag{4.36}$$

where, from (4.20),

$$\mathbf{B} = \mathbf{B}_L \mathbf{J}_D,$$

and where $\mathbf{M}$ and $\mathbf{G}$ in element form are defined in (4.31) and (4.32) respectively.

It is still required to evaluate the two definite integrals $\mathbf{K}_I$ and $\mathbf{K}_{II}$, and hence $\mathbf{K}$. This can be carried out by applying Gaussian quadrature or other accurate numerical integration methods to the two integrals in (4.35) and (4.36). Once $\mathbf{K}$ is found, the next step is to solve the matrix equation (4.34) for the approximate displacement δu of the incremental equilibrium equation.

4.4.3 Residual load

It has been derived from the last section that the matrix equation (4.34) is the approximate equation for the incremental equilibrium equation (4.24).

This approximate equation is a linear matrix equation, and it can be solved accurately for δu by standard methods of linear algebra. This solution can be taken as an approximate solution of the original incremental equilibrium equation in (4.24). It is necessary to seek ways to refine this approximate solution.

The simplest and the most direct approach would be to reduce the size of the third term $\int_\Omega [\delta \mathbf{B}_{NL}]^T \delta\sigma d\Omega$ in equation (4.24), which is the omitted term and is therefore the actual difference between the two equations. This could be achieved by simply reducing the size of each incremental load, and hence the product of the two increment terms that follow would also be reduced accordingly. It would give rise to a more accurate approximate solution. However, if the size of the incremental load is too small, the number of incremental steps will have to be increased accordingly, and this in turn would affect the efficiency of the method. Furthermore, this would create the unneccessary accumulation of computation errors which would reduce the overall accuracy of the method.

An alternative and better method would be the use of an iterative method based on the idea of residual load (or residual error).

Suppose that in the kth iteration of the residual load when the nth incremental load is being applied to the system, the incremental equilibrium equation takes the form

$$\widehat{\mathbf{K}}\delta\mathbf{u}_n^{(k)} = -\delta\mathbf{f}_n^{(k)} \tag{4.37}$$

where

$\widehat{\mathbf{K}}$ is the stiffness matrix, as defined in equation (4.34), updated to the kth iteration,

$\delta \mathbf{u}_n^{(k)}$ is displacement increment in the kth iteration, and

$\delta \mathbf{f}_n^{(k)}$ is the sum of the nth incremental load and all residual loads up to and including the $(k-1)$th iteration.

Once $\delta \mathbf{u}_n^{(k)}$ is found, the accumulated displacement $\mathbf{u}_n^{(k)}$ can be obtained from the equation

$$\mathbf{u}_n^{(k)} = \mathbf{u}_n^{(k-1)} + \delta \mathbf{u}_n^{(k)}, \tag{4.38}$$

and with this updated value of $\mathbf{u}_n^{(k)}$, the updated stiffness matrix $\widehat{\mathbf{B}}$ can be calculated.

From the relationship

$$\delta \sigma_n^{(k)} = \mathbf{D}\, \widehat{\mathbf{B}}\, \delta \mathbf{u}_n^{(k)}, \tag{4.39}$$

the stress in the kth iteration, $\delta \sigma_n^{(k)}$, can be found and hence the accumulated stress, $\sigma_n^{(k)}$, can be updated from the relationship

$$\sigma_n^{(k)} = \sigma_n^{(k-1)} + \delta \sigma_n^{(k)}. \tag{4.40}$$

Define the residual load (or residual error) by

$$\mathbf{r}_n^{(k)} = \delta \mathbf{f}_n^{(k)} + \int_\Omega \widehat{\mathbf{B}}^T \delta \sigma_n^{(k)} d\Omega, \tag{4.41}$$

where

$\mathbf{r}_n^{(k)}$ is kth residual load,

$\delta \mathbf{f}_n^{(k)}$ is the sum of the nth incremental load and all residual loads up to and including the $(k-1)$th iteration,

$\widehat{\mathbf{B}}$ is the new, updated stiffness matrix due to the accumulated displacement $\mathbf{u}_n^{(k)}$ defined by equation (4.38), and

$\sigma_n^{(k)}$ is the accumulated stress in the kth iteration.

As the updated values in (4.38) and (4.40) are used in the integrand in equation (4.41), the residual load $\mathbf{r}_n^{(k)}$ is effectively the vector that contains any surplus in the orginal incremental equilibrium equation when the accumulated displacement and stress are used. In order to refine the approximate solution, the aim here is to reduce $\mathbf{r}_n^{(k)}$ to a zero vector, or at least to make it converge under certain prescribed criteria. However, it cannot be

entirely certain that small residuals imply correct answers.

To overcome this problem, introduce the residual ratio $\rho^{(k)}$ as

$$\rho^{(k)} = \frac{\|\mathbf{r}_n^{(k)}\|}{\|\mathbf{r}_n^{(k-1)}\|} \tag{4.42}$$

This residual ratio $\rho^{(k)}$ is a factor which can be used to monitor the relative ratio of the norms of the two consecutive residual loads. It can give an indication whether the error is becoming smaller, and hence the iteration is converging.

Further, a tolerance factor can be prescribed so that when the residual ratio $\rho^{(k)}$ is smaller than this factor, the error can be regarded as small enough to be neglected, or insignificant in the context of this iteration. Hence it can be used as a factor to determine when the iteration can be terminated and the computation can proceed to the next incremental step. However, it is of vital importance that this factor must be small enough, so that it reflects a fair judgement on the convergence of the iteration.

If the residual ratio is greater than the tolerance factor, the approximate incremental equilibium equation

$$\widehat{\mathbf{K}}\delta\mathbf{u}_n^{(k+1)} = -\delta f_n^{(k+1)},$$

must be solved for $\delta\mathbf{u}_n^{(k+1)}$, and with this solution, the displacement vector must be accumulated to form a new stiffness matrix, and the whole procedure has to be repeated.

Note that in large displacement analysis, the cartesian derivatives of the shape functions (terms such as $\frac{\partial N_i}{\partial x}$) can no longer be assumed to be constant when they are used to evaluate the matrix $\widehat{\mathbf{B}}$ in this section. The new coordinates of the nodes in the deformed body have to be found first by adding the current nodal displacement $\delta\mathbf{u}_n^{(k)}$ to the original cartesian coordinates, and this vector can be used to form the matrix $\widehat{\mathbf{B}}$. Therefore $\widehat{\mathbf{B}}$ will change slightly after each iteration.

To ensure validity of the results, the residual ratio in each iteration should be convergent. If not, the resultant displacement vector is infinite. It implies that either the material property of the body is used incorrectly, or the applied load exceeds the critical load so that the bending moments are too big. In either case, it causes the deformation to collapse.

4.5 Euler Buckling

To validate the theory of large displacement analysis, the following example in column buckling is analysed with the algorithm set out in the last section.

4.5.1 A simple example - buckling of a uniform slender column

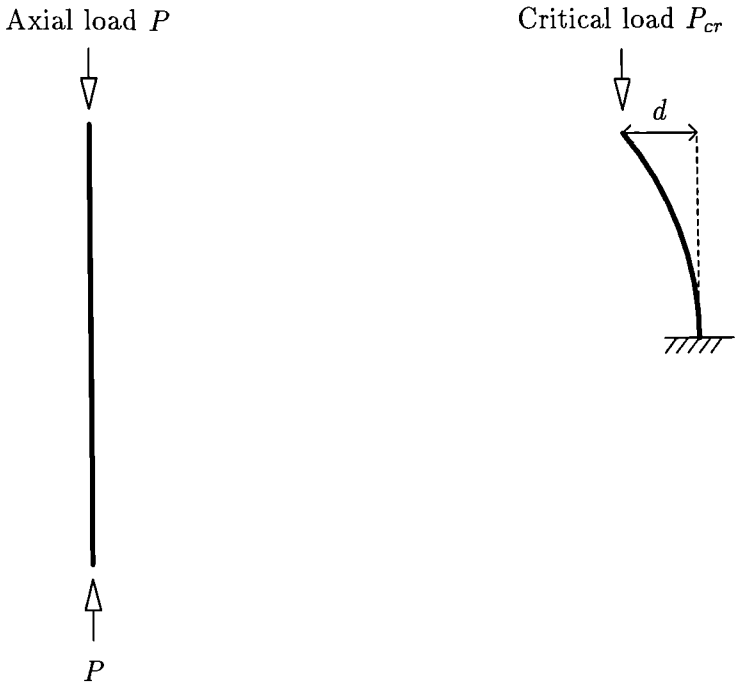

(a) Full beam (b) Half beam

Figure 4.2: Slender column

This buckling problem is concerned with the calculation of deflection caused by applying axial loads to a column. It can also be used to calculate the critical loads which cause elastic instability of a structure. In this particular example, buckling of a thin column of uniform cross-section is considered. The concept and the theoretical approach on buckling can be found in many standard textbooks, such as Timoshenko (1951) and Meek (1971), and Pan (1988) used the large displacement analysis in the finite element method to analysis the same problem numerically.

For the finite element discretization, the column is modelled by eight-noded two dimensional plane stress elements throughout. The column used is assumed to be made of homogenous, isotropic, and perfectly linear elastic material.

Consider a slender pin-jointed column which is free to move in the axial direction at

both end with a compressive axial force P, as shown in Figure 4.2(a). For convenience of imposing constraints on displacement, only half the column is modelled, as shown in Figure 4.2(b). The half column is fixed at one end and free to move in the other with P. The finite element mesh for the half column is shown in Figure 4.3. In this model, the column remains linearly elastic when subject to large strain, so that direct comparsion can be made between the computed buckling load and that predicted by Euler's theory.

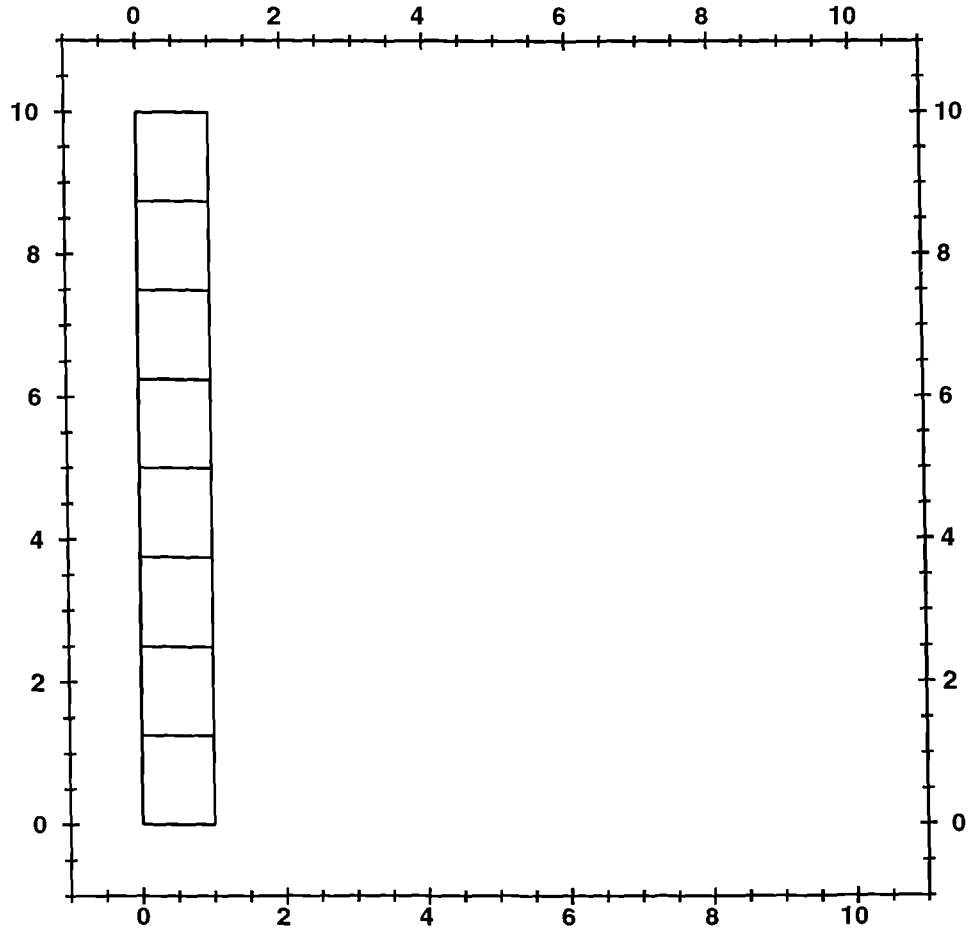

Figure 4.3: Finite element mesh of elastic column

In a finite element analysis, in addition to the axial load P, it is necessary to apply a small lateral load βP perpendicular to the free end of the column, in order to initiate nonlinear bending behaviour. The values of β are small so that this lateral load does not significantly affect the stress distribution according to the theory of infinitesimal strain. In this model, the value of β lies between 0.1% and 0.05%. Further, the element at the

top of the free end of this column is subject to both axial and lateral loads. They are applied along the two sides as surface traction, and the details of this element are shown in Figure 4.4.

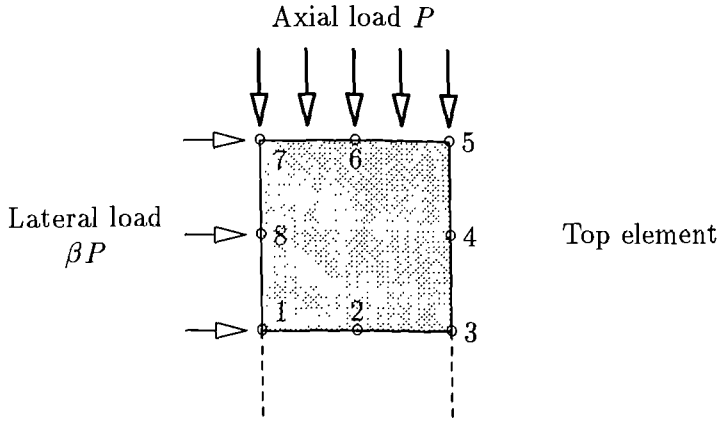

Figure 4.4: Details of top element

The program incorporating the large displacement theory predicts a collapse at about $0.97P_{cr}$ where P_{cr} is the maximum permissible axial load (critical load) given by Euler's formula

$$P_{cr} = \frac{\pi^2 EI}{4L^2}$$

where E is Young's modulus of material of the column,

I is the moment of inertia, and

L is the length of the half column.

Figure 4.5 shows the deformation (without exaggeration) of the half column of length 10m when an axial load of $0.97P_{cr}$, together with a small lateral load with $\beta = 0.1\%$ are applied to the free end of the column. These loads are applied in 16 equal increments. The Young's modulus of the beam is taken as $E = 0.2 \times 10^6 \text{N/m}^2$, with Poisson's ratio $\nu = 0.3$. In the computation of the residual load, a tolerance ratio of 0.1% is used.

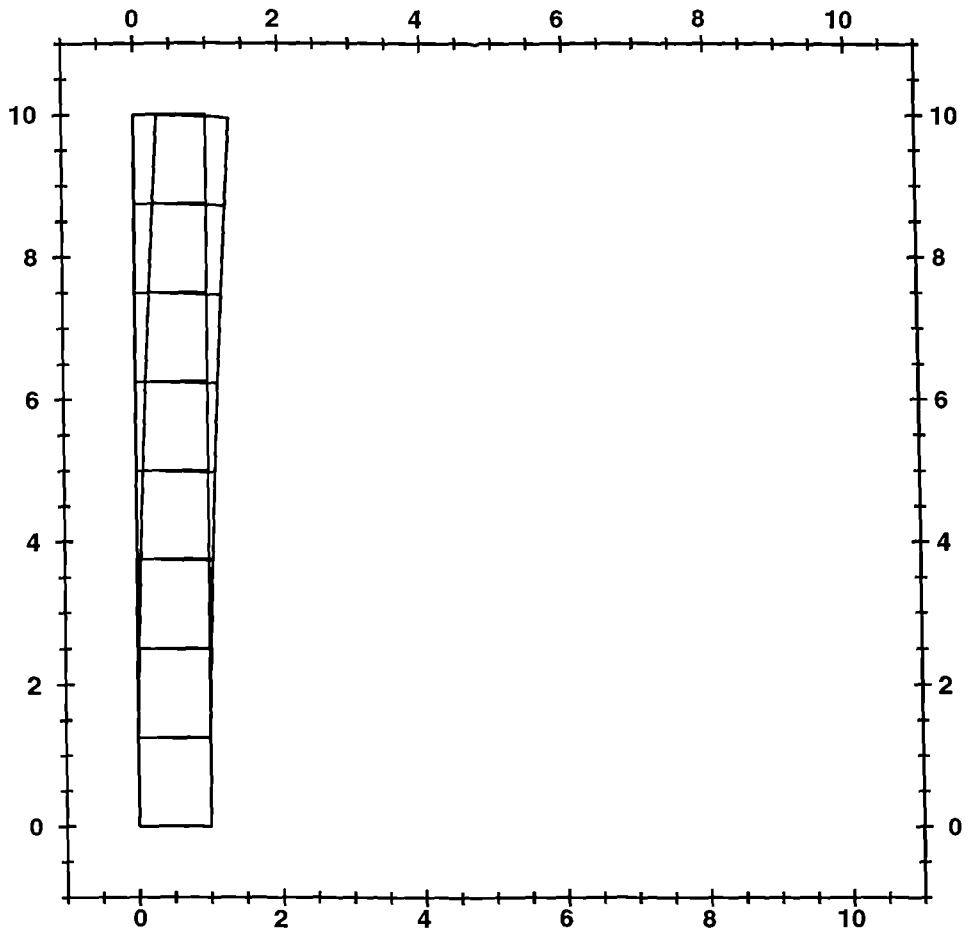

Figure 4.5: Deformation of column (Actual size)

4.5.2 Prediction of Critical load

In order to determine the critical load of the column, different trial values of the axial loads and β are used for further calculations and comparisons. The following table shows values of lateral displacements (in m) in the x direction of a half column u as a function of applied load P, computed by the program and according to large displacement bending theory with iterations performed on its residual loads. Material properties and number of equal increments used are the same as the model in Figure 4.4. Nodes 5, 6, and 7 are used as reference points in these computations.

load ($\times 10^3$N)	$\beta = 0.1\%$		
	node 5	node 6	node 7
0.20	0.00844	0.0083	0.00814
0.25	0.0136	0.00134	0.0132
0.30	0.0233	0.0231	0.0229
0.35	0.0478	0.0475	0.0473
0.38	0.0964	0.0962	0.0960
0.39	0.14	0.14	0.14
0.40	0.248	0.248	0.248
0.41	—	—	—
	$\beta = 0.05\%$		
	node 5	node 6	node 7
0.20	0.0038	0.0036	0.0035
0.25	0.00671	0.0651	0.00634
0.30	0.0113	0.0111	0.0109
0.35	0.023	0.0227	0.0225
0.38	0.0462	0.0459	0.0456
0.39	0.0671	0.0668	0.0666
0.40	0.119	0.118	0.118
0.41	—	—	—

Table 4.1: Calculated displacement values

Using node 5 as the reference, the computed values in the above table for the two different values of β are plotted in Figure 4.6. In can be seen from the figure that the characteristics of these two plotted graphs are very similar, and they both give rise to the same asymptotic value. This asymptotic value is taken as the computed critical load of the pin-jointed column. It shows that the critical load is independent of the values of β, provided of course that the value of β remains very small, and the computed critical load agrees with the theoretical solution provided by Euler's formula. It can be shown that similar graphs will be obtained if values for other nodes are used.

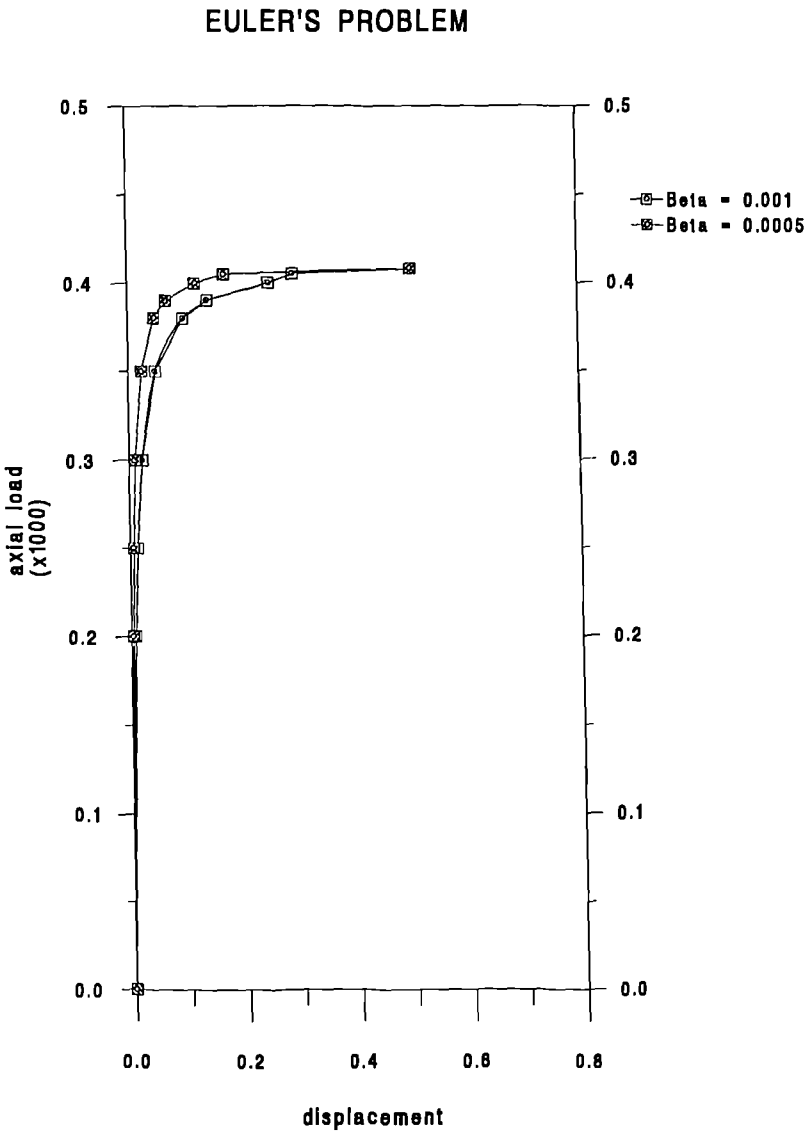

Figure 4.6: Column buckling - prediction of critical load of the beam

If the program is run when the small displacement theory is used instead, a similar buckling characteristic will occur. However, it has been found that the displacement at each increment step is linear, and is also linearly proportional to the axial stress applied to the top free hand. Therefore, when the displacement-load graph is plotted, it would only be possible to obtain a straight line which shows that it would be impossible for the small displacement theory to predict collapse, even when the thin column is under large axial stress, as shown in Figure 4.7.

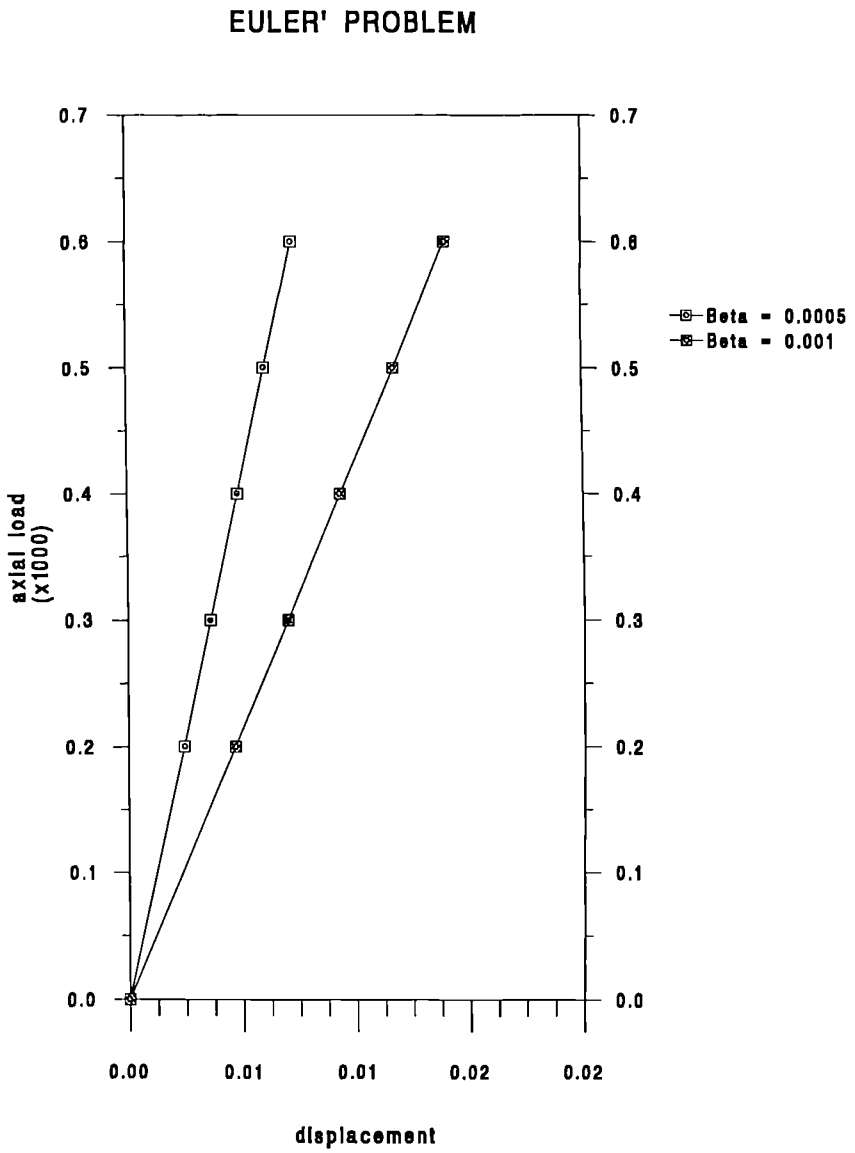

Figure 4.7: Column buckling using small displacement analysis

4.6 Conclusions and discussions

In this chapter, the standard finite element method for eight-noded parametric elements for two-dimensional elasticity problem has been extended to deal with nonlinear geometric behaviour. The main feature of this large displacement formulation is the use of a simple and easy to understand iterative method to calculate the residual load of the incremental equilibrium equation. This algorithm has been incorporated fully into the program and is used as a standard procedure.

This algorithm seems to be quite effective for most applications. However, its drawback can be fully seen when it is required to calculate the critical load, or to predict the collapse of the object. The number of iterations required to perform this analysis is simply too large to be efficient. Further, there is no algorithm or valid error analysis to predict the collapse of the object, ie. to show when the critical load has been exceeded. It can only be observed when the residual load fails to converge during the iteration process. This procedure is unreliable and is too time consuming. In order to enhance the appeal of the method, attempts will be made in Chapter 9 to investigate a different but more efficient approach to deal with residual loads.

The large displacement analysis presented in this chapter assumes linear behaviour of structures, and the medium which it is applied on is modelled by eight-noded isoparametric elements. An immediate extension of this theory would be to adapt it to three-dimensional problems, perhaps together with nonlinear material characteristic. Further, as one of the main features of the finite element method is to allow the structure to be represented in a mesh of different types of element, it would be appropriate to consider applying the theory to other types of element. The latter is the aim of the chapters that follow.

Chapter 5

Implementation of Bar Element in Finite Element Analysis

5.1 Introduction

In the last two chapters, the theory for both small and large displacement formulations has been established for the use of eight-noded isoparametric quadrilateral elements in the finite element analyses of some plane stress and plane strain problems. In this analysis, all members forming the frame must be able to be discretised by eight-noded isoparametric elements, and although in some simple cases, this may be possible, it will be more effective if members of different shapes can also be discretised by other more relevant types of elements. For example, a bar element is an ideal element to model structures which are one-dimensional and are infinitely thin such as rod, plane truss etc. It is also important in the development of finite element models of rockbolts.

One of the main problems with using different types of elements inside a mesh is that algorithms for these elements must be compatible within the solution procedure framework of the whole structure, and that they can be implemented in a computer program. With this requirement in mind, the theory established in earlier chapters will be modified and adapted, so that algorithms for bar and other one-, two- and three-dimensional elements can be established with a similar approach.

In this chapter, the use of a three-noded one-dimensional bar element in both the small and large displacement analyses will be implemented to analyse similar elasticity problems that involve thin rods. It should be noted that, in the bar element discretization of a thin

rod, the element couples longtitidinal strain with shear strain, but it does not any bending stiffness. This phenonemon features throughout this chapter.

Throughout this chapter, the cartesian derivative of the shape function N_i is denoted by N_i', and the coordinates in the rotated axes by x' and y'.

5.2 Geometry of a three-noded bar element

A two-noded bar element and a three-noded bar element share the same characteristics. Therefore, for the purpose of illustration, only the three-noded bar element is described here.

Suppose that a thin bar is discretised by a number of bar elements. The geometry of a standard three-noded one-dimensional element is shown in Figure 5.1. Initially, the bar element lies along the global axis x.

When loading is applied to the thin rod, the rod deforms and at some stage, it causes the bar element to move its local axes to x' and y', (with x' coincident with the bar's axis ξ), which are inclined at an angle of β to its original axes. This one-dimensional element allows variation only in the ξ direction, so that $\frac{\partial u'}{\partial y'} = \frac{\partial v'}{\partial y'} = 0$. This element is of length L, and each node has two translational degrees of freedom. The nodes are located at $\xi = -1, 0 + 1$, and the bar extends from $x' = 0$ to $x' = L$ (see Figure 5.2).

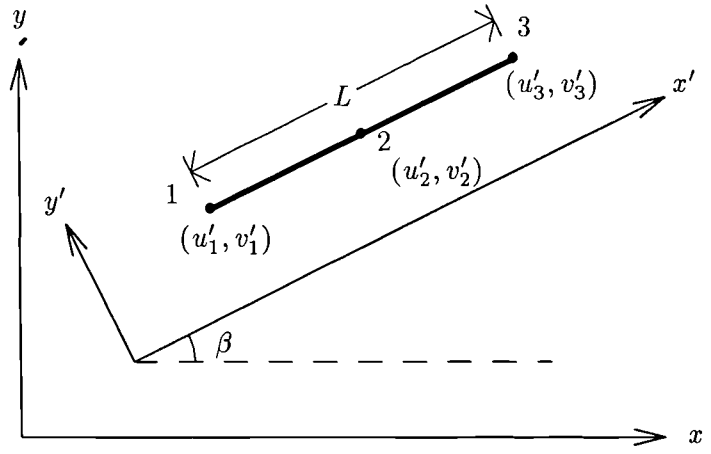

Figure 5.1: General geometry of a three-noded bar element in a rotated axis

From this figure, it can be seen that the relationship between any local displacements

u' and v', and the global displacements u and v can be expressed in matrix form

$$\mathbf{U}' = \mathbf{Q}\,\mathbf{U} \tag{5.1}$$

where $\mathbf{U} = (u,\, v)^T$ and $\mathbf{U}' = (u',\, v')^T$ and $\mathbf{Q}$ is the rotation matrix

$$\mathbf{Q} = \begin{bmatrix} \cos\beta & \sin\beta \\ -\sin\beta & \cos\beta \end{bmatrix} \tag{5.2}$$

To evaluate this angle β for a three-noded one-dimensional bar element, let

$$a_x = \sum_{i=1}^{3} N_i'(\xi)\, x_i, \qquad \text{and} \qquad a_y = \sum_{i=1}^{3} N_i'(\xi)\, y_i,$$

where N_i' is defined as the derivative of the shape function for the bar element

$$N_i' = \frac{dN_i}{dx'} = \frac{dN_i}{d\xi}\,\frac{d\xi}{dx'}.$$

Then, β can be found from the relationship

$$\sin\beta = \frac{a_y}{\sqrt{{a_x}^2 + {a_y}^2}} \qquad \text{or} \qquad \cos\beta = \frac{a_x}{\sqrt{{a_x}^2 + {a_y}^2}} \tag{5.3}$$

A proof of this relationship can be found in Chapter 7.

5.3 Small Displacement Analysis

To develop some new formulations for a three-noded one-dimensional bar element in small displacement analysis, recall that the linear $\mathbf{B}$ matrix for a two-dimensional, eight-noded isoparametric element e is

$$\mathbf{B}^e = [\mathbf{B}_1\ \ \mathbf{B}_2\ \cdots\ \mathbf{B}_8], \tag{5.4}$$

where for each node i in this element,

$$\mathbf{B}_i = [\mathbf{B}]_i = \begin{bmatrix} \frac{\partial N_i}{\partial x} & 0 \\ 0 & \frac{\partial N_i}{\partial y} \\ \frac{\partial N_i}{\partial y} & \frac{\partial N_i}{\partial x} \end{bmatrix}, \tag{5.5}$$

while the elasticity matrix $\mathbf{D}$ for plane stress is

$$\mathbf{D} = \frac{E}{1-\nu^2}\begin{bmatrix} 1 & \nu & 0 \\ \nu & 1 & 0 \\ 0 & 0 & \frac{1-\nu}{2} \end{bmatrix}, \tag{5.6}$$

and for plane strain,

$$\mathbf{D} = \frac{E(1-\nu)}{(1+\nu)(1-2\nu)} \begin{bmatrix} 1 & \frac{\nu}{(1-\nu)} & 0 \\ \frac{\nu}{(1-\nu)} & 1 & 0 \\ 0 & 0 & \frac{1-2\nu}{2(1-\nu)} \end{bmatrix}. \tag{5.7}$$

Suppose the Young's modulus and shear modulus of the bar are respectively E_b and G_b. The normal stress and strain in the bar can be defined by

$$\sigma_{x'}{}^b = E_b \, \epsilon_{x'}{}^b \tag{5.8}$$

where

$$\epsilon_{x'}{}^b = -\frac{du_b{}'}{dx'} = -\sum_{i=1}^{3} N_i'(\xi)\, u_i' \tag{5.9}$$

The shear stress and strain are related by the simple form

$$\tau_{x'y'}{}^b = G^b \, \nu_{x'y'}{}^b$$

where

$$\nu_{x'y'}{}^b = -\frac{dv_b{}'}{dx'} = -\sum_{i=1}^{3} N_i'(\xi)\, v_i' \tag{5.10}$$

As described in earlier chapters, the displacement, strain and stress in local axis are related by the equations

$$\epsilon = \mathbf{B}' \, \mathbf{U}' \tag{5.11}$$

and

$$\sigma = \mathbf{D}\, \epsilon \tag{5.12}$$

where in the element e,

$$\epsilon = (\epsilon_{x'}{}^b \;\; \gamma_{x'y'}{}^b)^T \qquad \text{and} \qquad \sigma = (\sigma_{x'}{}^b \;\; \tau_{x'y'}{}^b)^T$$

By comparing equations (5.4) to (5.8), the matrices $\mathbf{B}'$ and $\mathbf{D}$ for the bar element become

$$\mathbf{B}' = \begin{bmatrix} -N_1{}' & 0 & -N_2{}' & 0 & -N_3{}' & 0 \\ 0 & -N_1{}' & 0 & -N_2{}' & 0 & -N_3{}' \end{bmatrix} \tag{5.13}$$

and

$$\mathbf{D} = \begin{bmatrix} E_b & 0 \\ 0 & G_b \end{bmatrix} \tag{5.14}$$

where the values of E_b and G_b can be taken as

$$E_b = E\,, \qquad \text{and} \qquad G_b = \frac{E}{2(1+\nu)},$$

and the derivative of the shape function in local axis in $\mathbf{B}'$ can be found by

$$N_i' = \frac{dN_i}{dx'} = \frac{dN_i}{d\xi}\,\frac{d\xi}{dx'}.$$

For example, in a three-noded bar element, the relationship between x' and ξ is

$$x' = \frac{(\xi+1)L}{2},$$

and hence

$$N_i' = \frac{2}{L}\,\frac{dN_i}{d\xi}.$$

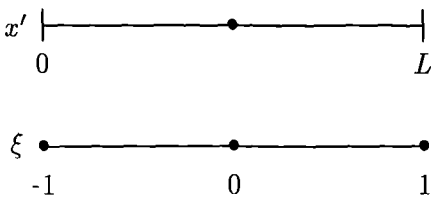

Figure 5.2: Relationship between x' and ξ for a three-noded bar element

Following equation (5.11), the displacement and strain in the local and global axes are related by the matrix equation

$$\begin{aligned}\epsilon &= \mathbf{B}'\,\mathbf{U}' = \sum_i [\mathbf{B}']_i \mathbf{U}_i' \\ &= \sum_i [\mathbf{B}']_i\,\mathbf{Q}\,\mathbf{U}_i = \sum_i [\mathbf{B}]_i \mathbf{U}_i,\end{aligned} \tag{5.15}$$

with

$$[\mathbf{B}']_i = \begin{bmatrix} N_i' & 0 \\ 0 & N_i' \end{bmatrix},$$

since the two element matrices $[\mathbf{B}_i]$ and $[\mathbf{B}']_i$ in the global and the local axes respectively are related by

$$[\mathbf{B}]_i = [\mathbf{B}']_i\,\mathbf{Q} \tag{5.16}$$

From this relationship and (5.13), the element $\mathbf{B}$ matrix can now be written in the form

$$\mathbf{B} = \begin{bmatrix} -N_1'\cos\beta & -N_1'\sin\beta & -N_2'\cos\beta & -N_2'\sin\beta & -N_3'\cos\beta & -N_3'\sin\beta \\ N_1'\sin\beta & -N_1'\cos\beta & N_2'\sin\beta & -N_2'\cos\beta & N_3'\sin\beta & -N_3'\cos\beta \end{bmatrix} \tag{5.17}$$

with its associated element displacement vector

$$\mathbf{u} = (u_1 \;\; v_1 \;\; u_2 \;\; v_2 \;\; u_3 \;\; v_3)^T.$$

With this element $\mathbf{B}$ matrix, the usual operation $\int_\Omega \mathbf{B}^T\mathbf{D}\mathbf{B}\; d\Omega$ will give rise to the element stiffness matrix. This formulation can then be used to calculate the deformation of the linear bar, as described earlier.

5.4 Large Displacement Analysis

The derivation of nonlinear stiffness matrices is necessary for analysing large deflection and stability problems. This study has been underway since 1958, but only a portion of the early work has appeared in general technical literature. In 1960, Turner *et al* took the first major step by considering incremental steps and a new class of stiffness matrices associated with geometric nonlinear problems. Since then, attention has also been turned to analyse large deflection problems of one-dimensional elements. However, most of these works focused on the representation of column by beam elements, but very little work has been done on bar element discretization.

The goal of the next section is to carry forward the various formulations that have been derived in the last chapter for a standard two-dimensional, eight-noded isoparametric element, and to propose a modification to form a nonlinear stiffness matrix for a one-dimensional bar element for large displacement analysis. This suggested formulation will then be applied to some practical everyday problems to illustrate its use and its deficiencies in soil mechanics.

5.4.1 Derivation of a nonlinear element stiffness matrix

From the last chapter, it can be recalled that in the large displacement analysis for eight-noded isoparametric quadrilateral elements, the nonlinear incremental strain matrix $\delta\mathbf{B}_{NL}$ at node i has been established in equation (4.27), and it can be written in the form

$$[\delta\mathbf{B}_{NL}]_i = \begin{bmatrix} \frac{\partial \delta u_n}{\partial x}\frac{\partial N_i}{\partial x} & \frac{\partial \delta v_n}{\partial x}\frac{\partial N_i}{\partial x} \\ \frac{\partial \delta u_n}{\partial y}\frac{\partial N_i}{\partial x} & \frac{\partial \delta v_n}{\partial y}\frac{\partial N_i}{\partial y} \\ \frac{\partial \delta u_n}{\partial y}\frac{\partial N_i}{\partial x} + \frac{\partial \delta u_n}{\partial x}\frac{\partial N_i}{\partial y} & \frac{\partial \delta v_n}{\partial y}\frac{\partial N_i}{\partial x} + \frac{\partial \delta v_n}{\partial x}\frac{\partial N_i}{\partial y} \end{bmatrix} \tag{5.18}$$

For a one-dimesional bar element along the axis x, the following can be assumed:

$$\frac{\partial u_n}{\partial y} = 0, \qquad \frac{\partial \delta v_n}{\partial y} = 0, \qquad \text{etc.} \tag{5.19}$$

Consequently, when the bar element is lying in the local coordinates x', equation (5.18) can be modified to

$$[\delta\mathbf{B}'_{NL}]_i^T = \begin{bmatrix} \frac{\partial \delta u_n'}{\partial x'}\frac{\partial N_i}{\partial x'} & \frac{\partial \delta v_n'}{\partial x'}\frac{\partial N_i}{\partial x'} \\ 0 & 0 \end{bmatrix}^T$$

$$= \begin{bmatrix} N_i' & 0 \\ 0 & N_i' \end{bmatrix} \begin{bmatrix} \frac{\partial \delta u_n'}{\partial x'} & 0 \\ \frac{\partial \delta v_n'}{\partial x'} & 0 \end{bmatrix}$$

$$= [\mathbf{G}]_i^T [\delta \mathbf{A}]_i^T \tag{5.20}$$

Therefore, it can be observed that

$$[\delta \mathbf{B}'_{NL}]_i^T \sigma_i = [\mathbf{G}]_i^T [\delta \mathbf{A}]_i^T \sigma_i = [\mathbf{G}]_i^T \begin{bmatrix} \frac{\partial \delta u_n'}{\partial x'} \sigma_x \\ \frac{\partial \delta v_n'}{\partial x'} \sigma_x \end{bmatrix} \qquad \text{since} \qquad \sigma = (\sigma_x \ \tau_{xy})^T$$

$$= [\mathbf{G}]_i^T \begin{bmatrix} N_i'\sigma_x & 0 \\ 0 & N_i'\sigma_x \end{bmatrix} \begin{bmatrix} \delta u_i' \\ \delta v_i' \end{bmatrix}$$

$$= [\mathbf{G}]_i^T \sigma_x \mathbf{I} [\mathbf{G}]_i \delta \mathbf{u}_i'$$

$$= [\mathbf{G}]_i^T \mathbf{M} [\mathbf{G}]_i \mathbf{Q} \delta \mathbf{u}_i \qquad \text{since} \qquad \delta \mathbf{u}_i' = \mathbf{Q} \delta \mathbf{u}_i \tag{5.21}$$

where

$$[\mathbf{G}]_i = \begin{bmatrix} N_i' & 0 \\ 0 & N_i' \end{bmatrix}$$

and

$$\mathbf{M} = \sigma_x \mathbf{I}$$

Analogous to (5.16), the incremental nonlinear matrices in different coordinate systems are related by

$$[\delta \mathbf{B}_{NL}]_i = [\delta \mathbf{B}'_{NL}]_i \mathbf{Q} \tag{5.22}$$

Combining equations (5.21) and (5.22), it can be seen that in the global coordinates,

$$[\delta \mathbf{B}_{NL}]_i^T \sigma_i = [\delta \mathbf{B}'_{NL} \mathbf{Q}]_i^T \sigma_i = \mathbf{Q}^T [\delta \mathbf{B}'_{NL}]_i^T \sigma_i$$

$$= \mathbf{Q}^T [\mathbf{G}]_i^T \mathbf{M} [\mathbf{G}]_i \mathbf{Q} \delta \mathbf{u}_i = [\widehat{\mathbf{G}}]_i^T \mathbf{M} [\widehat{\mathbf{G}}]_i \delta \mathbf{u}_i \tag{5.23}$$

where

$$[\widehat{\mathbf{G}}]_i = [\mathbf{G}]_i \mathbf{Q} = \begin{bmatrix} N_i' \cos\beta & N_i' \sin\beta \\ -N_i' \sin\beta & N_i' \cos\beta \end{bmatrix} \tag{5.24}$$

From the earlier chapters on the use of the eight-noded isoparametric quadrilateral element in the finite element method, the nonlinear **B** matrix for node i has been established, and it can be written in the form

$$[\mathbf{B}]_i = [\mathbf{B}_L]_i + [\mathbf{B}_{NL}]_i$$

$$
\begin{aligned}
&= \begin{bmatrix} \frac{\partial N_i}{\partial x} & 0 \\ 0 & \frac{\partial N_i}{\partial y} \\ \frac{\partial N_i}{\partial y} & \frac{\partial N_i}{\partial x} \end{bmatrix} + \begin{bmatrix} \frac{\partial u_n}{\partial x}\frac{\partial N_i}{\partial x} & \frac{\partial v_n}{\partial x}\frac{\partial N_i}{\partial x} \\ \frac{\partial u_n}{\partial y}\frac{\partial N_i}{\partial y} & \frac{\partial v_n}{\partial y}\frac{\partial N_i}{\partial y} \\ \frac{\partial u_n}{\partial y}\frac{\partial N_i}{\partial x} + \frac{\partial u_n}{\partial x}\frac{\partial N_i}{\partial y} & \frac{\partial v_n}{\partial y}\frac{\partial N_i}{\partial x} + \frac{\partial v_n}{\partial x}\frac{\partial N_i}{\partial y} \end{bmatrix} \\
&= [\mathbf{B}_0]_i \, \mathbf{J}_D \qquad (5.25)
\end{aligned}
$$

where

$$
\mathbf{J}_D = \begin{bmatrix} \frac{\partial x_n}{\partial x} & \frac{\partial y_n}{\partial x} \\ \frac{\partial x_n}{\partial y} & \frac{\partial y_n}{\partial y} \end{bmatrix} \qquad (5.26)
$$

The relationships between displacements given in (4.17) can be modified to the form

$$
u_n = x_n - x_0, \qquad v_n = y_n - y_0
$$

and

$$
\frac{\partial x_0}{\partial x} = 1, \qquad \frac{\partial y_0}{\partial y} = \frac{\partial x_0}{\partial y} = \frac{\partial y_0}{\partial x} = 0.
$$

Together with conditions (5.19), equation (5.25) can be simplified to give the **B** matrix for the one-dimensional bar element for node i along the local coordinates x', *viz.*

$$
\begin{aligned}
[\mathbf{B}']_i &= \begin{bmatrix} N_i' & 0 \\ 0 & N_i' \end{bmatrix} + \begin{bmatrix} \frac{\partial u_n'}{\partial x'} N_i' & \frac{\partial v_n'}{\partial x'} N_i' \\ 0 & 0 \end{bmatrix} \\
&= \begin{bmatrix} N_i' \frac{\partial x_n'}{\partial x'} & N_i' \frac{\partial y_n'}{\partial x'} \\ 0 & N_i' \end{bmatrix} \\
&= \begin{bmatrix} N_i' & 0 \\ 0 & N_i' \end{bmatrix} \begin{bmatrix} \frac{\partial x_n'}{\partial x'} & \frac{\partial y_n'}{\partial x'} \\ 0 & 1 \end{bmatrix} \\
&= [\mathbf{B}_0'] \, \mathbf{J}_D' \qquad (5.27)
\end{aligned}
$$

where

$$
\mathbf{J}_D' = \begin{bmatrix} \frac{\partial x_n'}{\partial x'} & \frac{\partial y_n'}{\partial x'} \\ 0 & 1 \end{bmatrix} \qquad (5.28)
$$

From the stress-displacement relationship $\epsilon' = \mathbf{B}' \, \mathbf{U}'$ and (5.27), it can be seen that

$$
\epsilon_{x'} = \sum (N_i' \, u_i' + \frac{\partial u_n'}{\partial x'} N_i' \, u_i' + \frac{\partial v_n'}{\partial x'} N_i' \, v_i') \qquad (5.29)
$$

and

$$
\nu_{x'y'} = \sum N_i' \, v_i' \qquad (5.30)
$$

where the shape functions N_i for the three-noded one-dimensional bar element are now dependent only on x', with

$$\left.\begin{aligned} N_1(\xi) &= \tfrac{1}{2}\xi(\xi-1) \\ N_2(\xi) &= 1-\xi^2 \\ N_3(\xi) &= \tfrac{1}{2}\xi(\xi+1) \end{aligned}\right\} \qquad (5.31)$$

with

$$x' = \frac{(\xi+1)L}{2}, \qquad \text{and} \qquad N_i' = \frac{dN_i}{dx'}.$$

From the displacement function $x_n = \sum N_i\, x_i$, the term $\dfrac{\partial {x_n}'}{\partial x'}$ can be evaluated by the equation

$$\frac{\partial {x_n}'}{\partial x'} = \sum N_i'\, {x_i}' = \sum N_i' (x_i \cos\beta + y_i \sin\beta).$$

Once the element stiffness matrix is formed, incremental steps and iterations on residuals to refine the results could be carried out. Algorithms and procedures to perform these are exactly the same as the one described in the previous chapter for eight-noded isoparametric element.

Because the movement of the bar element is dependent upon ξ only, this one-dimensional analysis can greatly reduce the number of computations involved in the program, and formulations for bar elements seem to be a lot easier to implement than before. However, when the small and the large displacement formulations are used in some practical examples, the results thus obtained show that both analyses are far from being ideal. To illustrate the weaknesses of these algorithms, a simple example is described in the next section.

5.5 An example

To explore how the theory derived above for a bar element can be implemented, a worked example and a practical example are being used below.

5.5.1 A worked example

In this worked example, the stiffness matrix of a bar element will be worked out by the exact finite element calculation as described in earlier sections.

A uniform thin rod of length L and radius r is placed horizontally in its plane of symmetry as shown in Figure 5.3(a). It is fixed at one end, and at the other end (which is

free to move in both x and y directions), a point load P is applied vertically downwards. The thin rod is modelled by a number of three-noded bar elements.

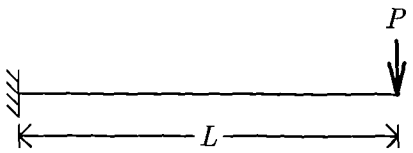

(a) thin rod

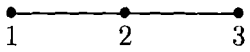

(b) bar element discretization of thin rod

Figure 5.3: Deflection of thin rod

Consider a particular bar element e. Suppose it is of length l. With the shape functions given in (5.31) for a three-noded bar element, the $\mathbf{B}^e$ matrix from (5.13) becomes

$$\mathbf{B}^e = \begin{bmatrix} -\frac{1}{l}(2\xi-1) & 0 & \frac{4}{l}\xi & 0 & -\frac{1}{l}(2\xi+1) & 0 \\ 0 & -\frac{1}{l}(2\xi-1) & 0 & \frac{4}{l}\xi & 0 & -\frac{1}{l}(2\xi+1) \end{bmatrix},$$

so that the matrix product $\mathbf{B}^{eT}\mathbf{D}\mathbf{B}^e$ can be written as

$$\frac{1}{l^2}\begin{bmatrix} (2\xi-1)^2E & 0 & -4\xi(2\xi-1)E & 0 & (4\xi^2-1)E & 0 \\ 0 & (2\xi-1)^2G & 0 & -4\xi(2\xi-1)G & 0 & (4\xi^2-1)G \\ -4\xi(2\xi-1)E & 0 & 16\xi^2E & 0 & -4\xi(2\xi+1)E & 0 \\ 0 & -4\xi(2\xi-1)G & 0 & 16\xi^2G & 0 & -4\xi(2\xi+1)G \\ (4\xi^2-1)E & 0 & -4\xi(2\xi+1)E & 0 & (2\xi+1)^2E & 0 \\ 0 & (4\xi^2-1)G & 0 & -4\xi(2\xi+1)G & 0 & (2\xi+1)^2G \end{bmatrix}.$$

The stiffness matrix for this element can be obtained from the integration

$$\int\int_\Omega \mathbf{B}^{eT}\mathbf{D}\mathbf{B}^e \, d\Omega,$$

while the load vector (for the element at the free end) is

$$\mathbf{F}^e = (0 \;\; 0 \;\; 0 \;\; 0 \;\; 0 \;\; -P)^T.$$

To perform this integration analytically, the first entry, for example, can be obtained by the operation

$$\frac{1}{l^2}\int_0^l (2\xi-1)^2 E\, A\, dx = \frac{AE}{l^2}\int_{-1}^1 (2\xi-1)^2 \frac{l}{2}\, d\xi = \frac{7AE}{3l}, \qquad \text{where} \qquad A = \pi r^2.$$

Likewise, other entries in the matrix can be found, and hence the element stiffness matrix becomes

$$\mathbf{K}^e = \frac{A}{3l}\begin{bmatrix} 7E & 0 & -8E & 0 & E & 0 \\ 0 & 7G & 0 & -8G & 0 & G \\ -8E & 0 & 16E & 0 & -8E & 0 \\ 0 & -8G & 0 & 16G & 0 & -8G \\ E & 0 & -8E & 0 & 7E & 0 \\ 0 & G & 0 & -8G & 0 & 7G \end{bmatrix}.$$

If a two-point Gaussian quadrature rule is used to numerically integrate the matrix product $\mathbf{B}^{eT}\mathbf{D}\mathbf{B}^e$ term by term, the result would be very similar, as, for example,

$$\begin{aligned}\int_{-1}^{1}(2\xi-1)^2\,d\xi &\simeq (2\times(-0.5773502)-1)^2+(2\times(0.5773502)-1)^2 \\ &= 4.6666666 \text{ (correct to 7d.p.)},\end{aligned}$$

which explains why this numerical method for integration is accurate when the integrand is of lower degree.

After assembling all element stiffness matrices to form a global stiffness matrix for the whole mesh, the stiffness equation becomes

$$\mathbf{K}\,\mathbf{u} = \mathbf{f}.$$

For a one-element mesh, the finite element solution can be obtained by solving the matrix equation

$$\frac{A}{3l}\begin{bmatrix} 7E & 0 & -8E & 0 & E & 0 \\ 0 & 7G & 0 & -8G & 0 & G \\ -8E & 0 & 16E & 0 & -8E & 0 \\ 0 & -8G & 0 & 16G & 0 & -8G \\ E & 0 & -8E & 0 & 7E & 0 \\ 0 & G & 0 & -8G & 0 & 7G \end{bmatrix}\begin{bmatrix} u_1 = 0 \\ v_1 = 0 \\ u_2 \\ v_2 \\ u_3 \\ v_3 \end{bmatrix} = \begin{bmatrix} R_x \\ R_y \\ 0 \\ 0 \\ 0 \\ -P \end{bmatrix} \tag{5.32}$$

where R_x and R_y are the respective horizontal and vertical components of the reaction force acting at node 1.

As the horizontal displacements for the three nodes are zero, i.e. $u_1 = u_2 = u_3 = 0$,

equation (5.32) reduces to

$$\frac{AG}{3l}\begin{bmatrix} 7 & -8 & 1 \\ -8 & 16 & -8 \\ 1 & -8 & 7 \end{bmatrix}\begin{bmatrix} 0 \\ v_2 \\ v_3 \end{bmatrix} = \begin{bmatrix} R_y \\ 0 \\ -P \end{bmatrix}$$

which gives a solution of $v_3 = -\frac{Pl}{AG}$. This is analogous to the displacement solution of a similar uniform bar when an axial load P is applied directly at its end.

The analytic solution for the deflection at the free end of a beam of length L is (Meek 1971):

$$v = -\frac{PL^3}{3EI} - \frac{6PL}{5AG}, \tag{5.33}$$

where the first term is the displacement due to bending, and the second is the displacement due to shear. In the latter term, a parabolic distribution of shear stress over the beam cross-section is assumed; if a uniform distribution of shear stress is used instead, the displacement due to shear is identical to that derived from the finite element analysis above.

5.5.2 Deflection of a thin bar partly embedded in ground

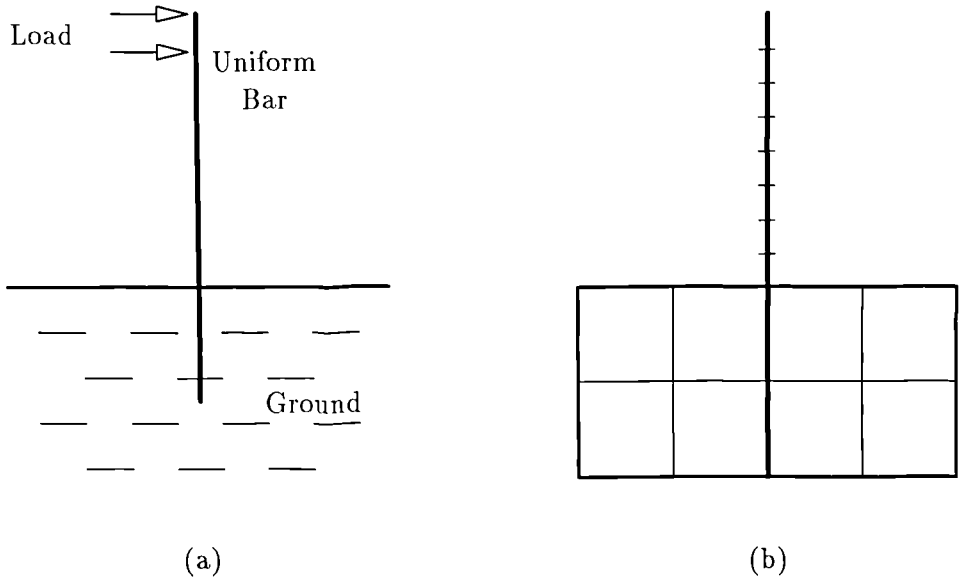

Figure 5.4: Thin bar partly embedded in ground

Consider a slender long cylindrical rod of uniform cross-section, partly embedded in an even ground. To set up the problem, it is assumed that the free end of the rod and the part that is embedded in the ground is free to move in both x and y directions. The whole

rod is rigidly fixed at its lowest end point which is inside the ground soil, as shown in Figure 5.4(a). The entire rod and the ground soil are taken to be homogeneous, isotropic and linearly elastic throughout.

In order to show how the rod will deform when it is discretised by bar elements, its free end is subject to different types of loadings, and the Young's modulus of the rod is taken to be much larger than that of the ground soil, so that the rod is modelled to be made up of a much stiffer material.

For finite element discretization, the rod is modelled by a total of ten bar elements; the free end that is above the ground is modelled by eight shorter, but identical, bar elements, while the part that is embedded in the ground is modelled by two identical bar elements. All bar elements are rigidly joined together to form a uniform long rod. The ground soil is modelled by eight identical eight-noded isoparametric quadrilateral elements. The finite element mesh used in this model is shown in Figure 5.4(b).

Different types of loading are applied perpendicularly from the left to the free end of the rod. Using the small displacement analysis discussed in this chapter and executed by the computer, the following is observed:

1. *Point Load*

   A single point load is applied to the top end of the rod. Figure 5.5 shows the results of the deformation when small displacement analysis is used.

   The results show that the deformation of the rod is divided into two parts; the part that is embedded in the ground, and also the ground soil, remain unperturbed by the loading, while the free end of the rod, ie. the part that is above the ground, is uniformly stressed and is deformed to a straight line. This example carries the characteristics of a thin rod with no moment of inertia and hence no bending stiffness, so that the loading has no effect on the embedded part and the ground soil.

   With a point load of magnitude 0.1×10^{-9}N, the numerical results obtained in this computation for the free end is -0.637×10^{-12}m, against the shear term of the theoretical results obtained by Meek in (5.33) of -0.636×10^{-12}m.

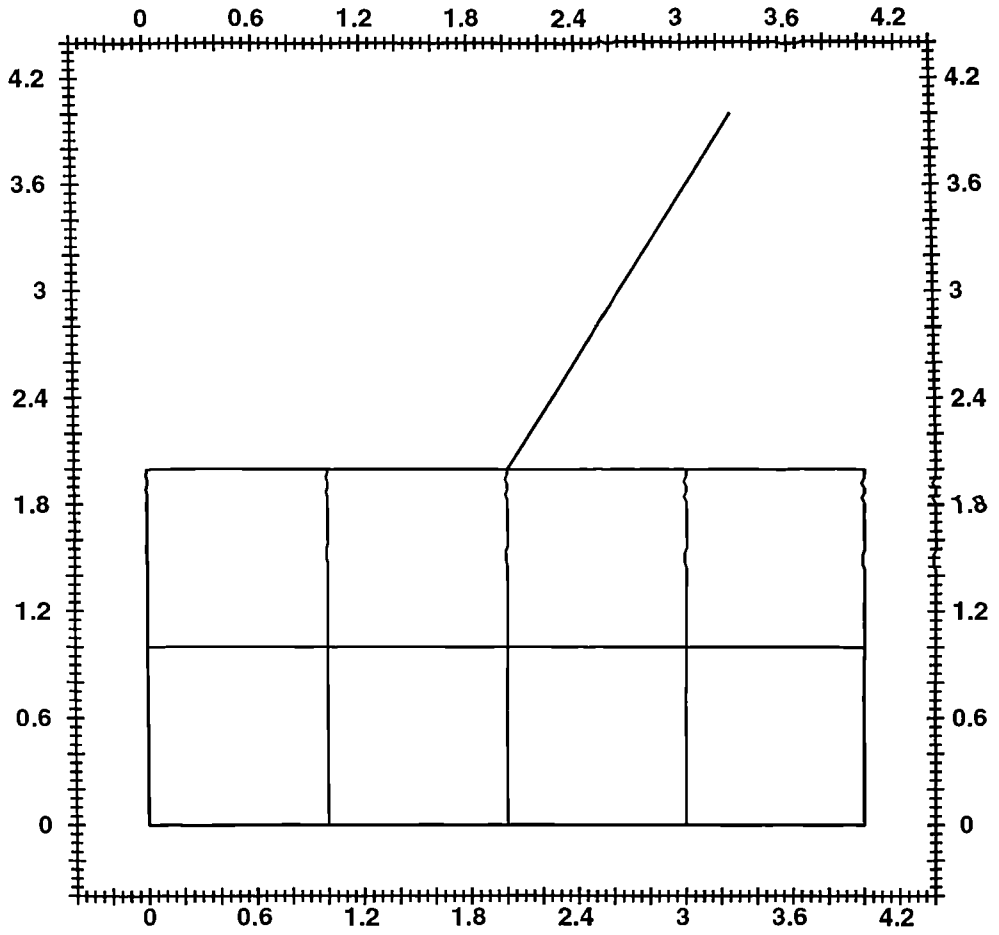

Figure 5.5: Deformation of a rod subject to a point load

To explore this further, different trial values of point loads are applied to the rod. The results shows that the deformation characteristics of the rod and the ground soil is the same as before. Indeed, if point loads are applied to any two points at the free end, the part of the rod that lie between these two points will be uniformly stressed and deformed to a straight line, and the slope of this straight line depends solely on the strength of the applied point loads, while the embedded part of the rod and the ground soil remain stationary (see Figure 5.6).

This behaviour does not reflect the natural curve bending phenomenon of a thin rod. The nodal deflection of a bar element can only provide a rigid body

translation for the element, but not the angular moments that may exist between elements. In order to produce a more realistic deformation, additional rotational degrees of freedom must be incorporated with some nodes of an element. This range of elements will be discussed in full in the next chapter.

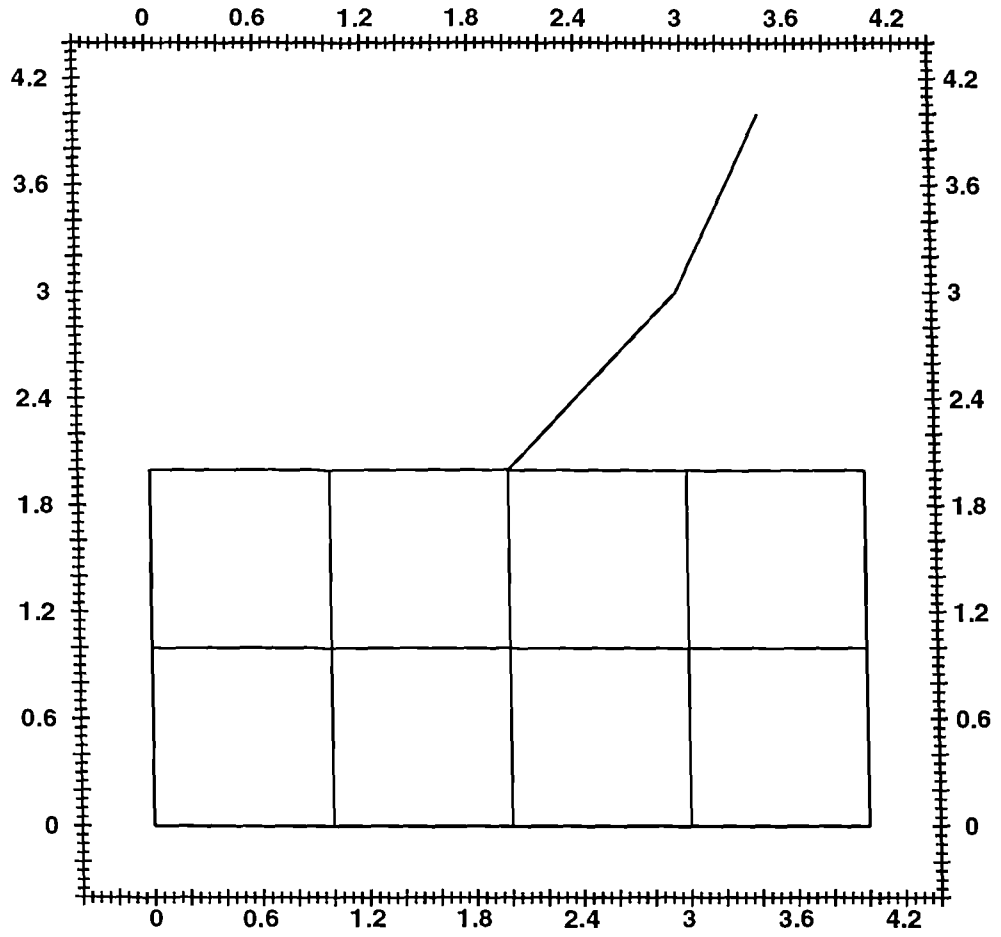

Figure 5.6: Deformation of a rod subject to two identical point loads

2. *Uniform Surface Traction*

Surface traction is applied uniformly and perpendicularly to the whole of the free end of the rod above the ground. Figure 5.7 shows the deformation of the rod and the ground when small displacement analysis is used.

Although the rod exhibits a more natural bending action at the free end, it is

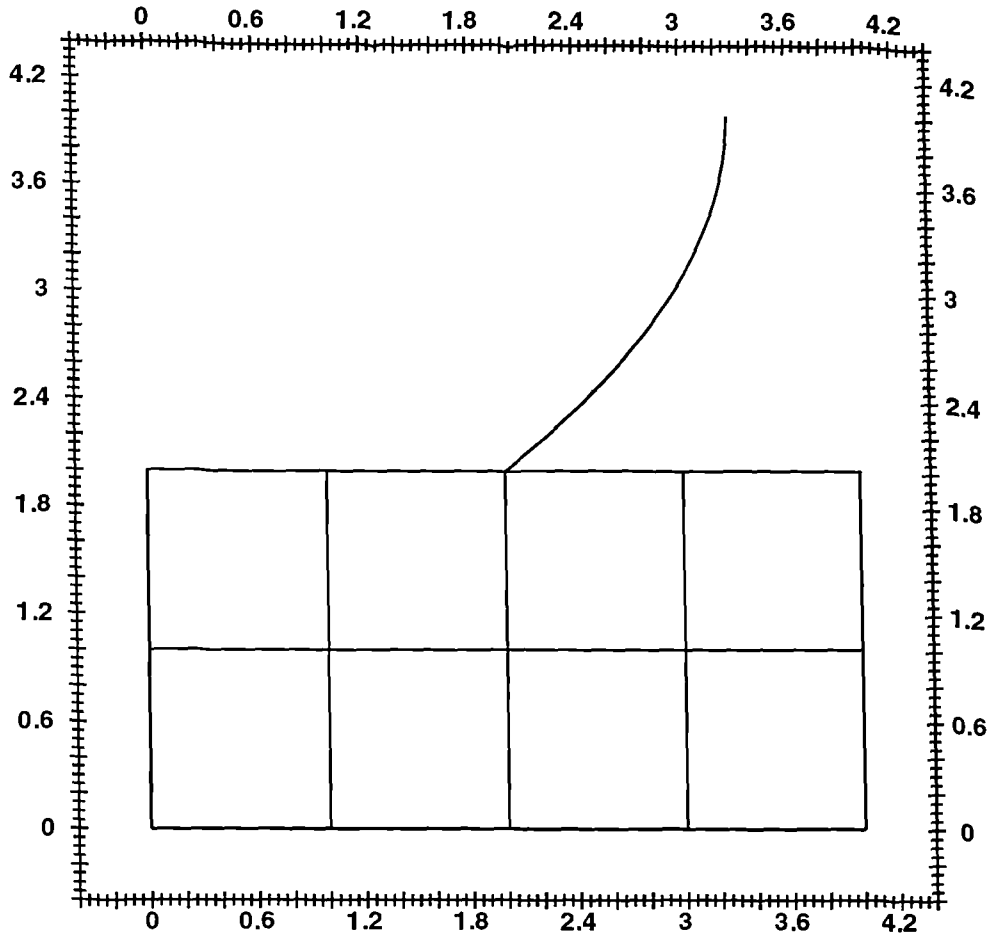

Figure 5.7: Deformation of a rod subject to uniform surface traction

attributed mainly because uniform traction is applied. Any angular moments that may exist between elements are still absent. Further, the embedded rod and the ground soil remain unmoved. This situation is similar to the above case when a point load is applied, and the rod still behaves like a pin-jointed truss. This type of rod element could be used to model cable rockbolts (with some initial stress to represent pre-tensioning). It has also been used by Aydan and others as the bolt in an element modelling a grouted rockbolt; here, the linking of the end-nodes with the rock via the grout imposes a surface traction along its length. The results above lead us to conclude, however, that the absence of inter-element torsional stiffness makes the rod element a poor model for the steel bolt, and completely inadequate for ungrouted rockbolts.

Efforts have also been made to experiment with different number of increments with unequal steps, and it has been found that the results are very similar. It shows this analysis is independent of the number of load increments used.

The large displacement analysis has also been used in this example, but no improvement on the bending characteristics can be found. In fact, its results are basically in line with the one obtained by small displacement analysis. The only difference is that the displacements are slightly larger due to the nonlinear parts.

5.6 Conclusions

Bar elements with only tranlational degrees of freedom have been considered in this chapter, and it has been shown that with this restriction, members forming the frame are modelled to be pinned together at the connecting points, and no angular bending actions can take place if the members are assumed to be weightless and external loads are applied only at the joints. The members are then uniformly stressed in tension or compression. Further, bar element discretization does not allow the stress to be transmitted between elements, so that there is an obvious absence of inter-related stress and deformation. Thus the results obtained are very similar to the deformation of a plane truss or framework.

Nowadays, most connections in structural steelwork are bolted and welded. This will restrain the slight angular movement which, in a pin-jointed structure, tends to occur as the member lengths alter under the action of the axial forces, so that some secondary bending action will take place. This secondary bending will allow the structure to bend in a curved shape. To obtain this type of deformation, it is clear that the bar elements are not the ideal elements in the finite element discretization these structures. Therefore it calls for a different range of elements which can transmit not only forces, but also moments.

Chapter 6

Beam Element

6.1 Introduction

The analysis and design of linear elements supporting lateral loading is one of the most frequent tasks undertaken by the structural engineer. The resistance of a beam to lateral loads depends characteristically on the flexural stiffness and, in some cases, the torsion stiffness, of the member.

In the preceding chapters, it has been shown that under load, the bending exhibited by the quadrilateral and bar elements for rigid bodies and discrete elements of frame structures have only translational degrees of freedom, and therefore can only transmit forces directly from element to element, with the nodes effectively acting as pin joints.

This type of deformation cannot represent the normal bending phenomenon of a beam supporting a lateral load system. To obtain a more realistic solution, it is necessary to investigate the use of another very useful and important range of beam elements which can transmit not only forces, but also moments, by specifying both translational and rotational degrees of freedom at their end nodes. With these elements, the external reactions may be calculated from the overall equilibrium conditions. The internal shear forces and bending moments can then be determined for sections selected at intervals along the length of the beam. The fundamental engineering beam theory has been discussed in detail by Timoshenko and Goodier (1951), and some elementary theory and application of finite element discretization of beam by Ross (1990).

The aim of this chapter is to first of all examine the nature of bending under load in

beams, and then to investigate the relations between the factors which govern the behaviour of beams.

The beam element is important to the development of a rockbolt element. During the last decade, Aydan's (1989) type rockbolt element has been subject to much research in the finite element modelling of tunnelling. In its coupled form, the rockbolt element and its many modified forms use rod element to model the steel bolt. As it will be seen in this chapter, a beam element can make a substantial improvement over a bar element in the discretization of a thin rod in a bending problem, and it can give a more realistic bending characteristic. It can be envisaged that, if the steel bolt is modelled by a series of beam elements instead of bar elements, the characteristics of a rockbolt can be better represented by the new element. The investigation of this new type of rockbolt element is the main aim of this research.

6.1.1 An example - Bridge girder

A simple everyday example of this type of flexural deformation is a bridge girder, where the external loads imposed are due to the weight of the parts of the bridge supported by the girder, and the live loads from the traffic using the bridge. The system can be represented by a simple beam structure subjected to an equivalent but greatly simplified loading such as the one shown in Figure 6.1(a). The concentrated forces represent the load imposed on the girder by transverse members and vehicle wheels, and the uniformly distributed load allows for the self weight of the system. The reactive forces V_1 and V_2 are necessary to maintain the beam in a state of static equilibrium.

As the beam is made from material which deforms under load, it is clear that bending or flexure will occur, and the beam will take up some final deflected shape of the form shown in Figure 6.1(b). Of course the manner and the shape of the deformation depends on the strength of the material of the beam, the length and the thickness of the beam, the magnitude of the loads, and where these loads are applied.

The static analysis of rigid-jointed frames and continuous beams is one of the most important aspects of structural engineering. Rigid-jointed frames take many and varied forms, and appear in many different branches of engineering, varying from ships to aircrafts, and motor cars to offshore drilling rigs.

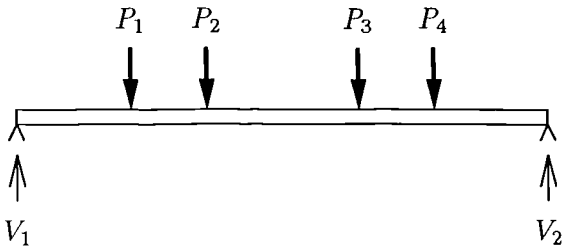

(a) Before loading

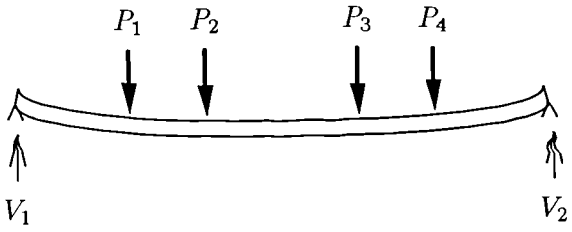

(b) After loading

Figure 6.1: Beam with bending moments

Most rigid-jointed frames can be modelled by a combination of different types of elements, including beam elements. With beam elements, rotational degrees of freedom are imposed on their end nodes, and hence bending moments are allowed to be transmitted through the elements to produce the natural curve bending phenomenon of a beam. Therefore structures such as thin rods can be satisfactorily modelled by this type of beam elements. In this chapter, the existing theory on small displacement of beam elements will be extended to develop a new large displacement formulation for the stiffness matrix of a two-noded beam element. Later, this theory will be adapted to three-noded beam elements.

6.2 Geometrical non-linearity

To investigate the deformation of an object under load, it is necessary to consider geometrically nonlinear behaviour, and in some cases, the material non-linearity, of the object.

The difficulty in applying the stiffness analysis to problems involving instability is that any compressive axial load on a structural member will tend to decrease its bending stiffness and vice versa for a tensile axial load. Thus, if a structural member is subject

to compressive axial load, buckling will occur when the bending stiffness is decreased, so that any small bending caused by the offset of the load will be larger than the bending resistance of the structure. This problem has been investigated in the Euler strut example in the large displacement theory for two-dimensional elements in Chapter 4. Such analysis is further complicated by the effects of material non-linearity where the stress in certain parts of the structure has exceeded the limit of proportionality.

In the matrix method of analysing the instability of such structures, it is usual to model the effects by adding a geometrical stiffness matrix to the linear stiffness matrix. The latter matrix usually considers the change of stiffness due to internal forces in the structure, thus imposing a nonlinear load-displacement relationship.

Therefore for each element, the resulting element stiffness matrix has to be modified to the form

$$[\mathbf{K}^e] = [\mathbf{K}_0^e] + [\mathbf{K}_G^e] \tag{6.1}$$

where $[\mathbf{K}_0^e]$ is a linear element stiffness matrix and $[\mathbf{K}_G^e]$ is the element geometrical stiffness matrix which depends on the internal forces in the element.

The total stiffness matrix in global coordinates is given by

$$[\mathbf{K}] = [\mathbf{K}_0] + [\mathbf{K}_G] \tag{6.2}$$

and the load-displacement relationship is

$$\mathbf{q} = ([\mathbf{K}_0] + [\mathbf{K}_G])\,\mathbf{u}_i \tag{6.3}$$

where

$[\mathbf{K}_0] = \Sigma[\mathbf{K}_0^e]$ is the system linear stiffness matrix in global coordinates, and
$[\mathbf{K}_G] = \Sigma[\mathbf{K}_G^e]$ is the system geometrical stiffness matrix in global coordinates.

In the last chapter, the process is carried out by a series of incremental loads, where the load is increased in small steps and the effects of geometrical nonlinearity are considered for each step and summed together to give the overall effect at the end of each step. This incremental step procedure was introduced by Turner *et al* (1960), and it has since been implemented for all geometrical nonlinear finite element analyses.

As in previous chapters, the problem concerning nonlinearity within the elastic limit will be considered. Therefore there is no material nonlinearity, and this nonlinearity comes only from the strain-displacement equation.

6.3 Geometrical stiffness matrix

While detailed computations of a two-dimensional element system are performed using the computer, a simple hand calculation on a one-dimensional finite element of the beam can be performed. This will allow the introduction of the concept of generalised stresses and strains in a simple but constructive manner.

In this chapter, efforts are concentrated on the development of an algorithm for two- and three-noded beam elements, which are the two types of beam element that will be used throughout this research project.

6.3.1 Two-noded beam element

In two-dimensional bending poblems, the simple Euler-Bernouilli theory assumes that the plane sections of the beam remain remain plane after bending, and that each longitudinal fibre of the beam behaves as if in uniaxial compression or tension independent of others.

Consider a two-noded beam element described in Figure 6.2. It is assumed for simplicity that the cross-section of the beam has a uniform area A (or uniform radius r), and is constant along the length of the beam. Further, it is assumed that the beam has modulus of elasticity E, Poisson ratio ν, and the beam element is of length L. The end nodes 1 and 2 are subject to shear forces and moments which result in translations and rotations, with nodal bending slopes θ_1 and θ_2 respectively. The element shown has flexural stiffness factor EI. It lies in the xy plane both before and after deformation takes place. Initially it is oriented along the x axis.

Here it will be necessary to consider both the axial displacement function of the beam, together with that in flexure, to simulate the bending effect.

The axial displacement function $u(x)$ is one-dimensional along the x direction. With

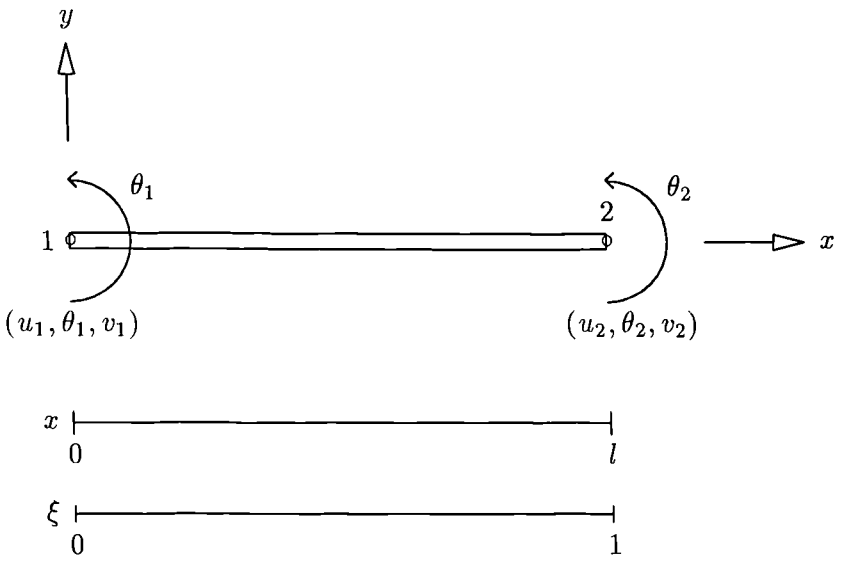

Figure 6.2: Two-noded beam element

the usual shape functions attached to a bar element, $u(x)$ can be represented by

$$u(x) = \sum_{i=1}^{2} N_i(\xi) u_i \tag{6.4}$$

where x and ξ are related by

$$\xi = \frac{x}{L}$$

and so

$$\frac{d\xi}{dx} = \frac{1}{L}.$$

However, due to the two extra rotational degrees of freedom, namely θ_1 and θ_2, that are introduced to the two end nodes of the beam element, the flexure function $v(x)$ in the y direction must satisfy the condition $\frac{dv}{dx} = \theta$, so it is necessary to introduce higher-degree shape functions $H_i(\xi)$ and $m_i(\xi)$ for all nodes i, and write

$$v(x) = \sum_{i=1}^{2} H_i(\xi) v_i + L \sum_{i=1}^{2} m_i(\xi) \theta_i. \tag{6.5}$$

To determine these shape functions for each i, it can be assumed that $N_i(\xi)$, $H_i(\xi)$ and $m_i(\xi)$ are of the forms

$$N_i(\xi) = a_0 + a_1 \xi$$

$$H_i(\xi) = b_0 + b_1 \xi + b_2 \xi^2 + b_3 \xi^3 \tag{6.6}$$

and

$$m_i(\xi) = c_0 + c_1 \xi + c_2 \xi^2 + c_3 \xi^3$$

where a_i, b_i, c_i are some constants to be determined by the constraints for the shape functions:

$$N_i(\xi_j) = \begin{cases} 1 & : \quad i = j \\ 0 & : \quad i \neq j \end{cases}$$

$$H_i(\xi_j) = \begin{cases} 1 & : \quad i = j \\ 0 & : \quad i \neq j \end{cases}$$

$$m_i(\xi_j) = \begin{cases} 0 & : \quad i = j \\ 0 & : \quad i \neq j \end{cases}$$

$$H_i'(\xi_j) = \begin{cases} 0 & : \quad i = j \\ 0 & : \quad i \neq j \end{cases}$$

and

$$m_i'(\xi_j) = \begin{cases} 1 & : \quad i = j \\ 0 & : \quad i \neq j \end{cases}$$

where $m_i'(\xi) = \dfrac{dm_i}{d\xi}$.

After some simple calculations, it can be shown that $N_i(\xi), H_i(\xi)$ and $m_i(\xi)$ can be taken as:

$$N_1(\xi) = 1 - \xi$$

$$N_2(\xi) = \xi$$

$$H_1(\xi) = 1 - 3\xi^2 + 2\xi^3$$

$$H_2(\xi) = 3\xi^2 - 2\xi^3 \tag{6.7}$$

and

$$m_1(\xi) = \xi - 2\xi^2 + \xi^3$$

$$m_2(\xi) = -\xi^2 + \xi^3$$

From the elementary beam theory, Martin (1966) formulated the nonlinear strain-displacement equation in the 'x' direction of any fibre at a distance 'y' from the neutral axis of the beam, by the equation

$$\epsilon_x = \frac{du}{dx} + \frac{1}{2}\left(\frac{dv}{dx}\right)^2 - \frac{d^2v}{dx^2}\, y \tag{6.8}$$

where

$\frac{1}{2}\left(\frac{dv}{dx}\right)^2$ is the additional strain due to large displacement deflection, and

$-\frac{d^2v}{dx^2}\,y$ is the bending contribution to the strain at a distance 'y' from the neutral axis.

The strain energy stored in the beam is given by

$$U_e = \frac{E}{2}\int_V \epsilon_x^2\, dV. \tag{6.9}$$

Substituting (6.8) into (6.9), the cubic and higher terms in (6.9) can be neglected. Further, since

$$\int_{-r}^{r} -2\,\frac{du}{dx}\,\frac{d^2v}{dx^2}\,y\,dy = 0,$$

it can be seen that

$$U_e = \frac{E}{2}\int_V \left\{\left(\frac{du}{dx}\right)^2 + \frac{du}{dx}\left(\frac{dv}{dx}\right)^2 + \left(\frac{d^2v}{dx^2}\right)^2 y^2\right\} dV. \tag{6.10}$$

For convenience, U_e in equation (6.10) can be written into two parts

$$U_e = U_1 + U_2$$

where

$$U_1 = \frac{EA}{2}\int_0^L \left\{\left(\frac{du}{dx}\right)^2 + \frac{du}{dx}\left(\frac{dv}{dx}\right)^2\right\} dx \tag{6.11}$$

and

$$\begin{aligned} U_2 &= \frac{E}{2}\int_V \left\{\left(\frac{d^2v}{dx^2}\right)^2 y^2\right\} dV \\ &= \frac{E}{2}\int_0^L \left(\frac{d^2v}{dx^2}\right)^2 \left(\int_V y^2\, dA\right) dx \\ &= \frac{EI}{2}\int_0^L \left(\frac{d^2v}{dx^2}\right)^2 dx \end{aligned} \tag{6.12}$$

with A as the cross-sectional area of the beam and EI as the flexural stiffness factor, where

$$I = \int_V y^2\, dA$$

represents the moment of inertia of the cross section of the beam with respect to the neutral axis.

For example, for a beam with elliptic cross section, $I = \frac{1}{4}\pi a^3 b$ where a and b are the major and minor axes respectively of the ellipse; with circular cross section with radius

r, $I = \frac{1}{4}\pi r^4$; and with rectangular cross section, $I = \frac{1}{12}cd^3$ where c is the width of the cross section the force is acting upon, and d is the depth of the rectangular bar. (see Figure 6.3)

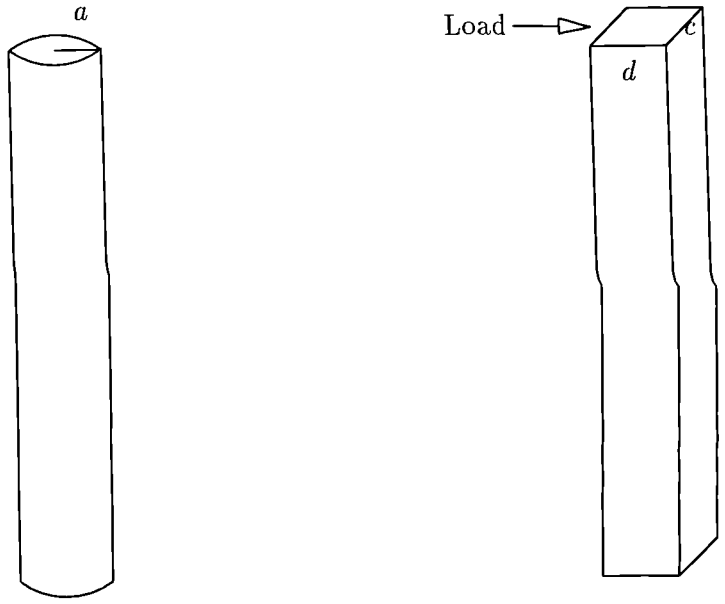

(a) Circular beam (b) Rectangular beam

Figure 6.3: Moment of Inertia for uniform beams

To find the stiffness matrix for the beam element, it is necessary to apply Castigliano's first theorem, which states that the stiffness coefficient k_{ij}^e of an element stiffness matrix can be obtained from the operation

$$k_{ij}^e = \frac{\partial^2 U_e}{\partial u_i \, \partial u_j}. \tag{6.13}$$

When applying partial differentiation to U_1 with respect to v_i and θ_i, the term

$$\frac{du}{dx}$$

in the integral

$$\int_0^L \frac{du}{dx}\left(\frac{dv}{dx}\right)^2 dx$$

may present some problems, as the value of this term varies in each increment step. However, at the start of the computation in the first increment step, it is known that $\frac{du}{dx} = \frac{1}{L}(u_2 - u_1)$, and hence it can be treated as a constant independent of v_i's and θ_i's. This is the assumption which is adopted in most currently used algorithms for a beam

element (see Ross 1990). However, in all other increment steps, this assumption can no longer hold true, as $\frac{du}{dx}$ is no longer a constant. Consequently the second term in equation (6.11) has to be dealt with differently. This will be discussed in a later part.

With this assumption, the stiffness matrix can be obtained analytically by first observing that U_1 in equation (6.11) can be simplified to

$$U_1 = \frac{EA}{2}\int_0^L \left(\frac{du}{dx}\right)^2 dx + \frac{F}{2}\int_0^L \left(\frac{dv}{dx}\right)^2 dx \tag{6.14}$$

where

$$F = EA\,\frac{du}{dx}$$

is the axial force in the bar, and is considered to be a constant here. This consideration can be justified at the start of the first increment step as $\frac{du}{dx}$ is assumed to be a constant, and E and A are the modulus of elasticity and the uniform cross-sectional area of the rod respectively.

To express U_e in explicit form, recall that the displacement functions are defined as

$$u(x) = \sum_{i=1}^{2} N_i(\xi)u_i$$

and

$$v(x) = \sum_{i=1}^{2} H_i(\xi)v_i + L\sum_{i=1}^{2} m_i(\xi)\theta_i$$

Hence,

$$\frac{du}{dx} = \frac{1}{L}\sum_{i=1}^{2} N_i'(\xi)u_i, \tag{6.15}$$

$$\frac{dv}{dx} = \frac{1}{L}\sum_{i=1}^{2} H_i'(\xi)v_i + \sum_{i=1}^{2} m_i'(\xi)\theta_i,$$

and

$$\frac{d^2v}{dx^2} = \frac{1}{L^2}\sum_{i=1}^{2} H_i''(\xi)v_i + \frac{1}{L}\sum_{i=1}^{2} m_i''(\xi)\theta_i, \tag{6.16}$$

denoting $N_i'(\xi) = \frac{dN_i(\xi)}{d\xi}$ and $H_i''(\xi) = \frac{d^2H_i(\xi)}{d\xi^2}$ etc.

Substituting (6.15) and (6.16) into (6.10), it can be observed that

$$\begin{aligned}\frac{\partial U_e}{\partial u_i} &= \frac{EA}{2}\int_0^L \left\{\frac{\partial}{\partial u_i}\left(\frac{du}{dx}\right)^2\right\} dx \\ &= \frac{EA}{L}\int_0^1 N_i'(\xi)\left(\sum_{j=1}^{2} N_j'(\xi)u_j\right) d\xi,\end{aligned} \tag{6.17}$$

and

$$\begin{aligned}
\frac{\partial U_e}{\partial v_i} &= \frac{EI}{2}\int_0^L \left\{\frac{\partial}{\partial v_i}\left(\frac{d^2v}{dx^2}\right)^2\right\} dx + \frac{F}{2}\int_0^L \left\{\frac{\partial}{\partial v_i}\left(\frac{dv}{dx}\right)^2\right\} dx \\
&= \frac{EI}{2}\int_0^L \left\{\frac{\partial}{\partial v_i}\left(\frac{1}{L^2}\sum_{j=1}^{2} H_j''(\xi)u_j + \frac{1}{L}\sum_{j=1}^{2} m_j''(\xi)\theta_j\right)^2\right\} dx \\
&\quad + \frac{F}{2}\int_0^L \left\{\frac{\partial}{\partial v_i}\left(\frac{1}{L}\sum_{j=1}^{2} H_j'(\xi)u_j + \sum_{j=1}^{2} m_j'(\xi)\theta_j\right)^2\right\} dx \\
&= \frac{EI}{L}\int_0^1 H_i''(\xi)\left(\frac{1}{L^2}\sum_{j=1}^{2} H_j''(\xi)u_j + \frac{1}{L}\sum_{j=1}^{2} m_j''(\xi)\theta_j\right) d\xi \\
&\quad + F\int_0^1 H_i'(\xi)\left(\frac{1}{L}\sum_{j=1}^{2} H_j''(\xi)u_j + \sum_{j=1}^{2} m_j''(\xi)\theta_j\right) d\xi, \qquad (6.18)
\end{aligned}$$

Likewise,

$$\begin{aligned}
\frac{\partial U_e}{\partial \theta_i} &= EI\int_0^1 m_i''(\xi)\left(\frac{1}{L^2}\sum_{j=1}^{2} H_j''(\xi)u_j + \frac{1}{L}\sum_{j=1}^{2} m_j''(\xi)\theta_j\right) d\xi \\
&\quad + FL\int_0^1 m_i'(\xi)\left(\frac{1}{L}\sum_{j=1}^{2} H_j'(\xi)u_j + \sum_{j=1}^{2} m_j''(\xi)\theta_j\right) d\xi \qquad (6.19)
\end{aligned}$$

Performing partial differentiation once more, the following can be obtained:

$$\frac{\partial^2 U_e}{\partial u_i \partial u_j} = \frac{EA}{L}\int_0^1 \left\{N_i'(\xi)\; N_j'(\xi)\right\} d\xi \qquad (6.20)$$

$$\frac{\partial^2 U_e}{\partial v_i\, \partial v_j} = \frac{EI}{L^3}\int_0^1 H_i''(\xi)\; H_j''(\xi)d\xi + \frac{F}{L}\int_0^1 H_i'(\xi)\; H_j'(\xi)d\xi \qquad (6.21)$$

and

$$\frac{\partial^2 U_e}{\partial \theta_i\, \partial \theta_j} = \frac{EI}{L}\int_0^1 m_i''(\xi)\; m_j''(\xi)d\xi + F\int_0^1 m_i'(\xi)\; m_j'(\xi)d\xi \qquad (6.22)$$

etc.

Substituting the shape functions and their derivatives established in equation (6.7) to (6.20), (6.21) and (6.22), and using Castigliano's first theorem in (6.13) to establish $k_{ij}{}^e$, the stiffness matrix of the beam element $[\mathbf{K}^e]$ in local coordinates can be found as

$$[\mathbf{K}^e] = [\mathbf{K}_0^e] + [\mathbf{K}_G^e]$$

$$= \frac{EI}{L^3}\begin{bmatrix} \frac{AL^2}{I} & 0 & 0 & -\frac{AL^2}{I} & 0 & 0 \\ 0 & 12 & 6L & 0 & -12 & 6L \\ 0 & 6L & 4L^2 & 0 & -6L & 2L^2 \\ -\frac{AL^2}{I} & 0 & 0 & \frac{AL^2}{I} & 0 & 0 \\ 0 & -12 & -6L & 0 & 12 & -6L \\ 0 & 6L & 2L^2 & 0 & -6L & 4L^2 \end{bmatrix}$$

$$+\frac{F}{L}\begin{bmatrix} 0 & 0 & 0 & 0 & 0 & 0 \\ 0 & \frac{6}{5} & -\frac{L}{10} & 0 & -\frac{6}{5} & \frac{L}{10} \\ 0 & -\frac{L}{10} & \frac{2L^2}{15} & 0 & \frac{L}{10} & -\frac{L^2}{30} \\ 0 & 0 & 0 & 0 & 0 & 0 \\ 0 & -\frac{6}{5} & \frac{L}{10} & 0 & \frac{6}{5} & -\frac{L}{10} \\ 0 & \frac{L}{10} & -\frac{L^2}{30} & 0 & -\frac{L}{10} & \frac{2L^2}{15} \end{bmatrix}, \tag{6.23}$$

and the displacement vector that is associated with this stiffness matrix is

$$\mathbf{u} = (u_1 \;\; v_1 \;\; \theta_1 \;\; u_2 \;\; v_2 \;\; \theta_2)^{\mathrm{T}} \tag{6.24}$$

Note that the element stiffness matrix expressed in (6.23) is obtained by integrating term by term analytically at the beginning of the first increment step when $\frac{du}{dx}$, and subsequently the factor F, is taken as a constant. However, after the first iteration in the first increment is carried out, the element starts to deform and hence $\frac{du}{dx}$ is no longer a constant. Therefore, the integral

$$\frac{\partial^2}{\partial u_i \, \partial u_j} \int_0^L \frac{du}{dx}\left(\frac{dv}{dx}\right)^2 dx = \int_0^L \left\{ \frac{\partial^2}{\partial u_i \, \partial u_j} \left[\frac{du}{dx}\left(\frac{dv}{dx}\right)^2 \right] \right\} dx \tag{6.25}$$

has to be calculated by some numerical methods, such as Gaussian quadrature, which is the method used for numerical integration throughout this thesis.

The displacement functions $u(x)$ and $v(x)$ for a two-noded beam element are linear and cubic respectively, therefore it is accurate enough to use the two-point Gaussian quadrature rule to perform the above numerical integration: if a function $f(x)$ is defined

for the variable x, then the integral can be approximated by the sum

$$\int_{-1}^{1} f(x)\,dx = \sum_{i=1}^{2} w_i f_i$$

where the Gauss weights $w_1 = w_2 = 1$, and f_i are the values of $f(x)$ at the two Gauss points $\pm\frac{1}{\sqrt{3}}$. The error of this numerical intergation is of the order $f^4(\xi)$ and therefore it will not significantly affect the overall accuracy of the algorithm.

Efforts have also been made to perform the numerical integration of (6.25) by 3- or higher-point Gaussian quadrature rule, and almost identical results have been obtained. While it is necessary to use higher-point Gaussian quadrature rule to deal with integrand of higher order, it would be impractical to use it when the integrand is of order 4. Further, the higher-point rule requires to perform a large number of computations, and consequently it will increase computation time and possibly accumulate noticeable computational errors. Therefore higher-point quadrature rule does not necessarily yield more accurate results.

As displacements are accumulated after each iteration, the element stiffness matrix will change slightly, and hence a new element stiffness matrix has to be recalculated and updated at each interation or increment step.

After the application of the first incremental load, or indeed the first iteration, deformations in both the x and the y directions occur, and hence the beam is now inclined at an angle β to the global axes. By writing $c - cos\beta$ and $s = sin\beta$, the elemental stiffness matrix in global coordinates can be obtained from the relationship

$$[\mathbf{K}^e]^0 = \mathbf{Q}^T[\mathbf{K}^e]\mathbf{Q} \tag{6.26}$$

where $\mathbf{Q}$ is the rotation matrix

$$\mathbf{Q} = \begin{bmatrix} c & s & 0 & 0 & 0 & 0 \\ -s & c & 0 & 0 & 0 & 0 \\ 0 & 0 & 1 & 0 & 0 & 0 \\ 0 & 0 & 0 & c & s & 0 \\ 0 & 0 & 0 & -s & c & 0 \\ 0 & 0 & 0 & 0 & 0 & 1 \end{bmatrix}$$

associated with the element e.

$[\mathbf{K}^e]^0$ is the *rotated* stiffness matrix for a two-noded beam element. In the incremental approach, if a body is discretised by several beam elements, the stiffness matrix for each element has to be found in the local coordinates first, and then it is rotated to the global axis by (6.26). The rotated matrices can then be assembled to form the global stiffness matrix $[\mathbf{K}]^0$, whence the incremental deformation for the whole body can be calculated. This process is repeated for all other incremental loads.

The advantage of using the rotation matrix $\mathbf{Q}$ is to ensure that in this two-dimensional problem, the local axis always lies along the direction of the element in each iteration or increment step, and by using this axis as reference, the element stress-strain behaviour can be reduced to one-dimensional and therefore the amount of calculations can be minimized.

6.3.2 Three-noded beam element

The development of this section for a three-noded beam element follows a very similar pattern to the previous section for a two-noded element.

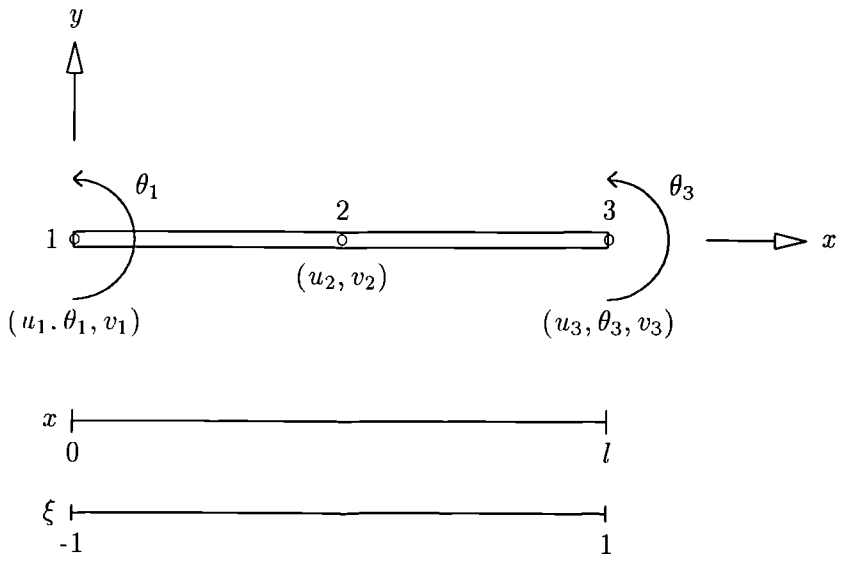

Figure 6.4: Three-noded beam element

Figure 6.4 shows a typical three-noded beam element. It is assumed that the element has a uniform cross-sectional area A, modulus of elasticity E, and length L, while the flexural stiffness factor is taken as EI.

The middle node 2 has translational degrees u_2, v_2 only, while nodes 1 and 3 lie at opposite ends of the element, and they have, in addition, nodal bending slopes θ_1 and θ_3,

together with translational degrees u_1, v_1 and u_3, v_3 respectively. Unlike the bar element, the additonal nodal bending slopes enable the beam to transmit nodal moments, and therefore it will give the structure, when modelled by these elements, a curved bending shape under loading. The beam lies in the xy plane both before and after deformation takes place. Initially it is oriented along the x axis in local coordinates.

In the x direction, the axial displacement function $u(x)$ can be represented by

$$u(x) = \sum_{i=1}^{3} N_i(\xi) u_i \tag{6.27}$$

where the N_i are the usual shape functions for bar elements, and are defined by

$$\begin{aligned} N_1(\xi) &= \frac{1}{2}\xi(\xi - 1) \\ N_2(\xi) &= 1 - \xi^2 \\ N_3(\xi) &= \frac{1}{2}\xi(\xi + 1) \end{aligned} \tag{6.28}$$

and where x and ξ are related by

$$x = \frac{(\xi + 1)L}{2}.$$

As in the case of a two-noded beam element, the flexure function $v(x)$ in the y direction can be written as

$$v(x) = \sum_{i=1}^{3} H_i(\xi) u_i + L \sum_{i=1,3} m_i(\xi)\theta_i \tag{6.29}$$

Under a similar system of constraints for $H_i(\xi), m_i(\xi)$ as in the two-noded beam element, the shape functions $H_i(\xi)$ and $m_i(\xi)$ are quartic and have been found to be

$$\begin{aligned} H_1(\xi) &= \frac{1}{4}(-3\xi + 4\xi^2 + \xi^3 - 2\xi^4) \\ H_2(\xi) &= 1 - 2\xi^2 + \xi^4 \\ H_3(\xi) &= \frac{1}{4}(3\xi + 4\xi^2 - \xi^3 - 2\xi^4) \end{aligned} \tag{6.30}$$

and

$$\begin{aligned} m_1(\xi) &= \frac{1}{4}(-\xi + \xi^2 + \xi^3 - \xi^4) \\ m_3(\xi) &= \frac{1}{4}(-\xi - \xi^2 + \xi^3 + \xi^4). \end{aligned} \tag{6.31}$$

The strain energy stored in the bar is given by equation (6.9),

$$U_e = \frac{E}{2}\int_V \epsilon_x^2 \, dV \tag{6.32}$$

where

$$\epsilon_x = \frac{du}{dx} + \frac{1}{2}\left(\frac{dv}{dx}\right)^2 - \frac{d^2v}{dx^2}\, y$$

and hence U_e becomes

$$\begin{aligned} U_e &= \frac{E}{2}\int_V \left\{ \left(\frac{du}{dx}\right)^2 + \frac{du}{dx}\left(\frac{dv}{dx}\right)^2 + \left(\frac{d^2v}{dx^2}\right)^2 y^2 \right\} dV \\ &= U_1 + U_2 \end{aligned} \tag{6.33}$$

where

$$U_1 = \frac{EA}{2}\int_0^L \left\{ \left(\frac{du}{dx}\right)^2 + \frac{du}{dx}\left(\frac{dv}{dx}\right)^2 \right\} dx \tag{6.34}$$

and

$$\begin{aligned} U_2 &= \frac{E}{2}\int_0^L \left(\frac{d^2v}{dx^2}\, y^2\right)^2 dx \\ &= \frac{EI}{2}\int_0^L \left(\frac{d^2v}{dx^2}\right)^2 dx \end{aligned} \tag{6.35}$$

Following a similar procedure as described in the last section for a two-noded beam element, it has been found that the stiffness matrix for the three-noded beam element in local coordinates is

$$[\mathbf{K}^e] = [\mathbf{K}_0^e] + [\mathbf{K}_G^e]$$

$$= \frac{EI}{L^3}\begin{bmatrix}
\frac{7AL^2}{3I} & 0 & 0 & -\frac{8AL^2}{3I} & 0 & \frac{AL^2}{3I} & 0 & 0 \\
0 & 8(\frac{79}{10}) & 8(\frac{47}{10})L & 0 & 8(-\frac{64}{5}) & 0 & 8(\frac{49}{10}) & 8(-\frac{17}{10})L \\
0 & 8(\frac{47}{10})L & 8(\frac{18}{5})L^2 & 0 & 8(-\frac{32}{5})L & 0 & 8(\frac{17}{10})L & 8(-\frac{3}{5})L^2 \\
-\frac{8AL^2}{3I} & 0 & 0 & \frac{16AL^2}{3I} & 0 & -\frac{8AL^2}{3I} & 0 & 0 \\
0 & 8(-\frac{64}{5}) & 8(-\frac{32}{5})L & 0 & 8(\frac{128}{5}) & 0 & 8(-\frac{64}{5}) & 8(\frac{32}{5})L \\
\frac{AL^2}{3I} & 0 & 0 & -\frac{8AL^2}{3I} & 0 & \frac{7AL^2}{3I} & 0 & 0 \\
0 & 8(\frac{49}{10}) & 8(\frac{17}{10})L & 0 & 8(-\frac{64}{5}) & 0 & 8(\frac{79}{10}) & 8(-\frac{47}{10})L \\
0 & 8(-\frac{17}{10})L & 8(-\frac{3}{5})L^2 & 0 & 8(\frac{32}{5})L & 0 & 8(-\frac{47}{10})L & 8(\frac{18}{5})L^2
\end{bmatrix}$$

$$+\frac{2F}{L}\begin{bmatrix} 0 & 0 & 0 & 0 & 0 & 0 & 0 & 0 \\ 0 & \frac{127}{105} & \frac{29}{210}L & 0 & -\frac{128}{105} & 0 & \frac{1}{105} & \frac{13}{210}L \\ 0 & \frac{29}{210}L & \frac{16}{105}L^2 & 0 & -\frac{8}{105}L & 0 & -\frac{13}{210}L & \frac{1}{21}L^2 \\ 0 & 0 & 0 & 0 & 0 & 0 & 0 & 0 \\ 0 & -\frac{128}{105} & -\frac{8}{105}L & 0 & \frac{256}{105} & 0 & -\frac{128}{105} & \frac{8}{105}L \\ 0 & 0 & 0 & 0 & 0 & 0 & 0 & 0 \\ 0 & \frac{1}{105} & -\frac{13}{210}L & 0 & -\frac{128}{105} & 0 & \frac{127}{105} & -\frac{29}{210}L \\ 0 & \frac{13}{210}l & \frac{1}{21}L^2 & 0 & \frac{8}{105}L & 0 & -\frac{29}{210}L & \frac{16}{105}L^2 \end{bmatrix}, \tag{6.36}$$

and the displacement vector that is associated with this stiffness matrix is

$$\mathbf{u} = (u_1 \;\; v_1 \;\; \theta_1 \;\; u_2 \;\; v_2 \;\; u_3 \;\; v_3 \;\; \theta_3)^T \tag{6.37}$$

As in the case of a two-noded beam element, the element stiffness matrix expressed in (6.36) is only valid at the start of the computation in the first increment when the factor $\frac{du}{dx}$ is a constant. However, when deformations occur after the first increment step is carried out, this factor becomes a variable and so the matrix $[\mathbf{K}_G^e]$ has to be evaluated at each step by a numerical method, such as Gaussian quadrature.

The shape functions for the displacement functions $u(x)$ and $v(x)$ are quadratic and quartic respectively, it is necessary to use three-point Gaussian quadrature formula to perform the integration, so that while accurate results can be obtained for the integral, the overall accuracy of the method will not be affected by the computational error introduced by this numerical method. For comparison, four- or more point formuluae have also been used in this algorithm, and the overall results have been found to be almost identical. Therefore it is fair to say that higher point Gaussian quadrature formula is deemed unneccessary.

By writing $c = cos\beta$ and $s = sin\beta$, where β is the inclined angle of the bar to the global axes, the element stiffness matrix in global coordinates can be obtained from the relationship

$$[\mathbf{K}^e]^0 = \mathbf{Q}^T[\mathbf{K}^e]\mathbf{Q} \tag{6.38}$$

where $\mathbf{Q}$ is the rotation matrix

$$\mathbf{Q} = \begin{bmatrix} c & s & 0 & 0 & 0 & 0 & 0 & 0 \\ -s & c & 0 & 0 & 0 & 0 & 0 & 0 \\ 0 & 0 & 1 & 0 & 0 & 0 & 0 & 0 \\ 0 & 0 & 0 & c & s & 0 & 0 & 0 \\ 0 & 0 & 0 & -s & c & 0 & 0 & 0 \\ 0 & 0 & 0 & 0 & 0 & c & s & 0 \\ 0 & 0 & 0 & 0 & 0 & -s & c & 0 \\ 0 & 0 & 0 & 0 & 0 & 0 & 0 & 1 \end{bmatrix}$$

associated with the element e.

6.4 Incremental load

In the analysis of nonlinear deformation, loads are applied to the structure in a series of increments, and it is assumed that the material of the structure is linearly elastic in each increment step. The large displacement analysis for quadrilateral elements has been discussed in full in Chapter 4, and a similar approach is now being adopted for beam elements.

Suppose an incremental load $\delta\mathbf{f}$ is applied to the system. Denote

$$\begin{aligned} \delta\mathbf{f} &= \mathbf{f}^n - \mathbf{f} \\ \delta\mathbf{u} &= \mathbf{u}_n - \mathbf{u} \\ \delta\mathrm{K} &= \mathrm{K}^n - \mathrm{K} \end{aligned} \tag{6.39}$$

where $\delta\mathbf{u}$ is the displacement during any one increment step etc.

It has been shown that the incremental equilibrium equation used in Chapter 4 for isoparametric elements provides a more realistic apporach to obtain a satisfactory solution for large displacement analysis. However, the iterative process involved in this approach in calculating residual loads requires the use of incremental stress, and there seems to be no equation that involves incremental stress for the beam element. Therefore, an alternative form for the incremental stiffness equation is proposed.

Consider the stiffness equation

$$\mathrm{K}\,\mathbf{u} = \mathbf{f}.$$

Substituting the incremental factors as defined in equation (6.39) into the stiffness equation, it can be rewritten as

$$\{\mathrm{K} + \delta\mathrm{K}\}\ \{\mathbf{u} + \delta\mathbf{u}\} = \mathbf{f} + \delta\mathbf{f} \tag{6.40}$$

Expanding equation (6.40),

$$\mathrm{K}\,\mathbf{u} + \delta\mathrm{K}\,\mathbf{u} + \mathrm{K}\,\delta\mathbf{u} + \delta\mathrm{K}\,\delta\mathbf{u} = \mathbf{f} + \delta\mathbf{f} \tag{6.41}$$

or, after simplification,

$$\delta\mathrm{K}\,\mathbf{u} + \mathrm{K}\,\delta\mathbf{u} + \delta\mathrm{K}\,\delta\mathbf{u} = \delta\mathbf{f} \tag{6.42}$$

which is now the incremental stiffness equation for the incremental load $\delta\mathbf{f}$.

This is a nonlinear matrix equation in $\delta\mathbf{u}$. To reduce it to an approximate linear matrix equation, it can be observed that the third term $\delta\mathrm{K}\ \delta\mathbf{u}$ in equation (6.42) is infinitesimal and can be neglected, as this term involves product of two relatively small incremental factors. The interest here is to find an approximate incremental stiffness matrix. Therefore, the first term $\delta\mathrm{K}\ \mathbf{u}$ of (6.42) can be neglected so that the approximate incremental stiffness equation reduces to

$$\mathrm{K}\delta\mathbf{u} = \delta\mathbf{f}. \tag{6.43}$$

Approximate solution to this linear matrix equation can now be improved by using a procedure based on the idea of residual loads which has been described in detail in Chapter 4.

6.5 Convergence of large displacement analysis by using Residual load

From the last section, the solution δu of the matrix equation

$$\mathrm{K}\delta u = \delta\mathbf{f}$$

is the approximate solution of the incremental stiffness equation (6.42).

In Chapter 4, an iterative method based on the idea of residual load (or residual error) has been used to refine this approximation, and appears to work well. That method will

be adapted here to perform a similar task.

Suppose that in the kth iteration of the residual load when the nth incremental load is being applied to the system, the incremental stiffness equation takes the form

$$\widehat{\mathbf{K}}\delta\mathbf{u}_n^{(k)} = \delta\mathbf{f}_n^{(k)} \tag{6.44}$$

where

- $\mathbf{K}$ is the global stiffness matrix, as defined in equation (6.43), updated to the kth iteration,
- $\delta\mathbf{u}_n^{(k)}$ is displacement in the kth iteration, and
- $\delta\mathbf{f}_n^{(k)}$ is the sum of the nth incremental load and all residual loads up to and including the $(k-1)$th iteration.

Then the accumulated displacement $\mathbf{u}_n^{(k)}$ becomes

$$\mathbf{u}_n^{(k)} = \mathbf{u}_n^{(k-1)} + \delta\mathbf{u}_n^{(k)}$$

Define the residual load (or residual error) as

$$\mathbf{r}_n^{(k)} = \delta\mathbf{f}_n^{(k)} - \widehat{\mathbf{K}}\delta\mathbf{u}_n^{(k)} \tag{6.45}$$

where

- $\mathbf{r}_n^{(k)}$ is kth residual load,
- $\delta\mathbf{f}_n^{(k)}$ is the sum of the nth incremental load and all residual loads up to and including the $(k-1)$th iteration, and
- $\widehat{\mathbf{K}}$ is the updated stiffness matrix due to the accumulated displacement $\mathbf{u}_n^{(k)}$.

and the residual ratio $\rho^{(k)}$ as

$$\rho^{(k)} = \frac{\|\mathbf{r}_n^{(k)}\|}{\|\mathbf{r}_n^{(k-1)}\|}. \tag{6.46}$$

This ratio can be used as a factor to monitor whether the iteration is converging or not. It is necessary to prescribe a tolerance factor, so that when the residual ratio is less than this factor, the iteration can be terminated and the next incremental step can be proceeded. Otherwise, further iteration is necessary to refine the results.

6.6 Examples of beam bending

The following examples in beam bending can illustrate how the algorithms developed in this chapter will work in practice. Large (or small, if appropriate) displacement analysis is implemented in the computer program, and the results are executed by the computer.

6.6.1 Column bending

Consider a very thin rod that is rigidly fixed in both the x and the y directions at one end, although the bending angle at that end is not fixed, and is free to move in the other (see Figure 6.5(a)). Initially the rod is hanging freely at A. To support the rod so that it can lie in equilbrium horizontally, and that it will not merely rotate at its fixed point A, it is imposed that the rod is rigidly supported at node B. The rod is uniform, and it is assumed to be homogeneous, linearly elastic and istropic. A point load is applied perpendicularly downwards at C, the free end of the rod, to initiate deformation.

For the finite element discretization, the rod is modelled by eight identical 3-noded beam elements, and the finite element mesh is shown in Figure 6.5(b).

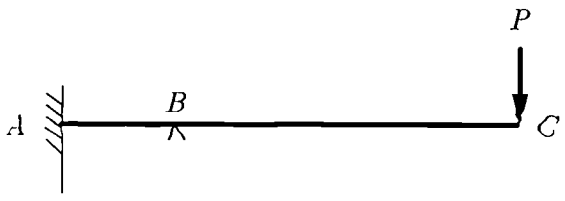

(a) Thin rod

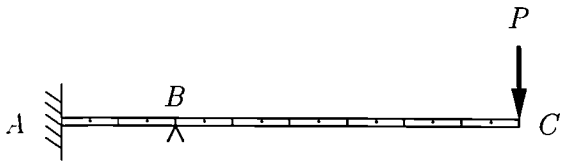

(b) Element discretization of example

Figure 6.5: Example of column bending

Figure 6.6 shows the lateral displacement of the rod computed by the program and according to the large displacement bending theory introduced in this chapter, together with iterations performed on its residual loads. The results clearly show that, with the addition of rotational degrees of freedom imposed on the two end-nodes of each beam

element, the internal shear force and bending moments will be transmitted from element to element, and hence the overall effect will give rise to a continuous curve bending shape of the deformed rod. This deformation is in line and agrees with the natural bending phenomenon of beams, and it shows a marked improvement over bar element discretization of similar problems.

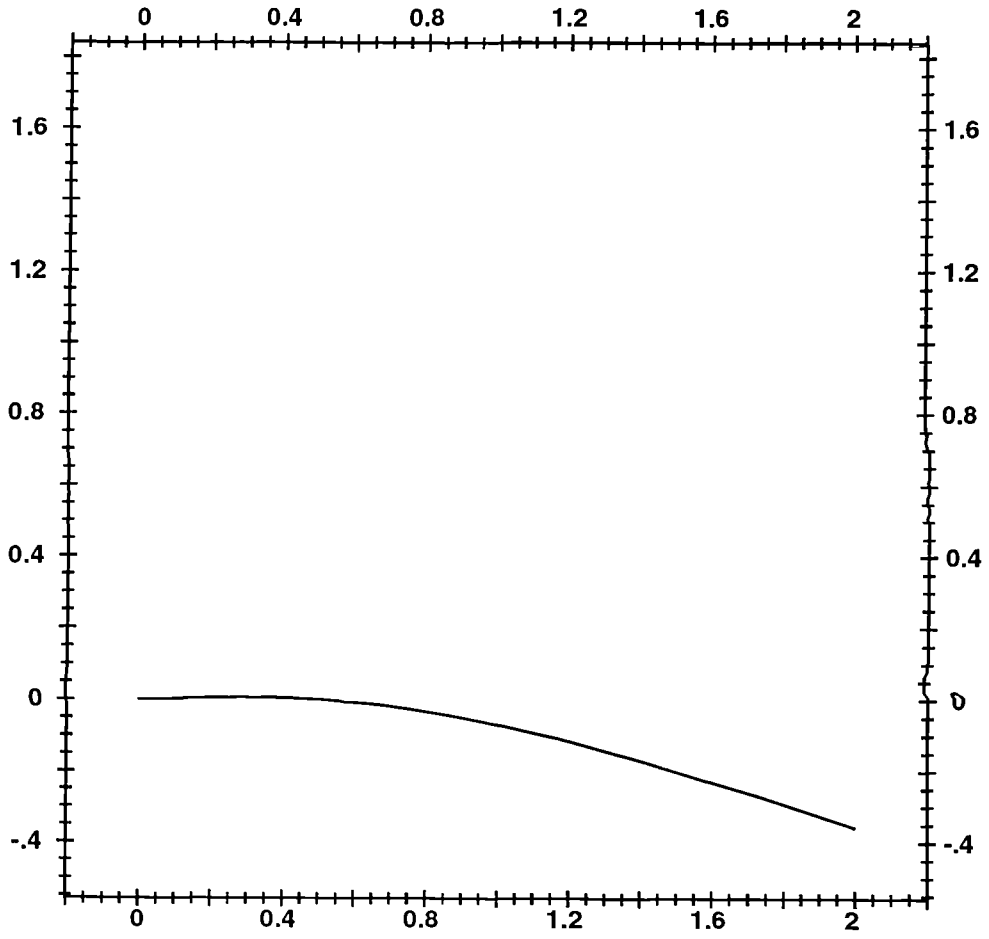

Figure 6.6: Deformation of thin rod using a point load (with exeggeration factor = 5×10^{12})

With a point load of 0.1×10^{-10}N, the displacement for the free end obtained by the large displacement formulation is 0.742×10^{-13}m, which works out to be 91% of the value from the analytical formula derived by Meek in (5.33).

6.6.2 Some observations

If the small displacement theory is used instead in the program, the bending characteristic of the deformed thin rod will be very similar to the nonlinear case. However, it has been found that when incremental loads are applied, displacement in each increment step is linearly and directly proportional to the size of the incremental load.

Further experiments using small displacement theory with different point loads have been carried out, and when these results are plotted in a displacement-load graph, a straight line curve is thus obtained. It shows that the small displacement theory will never break down, even when a point load with unrealistic large magnitude is applied to the rod. Therefore, as in the case of the eight-noded isoparametric elements, the small displacement theory can only be used as an approximation when the point load is small, and it becomes increasing inaccurate when the point load becomes bigger. Further, it cannot be used to predict the critical load and the collapse of the thin rod.

In section 6.3.1, the nonlinear stiffness matrix of an one-dimensional, two-noded beam element has been established. To compare the effect of using this type of element directly with its three-noded equivalent in a practical situation, the above column bending problem has been repeated. In this problem, the same set of parameters for the material properties of the thin rod and for the loadings is retained, except that the uniform thin rod in Figure 6.5 is now discretised by a mesh of eight identical one-dimensional, two-noded beam elements.

From the computed displacements obtained from the modified program with the new stiffness matrix given in (6.23), the results are shown in Fugure 6.7. It can be seen that the bending characteristics of the rod is virtually the same as before, except that the angle of rotation of each node becomes slightly flatter, although the difference is hardly noticeable. If the number of two-noded beam elements is increased in the discretization, the bending becomes smoother, and it approaches a similar curvilinear bending characteristics of the three-noded beam elements.

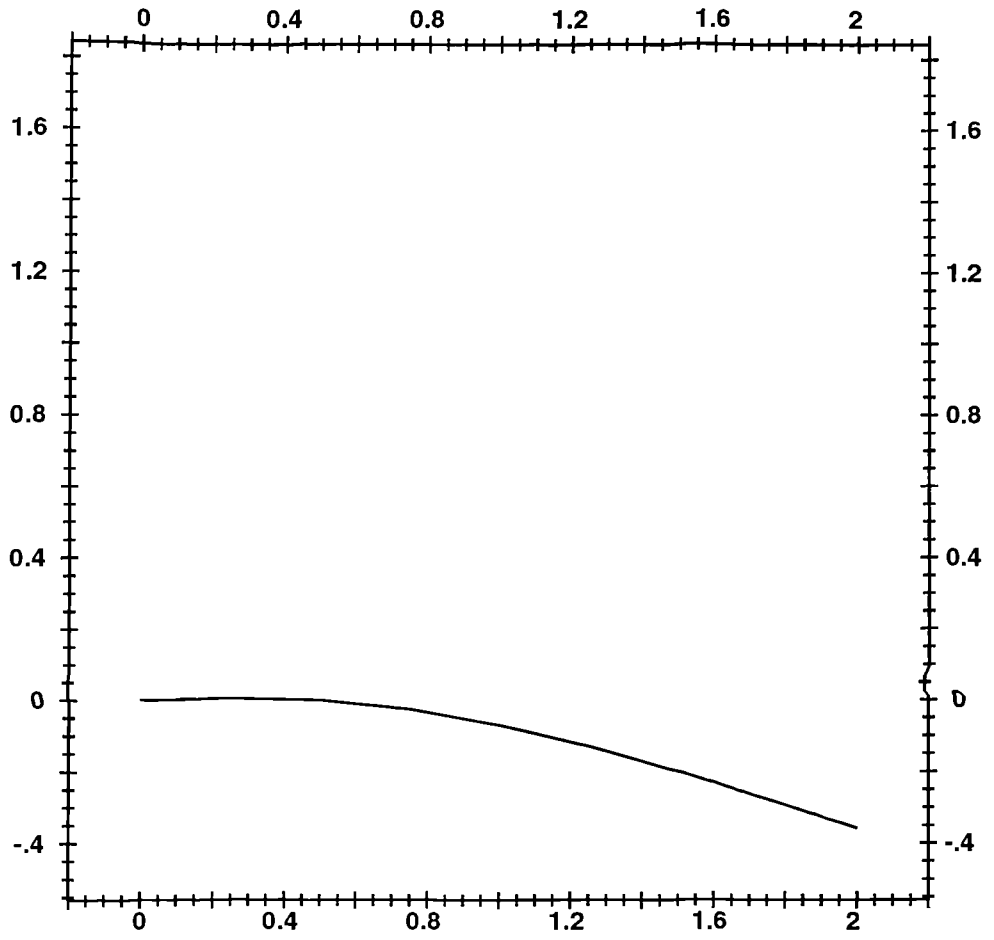

Figure 6.7: Deformation of a thin rod discretised by two-noded beam elements

6.6.3 Bending of a partly embedded thin bar

This example has been used in the last chapter when the thin bar was discretised by a number of bar elements (see Figure 5.3). It was concluded that with this discretization, the bar has been wrongly modelled as a pin-jointed truss, and that the stress were not allowed to transmit between elements.

To investigate whether beam element discretization of the same example would improve the overall bending characteristics, beam elements are used to model the thin bar, while the ground soil is modelled by eight identical eight-noded isoparametric elements. All parameters used here are the same as before, so that direct comparisons can be made. Figure 6.8 shows the results of the deformation when small displacement formulation are

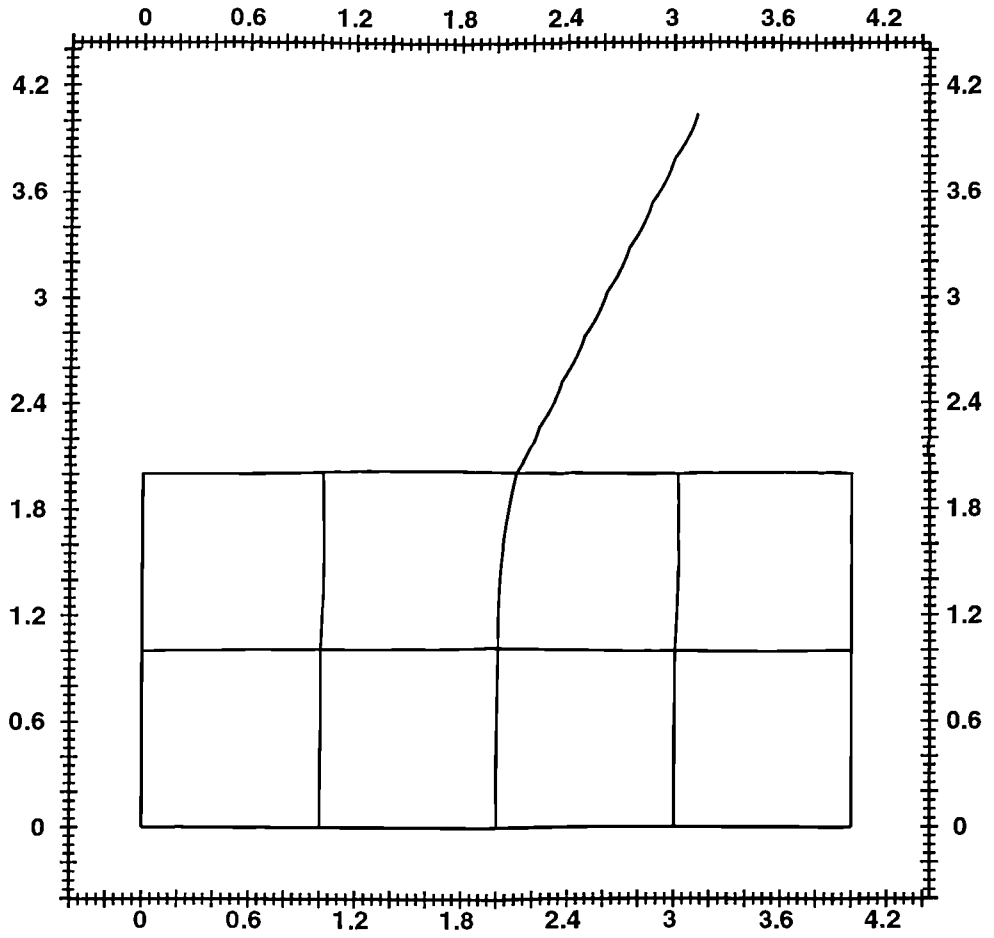

Figure 6.8: Bending of a thin rod using a point load

used for both types of element.

From this Figure, it can be readily seen that the stress from the free end of the rod can be transmitted into its embedded part and the ground soil, so that internal shear forces and angular moments are being considered. This part of the rod and the ground soil are now deformed in a natural curvilinear shape, so that it represents a marked improvement over bar element discretization. This beam-soil interaction will be an important mechanism in modelling rockbolts.

When large displacement theory is used, the model deforms with the same characteristic, but the problem is found to be very sensitive to the use of point load. When a

large point load is applied, one has to be very careful that this load does not exceed the critical load, otherwise the iteration procedure for the residual load will not converge, thus indicating the method fails, and that a total collapse has taken place. The problem of predicting critical load will be discussed in the following section.

6.7 Prediction of critical load

In order to predict the critical load of the thin rod as shown in Figure 6.5, a procedure similar to Section 4.5.2 is followed. Although the nature of this problem is different from Euler buckling, it would be useful to predict when the thin rod will collapse.

In this experiment, large displacement theory is used. At the free hand of the thin rod, trial values of point loads are increased gradually, and each time, the displacement is noted. Initially this algorithm can always predict deformation similar to Figure 6.6. However, after the point load reaches a certain value, the rod collapses very quickly and suddenly when the load is increased very slightly. In the displacement-load graph thus plotted in Figure 6.9, it can be seen that the first part of the curve behaves like a straight line, and after a certain point is reached, the displacement suddenly goes to infinity. At this point, the critical load is reached.

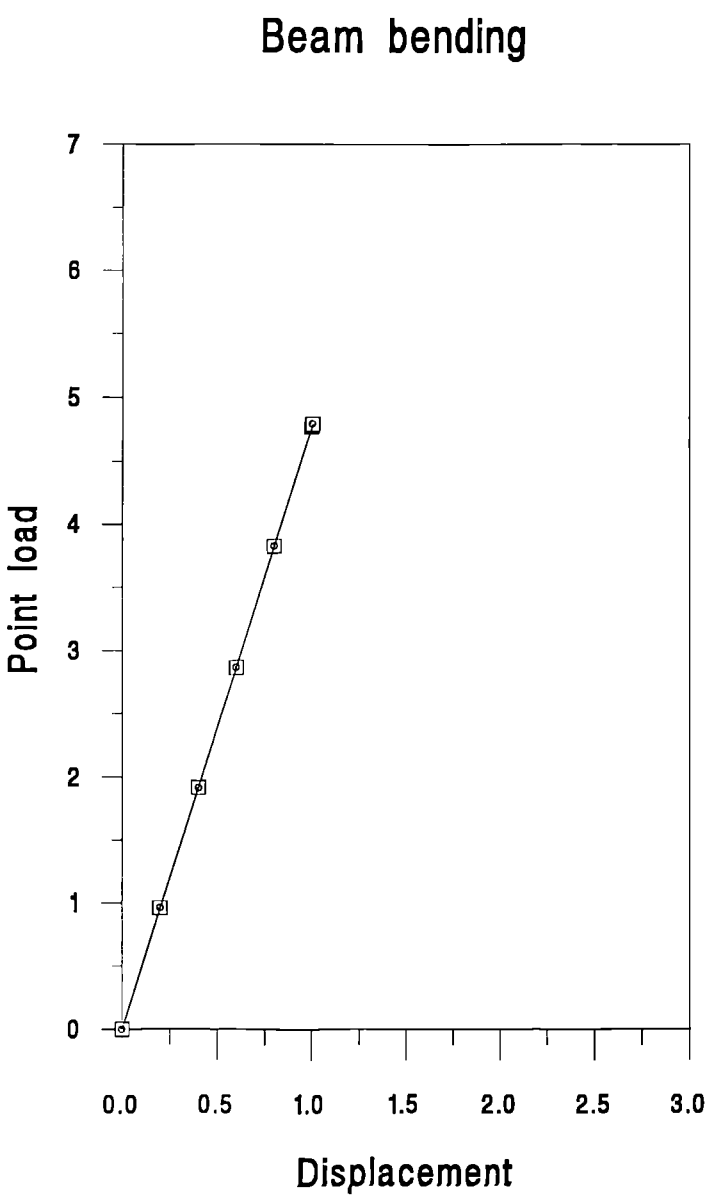

Figure 6.9: Displacement-load graph of beam bending

When comparing this graph with Figure 4.6, when the thin rod is discretised by eight-noded isoparametric elements, this sudden collapse may be caused by the fact that the rod is made of very thin material. To demonstrate this point, the problem of column buckling in Section 4.5 is repeated with a drastic reduction on the width of the column. The resulting displacement-load curve will become less smooth near the critical load, and it bears a similar characteristic to Figure 6.9. Further, it may worth pointing out that it is imortant to relate the width of the beam to its length. If rod is relatively thin, the beam is prone to collpase very easily, even if the applied load is relatively small.

The same experiement is being repeated with the second example shown in Figure 5.3, and the resulting displacement-load curve of the top node at the free end has the same shape as in Figure 6.9. It confirms that great care is needed to predict the critical load of a thin rod.

6.8 Discussion and practical implications

Beams are frequently connected together in both horizontal and vertical directions to form rigidly-jointed framed structures. These frames are most commonly encountered in building structures, and transmit loads primarily by bending actions. Although axial forces must always be present, their influence is usually small compared to the flexural effects.

With the development of beam elements in this chapter, the internal shear forces and the bending moments are being considered. From the examples of rod bending with bar element and beam element discretizations, it can be concluded that beam elements are superior to bar elements, and the former should be preferred in the finite element discretization of thin material. However it must be noted that because of the fine width of the material, critical load can be easily reached even if the applied load is relatively small. Therefore great care must be exercised when these elements are used. But its clear advantage over other type of elements has made it worthwhile to spend more time to experiment with its use. Of course, if beam elements are used as part of the element discretization of an object, then the superiority of these elements can be more readily seen. In Chapter 8, investigations will be carried out to examine the effect of using beam elements to discretise part of a grouted rockbolt, and the results will be compared.

Chapter 7

Joint Element

In the finite element analysis of solid mechanics, situations arise where discontinuous behaviour occurs between finite elements. In geotechnical situations, the discontinuities are intended to represent rock joints, faults and interfaces. The physical behaviour of such systems involves debonding and slip along the discontinuity. The term debonding describes the separation of two blocks of continuum adjacent to the joint surface which were initially in contact. Subsequent contact can also be developed by the movement of the two blocks towards each other. The term slip defines the relative motion along the joint surface or fault when the shearing force exceeds the shear strength of the joint. A joint element discretises the space between these two interacting blocks.

The material model of the continuous part of the system may be linearly elastic, or nonlinear with any specified properties. The slip and debonding phenomena make the discontinuities physically nonlinear and therefore special techniques must be employed to obtain a realistic solution.

Previous attempts have been made to develop discrete elements to represent the joint behaviour. Goodman, Taylor & Brekke (1968) developed a simple rectangular two dimensional element with eight degrees of freedom. With this element, adjacent three-dimensional blocks of continuous elements can penetrate into each other. Zienkiewicz *et al* (1970) advocated the use of continuous isoparametric elements with a simple nonlinear material property for shear and normal stress, assuming uniform strain in the thickness direction. Numerical difficulties may arise from ill conditioning of the stiffness matrix due to very large off-diagonal terms or very small diagonal terms which are generated by these elements in certain cases. Beer (1985) developed a general small displacement algorithm

which can be used for three-dimensional or two-dimensional shell-to-shell, shell-to-solid or solid-to-solid elements. These elements have zero thickness, and they provide a good platform for the modelling of rock mass and fractures.

7.1 Introduction

The algorithm under investigation in this chapter is based on the theory developed by Beer (1985) for the three-dimensional shell-to-shell contact element for linearly elastic material. This theory will be adapted to the types of one-dimensional solid-to-solid joint elements that are going to be implemented throughout this project. Figure 7.1 shows how these joint elements are structured in a two-dimensional rock mass system.

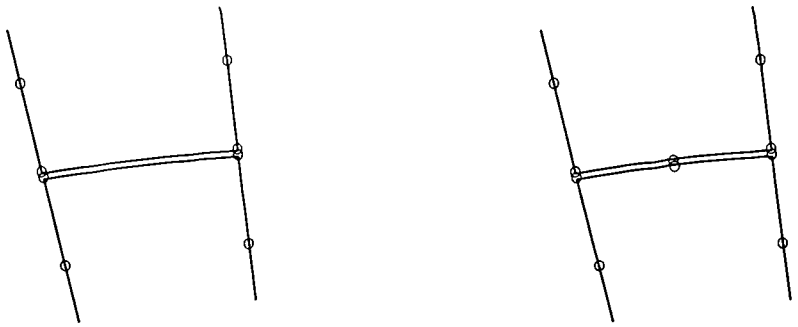

(a) Four-noded (b) Six-noded

Figure 7.1: Structures of two-dimensional joint elements

The joint element is made up of two identical one-dimensional sub-elements. It is assumed that the joint element has zero thickness, which has obvious advantages when modelling rock joints and fractures.

As the joint element is structured to model the joint or the space between rock mass, the two sub-elements initially lie in the same space and they are collinear with the overlying edge of the two adjoining rock elements. However, as the two sub-elements are modelled to be attached to different media which can have different material properties, or can be subject to different stresses, they are liable to deform in a different manner under loads.

In finite element discretization, these two sub-elements are theoretically detached from each other, with the top sub-element intuitively lying on top of the bottom one, and they

share the same nodes on their common edge. Likewise, the bottom sub-element is attached to the top element of the underlying medium, and they share the same nodes on their common edge. Therefore, the corresponding nodes of these two sub-elements must be regarded as lying on different edges, and they are distinguished by the use of different node numbers. The structures and the node details of a four-noded and a six-noded element are shown in Figures 7.4 and 7.5 respectively.

In this study, the top and the bottom media are continuous rock masses, and they are assumed to be without cracks and inhomogeneities. They are modelled by eight-noded isoparametric elements in the usual manner, while the two sub-elements that make up the joint element are modelled by one-dimensional, two- or three-noded elements. Further, every node in the joint element assumes two degrees of freedom.

7.2 Derivation of a general formula

In this chapter, the theory for the shell element will be investigated first. The shell-to-shell contact element in three dimensions is the most complex case in the modelling of joints. Details about the shell element have been described in full by *Zienkiewicz & Taylor (1991)*.

7.2.1 Shell-to-shell element

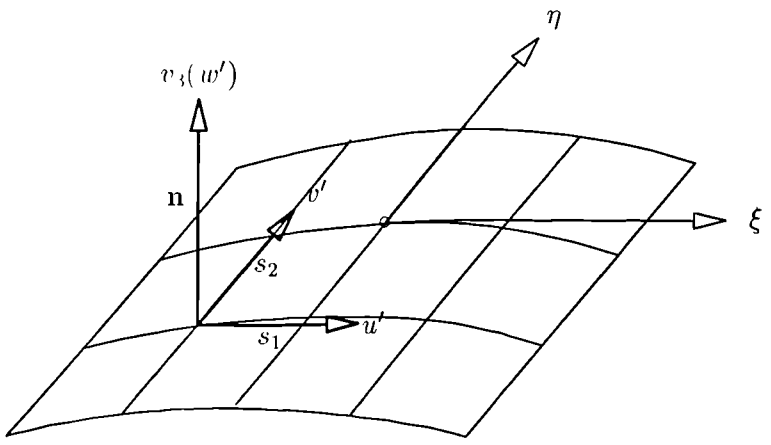

Figure 7.2: Vector definition in a three-dimesional shell element (top surface)

Consider the top surface of a typical three-dimensional shell element as shown in Figure 7.2. The external faces of the element are curved, while the section across the thickness is generated by straight lines. Pairs of corresponding points, i_{top} and i_{bottom}, each with given Cartesian coordinates, lie on the top and the bottom surface of the element which

has a certain thickness.

In a local coordinate system, it is usually convenient to define a vector between a corresponding point on the top and the bottom surfaces of this shell element, and this vector can be taken as the vector normal to the contact surface at the point of contact. Thus, the normal $\mathbf{v}_3$ can be obtained by simply taking

$$\mathbf{v}_3 = \begin{bmatrix} x_i \\ y_i \\ z_i \end{bmatrix}_{top} - \begin{bmatrix} x_i \\ y_i \\ z_i \end{bmatrix}_{bottom},$$

and the length of this vector is the thickness of the shell.

However, the shell is assumed to have *no thickness here, and so the two points* i_{top} and i_{bottom} are taken to coincide. Hence the above form is no longer valid. To overcome this problem, an alternative method for finding the normal vector can be obtained by considering the cross product

$$\mathbf{v}_3 = \begin{bmatrix} \frac{\partial x}{\partial \xi} \\ \frac{\partial y}{\partial \xi} \\ \frac{\partial z}{\partial \xi} \end{bmatrix} \times \begin{bmatrix} \frac{\partial x}{\partial \eta} \\ \frac{\partial y}{\partial \eta} \\ \frac{\partial z}{\partial \eta} \end{bmatrix}. \tag{7.1}$$

After normalisation, the unit vector of this normal becomes

$$\mathbf{n} = \frac{\mathbf{v}_3}{L}$$

where L is the length of this vector.

The two normalised tangent vectors $\mathbf{s}_1$ and $\mathbf{s}_2$ at the same contact point, which are shown in Figure 7.2, can be constructed by taking the cross products

$$\mathbf{s}_1 = \begin{bmatrix} 1 \\ 0 \\ 0 \end{bmatrix} \times \mathbf{n}$$

and

$$\mathbf{s}_2 = \begin{bmatrix} 0 \\ 1 \\ 0 \end{bmatrix} \times \mathbf{n},$$

so that they lie on the same contact plane which is tangential to the shell at the contact point. Hence the vectors $\mathbf{s}_1$, $\mathbf{s}_2$, and $\mathbf{v}$ define the three axes at the contact point of the shell.

7.2.2 Solid-to-solid element

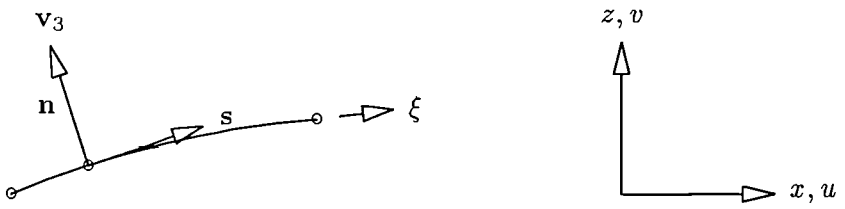

Figure 7.3: Two-dimensional joint element

In a two dimensional space shown in Figure 7.3, the η direction will no longer be considered. Hence, from equation (7.1), the normal vector $\mathbf{v}_3$ at the contact point can be found by taking the cross product

$$\mathbf{v}_3 = \begin{bmatrix} \frac{\partial x}{\partial \xi} \\ \frac{\partial y}{\partial \xi} \\ 0 \end{bmatrix} \times \begin{bmatrix} 0 \\ 0 \\ 1 \end{bmatrix} = \begin{bmatrix} \frac{\partial y}{\partial \xi} \\ -\frac{\partial x}{\partial \xi} \\ 0 \end{bmatrix},$$

with its unit vector

$$\mathbf{n} = \frac{1}{\sqrt{\left(\frac{\partial x}{\partial \xi}\right)^2 + \left(\frac{\partial y}{\partial \xi}\right)^2}} \begin{bmatrix} \frac{\partial y}{\partial \xi} \\ -\frac{\partial x}{\partial \xi} \\ 0 \end{bmatrix},$$

while the normalised tangent vector at the same contact point becomes

$$\begin{aligned} \mathbf{s} &= \begin{bmatrix} 0 \\ 0 \\ 1 \end{bmatrix} \times \frac{1}{\sqrt{\left(\frac{\partial x}{\partial \xi}\right)^2 + \left(\frac{\partial y}{\partial \xi}\right)^2}} \begin{bmatrix} \frac{\partial y}{\partial \xi} \\ -\frac{\partial x}{\partial \xi} \\ 0 \end{bmatrix} \\ &= \frac{1}{\sqrt{\left(\frac{\partial x}{\partial \xi}\right)^2 + \left(\frac{\partial y}{\partial \xi}\right)^2}} \begin{bmatrix} \frac{\partial x}{\partial \xi} \\ \frac{\partial y}{\partial \xi} \\ 0 \end{bmatrix}. \end{aligned}$$

These two vectors can be simply taken as

$$\mathbf{n} = \frac{1}{\sqrt{\left(\frac{\partial x}{\partial \xi}\right)^2 + \left(\frac{\partial y}{\partial \xi}\right)^2}} \begin{bmatrix} \frac{\partial y}{\partial \xi} \\ -\frac{\partial x}{\partial \xi} \end{bmatrix},$$

and

$$\mathbf{s} = \frac{1}{\sqrt{\left(\frac{\partial x}{\partial \xi}\right)^2 + \left(\frac{\partial y}{\partial \xi}\right)^2}} \begin{bmatrix} \frac{\partial x}{\partial \xi} \\ \frac{\partial y}{\partial \xi} \end{bmatrix}, \tag{7.2}$$

when the third dimension is not considered.

The displacements in the directions normal and tangential to the contact surface can be defined in matrix form by

$$\begin{bmatrix} u' \\ v' \end{bmatrix} = \theta^T \begin{bmatrix} u \\ v \end{bmatrix}, \tag{7.3}$$

with

$$\theta = [\mathbf{s},\ \mathbf{n}] = \frac{1}{\sqrt{\left(\frac{\partial x}{\partial \xi}\right)^2 + \left(\frac{\partial y}{\partial \xi}\right)^2}} \begin{bmatrix} \frac{\partial x}{\partial \xi} & \frac{\partial y}{\partial \xi} \\ \frac{\partial y}{\partial \xi} & -\frac{\partial x}{\partial \xi} \end{bmatrix}. \tag{7.4}$$

Further, the displacements at any point on the bottom surface of the top shell element are given in the usual form

$$\begin{bmatrix} u \\ v \end{bmatrix}_{top} = \mathbf{N}_{top}\mathbf{a}_{top}, \tag{7.5}$$

where $\mathbf{N}_{top}$ is a matrix containing shape functions of a n-noded one-dimensional element, and can be defined as

$$\mathbf{N}_{top} = [\mathbf{N}_1\ \mathbf{N}_2\ \cdots\ \mathbf{N}_n]_{top},$$

with

$$\mathbf{N}_i = N_i\mathbf{I},$$

and $\mathbf{I}$ is a 2×2 unit matrix, and the displacement vector

$$\mathbf{a}_{top} = \begin{bmatrix} \mathbf{a}_1 \\ \vdots \\ \mathbf{a}_n \end{bmatrix}_{top}$$

The bottom element is of the same form as the top element, and therefore it can be similarly written

$$\begin{bmatrix} u \\ v \end{bmatrix}_{bot} = \mathbf{N}_{bot}\mathbf{a}_{bot},$$

etc., with $\mathbf{N}_{top} = \mathbf{N}_{bot}$.

The relative displacements at the interface are the difference in displacements between the top and the bottom elements, and they can be expressed as

$$\begin{bmatrix} \delta_s \\ \delta_n \end{bmatrix} = \begin{bmatrix} u' \\ v' \end{bmatrix}_{top} - \begin{bmatrix} u' \\ v' \end{bmatrix}_{bot}. \tag{7.6}$$

Combining (7.3) and (7.5), equation (7.6) becomes

$$\begin{bmatrix} \delta_s \\ \delta_n \end{bmatrix} = \theta^T \mathbf{N}_{top}\mathbf{a}_{top} - \theta^T \mathbf{N}_{bot}\mathbf{a}_{bot}, \tag{7.7}$$

and it can be simplified in matrix algebra form as

$$\delta = \mathbf{B}\,\mathbf{a}^e \tag{7.8}$$

where

$$\mathbf{B} = \theta^T \mathbf{N} \tag{7.9}$$

and

$$\mathbf{a}^e = \begin{bmatrix} \mathbf{a}_{top} \\ \mathbf{a}_{bot} \end{bmatrix}$$

with

$$\mathbf{N} = [\mathbf{N}_{top} \; -\mathbf{N}_{bot}] \tag{7.10}$$

For an elastic joint element, the relationship between the shear and normal forces per unit length in the joint, and the relative displacement of the nodes is given by Goodman *et al* (1968) as

$$\begin{bmatrix} P_s \\ P_n \end{bmatrix} = \mathbf{D} \begin{bmatrix} u \\ v \end{bmatrix}.$$

where the associating elasticity matrix $\mathbf{D}$ is a diagonal material property matrix involving k_s and k_n, the joint stiffness per unit length in the tangential and normal directions respectively, and which are theoretically infinite. This matrix can be expressed as

$$\mathbf{D} = \begin{bmatrix} k_s & 0 \\ 0 & k_n \end{bmatrix}.$$

The stiffness matrix of this joint element in the small displacement analysis can be obtained from the standard procedure by minimizing the total potential energy U at the interface, where

$$U = \frac{1}{2}\,\mathbf{a}^{eT}\left(\int_A \mathbf{B}^T\mathbf{D}\mathbf{B}\,dA\right)\mathbf{a}^e,$$

so that the stiffness matrix for the contact element becomes

$$\mathbf{K}^e = \int_A \mathbf{B}^T\mathbf{D}\mathbf{B}\,dA.$$

In this research project, the joint element is modelled by one-dimensional four-noded or six-noded elements. It will be shown in the next several sections how the stiffness matrix of this contact element can be obtained analytically by using direct integration.

7.3 Four-noded joint element

In Figure 7.4, a four-noded joint element is shown. This four-noded joint element is modelled by two one-dimensional two-noded sub-elements, and the end nodes each have two degrees of freedom.

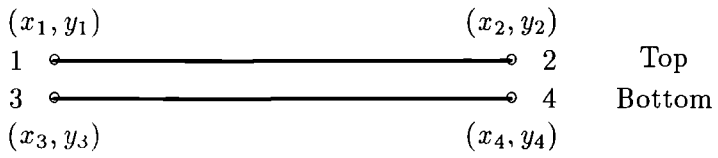

Figure 7.4: Four-noded joint element

These two sub-elements are of the same length and have the same characteristics. They describe the same surface and hence initially their corresponding nodes have the same coordinates, but they are distinguished by the use of different nodes with different numbers.

Consider a single standard one-dimensional two-noded element. The shape functions are defined by

$$N_1(\xi) = 1 - \xi$$

and

$$N_2(\xi) = \xi,$$

and any displacement along the two axes can be expressed in the form

$$x = \sum_{i=1}^{2} N_i(\xi) x_i$$

and

$$y = \sum_{i=1}^{2} N_i(\xi) y_i$$

Hence, the partial derivatives of x and y with respect to ξ in the local coordinate system become

$$\frac{\partial x}{\partial \xi} = x_2 - x_1$$

and

$$\frac{\partial y}{\partial \xi} = y_2 - y_1$$

As x_1, x_2 are the x- coordinates of the two end nodes of the bar element, they are related by

$$x_2 - x_1 = s_0. \qquad \text{and} \qquad y_2 = y_1$$

where s_0 is the length of the element.

With this relationship, the above partial derivatives reduce to

$$\frac{\partial x}{\partial \xi} = s_0 \tag{7.11}$$

and

$$\frac{\partial y}{\partial \xi} = 0. \tag{7.12}$$

Further, in equation (7.10), the two sub-elements are of the same length, and they have the same characteristics, and so

$$N_{top} = N_{bot}.$$

Together with (7.4), it can be seen that

$$\theta = \frac{1}{s_0} \begin{bmatrix} s_0 & 0 \\ 0 & -s_0 \end{bmatrix} = \begin{bmatrix} 1 & 0 \\ 0 & -1 \end{bmatrix}$$

and

$$\mathrm{N} = \begin{bmatrix} N_1 & 0 & N_2 & 0 & -N_1 & 0 & -N_2 & 0 \\ 0 & N_1 & 0 & N_2 & 0 & -N_1 & 0 & -N_2 \end{bmatrix}$$

With equation (7.9), the element **B** matrix takes the form

$$\begin{aligned}\mathbf{B} &= \theta^T \mathbf{N} \\ &= \begin{bmatrix} 1 & 0 \\ 0 & -1 \end{bmatrix} \begin{bmatrix} N_1 & 0 & N_2 & 0 & -N_1 & 0 & -N_2 & 0 \\ 0 & N_1 & 0 & N_2 & 0 & -N_1 & 0 & -N_2 \end{bmatrix} \\ &= \begin{bmatrix} N_1 & 0 & N_2 & 0 & -N_1 & 0 & -N_2 & 0 \\ 0 & -N_1 & 0 & -N_2 & 0 & N_1 & 0 & N_2 \end{bmatrix},\end{aligned} \tag{7.13}$$

so the matrix product $\mathbf{B}^T\mathbf{D}\mathbf{B}$ becomes

$$\begin{bmatrix} k_s N_1^2 & 0 & k_s N_1 N_2 & 0 & -k_s N_1^2 & 0 & -k_s N_1 N_2 & 0 \\ 0 & k_n N_1^2 & 0 & k_n N_1 N_2 & 0 & -k_n N_1^2 & 0 & -k_n N_1 N_2 \\ k_s N_1 N_2 & 0 & k_s N_2^2 & 0 & -k_s N_1 N_2 & 0 & -k_s N_2^2 & 0 \\ 0 & k_n N_1 N_2 & 0 & k_n N_2^2 & 0 & -k_n N_1 N_2 & 0 & -k_n N_2^2 \\ -k_s N_1^2 & 0 & -k_s N_1 N_2 & 0 & k_s N_1^2 & 0 & k_s N_1 N_2 & 0 \\ 0 & -k_n N_1^2 & 0 & -k_n N_1 N_2 & 0 & k_n N_1^2 & 0 & k_n N_1 N_2 \\ -k_s N_1 N_2 & 0 & -k_s N_2^2 & 0 & k_s N_1 N_2 & 0 & k_s N_2^2 & 0 \\ 0 & -k_n N_1 N_2 & 0 & -k_n N_2^2 & 0 & k_n N_1 N_2 & 0 & k_n N_2^2 \end{bmatrix} \tag{7.14}$$

and the stiffness matrix **K** for this joint element can be obtained from the integral

$$\mathbf{K}^e = \int_0^1 \mathbf{B}^T\mathbf{D}\mathbf{B}\, d\xi\ .$$

The analytical expression of this element stiffness matrix can be found by directly integrating each entry in the matrix (7.14), viz:

$$k_{11}^e = k_s \int_0^1 N_1^2\, d\xi = k_s \int_0^1 (1-\xi)^2\, d\xi = \frac{k_s}{3}$$

$$k_{33}^e = k_s \int_0^1 N_2^2\, d\xi = k_s \int_0^1 \xi^2\, d\xi = \frac{k_s}{3}$$

$$k_{13}^e = k_s \int_0^1 N_1 N_2\, d\xi = k_s \int_0^1 \xi\,(1-\xi)\, d\xi = \frac{k_s}{6}$$

etc.

Thus the element stiffness matrix becomes

$$\mathbf{K}^e = \frac{1}{6}\begin{bmatrix} 2k_s & 0 & k_s & 0 & -2k_s & 0 & -k_s & 0 \\ 0 & 2k_n & 0 & k_n & 0 & -2k_n & 0 & -k_n \\ k_s & 0 & 2k_s & 0 & -k_s & 0 & -2k_s & 0 \\ 0 & k_n & 0 & 2k_n & 0 & -k_n & 0 & -2k_n \\ -2k_s & 0 & -k_s & 0 & 2k_s & 0 & k_s & 0 \\ 0 & -2k_n & 0 & -k_n & 0 & 2k_n & 0 & k_n \\ -k_s & 0 & -2k_s & 0 & k_s & 0 & 2k_s & 0 \\ 0 & -k_n & 0 & -2k_n & 0 & k_n & 0 & 2k_n \end{bmatrix} \tag{7.15}$$

and the displacement vector that is associated with this element stiffness matrix is

$$\mathbf{u} = (u_1 \;\; v_1 \;\; u_2 \;\; v_2 \;\; u_3 \;\; v_3 \;\; u_4 \;\; v_4)^T$$

The formulation expressed in (7.15) agrees with the one derived by Goodman (1968) for the same four-noded joint element.

7.4 Six-noded joint element

This is an extension to the formulations developed in the last section, since a six-noded joint element has the same sturcture and characteristics of a four-noded element.

The following figure shows details of a six-noded joint element. This joint element is modelled by two one-dimensional three-noded elements, and each node has two degrees of freedom.

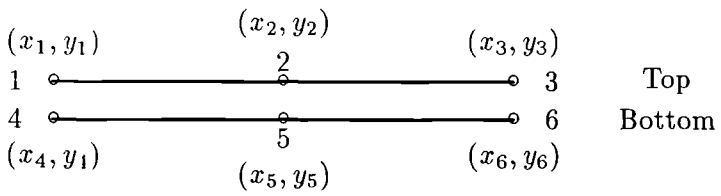

Figure 7.5: Six-noded joint element

For a standard one-dimensional three-noded element, the shape functions are given by

$$N_1(\xi) = \frac{1}{2}\xi(\xi - 1)$$

$$N_2(\xi) = 1 - \xi^2$$

and

$$N_3(\xi) = \frac{1}{2}\xi(\xi + 1)$$

Any displacement along the axes can be expressed by the displacement function

$$x = \sum_{i=1}^{3} N_i(\xi)x_i$$

and

$$y = \sum_{i=1}^{3} N_i(\xi)y_i$$

Performing partial differentiation,

$$\frac{\partial x}{\partial \xi} = (\xi - \frac{1}{2})x_1 - 2\xi x_2 + (\xi + \frac{1}{2})x_3 = \frac{1}{2}(x_3 - x_1) = \frac{1}{2}s_0$$

and

$$\frac{\partial y}{\partial \xi} = \frac{1}{2}(y_3 - y_1) = 0$$

Since x_1, x_2 and x_3 are the x- coordinates of the three nodes of the standard one-dimensional element,

$$2x_2 = x_1 + x_3,$$

and

$$x_3 - x_1 = s_0$$

where s_0 denotes the length of the element, and likewise,

$$2y_2 = y_1 + y_3,$$

Therefore by equations (7.4) and (7.10),

$$\theta = \frac{1}{\frac{1}{2}s_0}\begin{bmatrix} \frac{1}{2}s_0 & 0 \\ 0 & -\frac{1}{2}s_0 \end{bmatrix} = \begin{bmatrix} 1 & 0 \\ 0 & -1 \end{bmatrix}$$

and

$$\mathbf{N}_{top} = \begin{bmatrix} N_1 & 0 & N_2 & 0 & N_3 & 0 \\ 0 & N_1 & 0 & N_2 & 0 & N_3 \end{bmatrix}$$

with

$$\mathbf{N}_{bot} = \mathbf{N}_{top},$$

since the two sub-elements are of the same type.

It follows that the element **B** matrix becomes

$$\mathbf{B} = \begin{bmatrix} 1 & 0 \\ 0 & -1 \end{bmatrix} \begin{bmatrix} N_1 & 0 & N_2 & 0 & N_3 & 0 & -N_1 & 0 & -N_2 & 0 & -N_3 & 0 \\ 0 & N_1 & 0 & N_2 & 0 & N_3 & 0 & -N_1 & 0 & -N_2 & 0 & -N_3 \end{bmatrix}$$

$$= \begin{bmatrix} N_1 & 0 & N_2 & 0 & N_3 & 0 & -N_1 & 0 & -N_2 & 0 & -N_3 & 0 \\ 0 & -N_1 & 0 & -N_2 & 0 & -N_3 & 0 & N_1 & 0 & N_2 & 0 & N_3 \end{bmatrix} \tag{7.16}$$

and the matrix product $\mathbf{B}^T\mathbf{D}\mathbf{B}$ can be obtained as

$$\begin{bmatrix}
k_sM_{11} & 0 & k_sM_{12} & 0 & k_sM_{13} & 0 & -k_sM_{11} & 0 & -k_sM_{12} & 0 & -k_sM_{13} & 0 \\
0 & k_nM_{11} & 0 & k_nM_{12} & 0 & k_nM_{13} & 0 & -k_nM_{11} & 0 & -k_nM_{12} & 0 & -k_nM_{13} \\
k\,M_{12} & 0 & k_sM_{22} & 0 & k_sM_{23} & 0 & -k_sM_{12} & 0 & -k_sM_{22} & 0 & -k_sM_{23} & 0 \\
0 & k_n\,M_{12} & 0 & k_nM_{22} & 0 & k_nM_{23} & 0 & -k_nM_{12} & 0 & -k_nM_{22} & 0 & -k_nM_{23} \\
k_sM_{13} & 0 & k_sM_{23} & 0 & k_sM_{33} & 0 & -k_sM_{13} & 0 & -k_sM_{23} & 0 & -k_sM_{33} & 0 \\
0 & k_nM_{13} & 0 & k_nM_{23} & 0 & k_nM_{33} & 0 & -k_nM_{13} & 0 & -k_nM_{23} & 0 & -k_nM_{33} \\
-k_sM_{11} & 0 & -k_sM_{12} & 0 & -k_sM_{13} & 0 & k_sM_{11} & 0 & k_sM_{12} & 0 & k_sM_{13} & 0 \\
0 & -k_nM_{11} & 0 & -k_nM_{12} & 0 & -k_nM_{13} & 0 & k_nM_{11} & 0 & k_nM_{12} & 0 & k_nM_{13} \\
-k_sM_{12} & 0 & -k_sM_{22} & 0 & -k_sM_{23} & 0 & k_sM_{12} & 0 & k_sM_{22} & 0 & k_sM_{23} & 0 \\
0 & -k_nM_{12} & 0 & -k_nM_{22} & 0 & -k_nM_{23} & 0 & k_nM_{12} & 0 & k_nM_{22} & 0 & k_nM_{23} \\
-k_sM_{1} & 0 & -k_sM_{2} & 0 & -k_sM_{33} & 0 & k_sM_{13} & 0 & k_sM_{23} & 0 & k_sM_{33} & 0 \\
0 & -k_nM_{13} & 0 & -k_nM_{23} & 0 & -k_nM_{33} & 0 & k_nM_{13} & 0 & k_nM_{23} & 0 & k_nM_{33}
\end{bmatrix} \tag{7.17}$$

where

$$M_{ij} = N_iN_j.$$

From the integral

$$\mathbf{K}^e = \int_{-1}^{1} \mathbf{B}^T\mathbf{D}\mathbf{B}\, d\xi\,,$$

each entry of this element stiffness matrix $\mathbf{K}^e$ can be obtained analytically by using direct integration:

$$k_{ij}^e = k_{s/n} \int_{-1}^{1} N_iN_j\, d\xi.$$

For example,

$$k_{11}^e = k_s \int_{-1}^{1} N_1^2\, d\xi = k_s \int_{-1}^{1} \frac{1}{4}\,\xi^2\,(\xi-1)^2\, d\xi = \frac{4k_s}{15}$$

$$k^e_{33} = k_s \int_{-1}^{1} N_2^2 \, d\xi = k_s \int_{-1}^{1} (1-\xi^2)^2 \, d\xi = \frac{16k_s}{15}$$

$$k^e_{55} = k_s \int_{-1}^{1} N_3^2 \, d\xi = k_s \int_{-1}^{1} \frac{1}{4} \xi^2 (1+\xi)^2 \, d\xi = \frac{4k_s}{15}$$

$$k^e_{13} = k_s \int_{-1}^{1} N_1 N_2 \, d\xi = k_s \int_{-1}^{1} \frac{1}{2} \xi (\xi - 1)(1-\xi^2) \, d\xi = \frac{2k_s}{15}$$

$$k^e_{15} = k_s \int_{-1}^{1} N_1 N_3 \, d\xi = k_s \int_{-1}^{1} \frac{1}{4} \xi (\xi - 1) \xi (\xi + 1) \, d\xi = -\frac{k_s}{15}$$

$$k^e_{35} k_s \int_{-1}^{1} N_2 N_3 \, d\xi = k_s \int_{-1}^{1} \frac{1}{2} (1-\xi^2) \xi (\xi - 1) \, d\xi = \frac{2k_s}{15}$$

etc.

Hence, the stiffness matrix $\mathbf{K}^e$ for this joint element becomes

$$\mathbf{K}^e = \frac{1}{15} \begin{bmatrix}
4k_s & 0 & 2k_s & 0 & -k_s & 0 & -4k_s & 0 & -2k_s & 0 & k_s & 0 \\
0 & 4k_n & 0 & 2k_n & 0 & -k_n & 0 & -4k_n & 0 & -2k_n & 0 & k_n \\
2k_s & 0 & 16k_s & 0 & 2k_s & 0 & -2k_s & 0 & -16k_s & 0 & -2k_s & 0 \\
0 & 2k_n & 0 & 16k_n & 0 & 2k_n & 0 & -2k_n & 0 & -16k_n & 0 & -2k_n \\
-k_s & 0 & 2k_s & 0 & 4k_s & 0 & k_s & 0 & -2k_s & 0 & -4k_s & 0 \\
0 & -k_n & 0 & 2k_n & 0 & 4k_n & 0 & k_n & 0 & -2k_n & 0 & -4k_n \\
-4k_s & 0 & -2k_s & 0 & k_s & 0 & 4k_s & 0 & 2k_s & 0 & -k_s & 0 \\
0 & -4k_n & 0 & -2k_n & 0 & k_n & 0 & 4k_n & 0 & 2k_n & 0 & -k_n \\
-2k_s & 0 & -16k_s & 0 & -2k_s & 0 & 2k_s & 0 & 16k_s & 0 & 2k_s & 0 \\
0 & -2k_n & 0 & -16k_n & 0 & -2k_n & 0 & 2k_n & 0 & 16k_n & 0 & 2k_n \\
k_s & 0 & -2k_s & 0 & -4k_s & 0 & -k_s & 0 & 2k_s & 0 & 4k_s & 0 \\
0 & k_n & 0 & -2k_n & 0 & -4k_n & 0 & -k_n & 0 & 2k_n & 0 & 4k_n
\end{bmatrix} \tag{7.18}$$

with its associated displacement vector

$$\mathbf{u} = (u_1 \;\; v_1 \;\; u_2 \;\; v_2 \;\; u_3 \;\; v_3 \;\; u_4 \;\; v_4 \;\; u_5 \;\; v_5 \;\; u_6 \;\; v_6)^T.$$

7.5 Examples

To validate the theory developed for joint elements in the last few sections of this chapter, the following hypothetical models are now going to be investigated.

For a realistic analysis of the joint element in rock masses, it is appropriate to treat the rock mass as an aggregate of massive rock blocks, separated by joints with special and relevant material properties that as a rule will differ from the properties of the adjacent blocks.

7.5.1 A simple example - joint between two rock blocks

The following is a very simple example that illustrates the effect of using a joint element between two uniform rock blocks in the modelling of rock under loads.

In this example, suppose that there exists a joint between the rock blocks. The rock blocks are assumed to be linearly elastic, and they are represented by two blocks which are identical in size and have the same material properties. One block is placed on top of the other, and they are interconnected by a horizontal joint. It is assumed that the joint is also made of linearly elastic material, although its material properties may differ from those used for the rock blocks. In Figure 7.6(a), heavy lines are used to indicate the joint between the two rectangular rock blocks. The bottom end of the bottom block is rigidly fixed to the ground. A uniform surface traction is applied normally from the left to the vertical left-hand side of the top block.

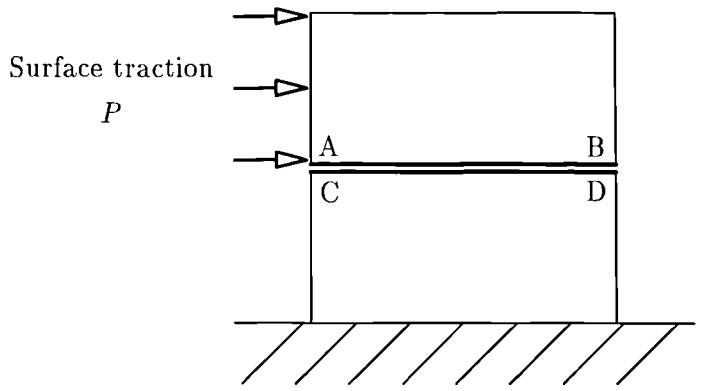

Figure 7.6(a): A simple example - joint between two rock blocks

For the finite element discretization, the mesh used in this example is shown in Figure

7.6(b). The joint between the rock blocks are modelled by four identical joint elements, while the two elastic rock blocks are each modelled by 16 identical eight-noded isoparametric elements, and the horizontal joint is modelled by four identical six-noded joint elements.

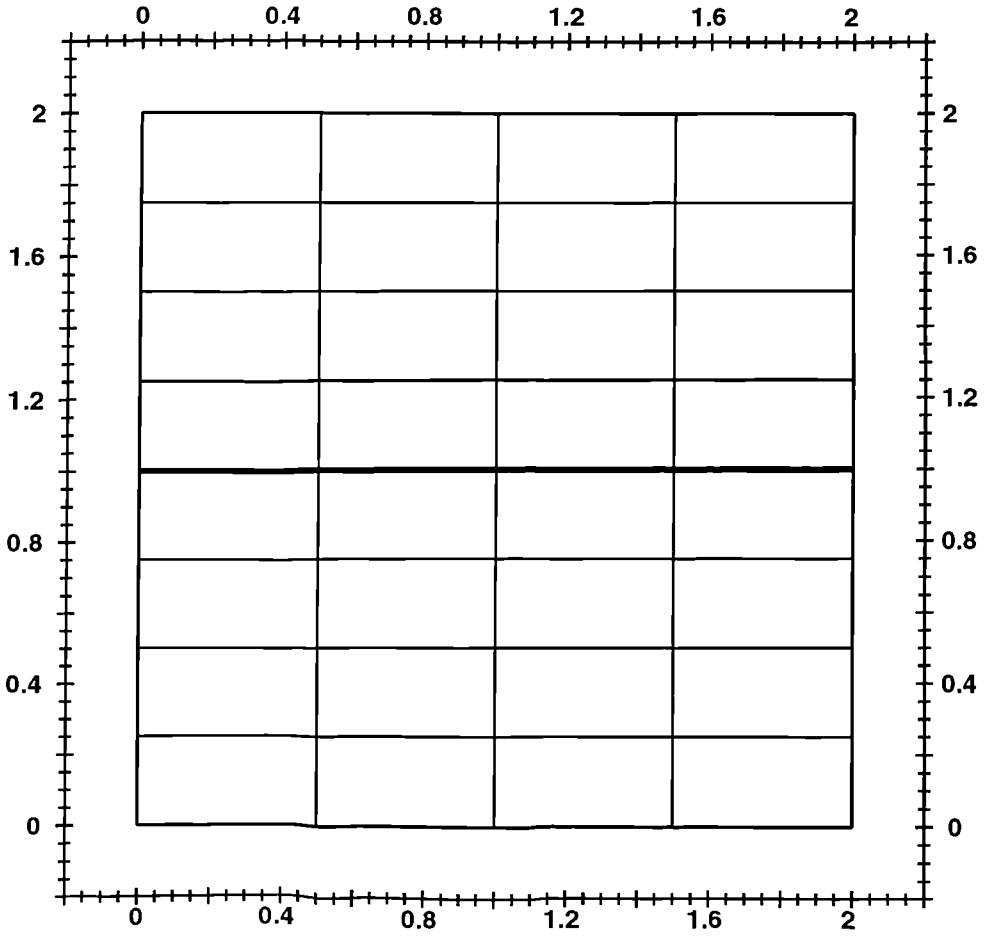

Figure 7.6(b): Element mesh

For direct comparision, different sets of experimental values of horizontal and vertical stiffness k_s and k_n are used, while the material properties for the blocks and the joint remain the same throughout.

Two examples with different k_s and k_n are shown in Figure 7.7. Figures 7.7(a) and 7.7(b) show the deformation of the two blocks, with the same exaggeration factor of 70, subject to the same surface traction of 200N, when algorithms for isoparametric elements

and joint elements are used. In both cases, it can be seen that the bottom block remains fairly stable, while the top block slides away slightly in the direction of the surface traction, and create a tendency to rotate at the centre of its lower end, thus causing the far bottom right end of the top block penetrates downwards into the bottom block. The amount of slide and penetration clearly depends on the values of the parameters k_s and k_n used.

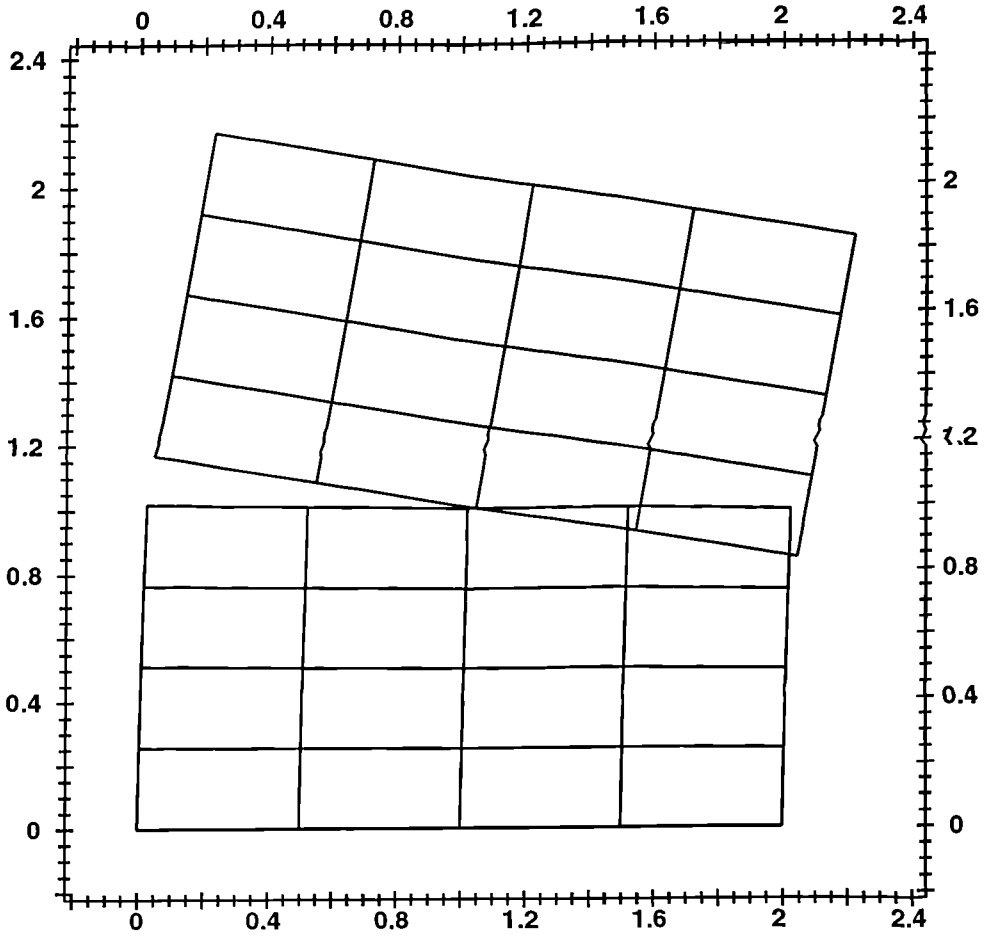

tangential component of the joint stiffness k_s $= 2 \times 10^6 \text{N/m}^2$

normal component of the joint stiffness k_n $= 5 \times 10^5 \text{N/m}^2$

Young's modulus of rock E_r $= 0.2 \times 10^6 \text{N/m}^2$

Poisson's ratio of rock ν_r $= 0.3$

Figure 7.7(a): Example of deformation due to joint element (exaggerated)

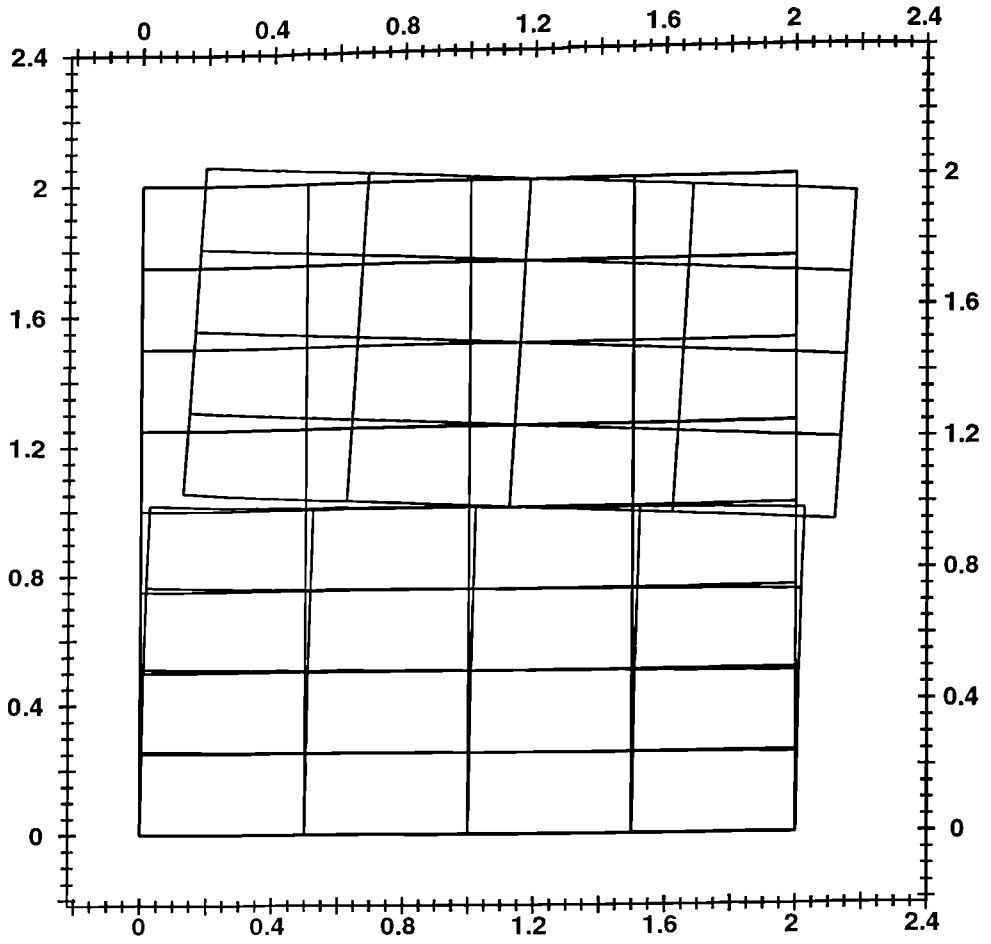

tangential component of the joint stiffness k_s $= 5 \times 10^5 \text{N/m}^2$

normal component of the joint stiffness k_n $= 2 \times 10^6 \text{N/m}^2$

Young's modulus of rock E_r $= 0.2 \times 10^6 \text{N/m}^2$

Poisson's ratio of rock ν_r $= 0.3$

Figure 7.7(b): Example of deformation due to joint element (exaggerated)

With different values of joint stiffness, the amount of deformation (all units are in meter) at different ends of the joint can be summarized in the following table.

		A	B	C	D
$k_s = 2 \times 10^6$	u	0.516×10^{-3}	0.440×10^{-3}	0.265×10^{-3}	0.248×10^{-3}
$k_n = 5 \times 10^5$	v	0.168×10^{-2}	-0.167×10^{-2}	0.187×10^{-3}	-0.176×10^{-3}
$k_s = 10^6$	u	0.769×10^{-3}	0.685×10^{-3}	0.264×10^{-3}	0.253×10^{-3}
$k_n = 10^6$	v	0.932×10^{-3}	-0.923×10^{-3}	0.187×10^{-3}	-0.180×10^{-3}
$k_s = 5 \times 10^5$	u	0.127×10^{-2}	0.118×10^{-2}	0.263×10^{-3}	0.257×10^{-3}
$k_n = 2 \times 10^6$	v	0.556×10^{-3}	-0.551×10^{-3}	0.186×10^{-3}	-0.182×10^{-3}

Table 7.1 Computed displacement values of Example 1

7.5.2 Goodman's joint examples

The following examples of the application of joint elements have been investigated by Goodman *et al* (1968). The main purpose of these examples is to examine the freedom to shift and rotate of blocks of arches and beams in a blocky rock system.

The behaviour in a complex structure must be analysed by a technique which can simulate block movements in a simple intersection. Figure 7.8 shows a mesh used to simulate the intersection of a through going and a staggered joint set. In this model, three elastic blocks are used, each comprises 16 isoparametric elements. The horizontal and vertical joints are made up of eight joint elements. They are indicated by heavy lines.

To elaborate on the structure of the mesh near the joint, Figure 7.9 shows the initial position of the eight joint elements and of the adjacent block elements.

At the intersection point, three nodal points with identical coordinates are used. In the examples that follow, six-noded joint elements are used, and the nodes details of the joints are shown in Figure 7.10.

In the finite element analysis of the blocks, the small displacement theory is first used.

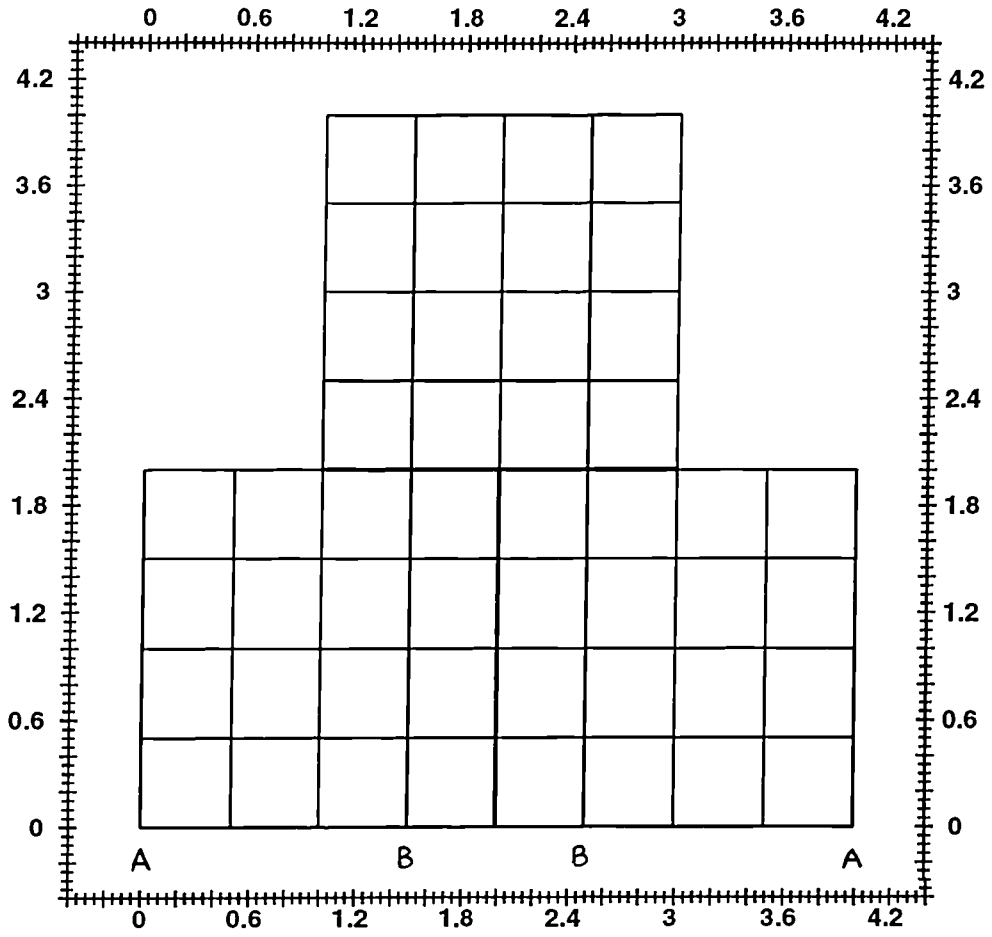

Figure 7.8: Element mesh of Goodman's joint

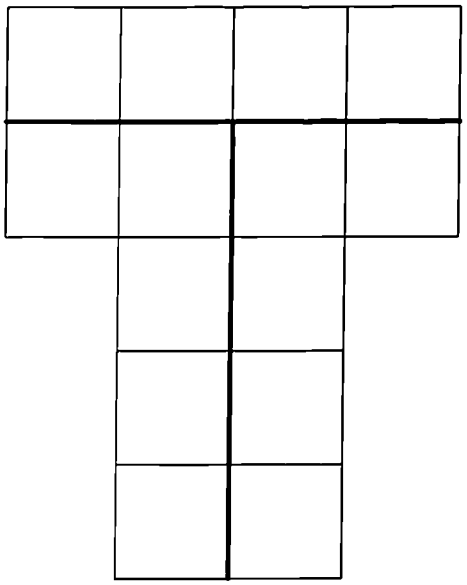

Figure 7.9: Joint elements at intersection

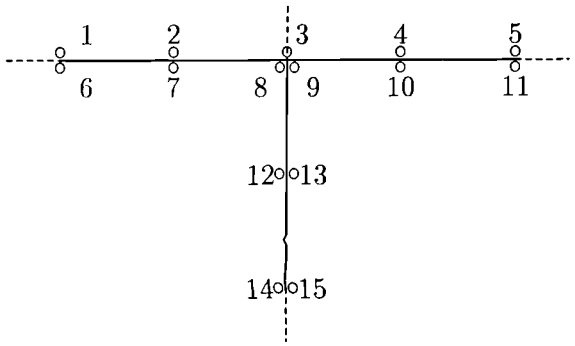

Figure 7.10: Nodes details of joints at intersection

To simulate a real life situation, two problems were run. In Problem 1, the support of the system was fixed in both the x and y directions in the outer corners at points A (see Figure 7.11(a)). This creates an unstable situation in which the top block tends to drop down with rotations about points A. In Problem 2, the supports were moved to points B (see Figure 7.11(b)). This created the tendency for opposite sense of rotation. In both problems, uniform surface traction is applied vertically downwards and normal to the top side of the top elastic block to initiate deformation.

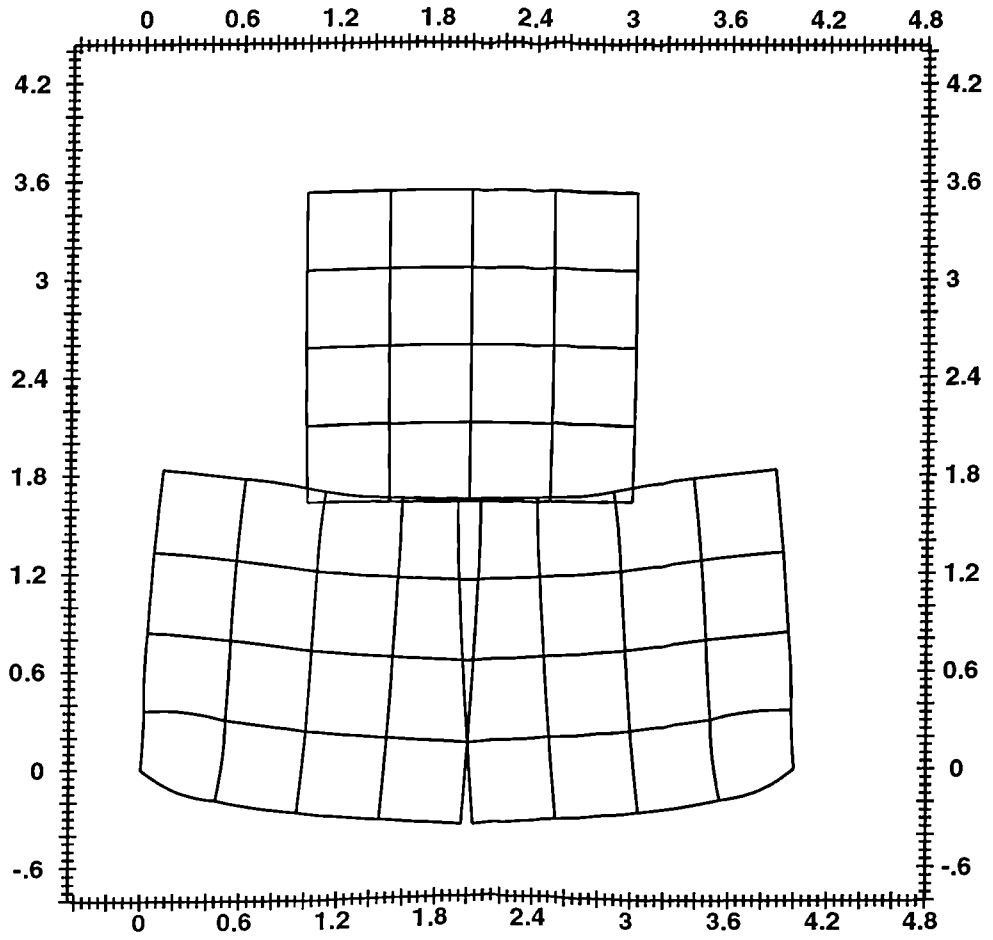

tangential component of the joint stiffness k_s $= 10^6 \text{N/m}^2$

normal component of the joint stiffness k_n $= 10^6 \text{N/m}^2$

Young's modulus of rock E_r $= 0.2 \times 10^6 \text{N/m}^2$

Poisson's ratio of rock ν_r $= 0.3$

surface traction $= 10\text{N}$

Figure 7.11(a): Problem 1 - Deformation of Goodman's joint (with exaggeration factor 300)

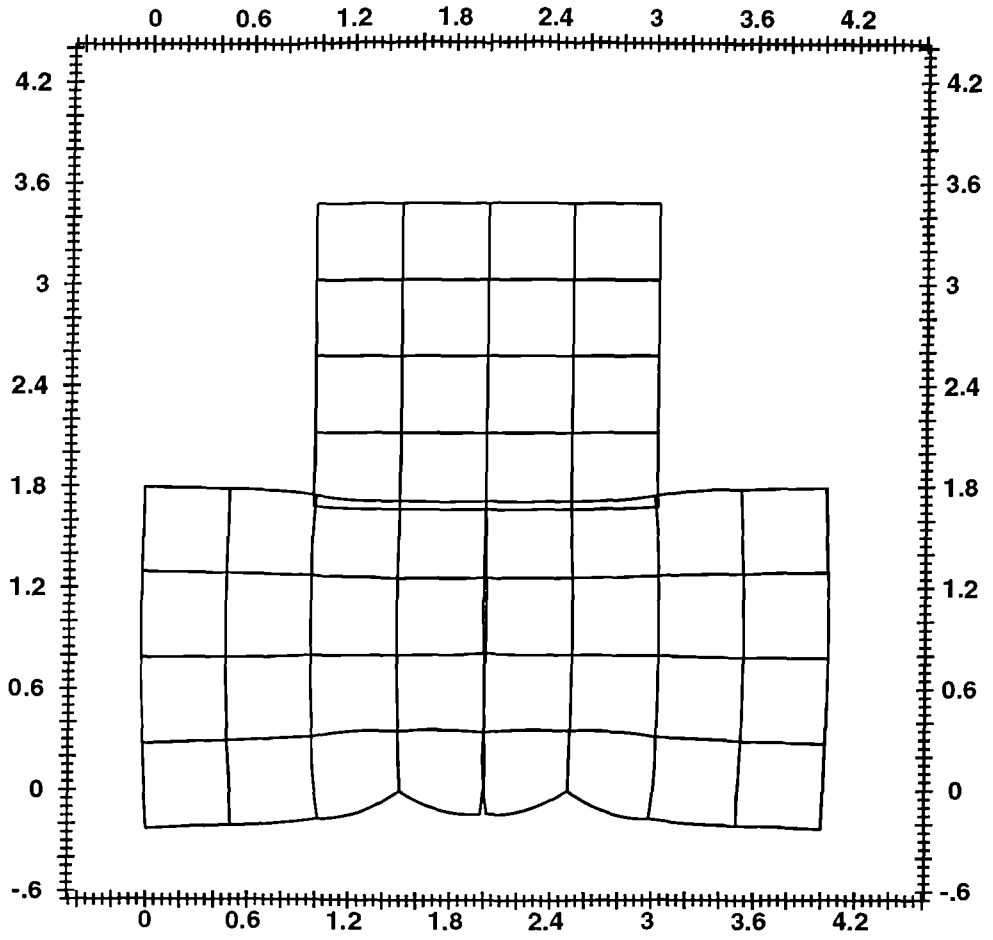

tangential component of the joint stiffness k_s $= 10^6 \text{N/m}^2$

normal component of the joint stiffness k_n $= 10^6 \text{N/m}^2$

Young's modulus of rock E_r $= 0.2 \times 10^6 \text{N/m}^2$

Poisson's ratio of rock ν_r $= 0.3$

surface traction $= 20\text{N}$

Figure 7.11(b): Problem 2 - Deformation of Goodman's joint (with exaggeration factor 2000)

For Problem 1, Figure 7.11(a) shows the partial opening of the lower part of the vertical joint, together with the mutual penetration of horizontal block elements. The downward movement of nodal points in the top side of the top elastic block is indicated by d.

For Problem 2, Figure 7.11(b) shows high stresses are being developed normal to the top elements of the vertical joint. It causes compression in all joint elements.

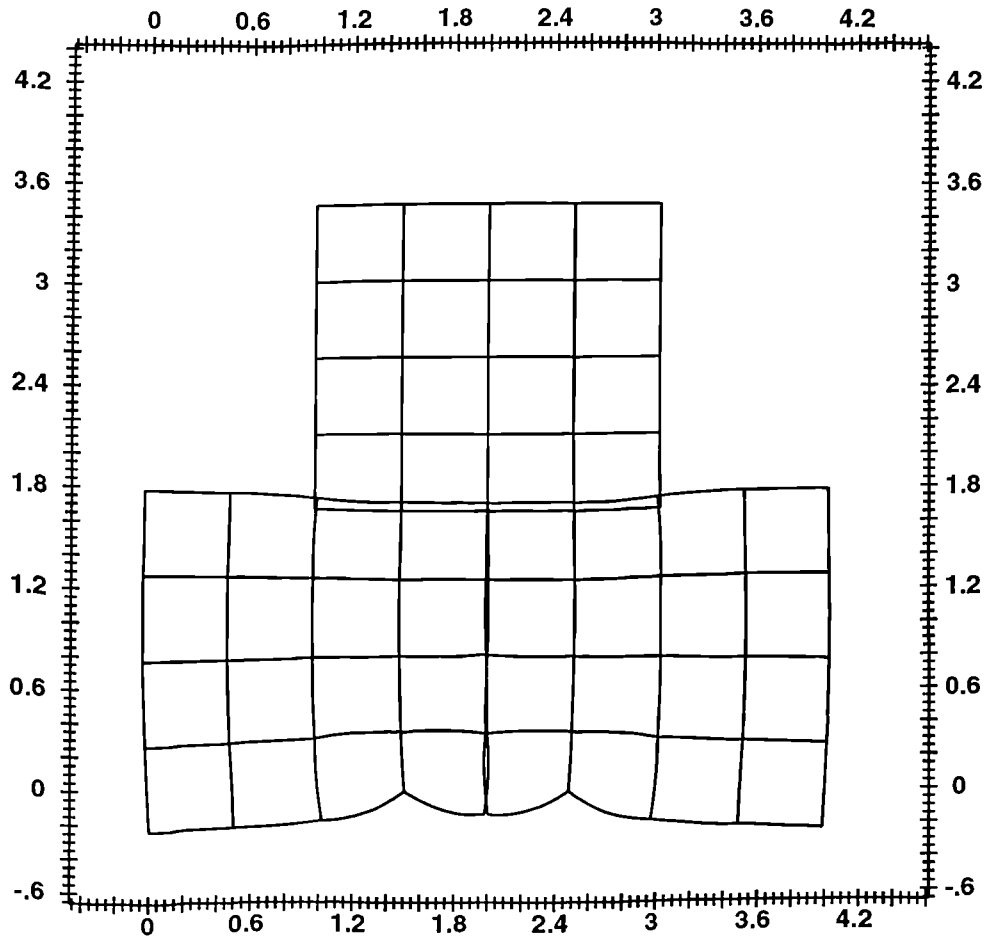

Figure 7.12: Problem 2 - Deformation of Goodman's joint (with exaggeration factor 2000) with supports fixed in the vertical direction only.

To distinguish between the effect of using different types of support under the same environment, the above two problems are run again. In both cases, the supports are placed at the same points, but they are fixed in the vertical direction only, so that the structure is free to slide horizontally at the supports. As before, a uniform surface tension of is applied vertically downwards and normal to the top side of the top elastic block. All other parameters, including the geometric properties of the rock mass and the stiffness of the

joint, remain the same throughout.

Using the same exaggeration factor of 2000 as before for direct comparison, Figure 7.12 shows how the structure deforms in Problem 2. When compared with Figure 7.11(b) when the supports are fixed in both x- and y-directions at points B, it can be seen that the overall shape of the deformations in these two cases are very similar. The most noticable difference is at the lower end of the vertical joint, where the structure opens up more than in the previous case. This is of course very reasonable, as the joints at points B allows the structure to slide horizontally and thus allows more horizontal movement sliding away from the centre of the structure.

To experiment the use of different parameters under different criteria, Problem 1 is executed again with the same set of parameters as before, but with the supports at points A both fixed in the vertical direction only. This means that when loading is applied, the supports and hence the base of the structure can slide freely along the horizontal direction. The program fails to give any solution, which indicates that total collapse of the structure has occured. Further experiments show that with careful choice of material properties of the rock block and the joint, this problem may be able to give some reasonable results. It shows that the Goodman joint is quite sensitive to the use of parameters. For example, if the wrong set of joint stiffness is used, the internal stress caused by the rock mass may cause the joint to slide away infinitely and hence cause the structure to collapse.

To compare these results with the original program tested by Goodman (1968), Figure 7.12(a) shows his deformed meshes for Problems 1 and 2. In his experiment, point A and B were supported by rollers which only allow horizontal movement at these points. Goodman showed that in Problem 1, the bottom blocks rotated as initial failure was taking place, thus total collapse was observed. In Problem 2, the upper three elements in the vertical joint failed, while the other joint elements were in compression. This model were found to be stable, despite the failure of the three joint elements. These findings had the same characteristics of those obtained in this chapter.

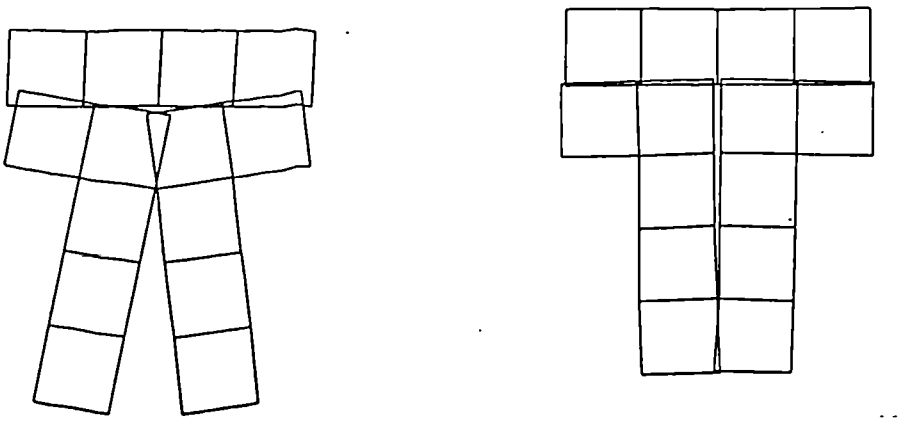

Problem 1 Problem 2

Figure 7.12(a) Results obtained by Goodman (1968)

Goodman's paper produces Figure 7.12(a), but does not give any values for displacements. However, it can be seen that the deformation characteristics in both cases are very similar. These similarities are indeed expected, since the formualtion of the stiffness matrix for a four-noded joint element in both cases is identical.

7.6 Large displacement analysis

In order to obtain a more realistic effect of using joints in rock mechanics, large displacement analysis must be used. However, because of the limitation of this thesis, only linear load-displacement analysis for the rock joint has been established. Therefore, it is proposed that, while linear analysis is used for joint elements, large displacement analysis is used for rock and other types of elements hereafter.

7.6.1 Residual loads

In §4.4.3, it has been discussed in full how residual loads are calculated in the iterative process in the large displacement analysis of eight-noded isoparametric rock elements. To analyse the deformation of a rock mass together with rock joints, the large displacement formulation, together with the algorithm for the residual load for rock elements, and the

small displacement formulation for the joints are mixed together in the program.

The implementations of these two algorithms are not the same, therefore extreme care must be exercised in order to make sure that residual loads are not considered for joint elements. This can be achieved by setting the values of the residual load to zero at all nodes of the joint elements with respect to the global displacement vector in all subsequent iterations. It implies that the displacements of these nodes are always zero during iteration, and hence the contribution from the joint elements for the whole system only comes from the first step in each incremental step.

7.6.2 Goodman's joint - an example

As an example, Problem 1 of Goodman's joint examples (see Figure 7.8) is run again with the above mixed algorithm. In this example, supports are placed at points A, and they are rigidly fixed in both the x- and y- directions. All other parameters used in this example are the same as before.

Figure 7.13 shows the results of the deformed mesh of Problem A in Goodman's joint, according to the above proposed mixed algorithm, and computed by the computer program. When compared with Figure 7.11(a), where small displacement analysis is used for all elements, the deformed meshes in both cases share a very similar characteristic. Indeed this should be the case, as nonlinear deformation of the rock mass should behave like a linear one when a relatively small loading is applied. As the loading increases, difference between the two analyses will become more significant. After some stage, the mixed algorithm fails, which indicates that the critical load of the structure has been reached, and total collapse has occurred. This situation only arises when large displacement analysis is used for the rock mass.

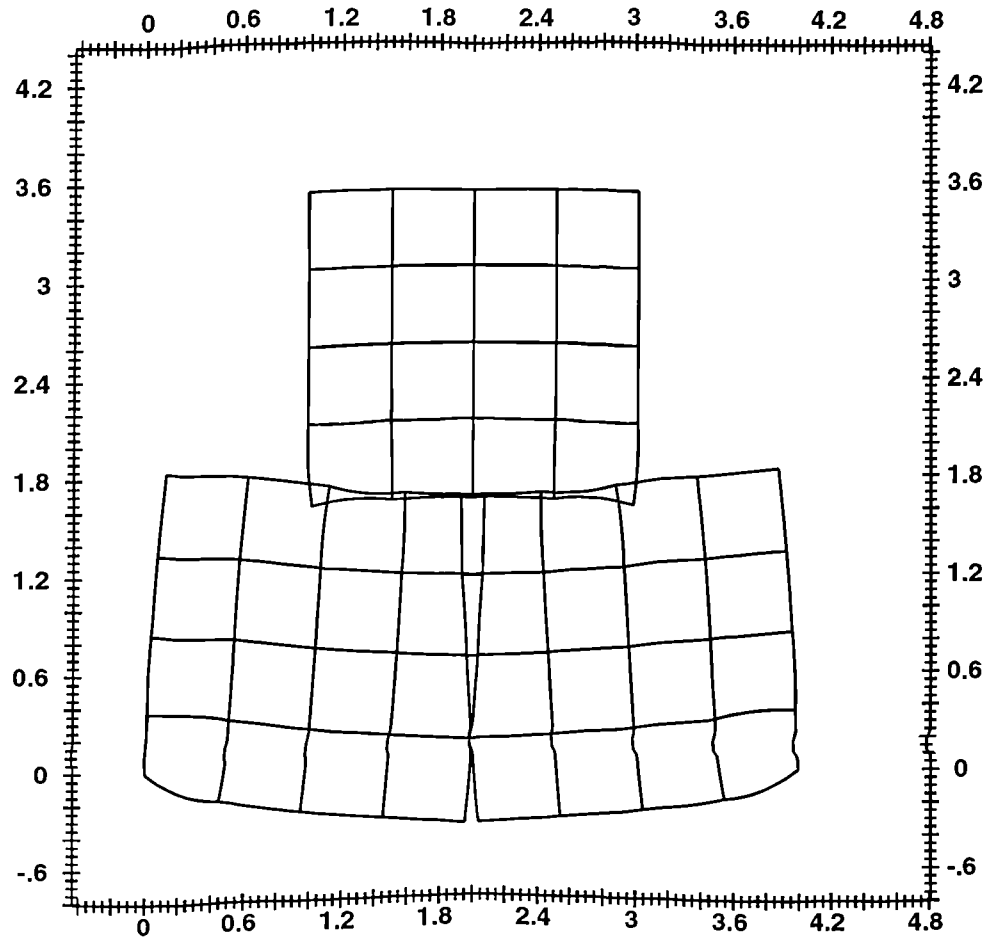

Figure 7.13: Problem 1 - Large displacement analysis of Goodman's joint (exaggeration factor 300) with supports fixed in x- and y- directions.

7.7 Discussion and conclusion

The joint element presented and the method of analysis discussed in this chapter seems to handle adequately such joint behavioral features as failure in tension, shear, rotation of blocks, development of arches, and even, to a certain extent, the collapse pattern of structures in jointed rock.

The formulation of the joint element introduced here can be used for shell-to-shell, shell-to-solid and solid-to-solid interfaces in either two or three dimensions. In the context

of this thesis, two-dimensional solid-to-solid type is used. One of the main properties of this joint element is that it assumes zero thickness, which is particularly suited for modelling rock joints and fractures. One of the main aims of developing this element is to apply it to the modelling of excavations in rock, where rock mass is traversed by bedding planes and fractures, and then the effect of using rockbolts as supports in jointed rocks.

The classification by means of stiffness, k_n and k_s, and strength seems profitable, as these properties directly describe the potential behaviour of the joint and can be used in finite element analysis. Direct measurements of the joint quantities mentioned is important, perhaps even more so than measuring the rock block properties.

Due to the limitation of this thesis, only linear analysis of joint element has been considered. Ways to incorporate it into the large displacement analysis of rock mass have been discussed, and although the overall results of the combined analyses are adequate, it would be more realistic and meaningful if nonlinear analysis is used for all types of elements throughout. This would, of course, open up a potential for further investigation.

Chapter 8

Rockbolt Element

In tunnel engineering, fully grouted untensioned rockbolts are one common type of support system that is used to prevent structural failure of the tunnel during excavation. Adequate analytical design methods for the length and spacing of rockbolts are not available for various ground conditions even though the use of these rockbolts is increasing. Numerical modelling is one design approach. However, this method requires a better understanding than is currently available of the mechanics involved in the transfer of load between the bolt and the surrounding rock mass.

In the numerical simulation of tunnel engineering, some problems require an adequate determination of rock properties and existing stresses, and an efficient modelling of the discontinuities and the structure in the post-elastic phase. Rock mass reinforcement is one such problem.

The action of the reinforcement system depends on the fixing conditions of the anchoring elements to the rock mass. This can be acheived by either fixing extreme points of the bolt (mechanically anchored), or continuously by grouting the whole length of the bolt (fully grouted). Mechanically anchored rockbolts are mainly employed in temporary short anchors in strong rock, while fully grouted rockbolts can be permanently used in both loose and cohesive soils. The mechanics of these two types of rockbolt are illustrated in Figure 8.1(a).

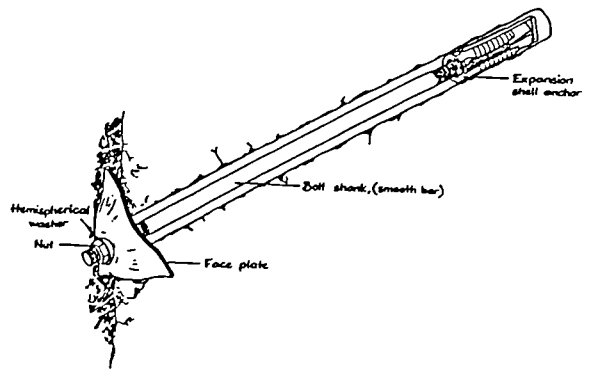

(a) Mechanically anchored rockbolt

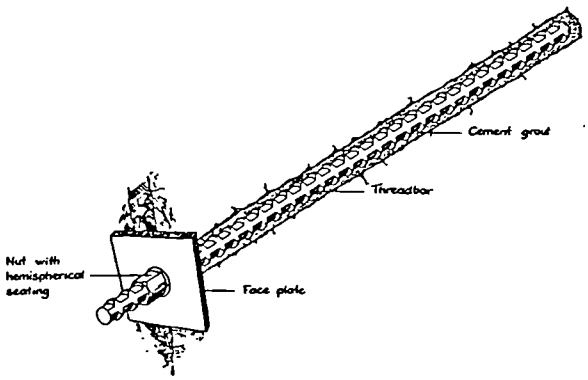

(b) Fully grouted rockbolt

Figure 8.1: (a) Mechanics of rockbolts (from Pellet 1994)

Rockbolts have made possible several new construction designs in civil engineering, and they can be used either as a temporary or permanent support measure.

To maximize the effect of using rockbolts as support in tunnel excavation, it is essential that rockbolts should be:

1. able to withstand high tensile strength of the rock mass and the deformation of the rockbolts;
2. corrosion resistant and durable, even under aggressive water and rock deformations;
3. made of materials appropriate to the particular characteristics of the applications;
4. flexible and can be set in most confined locations in tunnelling and mining sites.

Depending on the designs and intended uses, rockbolts come in different shapes and

sizes. Figure 8.1(b) shows examples of some of today's most commonly used grouted rockbolts in rock engineering.

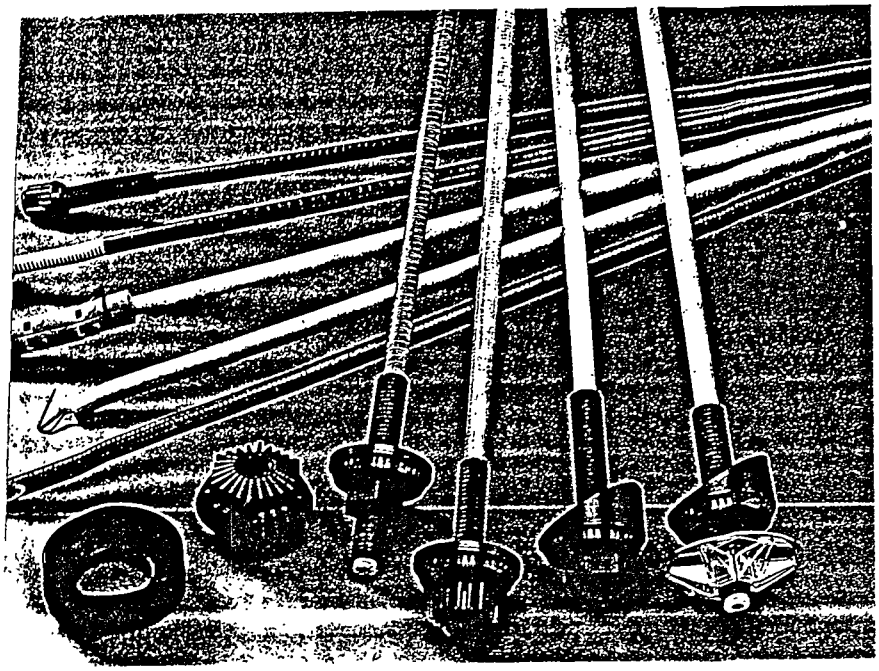

Figure 8.1(b): Examples of some commonly used grouted rockbolts in tunnel engineering (courtesy of H. Weidmann, Switzerland)

8.1 Introduction

Despite their popularity in tunnel engineering, the modelling of grouted rockbolts poses some particular problems. For example, the bolt does not produce a significant effect on the global model until a large amount of deflection has taken place. This occurs if the rock may have joint discontinuities or be in a plastic phase.

Another problem with the numerical technique to simulate the effect of using grouted rockbolts is the lack of an adequate global model of a grouted rockbolt. Development of such a model necessitates adequate definition of the interaction machanics between the rockbolt and the rock mass.

The finite element method has been established as an important numerical tool for modelling tunnels and excavations, and much literature has been published on the finite element modelling of grouted rockbolts. The purpose of this chapter is to further investigate the feasibility of using rockbolts as support in tunnel excavation, to explore its potential, and to develop an efficient and accurate algorithm for a rockbolt element when

the surrounding rock mass is under a full range of loadings. The final element will be incorporated into a commerically used package, FESTA, for validation on real-life data.

8.2 Finite element modelling of rockbolts

The general approach of the finite element method consists of replacing the actual structural system by a system of a finite number of elements interconnected at a finite number of nodal points. In earlier chapters, it has been shown how this method can be used to model rock mass, thin rods, and joints by using appropriate types of elements. For a rockbolt member, these finite elements have to be selected so that they can accurately represent the behaviour of the rock, grout and the steel reinforcement, and the interactions between the components.

The main aim of this chapter is focus on the finite element modelling of rockbolts, together with steel reinforcement characterized by beam-type behaviour, and grout that is attached to the rock mass. The rockbolts and their surrounding media are assumed to be homogeneous and isotropic throughout, and to have linearly elastic stress-strain relationships. The surrounding rock mass is discretised by two-dimensional eight-noded isoparametric elements, and the discontinuities or the spaces between two interacting rock blocks are discretised by two-dimensional six-noded joint elements; details of these types of elements can be found in earlier chapters. A mesh of six-noded rockbolt elements is used to discretise the rockbolt, as described in detail below.

8.2.1 Development of the rockbolt element - early models

Reinforcement of *in situ* soils and rocks has always been the subject of the engineer's considerations. Man had built superficial and underground structures for a long time, the earliest form of rockbolt was made of wood and was used to prevent rock falls. During the excavation of Mont-Cenis tunnel (1857-1871), Germain Sommeiller introduced the pneumatic hammer. This technique later evolved into the idea of installing steel bars for rock reinforcement.

The first fundamental studies on rockbolts were undertaken by Panek (1956). His efforts concentrated on the suspension and beam building effects of rockbolts. Works which led to the introduction of rockbolts into the New Austrian Tunnelling Method were ini-

tated by Rabcewicz (1964, 1965). Hugon & Costes (1959) derived formulae to calculate the optimum fixing force for a mechanical base and the fixing strength of rock. Ewoldsen & Goodman (1967) first used the finite element method to analyse rockbolts to investigate the axial, radial, and tangential stress components around a bolt fixed into elastic homogeneous rock.

Other early numerical models of rockbolt were considered by Barla and Cravero (1972), and Zienkiewicz (1977). Heuze & Goodman (1973) introduced the idea of the reinforcement effect of rockbolts at discontinuities. The rockbolts were represented by one-dimensional elements with axial stiffness. St. John & van Dillen (1983) used a three-dimensional element when the tangential stiffness of the bolt and the grout were taken into account. Lorig (1985) also considered this problem, but difficulties arose in the interpretation of real-life physical situations to reproduce the parameters used in this model.

8.2.2 Rockbolt element in coupled form

In a two-dimensional stress/strain problem, the use of rockbolt elements to simulate grouted rockbolts in a rock mass is in fact an effect-dominated technique. Therefore, rockbolt elements are only imaginary one-dimensional elastic elements that could have different strength, although in reality, rockbolts are three-dimensional objects and have physical weights etc.

In finite element analysis, the action of the rockbolt in the continuous rock mass near the joint is so complex that it is necessary to use two sub-elements to model a rockbolt element. This type of element was introduced by Aydan (1988). In its three-dimensional form, it consisted of an eight-noded element, two nodes connected to the steel bolt and six jointed onto the rock mass; the steel bolt was thus modelled by a one-dimensional two-noded linear bar element. In a two-dimensional problem, only four nodes were involved. This type of rockbolt has been widely adapted since, and based on this design, many different versions have been proposed.

Swoboda & Marenče (1991, 1992, 1995) and Marenče (1992) considered the special problem of the rockbolt dowel effect at the crossing with joints in rocks, when a specific type of element called the *bolt crossing joint* has been introduced. This element directly connected bolt elements on both sides of the discontnuity (joint element). It was mod-

elled as springs that describe bolt resistance according to movement at the joint. A brief description of this element can be found in Section 10.5

In another variation on Aydan's rockbolt element, Reed *el al* (1992a) used a three-noded quadratic bar element to model the bolt. The nonlinear analysis was derived from the fundamental nonlinear stress, strain and displacement relationships. Unfortunately the paper was unfinished and was deprived of any numerical results to justify its analytical approach. Egger & Pellet (1992) defined an interface element whose thickness corresponds to the distance between the two plastic hinges in the bolt. Pellet (1994) studied in detail the influence of the principal mechanical and geometrical characteristics on the shear process of the reinforced joint.

8.2.3 Other recent related developments

Based on the usual *ungrouted tensioned rockbolt theory*, *Labiouse (1996)* made three improvements by considering the elastic compression of the carrying ring surrounding the excavation due to the bolts preload; the transfer of the reaction force to the rock mass in the bolts anchoring zone; and the relative displacement of the bolt ends, which has an effect on their tension. Roy & Rajagopalan (1997) used the classical beam-column theory for evaluating passive rockbolt roof reinforcement by modelling each rockbolt as a linear spring and by allowing in the model for non-uniform bolt spacing. The performance of grouted rockbolts subject to close proximity blasting was evaluated by Stjern *et al* (1998). This consisted of pull-out tests of bolts and vibration measurements on both the rock and the bolts.

Unfortunately, the author cannot find any articles published in the past year or so which contain further developments of Aydan's bolt model.

This thesis uses the idea introduced by Reed *el al* as a springboard; it examines the viability of using a beam element to discretise the steel bolt, and it offers a different approach to establish a large displacement formulation for the new rockbolt element.

The use of bar and beam elements to discretise a thin rod has been discussed extensively in Chapters 5 and 6, and it was concluded that the beam element gives a much more realistic result than a bar element. In Aydan's rockbolt element, the steel bolt is discretised

by bar elements. It can be envisaged that improvement can be made if beam elements are chosen to model the steel bolt instead. In particular, a separate *bolt crossing joint* element should not be needed, as the beam element ensures continuity of curvature along the bolt.

8.2.4 Aydan's rockbolt element

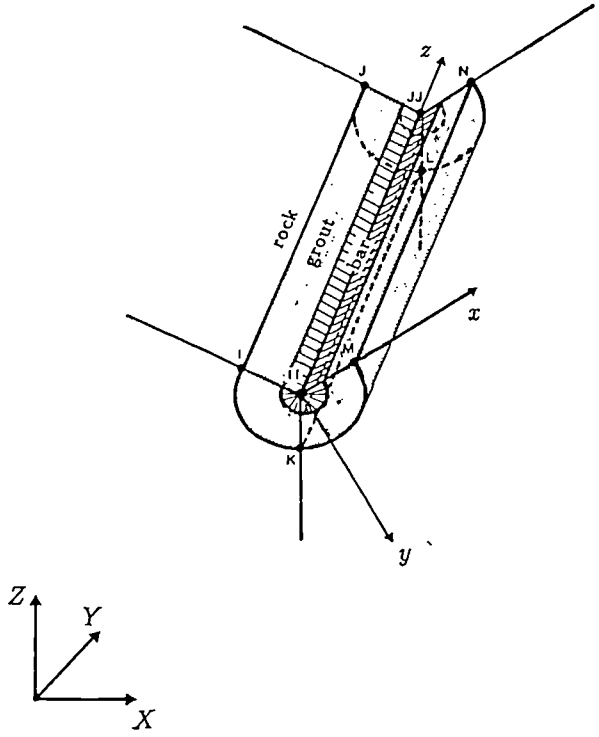

Figure 8.2: The three-dimensional representation of Aydan's rockbolt (from Aydan(1989))

Figure 8.2 shows Aydan's rockbolt element in three dimensions. This element has eight nodes, two connected to the bolt, and six jointed to the rock mass. The following mechanical responses of the rockbolt and their governing equations were considered by Aydan (1989):

1. Equilibrium equation for axial loading in the steel bar:

$$\frac{d\sigma^b_{zz}}{dz} = 0$$

where σ^b_{zz} is the axial stress in the bolt.

2. Equilibrium equation for shear loading in the steel bar:

$$\frac{d\tau^b_{zr}}{dz} = 0$$

where τ^b_{zr} is the shear stress in the bolt.

3. Equilibrium equation for shear loading in the grout annulus:

$$\frac{d\tau_{rz}^g}{dr} + \frac{\tau_{rz}^g}{r} = 0$$

where τ_{rz}^g is the shear stress in the annulus.

4. Equilibrium equation for normal loading in the grout annulus:

$$\frac{d\sigma_{rr}^g}{dr} + \frac{\sigma_{rr}^g}{r} = 0$$

where σ_{rr}^g is the normal stress in the grout.

The local element stiffness matrix in cylindrical coordinates can be expressed as

$$\mathbf{K}_{b,g} = \begin{bmatrix} [\mathbf{K}]_b & \\ & [\mathbf{K}]_g \end{bmatrix}$$

where $[\mathbf{K}]_b^e$ describes the contribution from the bolt, and it takes the form

$$[\mathbf{K}]_b^e = \begin{bmatrix} K_b^r & 0 & -K_b^r & 0 \\ 0 & K_b^z & 0 & -K_b^z \\ -K_b^r & 0 & K_b^r & 0 \\ 0 & -K_b^z & 0 & K_b^z \end{bmatrix}$$

with

$$K_b^r = \frac{G_b A}{L}, \qquad K_b^z = \frac{E_b A}{L}, \qquad \text{and} \qquad A = \pi r_b^2,$$

and L is the length of the element.

The matrix $[\mathbf{K}]_g$ represents the contribution from the grout annulus, and it takes the form

$$[\mathbf{K}]_g^e = \begin{bmatrix} 2K_g^r & 0 & K_g^r & 0 \\ 0 & 2K_g^z & 0 & K_g^z \\ K_g^r & 0 & 2K_g^r & 0 \\ 0 & K_g^z & 0 & 2K_g^z \end{bmatrix}$$

with

$$K_g^r = \pi E_g \frac{L}{3\ln(r_h/r_b)}, \qquad K_g^z = \pi G_g \frac{L}{3\ln(r_h/r_b)}$$

The disadvantage of this formulation is that only axial and shear stiffnesses are considered, thus neglecting the bending stiffness of the bolt.

There are two main modifications proposed in this thesis to the Aydan rockbolt element, namely, to replace bar elements by beam elements in the discretization of the steel bolt, and to consier dowel effect to model the transverse movements between the steel bolt and the grout-rock interface.

8.2.5 Properties of the rockbolt element

In this modification, a number of one-dimensional four- or six-noded rockbolt elements are normally used to model a grouted rockbolt. The number of rockbolt elements required in the analysis depends on the length of the rockbolt, the accuracy of the analysis, and the amount of storage space available in a computer. Figure 8.3(a) shows how a typical six-noded element is modelled to join onto a rock element, and its detailed node arrangement is shown in Figure 8.3(b).

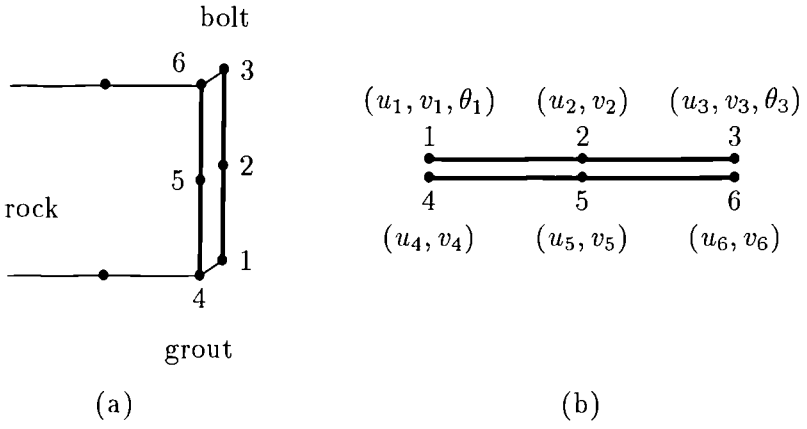

Figure 8.3: Details of a rockbolt element

In this finite element model, the grout is discretised by an interaction between bolt nodes 1, 2, 3, and rock nodes 4, 5 and 6. The latter share one edge of eight-noded isoparametric quadrilaterial elements which represents the rock mass that the rockbolt is grouted onto, and each node has two translational degrees of freedom. Throughout this thesis, the six-noded rockbolt element is strictly modelled to join onto one side of an eight-noded isoparametric rock element in the manner as shown in Figure 8.3(a).

One of the main concerns of this thesis is to use a beam element as the sub-element to

model the steel bolt, so that when internal shear forces and bending moments are considered, the steel bolt can exhibit a natural curvilinear bending characteristic when loading is applied to the rock mass. Therefore, in common with a beam element, the middle node of the beam element has two translational degrees of freedom, while each end-node has in addition a rotational degree of freedom, as shown in Figure 8.3(b). Initially, the corresponding nodes of the sub-elements that model the steel bolt and the grout share the same coordinates.

The new rockbolt element is based on Aydan's type of grouted rockbolt element, and so they share the same characteristics. Hence the properties of the latter can be essentially carried forward to the new element, viz:

1. Nodes 1, 2 and 3 are on the axis of the bolt, and they represent the steel bolt of the grouted rockbolt;

2. Nodes 4, 5 and 6 are on the outside surface of the bolt, which are attached to the rock mass;

3. Throughout this chapter, the numbering of these nodes for a rockbolt element is arranged strictly in the order as shown in Figure 8.3(b);

4. The relative deformation between the outside nodes 4, 5 and 6 and the central nodes 1, 2 and 3 produces the shear stress in the grout, which transfers loads from the rock mass around the grout to the steel bolt of the rockbolt.

The one-dimensional rockbolt element is uniform and is 'cylindrical', and the steel bolt and the grout are 'axisymmetrical', which means they both have measurable length and non-zero radius, and their axes are collinear. Further, the element is assumed to have no weight. The rockbolt is made of isotropic, homogeneous, and perfectly elastic material, and it can produce either linear or nonlinear deformation under loadings. It is also assumed that there is no slip in the interface between the steel bolt and the grout, and the interface between the grout and the rock mass. Materially nonlinear behaviours such as slip, debonding and plastic yield could be added to the element in later research, once the basic elastic element has been proved to perform acceptably.

8.2.6 Geometry of the rockbolt element

In common with other one-dimensional elements, the mechanics of a rockbolt element is generally described in relation to its local axial direction.

Initiallly the global x-axis is taken along the longitudinal direction of the element. When loading is applied, the element deforms and suppose at some stage, it lies on the local x'-axis, which is inclined at an angle β to the global x-axis, as shown in Figure 8.4.

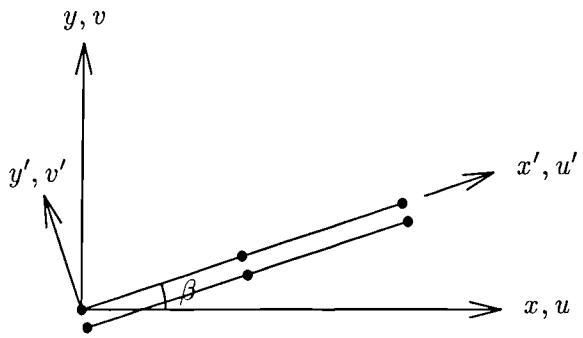

Figure 8.4: Element geometry

It has been seen in Chapter 5 that the angle β at a point can be obtained from equation (5.3) by

$$\sin\beta = \frac{a_y}{\sqrt{a_x^2 + a_y^2}} \qquad \text{or} \qquad \cos\beta = \frac{a_x}{\sqrt{a_x^2 + a_y^2}},$$

where a_x and a_y are the Cartesian derivatives of the displacement functions of the element in the axial and the radial directions respectively.

Suppose that node i has two translational degrees of freedom. Its displacement vector $\mathbf{u}_i'$ in terms of the rotated axes x', y' is related to the Cartesian displacement $\mathbf{u}_i$ in the global axis by

$$\mathbf{u}_i' = \begin{bmatrix} u_i' \\ v_i' \end{bmatrix} = \begin{bmatrix} \cos\beta & \sin\beta \\ -\sin\beta & \cos\beta \end{bmatrix} \begin{bmatrix} u_i \\ v_i \end{bmatrix} = \mathbf{R_2}\mathbf{u}_i \,, \tag{8.1}$$

and likewise, in the case of a beam element when the end-node i has an additional rotational degree of freedom θ_i, this relationship becomes

$$\mathbf{u}_i' = \begin{bmatrix} u_i' \\ v_i' \\ \theta_i \end{bmatrix} = \begin{bmatrix} \cos\beta & \sin\beta & 0 \\ -\sin\beta & \cos\beta & 0 \\ 0 & 0 & 1 \end{bmatrix} \begin{bmatrix} u_i \\ v_i \\ \theta_i \end{bmatrix} = \mathbf{R_3}\mathbf{u}_i \,. \tag{8.2}$$

Combining these relationships, for example, for a three-noded beam element e, the element 8×8 rotational matrix becomes

$$\mathbf{R}^e = \begin{bmatrix} \mathbf{R}_3 & \mathbf{0}_{3\times2} & \mathbf{0}_{3\times3} \\ \mathbf{0}_{2\times3} & \mathbf{R}_2 & \mathbf{0}_{2\times3} \\ \mathbf{0}_{3\times3} & \mathbf{0}_{3\times2} & \mathbf{R}_3 \end{bmatrix} \tag{8.3}$$

where $\mathbf{0}_{m\times n}$ is an $m \times n$ zero matrix.

8.3 Mechanical responses of rockbolt element - bar element discretization of steel bolt

The grout annulus together with the two interfaces between the bolt and the grout, and between the grout and the rock, is an important element for the stress transfer between the steel bar/beam and the surrounding medium. This transfer is mainly made through the shear response of the grout annulus. The transverse response of the grout annulus is also an important factor in evaluating the form of failure somewhere within the grout annulus and the dilatancy which may arise during the debonding process. In a two-dimensional elasticity problem, the following mechanical models are suggested to simulate the above responses, and they are evolved from the theory investigated by Aydan, and its full description can be found in Aydan (1989). Here, following earlier researchers, a bar element formulation for the bolt is used; a beam formulation will be considered in the following section.

In this section, a two-dimensional elasticity problem is described. It is necessary to first of all fully account for the effect of the mechanical responses of rockbolts, so that equations derived from these mechanisms can be combined to establish the small displacement formulations of the rockbolt element. This forms the fundamentals of the proposed rockbolt element.

The grout annulus is assumed to be of cyclindrical and axisymmetrical shape. The mechanical responses of the annulus against applied loads are assumed to consist of a shear response parallel to the longitudinal axis of the steel bolt and a normal response perpendicular to that axis.

8.3.1 Axial loading

From the theory of mechanics, the equilibrium equation in the axial direction of the bar is defined as

$$\frac{d\sigma^b_{x'}}{dx'} = 0, \tag{8.4}$$

where $\sigma^b_{x'}$ is the axial stress of the bolt, and x' is the local coordinate in the axial direction of the rockbolt element.

Then equation (8.4) has a solution

$$\sigma^b_{x'} = E_b\, \epsilon^b_{x'}, \tag{8.5}$$

which defines the stress-strain relationship, where

$$\epsilon^b_{x'} = -\frac{du'_b}{dx'} \tag{8.6}$$

at a point, with u'_b as the axial displacement of the steel bolt, which has Young's modulus $E_{b'}$.

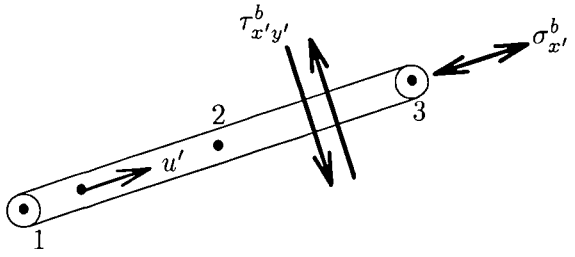

Figure 8.5: Normal stress/strain in bolt

In the local coordinate system, the displacement function of the steel bolt along its axial direction x' is defined by

$$u'_b(\xi) = N_1(\xi)u_1{}' + N_2(\xi)u_2{}' + N_3(\xi)u_3{}',$$

and so equation (8.6) can be written in matrix form as

$$\epsilon^b_{x'} = \begin{bmatrix} -N'_1 & -N'_2 & -N'_3 \end{bmatrix} \begin{bmatrix} u'_1 \\ u'_2 \\ u'_3 \end{bmatrix}, \tag{8.7}$$

where N'_i is the Cartesian derivative of the shape function $N_i(\xi)$.

For example, for a three-noded bar element of length L,

$$N'_i = \frac{dN_i}{dx'} = \frac{2}{L}\,\frac{dN_i}{d\xi}.$$

8.3.2 Shear strain in the bolt

The steel bolt is modelled by a three-noded one-dimensional bar element with certain bending and normal strength. This assumption is quite reasonable for thin steel bolts of small cross-section.

With this assumption, the axial displacements of the steel bolt are considered to be constant in the local transverse y' direction, and so it can be taken that

$$\frac{du_b'}{dy'} = 0.$$

The shear strain in the bolt is restricted by the shear stiffness of the bolt, and hence the equilibrium equation for the transverse direction of the bolt can be taken as

$$\frac{d\tau^b_{x'y'}}{dx'} = 0, \tag{8.8}$$

where $\tau^b_{x'y'}$ is the shear stress of the bolt. This equation has a solution

$$\tau^b_{x'y'} = G_b\, \gamma^b_{x'y'}$$

where the shear strain

$$\gamma^b_{x'y'} = -\frac{dv_b'}{dx'} \tag{8.9}$$

at a point, and G_b is the shear modulus of the bolt.

The y-displacement function of a bar element can be expressed in the form

$$v_b'(\xi) = \sum_{i=1}^{3} N_i(\xi) v_i', \tag{8.10}$$

and, as a bar element discretization is used here, this displacement functions also holds true for the bolt sub-element.

Hence, equation (8.9) can be written in matrix form as

$$\gamma^b_{x'y'} = [-N_1' \; -N_2' \; -N_3'] \begin{bmatrix} v_1' \\ v_2' \\ v_3' \end{bmatrix} \tag{8.11}$$

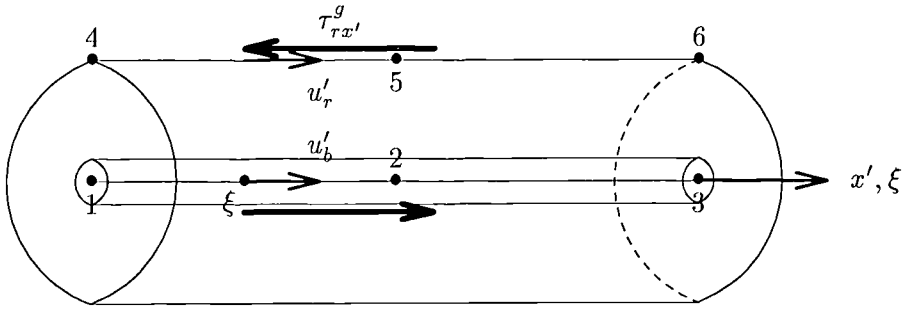

Figure 8.6: Shear stress in grout (in local coordinates)

8.3.3 Shear stress in the grout

By construction, the steel bolt and the grout are axisymmetric and cylindrical. Their cross-sections are concentric with radii r_b and r_h respectively, as shown in Figures 8.6 and 8.7.

With the usual notations, the displacement functions of the grout and the bolt are defined respectively by

$$u'_r = [N_1 \;\; N_2 \;\; N_3] \begin{bmatrix} u'_4 \\ u'_5 \\ u'_6 \end{bmatrix}$$

and

$$u'_b = [N_1 \;\; N_2 \;\; N_3] \begin{Bmatrix} u'_1 \\ u'_2 \\ u'_3 \end{Bmatrix}.$$

Aydan (1989) showed that the equilbrium equation for the shear stress of the grout $\tau^g_{rx'}$ is governed by the differential equation (in cylindrical coordinates)

$$\frac{d\tau^g_{rx'}}{dr} + \frac{\tau^g_{rx'}}{r} = 0 \tag{8.12}$$

where r is the radial distance from the centre of the steel bolt, or

$$\frac{1}{r}\,\frac{d}{dr}(r\tau^g_{rx'}) = 0. \tag{8.13}$$

The solution of the above differential equation can be written as

$$\tau^g_{rx'} = G_g\, \gamma^g_{rx'} \tag{8.14}$$

where

$$\gamma^g_{rx'} = -\frac{du'_g}{dr}, \tag{8.15}$$

which in fact defines the constitutive equation for the linear relationship between shear stress and strain.

The shear modulus of the grout G_g is a constant. Therefore, by combining the relationships in (8.14) and (8.15), equation (8.13) can be rewritten as

$$0 = \frac{1}{r}\frac{d}{dr}\left(r\,\frac{du'_g}{dr}\right) = \frac{d^2u'_g}{dr^2} + \frac{1}{r}\frac{du'_g}{dr} \tag{8.16}$$

Equation (8.13) has a simple solution

$$r\,\gamma^g_{rx'} = -k_1 \tag{8.17}$$

where k_1 is a constant independent of r.

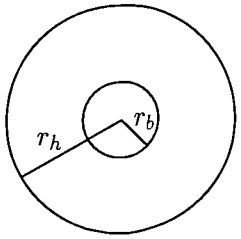

Figure 8.7: Radii of bolt and grout

To determine this constant, it can be observed that from equation (8.15), the boundary condition gives rise to

$$\int_{r_b}^{r_h} \gamma^g_{rx'}\,dr = -\left[u'_g\right]_{r_b}^{r_h} = u'_b - u'_r,$$

where u'_b and u'_r are the axial displacements of the bolt and the rock respectively.

From equation (8.17),

$$\int_{r_b}^{r_h} \gamma^g_{rx'}\,dr = \int_{r_b}^{r_h} -\frac{k_1}{r}\,dr = -k_1\,\ln\left(r_h/r_b\right)$$

which gives

$$-k_1 = \frac{u'_b - u'_r}{\ln\left(r_h/r_b\right)},$$

and therefore,

$$\gamma^g_{rx'} = \frac{1}{\ln\left(r_h/r_b\right)}\,\frac{u'_b - u'_r}{r}. \tag{8.18}$$

In the plane strain finite element discretization of the rockbolt, the radius variable r cannot be used directly, and $\gamma^g_{rx'}$ must be treated as a constant through the cross-section.

It will be approximated by using the value at the mid-radius $r = r = \dfrac{(r_b + r_h)}{2}$ so that

$$\gamma^g_{rx'} = \frac{1}{r \ln (r_h/r_b)} (u'_b - u'_r)$$

$$= \frac{1}{r\ell} [N_1 \;\; N_2 \;\; N_3 \;\; -N_1 \;\; -N_2 \;\; -N_3] \begin{bmatrix} u'_1 \\ u'_2 \\ u'_3 \\ u'_4 \\ u'_5 \\ u'_6 \end{bmatrix}$$

where

$$\ell = \ln (r_h/r_b)$$

or simply *in matrix form*,

$$\gamma^g_{rx'} = \frac{1}{r\ell} \mathbf{N}\, \mathbf{u} \tag{8.19}$$

8.3.4 Dowel effect

While the differential axial movement between bolt and rock is governed by the grout shear modelled above, it is equally important to greatly restrict differential transverse movements, ie. to prevent the bolt from penetrating into the rock mass. The simplest way of modelling this *dowel effect* is to introduce an artifically large stiffness modulus D governing this movement. This stiffness can be thought of as a spring between the steel bolt and the grout-rock interface nodes in transverse direction, as shown in Figure 8.8.

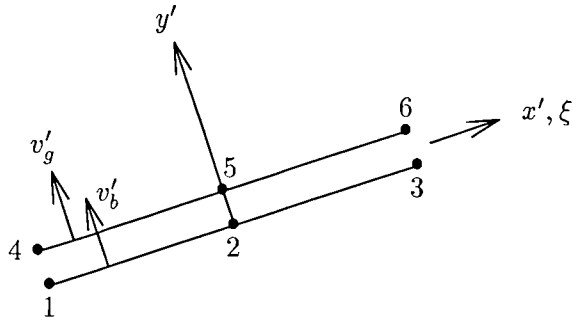

Figure 8.8: *Dowel effect*

The *dowel effect* is defined as the difference in the local transverse displacements of the bolt and the grout, that is,

$$\epsilon^g_{y'} = v'_b - v'_r \tag{8.20}$$

where

$$v_r' = [N_1 \;\; N_2 \;\; N_3] \begin{bmatrix} v_4' \\ v_5' \\ v_6' \end{bmatrix}$$

and

$$v_b' = [N_1 \;\; N_2 \;\; N_3] \begin{bmatrix} v_1' \\ v_2' \\ v_3' \end{bmatrix}$$

and so equation (8.20) can be written as

$$\epsilon_{y'} = [N_1 \;\; N_2 \;\; N_3 \;\; -N_1 \;\; -N_2 \;\; -N_3] \begin{bmatrix} v_1' \\ v_2' \\ v_3' \\ v_4' \\ v_5' \\ v_6' \end{bmatrix} \tag{8.21}$$

with constitutive equation

$$\sigma_{y'} = \mathbf{D}\, \epsilon_{y'}.$$

8.4 Element strain matrix - small displacement analysis

With the usual notation, the constitutive law for a linear elastic behaviour of the rockbolt says that the displacement, strain and stress vectors of the whole system are related in matrix forms by

$$\left.\begin{aligned} \epsilon &= \mathbf{B}'\, \mathbf{u}' \\ \sigma &= \mathbf{D}\, \epsilon. \end{aligned}\right\} \tag{8.22}$$

In an arbitary rockbolt element e, $\mathbf{D}$ is the constitutive elasticity matrix of the rockbolt element defined by the matrix

$$\mathbf{D} = \begin{bmatrix} E_b & 0 & 0 & 0 \\ 0 & G_b & 0 & 0 \\ 0 & 0 & G_g & 0 \\ 0 & 0 & 0 & D \end{bmatrix}, \tag{8.23}$$

where

E_b is Young's modulus of the steel bolt,

G_b is the shear modulus of the steel bolt,

G_g is the shear modulus of the grout,

D is stiffness modulus of the *dowel effect*,

with

$$\left.\begin{aligned} \epsilon &= \left(\epsilon^b_{x'} \;\; \gamma^b_{x'y'} \;\; \gamma^g_{rx'} \;\; \epsilon^g_{y'}\right)^T \\ \sigma &= \left(\sigma^b_{x'} \;\; \tau^b_{x'y'} \;\; \tau^g_{rx'} \;\; \sigma^g_{y'}\right)^T \end{aligned}\right\} \tag{8.24}$$

with respect to the displacement vector (in the local coordinates) of the rockbolt element

$$\mathbf{u}' = (u'_1 \;\; v'_1 \;\; u'_2 \;\; v'_2 \;\; u'_3 \;\; v'_3 \;\; u'_4 \;\; v'_4 \;\; u'_5 \;\; v'_5 \;\; u'_6 \;\; v'_6)^T. \tag{8.25}$$

By combining the matrices for the different mechanisms described in the last section, the element strain matrix of the rockbolt element can be obtained in a manner described below.

Let $\left[\mathbf{B}'_{b\ lt}\right]_i$ and $\left[\mathbf{B}'_{grout}\right]_i$ denote the strain sub-matrices related to the bolt and the grout respectively for node i of the rockbolt element. By assembling equations (8.7), (8.11), (8.19) and (8.21) according to (8.22) and (8.24) with respect to the displacement vector $\mathbf{u}$ defined in (8.25),

$$\left[\mathbf{B}'_{bolt}\right]_i = \begin{bmatrix} -N'_i & 0 \\ 0 & -N'_i \\ cN_i & 0 \\ 0 & N_i \end{bmatrix}, \tag{8.26}$$

with

$$c = \frac{1}{r\ell} = \frac{1}{r \ln (r_h/r_b)},$$

and

$$\left[\mathbf{B}'_{grout}\right]_i = \begin{bmatrix} 0 & 0 \\ 0 & 0 \\ -cN_i & 0 \\ 0 & -N_i \end{bmatrix} \tag{8.27}$$

for any node i in the grout.

The strain matrix for the rockbolt element is written in the form

$$\mathbf{B}' = \left[\mathbf{B}'_{bolt} \mid \mathbf{B}'_{grout}\right], \tag{8.28}$$

so that by assembling the above matrices for all nodes i in the element, it can be seen that

$$\mathbf{B}' = \begin{bmatrix} -N_1' & 0 & -N_2' & 0 & -N_3' & 0 & 0 & 0 & 0 & 0 & 0 & 0 \\ 0 & -N_1' & 0 & -N_2' & 0 & -N_3' & 0 & 0 & 0 & 0 & 0 & 0 \\ cN_1 & 0 & cN_2 & 0 & cN_3 & 0 & -cN_1 & 0 & -cN_2 & 0 & -cN_3 & 0 \\ 0 & N_1 & 0 & N_2 & 0 & N_3 & 0 & -N_1 & 0 & -N_2 & 0 & -N_3 \end{bmatrix}. \tag{8.29}$$

This element strain matrix is expressed in the local axis, it will be necessary to transform it into the global axis before the next step can be taken. This procedure will be shown in section 8.7.

8.5 Mechanical responses of rockbolt element - beam element discretization of steel bolt

The element strain matrix derived in the last section is based on the mechanisms that simulate various reponses of a rockbolt. The new rockbolt element proposed here shares the same characteristics of the old one, and fundamentally, it is subject to the same responses. Consequently the mechanisms mentioned in Section 8.3 are still valid. However, as the new element uses the three-noded beam element to model the steel bolt, modifications must be made to accomodate the different transverse displacement function in this element discertization.

Recall from Section 6.3.2 that the axial displacement function of a three-noded beam element can be expressed in the form

$$u_b'(\xi) = \sum_{i=1}^{3} N_i(\xi) v_i', \tag{8.30}$$

where $N_i(\xi)$'s are the usual shape functions associated with the local x'-displacement of a beam element, and in the transverse direction,

$$v_b'(\xi) = \sum_{i=1}^{3} H_i(\xi) v_i' + L \sum_{i=1,3} m_i(\xi)\theta_i, \tag{8.31}$$

where $H_i(\xi)$'s and $m_i(\xi)$'s are the shape functions in the local y'-displacement of a beam element, as defined in equations (6.30) and (6.31), and L is the length of the element.

The axial displacement functions of the bar and the beam elements are of the same form, so there is no need to modify the two mechanical responses involved in the local axial direction. However, it is necessary to interpret the transverse mechanical responses under the new displacement function in this direction.

In the second mechanism described in Section 8.3.2 where the shear strain in the bolt is simulated, the equilibrium equation for the transverse direction of the bolt in (8.7) is given by

$$\frac{d\tau^b_{x'y'}}{dx'} = 0, \tag{8.32}$$

By equation (8.30), its solution in $\gamma^b_{x'y'}$ can be modified to the form

$$\gamma^b_{x'y'} = [-H_1' \; - Lm_1', \; -H_2' \; - H_3' \; - Lm_3'] \begin{bmatrix} v_1' \\ \theta_1 \\ v_2' \\ v_3' \\ \theta_3 \end{bmatrix} \tag{8.33}$$

Further, in the fourth mechanism in Section 8.3.4 which simulates the dowel effect between the steel bolt and the grout-rock interface, the radial displacements become

$$v_r' = [N_1 \;\; N_2 \;\; N_3] \begin{bmatrix} v_4' \\ v_5' \\ v_6' \end{bmatrix}$$

and

$$v_b' = [H_1 \;\; Lm_1 \;\; H_2 \;\; H_3 \;\; Lm_3] \begin{bmatrix} v_1' \\ \theta_1 \\ v_2' \\ v_3' \\ \theta_3 \end{bmatrix}$$

and therefore the equation that governs the *dowel effect* in (8.20)

$$\epsilon^g_{y'} = v_b' - v_r'$$

can now be expressed in matrix form

$$\varepsilon_{y'} = [H_1 \;\; Lm_1 \;\; H_2 \;\; H_3 \;\; Lm_3 \;\; -N_1 \;\; -N_2 \;\; -N_3] \begin{bmatrix} v'_1 \\ \theta_1 \\ v'_2 \\ v'_3 \\ \theta_3 \\ v'_4 \\ v'_5 \\ v'_6 \end{bmatrix} \tag{8.34}$$

Equations (8.33) and (8.34) essentially describe the differences between the two sub-element discretizations. Each three-noded beam element involves two more degrees of freedom, so there is an increase in size in the resulting element strain matrix and hence the global stiffness matrix. However, it is worth noting that with today's ever increasing computing power and storage space, this increase, in practice, will not *dramatically affect* the overall efficiency of the method.

8.5.1 Element strain matrix

Since a beam element has in addition a rotational degree of freedom attached to its end-nodes, the displacement vector (in the local coordinates) of the *rockbolt element becomes*

$$\mathbf{u}' = (u'_1 \;\; v'_1 \;\; \theta_1 \;\; u'_2 \;\; v'_2 \;\; u'_3 \;\; v'_3 \;\; \theta_3 \;\; u'_4 \;\; v'_4 \;\; u'_5 \;\; v'_5 \;\; u'_6 \;\; v'_6)^T. \tag{8.35}$$

Matrices expressed in (8.33) and (8.34) supercede those in (8.11) and (8.21) respectively for the local transverse direction of the bolt, and by following the same procedure for combining the matrices that represent the four mechanisms, the element strain matrix of the new rockbolt element can be obtained.

Thus, the strain matrix for the middle-node of the bolt becomes

$$[\mathbf{B}'_{bolt}]_i = \begin{bmatrix} -N'_i & 0 \\ 0 & -H'_i \\ cN_i & 0 \\ 0 & H_i \end{bmatrix}, \tag{8.36}$$

and for the end-nodes,

$$[\mathbf{B}'_{bolt}]_i = \begin{bmatrix} -N'_i & 0 & 0 \\ 0 & -H'_i & -Lm'_i \\ cN_i & 0 & 0 \\ 0 & H_i & Lm_i \end{bmatrix} \tag{8.37}$$

with

$$c = \frac{1}{r\ell} = \frac{1}{r \ln (r_h/r_b)},$$

while for any node in the rock,

$$[\mathbf{B}'_{rock}]_i = \begin{bmatrix} 0 & 0 \\ 0 & 0 \\ -cN_i & 0 \\ 0 & -N_i \end{bmatrix}. \tag{8.38}$$

The element strain matrix is expressed in the partition form

$$\mathbf{B}' = [\mathbf{B}'_{bolt} \mid \mathbf{B}'_{rock}]_{4\times 14}, \tag{8.39}$$

and it can be seen by combining equations (8.36), (8.37) and (8.38) with respect to the displacement vector defined in (8.35) for all nodes i in the element,

$$\mathbf{B}'_{bolt} = \begin{bmatrix} -N'_1 & 0 & 0 & -N'_2 & 0 & -N'_3 & 0 & 0 \\ 0 & -H'_1 & -Lm'_1 & 0 & -H'_2 & 0 & -H'_3 & -Lm'_3 \\ cN_1 & 0 & 0 & cN_2 & 0 & cN_3 & 0 & 0 \\ 0 & H_1 & Lm_1 & 0 & H_2 & 0 & H_3 & Lm_3 \end{bmatrix} \tag{8.40}$$

and

$$\mathbf{B}'_{rock} = \begin{bmatrix} 0 & 0 & 0 & 0 & 0 & 0 \\ 0 & 0 & 0 & 0 & 0 & 0 \\ -cN_1 & 0 & -cN_2 & 0 & -cN_3 & 0 \\ 0 & -N_1 & 0 & -N_2 & 0 & -N_3 \end{bmatrix}. \tag{8.41}$$

This strain matrix is significantly different from the one defined in (8.29), and it highlights the essential difference between the finite element modelling of the steel bolt by the bar and the beam element. We have seen in earlier chapters the advantages of introducing rotational degrees of freedom to the end-nodes to transmit bending moments, and it will be interesting to see how much effect it will have on the steel bolt and hence on the rockbolt.

8.6 Element stiffness matrix in local axis

For the purpose of illustration, the beam element is taken as the sub-element to model the steel bolt throughout the rest of this chapter, so that all formulations thus derived are based on the new rockbolt element. For an equivalent formulation and analysis for the bar element discretization, the same procedure can be followed.

To determine the stiffness matrix of a rockbolt element, it is convenient to write the matrix product $\mathbf{B}'^T\mathbf{D}\mathbf{B}'$ in the partition form

$$\left[\begin{array}{c|c} \mathbf{M}_{bolt} & \mathbf{M}_{grout} \\ \hline \mathbf{M}_{grout}^T & \mathbf{M}_{rock} \end{array}\right]_{14\times 14}$$

where, for the ease of illustration, it can be written

$$\mathbf{M}_{bolt} = \mathbf{M}_1 + \mathbf{M}_2. \tag{8.42}$$

In the local axis with the element strain matrix $\mathbf{B}'$ defined in (8.39) and the constitutive matrix $\mathbf{D}$ defined in (8.23), it can be readily shown that after matrix multiplications, the sub-matrices $\mathbf{M}_1$ and $\mathbf{M}_2$ can be written respectively as

$$\mathbf{M}_1 = \begin{bmatrix} E_bN_1'^2 & 0 & 0 & E_bN_1'N_2' & 0 & E_bN_1'N_3' & 0 & 0 \\ 0 & G_bH_1'^2 & G_bLH_1'm_1' & 0 & G_bH_1'H_2' & 0 & G_bH_1'H_3' & G_bLH_1'm_3' \\ 0 & G_bLH_1'm_1' & G_bL^2m_1'^2 & 0 & G_bLH_2'm_1' & 0 & G_bLH_3'm_1' & G_bL^2m_1'm_3' \\ E_bN_1'N_2' & 0 & 0 & E_bN_2'^2 & 0 & E_bN_2'N_3' & 0 & 0 \\ 0 & G_bH_1'H_2' & G_bLH_2'm_1' & 0 & G_bH_2'^2 & 0 & G_bH_2'H_3' & G_bLH_2'm_3' \\ E_bN_1'N_3' & 0 & 0 & E_bN_2'N_3' & 0 & E_bN_3'^2 & 0 & 0 \\ 0 & G_bH_1'H_3' & G_bLH_3'm_1' & 0 & G_bH_2'H_3' & 0 & G_bH_3'^2 & G_bLH_3'm_3' \\ 0 & G_bLH_1'm_3' & G_bL^2m_1'm_3' & 0 & G_bLH_2'm_3' & 0 & G_bLH_3'm_3' & G_bL^2m_3'^2 \end{bmatrix}$$

and

$$\mathbf{M}_2 = \begin{bmatrix} G_g c^2 N_1^2 & 0 & 0 & G_g c^2 N_1 N_2 & 0 & G_g c^2 N_1 N_3 & 0 & 0 \\ 0 & DH_1^2 & DLH_1 m_1 & 0 & DH_1 H_2 & 0 & DH_1 H_3 & DLH_1 m_3 \\ 0 & DLH_1 m_1 & DL^2 m_1^2 & 0 & DLH_2 m_1 & 0 & DLH_3 m_1 & DL^2 m_1 m_3 \\ G_g c^2 N_1 N_2 & 0 & 0 & G_g c^2 N_2^2 & 0 & G_g c^2 N_2 N_3 & 0 & 0 \\ 0 & DH_1 H_2 & DLH_2 m_1 & 0 & DH_2^2 & 0 & DH_2 H_3 & DLH_2 m_3 \\ G_g c^2 N_1 N_3 & 0 & 0 & G_g c^2 N_2 N_3 & 0 & G_g c^2 N_3^2 & 0 & 0 \\ 0 & DH_1 H_3 & DLH_3 m_1 & 0 & DH_2 H_3 & 0 & DH_3^2 & DLH_3 m_3 \\ 0 & DLH_1 m_3 & DL^2 m_1 m_3 & 0 & DLH_2 m_3 & 0 & DLH_3 m_3 & DL^2 m_3^2 \end{bmatrix}, \tag{8.43}$$

while

$$\mathbf{M}_{grout} = \begin{bmatrix} -G_g c^2 N_1^2 & 0 & -G_g c^2 N_1 N_2 & 0 & -G_g c^2 N_1 N_3 & 0 \\ 0 & -DN_1 H_1 & 0 & -DN_2 H_1 & 0 & -DN_3 H_1 \\ 0 & -DLN_1 m_1 & 0 & -DLN_2 m_1 & 0 & -DLN_3 m_1 \\ -G_g c^2 N_1 N_2 & 0 & -G_g c^2 N_2^2 & 0 & -G_g c^2 N_2 N_3 & 0 \\ 0 & -DN_1 H_2 & 0 & -DN_2 H_2 & 0 & -DN_3 H_2 \\ -G_g c^2 N_1 N & 0 & -G_g c^2 N_2 N_3 & 0 & -G_g c^2 N_3^2 & 0 \\ 0 & -DN_1 H_3 & 0 & -DN_2 H_3 & 0 & -DN_3 H_3 \\ 0 & -DLN_1 m_3 & 0 & -DLN_2 m_3 & 0 & -DLN_3 m_3 \end{bmatrix}$$

and

$$\mathbf{M}_{rock} = \begin{bmatrix} G_g c^2 N_1^2 & 0 & G_g c^2 N_1 N_2 & 0 & G_g c^2 N_1 N_3 & 0 \\ 0 & DN_1^2 & 0 & DN_1 N_2 & 0 & DN_1 N_3 \\ G_g c^2 N_1 N_2 & 0 & G_g c^2 N_2^2 & 0 & G_g c^2 N_2 N_3 & 0 \\ 0 & DN_1 N_2 & 0 & DN_2^2 & 0 & DN_2 N_3 \\ G_g c^2 N_1 N_3 & 0 & G_g c^2 N_2 N_3 & 0 & G_g c^2 N_3^2 & 0 \\ 0 & DN_1 N_3 & 0 & DN_2 N_3 & 0 & DN_3^2 \end{bmatrix}, \tag{8.44}$$

where H_1, H_3, m_1 and m_3 are the shape functions of a beam element in the local y-displacement.

Each entry in this matrix product involves product of stiffness factors, shape functions and their derivatives. All of these are known functions and parameters so that it can be integrated term by term to form the element stiffmess matrix. This procedure can be

carried out either analytically or numerically by some standard accurate algorithms. This integration process will be described later in this chapter.

8.7 Element stiffness matrix in global axis

After the first incremental load is applied to the structure, deformation occurs and it is assumed that at some stage, the rockbolt element lies along the local axis, which is inclined at an angle of β to the global axis (see Figure 8.4). In finite element analysis, element stiffness matrices obtained in the local axes have to be converted to the global axis before it can be assembled to form the global stiffness matrix for the complete system.

In view of the rotational matrices introduced in equations (8.1) and (8.2) in the first section of this chapter, the strain sub-matrices for node i in the local and the global axes are related by

$$[\mathbf{B}_{bolt}]_i = [\mathbf{B}_{bolt}]'_i \, \mathbf{R}_i$$

etc.

Using these relationships, equations (8.36), (8.37) and (3.38) can be modified to become the strain sub-matrix for the middle-node of the bolt as

$$\begin{aligned}
[\mathbf{B}_{bolt}]_i &= \begin{bmatrix} -N'_i & 0 \\ 0 & -H'_i \\ cN_i & 0 \\ 0 & H_i \end{bmatrix} \begin{bmatrix} \cos\beta & \sin\beta \\ -\sin\beta & \cos\beta \end{bmatrix} \\
&= \begin{bmatrix} -N'_i\cos\beta & -N'_i\sin\beta \\ H'_i\sin\beta & -H'_i\cos\beta \\ cN_i\cos\beta & cN_i\sin\beta \\ -H_i\sin\beta & H_i\cos\beta \end{bmatrix},
\end{aligned} \tag{8.45}$$

and likewise for the end-nodes,

$$[\mathbf{B}_{bolt}]_i = \begin{bmatrix} -N'_i\cos\beta & -N'_i\sin\beta & 0 \\ H'_i\sin\beta & -H'_i\cos\beta & -Lm'_i \\ cN_i\cos\beta & cN_i\sin\beta & 0 \\ -H_i\sin\beta & H_i\cos\beta & Lm_i \end{bmatrix} \tag{8.46}$$

while, for the rock,

$$[\mathbf{B}_{rock}]_i = \begin{bmatrix} 0 & 0 \\ 0 & 0 \\ -cN_i\cos\beta & -cN_i\sin\beta \\ N_i\sin\beta & -N_i\cos\beta \end{bmatrix}. \tag{8.47}$$

These strain sub-matrices can replace their preceding ones so that by considering all nodes in the rockbolt element, the element strain matrix

$$\mathbf{B} = [\mathbf{B}_{bolt} \mid \mathbf{B}_{rock}]_{4\times 14}$$

can take the form

$$\mathbf{B}_{bolt} = \begin{bmatrix} -N_1'\cos\beta - N_1'\sin\beta & 0 & -N_2'\cos\beta - N_2'\sin\beta - N_3'\cos\beta - N_3'\sin\beta & 0 \\ H_1'\sin\beta & -H_1'\cos\beta - Lm_1' & H_2'\sin\beta & -H_2'\cos\beta \; H_3'\sin\beta & -H_3'\cos\beta - Lm_3' \\ cN_1\cos\beta & cN_1\sin\beta & 0 & cN_2\cos\beta \; cN_2\sin\beta \; cN_3\cos\beta & cN_3\sin\beta & 0 \\ -H_1\sin\beta & H_1\cos\beta & Lm_1 & -H_2\sin\beta \; H_2\cos\beta \; -H_3\sin\beta \; H_3\cos\beta & Lm_3 \end{bmatrix} \tag{8.48}$$

and

$$\mathbf{B}_{rock} = \begin{bmatrix} 0 & 0 & 0 & 0 & 0 & 0 \\ 0 & 0 & 0 & 0 & 0 & 0 \\ -cN_1\cos\beta & -cN_1\sin\beta & -cN_2\cos\beta & -cN_2\sin\beta & -cN_3\cos\beta & -cN_3\sin\beta \\ N_1\sin\beta & -N_1\cos\beta & N_2\sin\beta & -N_2\cos\beta & N_3\sin\beta & -N_3\cos\beta \end{bmatrix} \tag{8.49}$$

This element strain matrix is now expressed in the global axis, and we are ready to form the matrix multiplication and hence the element stiffness matrix. The next step is to examine the matrix integral $\int_V \mathbf{B}^T\mathbf{D}\mathbf{B}\, dV$ which advocates the use of some accurate numerical methods.

8.7.1 Integration

The stiffness matrix for the rockbolt element can be obtained by integrating term by term in the matrix integral

$$\int_V \mathbf{B}^T\mathbf{D}\mathbf{B}\, dV.$$

The integration is performed over the whole domain of the element, so it is necessary to first of all investigate its domain first.

Unlike other types of elements, the rockbolt element consists of two sub-elements, and they are of different shapes and sizes. The integration of this matrix product over volumes of these sub-elements must therefore be considered seperately, so that the operation can be performed over different domains under different schemes.

In the mechanisms for calculating the normal and the shear strain for the bolt, the bolt is assumed to be axisymmetrical and cylindrical, and it has a cross-sectional area of

$$A_b = \pi r_b^2,$$

over which the integrand is constant.

Hence in these two cases, the area A_b can be taken as the 'integration area', and the matrix integral reduces to a simple integral that involves only one variable (the bolt length), whence it can be evaluated numerically by some standard accurate numerical methods, such as Gaussian quadrature.

For the shear stress in the grout along the axial direction of the element, it has been seen from equation (8.19) that

$$\gamma^g_{rx'} = \frac{1}{\bar{r}\ell}\,\mathbf{N}\,\mathbf{u}.$$

.

For convenience, the strain matrix can be written in the form

$$\mathbf{B}(r,\xi) = \frac{1}{r\ell}\,\mathbf{N} = \frac{1}{r\ell}\,\mathbf{B}(\xi) \tag{8.50}$$

where

$$\mathbf{N} = [N_1\ N_2\ N_3\ -N_1\ -N_2\ -N_3\ ]$$

so that $\mathbf{B}(\xi) = \mathbf{N}$ is the matrix that primarily involves the shape functions $N_i's$ in the axial direction of the beam element.

The domain of the integral is over the grout, and hence the stiffness matrix for this component becomes

$$\begin{aligned}\int_V \mathbf{B}^T\mathbf{D}\mathbf{B}\,dV &= \int_0^L \int_A \mathbf{B}^T\mathbf{D}\mathbf{B}\,dA\,dx \\ &= \frac{2\pi}{\ell}\int_0^L \mathbf{B}^T\mathbf{D}\mathbf{B}\,dx,\end{aligned} \tag{8.51}$$

since

$$\begin{aligned}\int_A \mathbf{B}^T\mathbf{D}\mathbf{B}\, dA &= 2\pi \int_{r_b}^{r_h} \mathbf{B}^T\mathbf{D}\mathbf{B}\, r\, dr \\ &= 2\pi \int_{r_b}^{r_h} \frac{1}{r^2\ell^2}\mathbf{B}^T\mathbf{D}\mathbf{B}\, r\, dr \\ &= \frac{2\pi}{\ell}\, \bar{\mathbf{B}}^T\mathbf{D}\bar{\mathbf{B}}. \end{aligned} \tag{8.52}$$

Technically $\mathbf{B}(\xi)$ is not the 'true' shear strain-displacement matrix $\mathbf{B}(r,\xi)$, as it would not be possible to include the radius variable r in this analysis. Hence $\mathbf{B}$ can only be approximated (and also the term $\gamma(r)$) at the mid-radius

$$r = \frac{1}{2}(r_b + r_h).$$

The approximate strain matrix $\tilde{\mathbf{B}}$ can then be related by

$$\tilde{\mathbf{B}} = \mathbf{B}(\bar{r},\xi) = \frac{1}{r\ell}\bar{\mathbf{B}}, \tag{8.53}$$

i.e.

$$\mathbf{B} = r\ell\tilde{\mathbf{B}}, \tag{8.54}$$

or, from equation (8.50),

$$\mathbf{B} = \frac{r}{r}\tilde{\mathbf{B}}, \tag{8.55}$$

Hence,

$$\mathbf{B}^T\mathbf{D}\mathbf{B} = \frac{1}{r^2\ell^2}\mathbf{B}^T\mathbf{D}\mathbf{B}.$$

and it follows from (8.51) that the integral becomes

$$\begin{aligned}\int_V \mathbf{B}^T\mathbf{D}\mathbf{B}\, dV &= \frac{2\pi}{\ell}\int_0^L \mathbf{B}^T\mathbf{D}\mathbf{B}\, dx = \frac{2\pi}{\ell}\int_0^L r^2\ell^2\, \tilde{\mathbf{B}}^T\mathbf{D}\tilde{\mathbf{B}}\, dx \\ &= 2\pi\ell r^2 \int_0^L \tilde{\mathbf{B}}^T\mathbf{D}\tilde{\mathbf{B}}\, dx. \end{aligned} \tag{8.56}$$

The approximated matrix $\tilde{\mathbf{B}}$ and hence the matrix product in (8.56) involve only one variable x (or ξ) so that the integral is reduced to a single integral. Hence the 'integration area' of $2\pi r^2 \ln(r_h/r_b)$ can be assumed here.

The intergal expressed in (8.56) can be integrated numerically term by term, for example, by Gaussian quadrature by rewriting it in the form

$$\int_V \mathbf{B}^T\mathbf{D}\mathbf{B}\, dV = \pi\ell r^2 L \int_{-1}^{1} \tilde{\mathbf{B}}^T\mathbf{D}\tilde{\mathbf{B}}\, d\xi. \tag{8.57}$$

In the mechanism that simulates the *dowel effect*, the integration is over the space between the steel bolt and the grout-rock interface. This space has a uniform cross-sectional

grout area which is the area between the 'concentric' grout and the bolt, and therefore the 'integration area' of $\pi(r_h^2 - r_b^2)$ can be used.

Alternatively, by following the same arguments, integrals that relate the four mechanisms can be expressed in single integral forms that involve one variable. All entries in the matrices $\tilde{\mathbf{B}}$ and $\mathbf{D}$ are known, so that every entry in the matrix product $\tilde{\mathbf{B}}^T\mathbf{D}\tilde{\mathbf{B}}$ only involves product of known functions. Consequently they can be integrated analytically term by term. Of course this method is only efficient during the first incremental load, when the local axis is the same as the global axis. The formulation will get increasingly complicated after deformation occurs, whence the numerical method is much preferred.

8.8 Large displacement analysis

8.8.1 Introduction

Starting with a linear stress-strain relationship, the stiffness matrix of the rockbolt element has been derived in the last few sections. This formulation is a linear one, and it can only be used to predict linear deformation of a structure. In this section, a corresponding formulation for large displacement will be established.

Qu and Reed *(1992b)* carried out a full investigation on a rockbolt element. This element was of the same coupled form, except that bar element discretization was used for the steel bolt. The analysis started with the fundamental nonlinear displacement, strain and stress relationships, and these formulae were applied to the equilibrium equation and other fundamental laws in mechanics to derive the nonlinear element strain matrix.

Although these nonlinear relationships have already been considered earlier in establishing the large displacement analyses of other types of elements, including those of a beam element, it would be more practical and efficient if formulations of these analyses can be adapted directly for the rockbolt element. In particular, as it has been suggested that beam element discretization is used for modelling the steel bolt in a rockbolt, it seems appropriate that the large displacement formulation of a beam element can somehow be made use of in the new algorithm.

8.8.2 Stiffness matrix for the grout

In Section 8.5, the matrix product $\mathbf{B^T DB}$ for small displacement of a standard six-noded rockbolt has been written in the block matrix form

$$\left[\begin{array}{c|c} \mathbf{M}_{bolt} & \mathbf{M}_{grout} \\ - - + - - \\ \mathbf{M}_{grout}^{T} & \mathbf{M}_{rock} \end{array}\right]_{14\times 14}$$

where $\mathbf{M}_{bolt}$ is the linear matrix associated with a beam sub-element.

The nonlinear stiffness matrix for the rockbolt element is made up of a linear part and a nonlinear part. For the linear part, since the grout is connected to the surrounding rock interface, therefore the sub-matrices $\mathbf{M}_{grout}$ and $\mathbf{M}_{rock}$ remain unchanged, and they can be retained here. For the nonlinear part of this interface, the grout can be combined with the surrounding rock element, whence the established iteration scheme for the nonlinear part of an eight-noded isoparametric element can be brought in to deal with the grout. However, it is still required to find a suitable large displacement formulation for the steel bolt.

8.8.3 Stiffness matrix for the steel bolt

To bring in the large displacement formulation in the axial direction of the steel bolt, the simplest approach appears to be directly replacing $\int_{V^e} \mathbf{M}_{bolt}\, dV^e$ by the nonlinear stiffness matrix of a beam element as given in equation (6.32), taking $F = EA\dfrac{du}{dx}$ as a variable.

However, from equation (8.42), it can be seen that

$$\mathbf{M}_{bolt} = \mathbf{M}_1 + \mathbf{M}_2,$$

where the two matrices $\mathbf{M}_1$ and $\mathbf{M}_2$ involve factors $E_b, G_b, G_g,$ and D, which means that $\mathbf{M}_{bolt}$ contains contributions not only from the bolt, but also from the grout-rock interface. Thus, if $\mathbf{M}_{bolt}$ is replaced by the stiffness matrix of a beam element only, all contributions from the grout in this sub-matrix will be removed, and hence the resulting matrix only consists of contribution from the bolt, and therefore it cannot appropriately describe the

full effect of the grout.

In the partition form of the element stiffness matrix, the difficulty here is to find a way of replacing the linear stiffness matrix of the bar sub-element by a nonlinear one of the beam sub-element, while retaining contributions from the grout in $\mathbf{M}_{bolt}$.

In Swoboda & Marenče's (1992, 1992, 1995) investigation of the *bolt crossing joint* element, it was suggested that in the two-dimensional form of Aydan's four-noded rockbolt element (with the node order starting from the grout, as opposed to starting from the bolt, which is assumed throughout in this thesis), the stiffness matrix of this element could be modified to

$$\mathbf{K} = \begin{bmatrix} 2k_g & 0 & k_g & 0 & -2k_g & 0 & -k_g & 0 \\ 0 & k_s + k_d & 0 & -k_s & 0 & -k_d & 0 & 0 \\ k_g & 0 & 2k_g & 0 & -k_g & 0 & -2k_g & 0 \\ 0 & -k_s & 0 & k_s + k_d & 0 & 0 & 0 & -k_d \\ -2k_g & 0 & -k_g & 0 & k_b + 2k_g & 0 & -k_b + k_g & 0 \\ 0 & -k_d & 0 & 0 & 0 & k_d & 0 & 0 \\ -k_g & 0 & -2k_g & 0 & -k_b + k_g & 0 & k_b + 2k_g & 0 \\ 0 & 0 & 0 & -k_d & 0 & 0 & 0 & k_d \end{bmatrix}, \tag{8.58}$$

with stiffness factors

$$k_b = \frac{E_b A_b}{L}, \qquad k_s = \frac{G_b A_b}{L}, \qquad k_g = \pi\, G_g \frac{L}{3\ln(r_h/r_b)}, \tag{8.59}$$

and from the formula suggested by Brady & Lorig (1988),

$$k_d = E_b I \left[\frac{D}{2E_b I(r_h/r_b - 1)}\right]^{3/4}, \tag{8.60}$$

where E_b, G_b are respectively the Young's modulus and the shear modulus of the bolt, G_g, D the respective shear modulus and the Young's modulus of the grout, A_b the cross-sectional area of the bolt, L the length of the element, r_b and r_h are respectively the radii of the bolt and the grout, and k_d is the *dowel* stiffness.

Extracting the relevant part of (8.58) that relates to node i of the bolt

$$\begin{bmatrix} k_b + 2k_g & 0 \\ 0 & k_d \end{bmatrix}, \tag{8.61}$$

and comparing it with the equivalent part of M_{bolt} in (8.43)

$$\begin{bmatrix} E_b N_i'^2 + G_g c^2 N_i^2 & 0 \\ 0 & G_b H_i'^2 + D H_i^2 \end{bmatrix}, \tag{8.62}$$

it can be seen that both of them combine contributions from the bolt and the grout. In particular, in the first entries, the terms k_b and $E_b N_i'^2$ describe the contributions from the axial direction of the bolt. Therefore it seems appropriate that the term $E_b N_i'^2$ in (8.62) can be directly replaced by k_b, while retaining all other entries in the sub-matrix M_{bolt}. Specifically, k_b can be taken as the large displacement formulation of a beam element so that nonlinearity can be introduced without affecting contributions from the grout.

To execute this replacement in (8.43), the Young's modulus of the steel bolt, E_b, in the constitutive matrix of the rockbolt as defined in (8.4) can be simply set to zero, thus removing contributions from the axial direction of the bolt, whence the nonlinear stiffness matrix of the beam element can be added directly to this sub-matrix.

This replacement seems to work well, and in practice can produce satisfactory results. The significant advantage of this method is that it allows the use of some existing theories on various types of elements, so that the formulation and the manipulation of the rockbolt element carried out by computer can be kept *as simple as possible*, while retaining the overall properties and accuracies. In a computer program, the subroutines that are written to compute the deformations of isoparametric and beam elements can be recalled and re-used inside the rockbolt element subroutine, so that there is no need to write extra algorithms for this element.

8.8.4 Integration for the residual load

To calculate the elemental residual load in large displacement analysis, the integral

$$I_{R^e} = \int_{\Omega^e} \mathbf{B}^T \delta\sigma \, d\Omega^e \tag{8.63}$$

over the domain Ω^e for each element has to be considered in each incremental load.

Essentially, in a mesh of finite elements, the integral for calculating the residual in each iteration has to be carried out for each element by an appropriate accurate numerical scheme before it can be assembled into the global residual load vector. Therefore, an iteration scheme must be adapted for a rockbolt element.

Two sub-elements of different domains are used in this rockbolt element discretization, so it is necessary to consider these two integrals separately. The large displacement

formulation for beam element has been considered in Chapter 6, and as the steel bolt is modelled by a beam element, its iteration scheme can be used for the bolt sub-element for this purpose.

For the grout interface, the integral defined in (8.63) becomes

$$I_{R^e} = \int_0^L 2\pi \int_{r_b}^{r_h} \mathbf{B}^T \delta\sigma \; r \; dr \; dx, \tag{8.64}$$

which can be further simplified by (8.55) :

$$\begin{aligned} \int_{r_b}^{r_h} \mathbf{B}^T \delta\sigma \; r \; dr &= \int_{r_b}^{r_h} r \cdot \frac{r}{r} \tilde{\mathbf{B}}^T \delta\sigma \; dr \\ &= r\,(r_h - r_b)\,\tilde{\mathbf{B}}^T \delta\sigma \end{aligned} \tag{8.65}$$

Therefore, the integral associated with the grout for the iteration scheme carries an 'integration area' of

$$2\pi r\,(r_h - r_b) = 2\pi \cdot \frac{1}{2}\,(r_h + r_b)(r_h - r_b) = \pi\left(r_h^2 - r_b^2\right),$$

which in fact is the true cross-sectional area of the grout.

As before, the matrix $\mathbf{B}$ has to be approximated at the mid-radius $r = r = \frac{1}{2}(r_h + r_b)$, so that $\tilde{\mathbf{B}}$ and hence the integrand in (8.63) involves only one variable ξ. Hence, (8.63) can be integrated numerically, for example, by Gaussian quadrature.

Therefore, the aggregate 'integrating area' of

$$\pi\left(r_h^2 - r_b^2\right) \times \frac{1}{r\ell} = \frac{2\pi\,(r_h - r_b)}{\ell}$$

can be used to integrate $\mathbf{B}^T \delta\sigma$.

When the above methods are implemented, the residual load for the grout interface can be found by

$$\mathbf{r}^e = \delta\mathbf{f}^e + \int_{\Omega^e} \mathbf{B}^T \delta\sigma \; d\Omega^e$$

where $\mathbf{f}$ is the element load vector, so that the iteration scheme for examining the convergence of all subsequent residual loads in this sub-element can be carried out in exactly the same way as before.

This algorithm has proved to be a very efficient one in a practical sense. In the computer program that simulates deformation of rock mass, the iteration scheme for the grout

interface is the same as the one for the rock mass, and therefore it has the convenience of sharing the same subroutine without any need of writing an extra subroutine for the sub-element.

8.9 Examples

The purpose of using rockbolts in jointed rock is to increase its strength, so that partial or total collapse can be prevented. In the two-dimensional example described in section 7.5.1, a rock mass with internal cracks has been examined. When this rock mass is subject to a range of loadings, it has been demonstrated how the joint rocks are liable to slide away or penetrate into each other; and when the loadings are big enough, part of the jointed rock may slide away indefintely, thus causing instability in the structure.

To appreciate the effectiveness of using rockbolts as support in a rock mass, Figure 8.9 shows a two-dimensional model that is being used as a hypothetical example here. This model is very similar in construction to the first example used in Chapter 7 for examining joint elements, except that through the discontinuities between the rock mass, a rockbolt is bolted to serve as a reinforcement, so that direct comparisons can be made.

In this model, the two rock blocks, the joint and the grouted rockbolt are all assumed to be made of linearly elastic, homogeneous and isotropic materials with different material properties. The surrounding rock mass is modelled by two uniform rectangular rock blocks which are identical in size and have the same material properties. One rock block is rigidly placed on a rough horizontal plane, so that no sliding or tilting is allowed at the bottom end of the block. The other rock block is placed directly on top of the first block, so that the gap between these two blocks creates discontinuities within the rock mass, and the space can be characterized by a smooth horizontal joint. This joint assumes a certain set of moduli k_s and k_n, which are the joint stiffness per unit length in the tangential and normal directions respectively. With this joint, the two blocks can penetrate into each other, and/or the top block can slide away when the structure is subject to some loadings, as investigated in the previous chapter.

To restrict and stabilize the movement of these two rock blocks, a grouted rockbolt is bolted through them via the joint at an angle of $\frac{\pi}{4}$ to the horizontal, as shown in Figure

8.9. To initiate deformation, a uniform surface traction is applied horizontally from the left, and is normal to the vertical left hand surface of the top block .

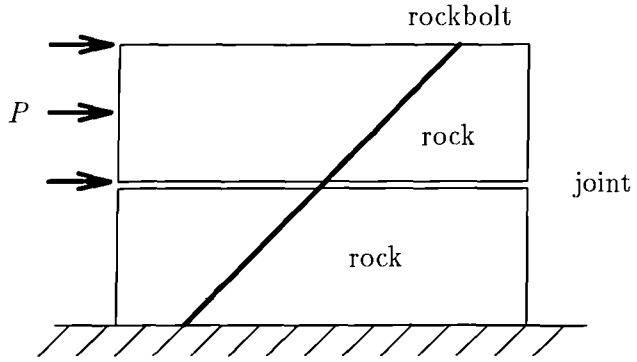

Figure 8.9: A simple example involving rockbolts

For finite element discretization, each rock block is modelled by a mesh of 32 eight-noded isoparametric elements, while the joint and the grouted rockbolt are respectively modelled by meshes of eight identical six-noded joint elements and eight identical six-noded grouted rockbolt elements. The rockbolt is bolted onto the rock, and is connected to the rock mass in a manner shown in Figure 8.3(a). It is also assumed that the rockbolt is rigidly fixed at its lower end. In this representation, the bolt shares one side of the neighbouring eight-noded isoparametric rock element, and hence initially the nodes of the bolt coincide with the corresponding nodes on the interface of this rock element.

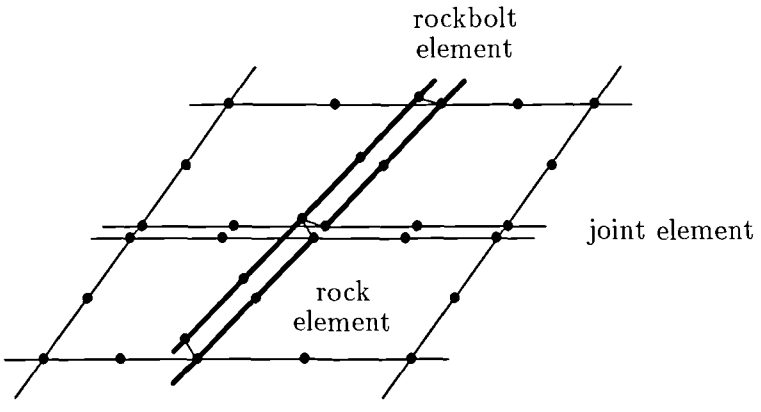

Figure 8.10: Element details of structure

The sub-elements that discretise the steel bolt are connected to the rock at the end-nodes. To elaborate on the element construction of the mesh where the rock block, the joints, and the grouted rockbolts meet, Figure 8.10 shows the initial details in the vicinity of this area. At this intersection, the nodes of these elements are inter-connected in the

manner shown in Figure 8.11. That is, the bolt is continuous across the joint, but the rock nodes are not.

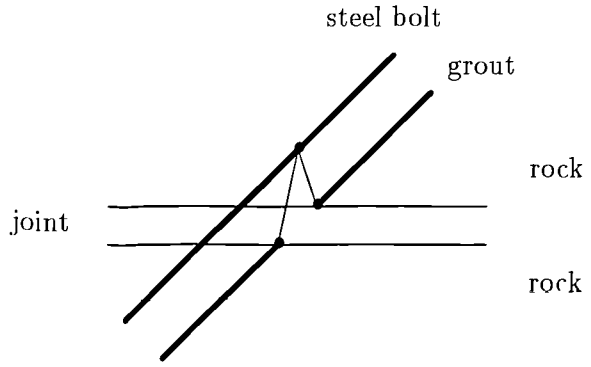

Figure 8.11: Node details at intersection

For direct comparision, two problems are run. In Problem 1, the steel bolt is modelled by a mesh of bar elements, while in Problem 2, beam elements are used. In both problems, the same mesh is used for the structure. All materials used are assumed to be linearly elastic, isotropic and homogeneous. The tangential and the normal components of the joint stiffness are both taken to be $10^6 N/m^2$. The following table gives the material property values for the rock masses and the rockbolt used in both problems:

	Elasticity modulus KN/m^2	Poisson's ratio	Shear modulus KN/m^2	Radius m
Rock	400.00	0.30		
Bolt	1600.00	0.30		0.04
Grout	800.00	0.30	400	0.08

Table 8.1: Material properties of the rockbolt

The purpose of this exercise is to use numerical simulation to examine the viability of the new rockbolt element by comparing the bar and beam element discretizations of steel bolt under identical situation. It is hoped that with the help of the results of these two problems, the performance of the new algorithm can be evaluated, and that the new algorithm can prove to be competitive and can offer greater finesse in the design of rockbolt models in tunnel engineering.

Note that in all experiments carried out in this section, an exaggeration factor of 300 is used throughout to produce the deformed mesh.

8.9.1 Problem 1: bar element discretization of steel bolt

This problem creates the situation where the original Aydan's type rockbolt element is modelled in the analysis to evaluate the use of rockbolts in jointed rocks, and the formulations are based on the algorithms derived from its simulated mechanical responses.

In the finite element discretization, the rockbolt is jointed onto the neighbouring rock element as shown in Figure 8.3(a), with its element details shown in Figure 8.3(b), except that the end-nodes of the steel bolt only have two translational degrees of freedom. For simplicity, only small displacement formulations are used.

From the linear strain matrix expressed in (8.29), a similar procedure as described in sections 8.4 and 8.5 has been followed to form the stiffness matrix for a rockbolt element in the global axis. For all other types of element, formulations are taken directly from those described in earlier chapters. With this arrangement, Figure 8.12 shows the results of this formulation, as executed by the computer.

The figure shows that, although the two rock blocks between joints can be stablised by the use of rockbolt, the overall effect is not entirely a satisfactory one, with a tendency for top rock block to rotate at the point where the rockbolt is bolted through the two rock blocks, while the bottom rock block remains relatively stable in relation to the top block. It can be seen that the left hand side of the top block tends to move away from the bottom block to open up a space between the joint, and in the right, the top block penetrates slightly into the bottom one.

It can be argued that the amount of rotation can somehow be reduced by increasing the stiffness of the joint, but in general, the existence of the rotation and the space between the two blocks in the left hand side suggests that the stability of the rock mass looks quite questionable, especially as these results are obtained in the small displacement analysis. If the loadings are increased slightly, it can be envisaged that further rotation may occur, and although the top rockbolt may not slide away completely, instability may occur in the rock mass.

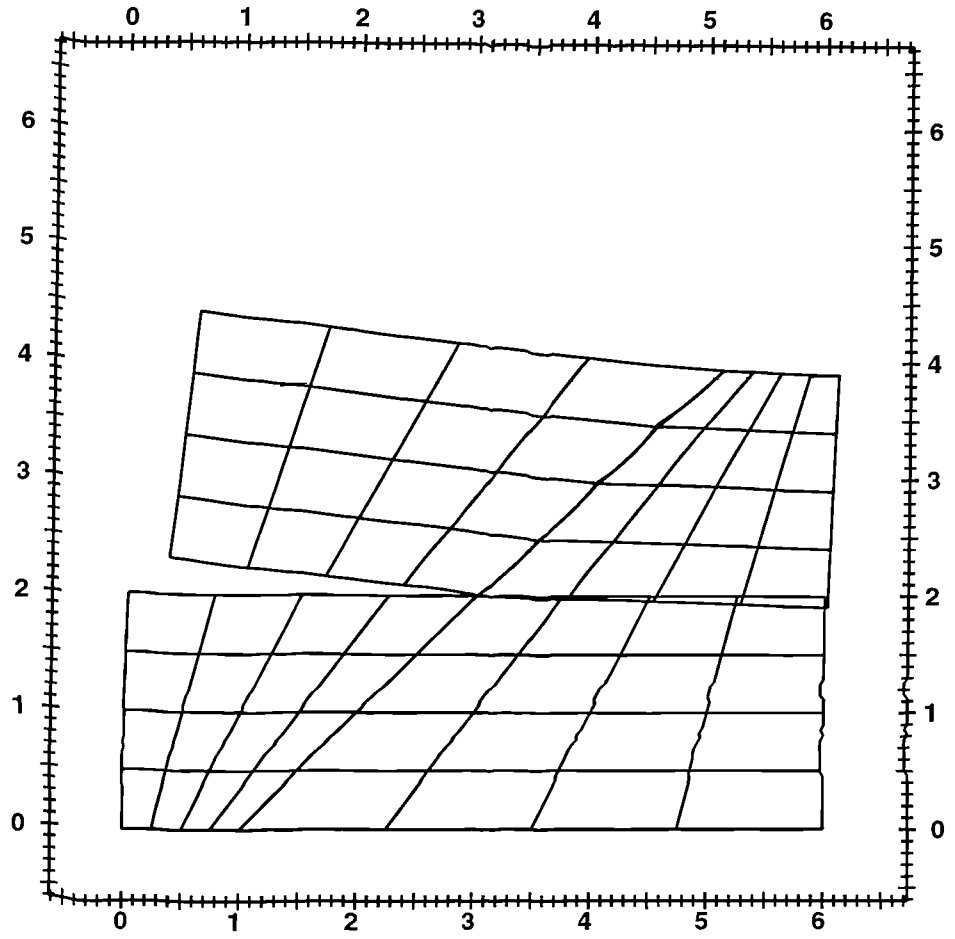

Figure 8.12: Problem 1 - bar element discretization of steel bolt

Further, it is interesting to note that the top half of the deformed rockbolt exhibits disjoint behaviour between its members. The deformation between members is not strictly strut like, but it owes more to the fact that the neighbouring rock element that the grout is attached to exhibits a natural deforming phenomenon. These 'discontinuities' between rockbolt elements echo the difficulties encountered before, and they reflect the unsatisfactory results obtained when bar elements are used to model a thin rod (please refer to Chapter 5). It confirms that bar elements may not be the ideal elements to model the steel bolt in rockbolt element.

Higher Gauss point integrating rules have also been used in this problem, but no

improvement could be observed.

8.9.2 Problem 2: beam element discretization of steel bolt

In this problem, the new rockbolt element replaces Aydan's element in the last Problem, while all other conditions are the same as before. Here, two trial runs are made. The first run uses small displacment formulations, while in the second, large displacement formulations are used.

1. **Small displacement analysis**

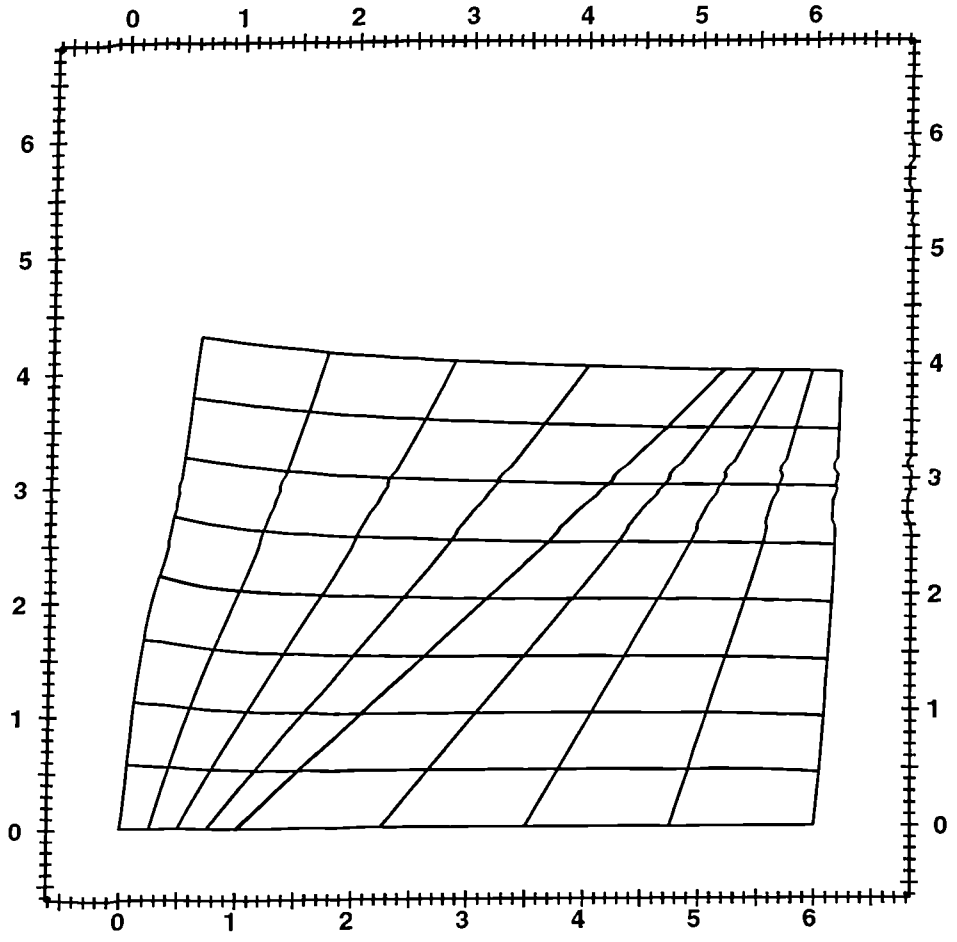

Figure 8.13: Problem 2 - beam element discretization of steel bolt (small displacement)

Figure 8.13 shows the results of the small displacement analysis, as executed by the computer. It suggests that the whole structure deforms as one unit, which effectively

means that the rockbolt has totally compensated the joint within the rock mass, so that no discontinuities within the rock mass have any effect on the structure. Consequently, the deformations between elements are much smoother, and the rockbolt can hold the rock blocks between the joints very well without rotation or penetration.

Further, it can be seen that the rockbolt is connected by its members to form a rigidly jointed frame, so that the rockbolt in this representation offers much more satisfactory results without exhibiting any 'discontinuities' between members. This is mainly because an additional rotational degree of freedom is allowed at the end-node of each beam element, and the bolt sub-elements are allowed to transmit bending actions between them. With the total absence of the strut like behaviour, together with a smooth deformation of the whole structure, it suggests that beam element discretization of the steel bolt offers greater flexibilty and stability than in Problem 1, and it reflects a much more realistic real life situation.

2. **Large displacement analysis**

To give a more realistic representation, Problem 2 is run again using large displacement formulations for all elements. Figure 8.14 shows the results of the computed results, and it can be seen that the general shape of the deformed body is very similar to Figure 8.13 when small displacement analysis is used, except that a very slight rotation of the top rock block is noticed. However, the amount of this rotation is very small, and it should not affect the stabilty of the whole structure. This confirms the superiority of beam element discretization, as the smoothness of the deformed structure offers greater stability, and in real life, this rockbolt system can act as a good support system to prevent structural failure of the tunnel during excavation.

8.9.3 Comparisons between trial examples using different parameters

As an experiment, further trial parameters are used in Problem 2. In particular, Figure 8.15 shows the results of the large displacement analysis when identical parameters are used in the same mesh, except that loadings are now applied to the structure from the right. The direction of the surface traction is against the inclination of the rockbolt, so that the rockbolt is subject to higher tensile strength of the rock mass. Again, it can be seen that the rockbolt can hold the rock blocks and the

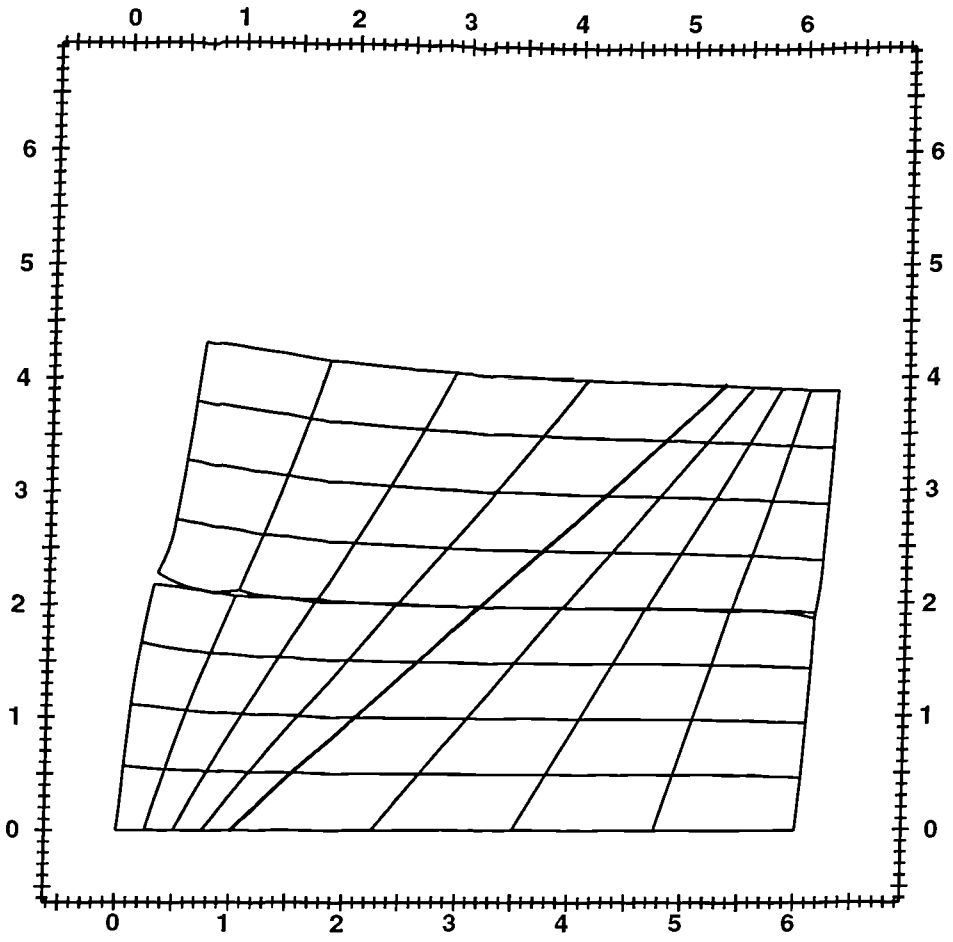

Figure 8.14: Problem 2 - beam element discretization of steel bolt (large displacement)

joint quite well with very small amount of rotation, and the whole structure deforms smoothly, as in Problem 2.

Comparisons between other trial values used in the same example were carried out, and it is found that the results are very similar. However, it must be pointed out that the use of parameters and material properties in this example plays a vital part in the overall results, as these quantities contribute significantly to the stiffness matrix of the structure, and hence the outcome of the deformation.

With a carefully chosen set of parameters which resembles closely a real-life situation, it can be concluded that the new algorithm proposed here represents a better mechanism to discretise rockbolts in tunnel engineering, and the use of beam elements is seen as a

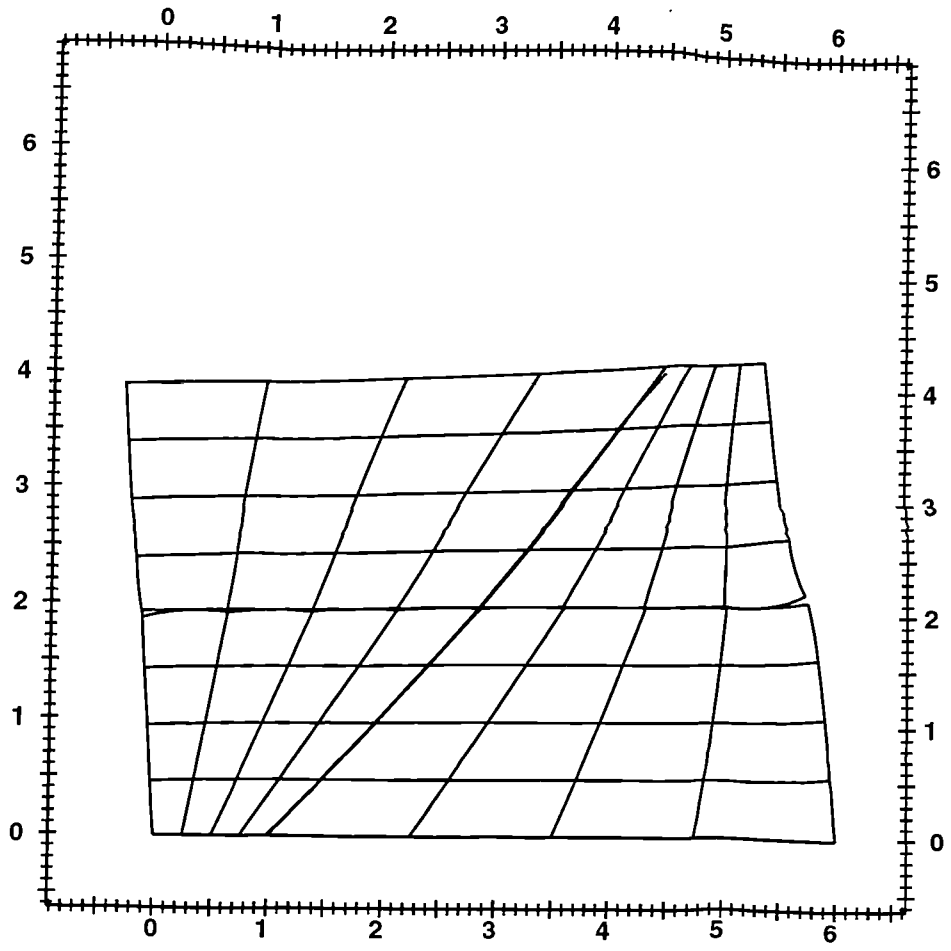

Figure 8.15: Problem 2a - uniform surface traction applying from the left

more desirable finite element discretization of the steel bolt.

8.9.4 Limitations of the joint element in these examples

Throughout this thesis, cracks and discontinuities between rock masses are discretised by joint elements as described in detail in Chapter 7. One of the main disadvantages of using this algorithm is that only small displacement formulation for joint element has been derived. Further, the two parameters which govern the movement of the joint are its normal and tangential stiffness. Although these linear factors can adequately control movement in the axial and the transverse directions, there is no mechanism to deal with the case when the rock masses start to seperate or to penetrate into each other between the joints. These phenomena are clearly evident in all examples set in this section, and

nonlinear mechanisms to govern joint opening and to prevent interpenetration are needed, to produce more realistic results.

8.10 Conclusions

In this Chapter, a new rockbolt element has been proposed. This element is in coupled form, and is based on the rockbolt element introduced by Aydan. It shares the same characteristics as Aydan's element, and it also has the same properties.

When the surrounding rock mass is subject to loadings, careful considerations have been made to the responses of the rockbolt due to the high tensile strength exerted by the rock mass. These considerations form the essential part of the algorithms of the proposed new rockbolt element.

In the last section, comparisons between the bar and the beam discretizations of steel bolt have been presented. Under an identical situation, it clearly shows that the new algorithm proposed in this chapter enjoys a better representation of a real-life situation, and the rockbolt performs its duty well as an effective reinforcement between discontinuities within the rock mass. With the help of an extra degree of freedom at the end-node of each beam element, internal shear forces and bending moments are allowed to transmit between elements, so that the resulting effects are much more realistic. Although the bar element discretization can also prevent the rock mass from sliding or collapsing, the rockbolt deforms as a strut-like structure, which is the problem highlighted in Chapter 5. Further, there is an absence of some smoothness between rock masses after deformation, when the gap between the joint within the rock masses start to open up, and the rock masses starts to rotate and penetrate into each other.

Geometric linearity and nonlinearity of the rockbolt element have also been presented. The small displacement formulation of the new rockbolt element is extended, so that it combines with the algorithms derived earlier for a beam element to form its large displacement equivalent. This method reduces the amount of algebraic manipulation considerably, and it calls for efficient use of all available formulae. Further, it would eliminate the need to derive new algorithms and to write a new subroutine in the computer program to simulate the analysis.

In order to keep the manipulation of data as simple as possible, it is intended throughout that simple algorithms are employed to solve the global stiffness equation and to conduct the iterative process for the residual loads in large displacement analysis. Although these algorithms are quite straightward and easy to understand, it may require many computations and iterations, which may in turn demand a large memory space and long computation time during execution, especially when a large number of elements is used in the analysis. This problem becomes more prominent when the loading applied to the structure is close to the critical load. Therefore, in order to maximize the efficiency of the analysis as a whole, it would be of benefit if efficient algorithms could be included within the analysis. This idea will be introduced in detail in the next chapter.

With the aid of an example, it can be observed that when the algorithm for the new rockbolt is used, the actual difference between geometric linearity and nonlinearity is quite small. Although there exist discontinuities within the rock mass, the small displacement analysis allows the rock masses to deform as one unit, whereas the large displacement analysis allows a small rotation between the two rock masses. In both cases, it can be taken that the new rockbolt element provides a better algorithm in finite element analysis to stabilise a discontinuous rock mass.

This study has clearly shown that it is possible to evaluate the effect of using rockbolts as reinforcement in rock mass both qualitatively and quantitatively, provided that the rockbolt, the surrounding rock mass and the stiffness of the joint are properly modelled by parameters which are closely related to a real-life situation. It is of paramount importance to study and understand the relationships between the materials and their properties of all the component involved in the body of the structure under investigation, otherwise it is possible to obtain results which may bear no significance to the real world.

The algorithm for the new rockbolt element is based on a two-dimensional elasticity problem. Naturally, the rockbolt element proposed here can be extended to deal with three-dimensional problems. Further, from the outset, the linear stress-strain relationship is used. While most materials exhibit this linear relationship up to the yield stress level, nonlinear behaviour is observed at higher stress levels. This phenomenon is called the plastic behaviour of material, and it can be characterized by an irreversible strain which is not time-dependent and which can only be sustained once a certain level of stress has

been reached.

The plastic behaviour of soil and metals allow a rational treatment of bearing capacities of foundations and the failure of slopes, excavations and tunnels. It also allows complete description of the stress-strain behaviour of soils so that soil deformations can be predicted right up to failure. Admittedly the behaviour of nonlinearity is more complex than elasticity. Therefore it is natural that the next stage of developement of the proposed algorithm is to adapt it to materials that exhibit plastic or nonlinear behaviour. Slip and debonding between bolt and grout, and between grout and rock, are other nonlinear mechanisms which it would be important to incorporate in future development of the rockbolt element.

Rockbolts have long been playing a big part in rock engineering as a practical way to stabilize the rock mass in tunnel excavations. It is hoped that the proposed algorithm for the new rockbolt element can be applied under most practical situations, so that the present study can be more widely and readily applied to other areas that involve rockbolting.

Chapter 9

Quasi-Newton methods

9.1 Introduction

In this thesis, the problem of large deformation of a perfectly elastic body under loadings has been investigated by the use of the finite element displacement method, and it is very often that one has to solve the resulting nonlinear stiffness equation

$$\mathbf{K}u = f$$

where $\mathbf{K}$ is the nonlinear global stiffness matrix.

Methods of solving this equation using residual loads have been discussed in full in the last few chapters, and they have been used extensively throughout. Although these methods are easy to understand and are fairly reliable, they are often not efficient enough and may require a large number of iterations to achieve reasonable accuracy.

Reed (1990, 1992) has proposed the use of variants of quasi-Newton minimization algorithms as an alternative to solve this nonlinear matrix equation in the finite element system. In this chapter, theories of these algorithms are summarized, and their performance will be compared with the aid of a standard problem in elasticity.

9.2 General quasi-Newton minimization algorithm

At present, variants of limited storage quasi-Newton algorithms have been widely used for minimizing any given function $f(x)$, where $x \in \Re^n$, assuming that $f(x)$ is at least twice continuously differentiable $\forall x \in \Re^n$.

In the full general quasi-Newton method, if x_1 is a given starting point, the kth iteration is defined by

$$x_{k+1} = x_k + \lambda_k p_k \tag{9.1}$$

where λ_k is the steplength which is to be found by a line search, and p_k is the search direction given by

$$p_k = -\mathbf{H}_k g_k, \tag{9.2}$$

with $g(x) = \nabla f(x)$ and $\mathbf{H}_k$ is the approximation to the inverse Hessian of $f(x)$, or the inverse of $\nabla^2 f(x)$, and is defined recursively from a symmetric positive definite matrix $\mathbf{H}_1$, which is the initial approximation of the inverse Hessian and is usually diagonal, by

$$\mathbf{H}_{k+1} = \mathbf{H}_k + \mathbf{U}_k, \qquad k = 1, 2, 3, \ldots, \tag{9.3}$$

where $\mathbf{U}_k$ is a symmetric rank one or rank two update.

Let

$$s_k = x_{k+1} - x_k \qquad \text{and} \qquad y_k = g_{k+1} - g_k,$$

then at each iteration, it is required that

$$\mathbf{U}_k y_k = s_k - \mathbf{H}_k y_k. \tag{9.4}$$

Some of the most commonly used formulae derived from this algorithm are defined for $\mathbf{U}_k$ by the following:

1. Symmetric Rank One (SR1) method

$$\mathbf{U}_k = \frac{1}{\alpha_k} u_k {u_k}^T \tag{9.5}$$

where

$$u_k = s_k - \mathbf{H}_k y_k \qquad \text{and} \qquad \alpha_k = {u_k}^T y_k.$$

2. The Broyden family of rank-two updates

$$\mathbf{U}_k = \frac{1}{\alpha_k} u_k {u_k}^T - \frac{1}{\beta_k} v_k {v_k}^T + \gamma_k w_k {w_k}^T, \tag{9.6}$$

where

$$u_k = s_k, \quad v_k = \mathbf{H}_k y_k, \quad \alpha_k = {u_k}^T y_k, \quad \beta_k = {v_k}^T y_k, \quad \text{and} \quad w_k = \frac{1}{\alpha_k} u_k - \frac{1}{\beta_k} v_k.$$

The value of γ_k in (9.6) characterizes the following different methods:

(a) DFP: $\gamma_k \equiv 0$;

(b) BFGS: $\gamma_k \equiv \beta_k$.

In the BFGS method, the updating in (9.3) and (9.6) can be rearranged to take the multiplicative form;

$$\mathbf{H}_{k+1} = \mathbf{V}_k^T \mathbf{H}_k \mathbf{V}_k + \rho_k s_k s_k^T \tag{9.7}$$

where $\rho_k = \dfrac{1}{\alpha_k}$ and $\mathbf{V}_k = \mathbf{I} - \rho_k y_k s_k^T$;

(c) Hoshino: $\gamma \equiv \dfrac{\alpha_k \beta_k}{\alpha_k + \beta_k}$.

In all of these algorithms, the whole $n \times n$ matrix H_k, or, when making use of the symmetry, the upper triangle of H_k, is stored.

Full details of the above and their convergence properties can be found in the standard texts such as Fletcher (1987) and Dennis & Schnabel (1983).

9.3 Limited storage algorithms

9.3.1 Introduction

Although the quasi-Newton methods described in the last section work well in practice, they require an approximation for the Hessian of f, or its inverse, and thus it is necessary to store an $n \times n$ matrix as the iteration proceeds. This will make the computation very expensive and thus the methods become impractical when n is large. Therefore, variants of the standard quasi-Newton algorithms are introduced in order to reduce the amount of storage.

In these limited storage quasi-Newton algorithms, the initial matrix, which is usually diagonal, is stored in compact form, together with a certain number of individual updates.

9.3.2 Approximation to the inverse Hessian of $f(x)$

In this section, the aim is to construct an iteration scheme to form $\mathbf{H}_k$ as an approximation to the inverse Hessian of $f(x)$.

In limited storage quasi-Newton algorithms, $\mathbf{H}_1$ and the information for the individual updates $\mathbf{U}_i$ are stored separately. Then when it is required, $\mathbf{H}_k$ can be constructed from

$$\mathbf{H}_k = \mathbf{H}_1 + \sum_{i=1}^{k-1} \mathbf{U}_i, \tag{9.8}$$

if the Broyden family of rank-two updates in the additive updating form of (9.6) is used, where $\mathbf{U}_i = \mathbf{U}_i(s_i, y_i, H_i y_i)$.

Assuming that storage for m updates are available, the two most commonly used limited storage algorithms are briefly described below:

1. In the VSCG algorithm of Buckley and LeNir (1983, 1985) where the additive form (9.6) is used, once all of the m update storages are filled, information on the first $m-1$ updates is retained, and at each subsequent iteration, the most recently formed one is replaced. Thus,

$$\mathbf{H}_{k+1} = \mathbf{H}_m + \mathbf{U}_k, \qquad k = m, m+1, \ldots \tag{9.9}$$

2. In the L-BFGS algorithm of Liu and Nocedal (1989) where the multiplicative form is used, once the storage is filled, the m most recently formed updates are retained, and at each subsequent iteration, the oldest update is replaced. Thus

$$\begin{aligned} \mathbf{H}_{k+1} &= (\mathbf{V}_k^T \ldots \mathbf{V}_{k-m+1}^T)\mathbf{H}_1(\mathbf{V}_{k-m+1} \ldots \mathbf{V}_k) \\ &+ \rho_{k-m+1}(\mathbf{V}_k^T \ldots \mathbf{V}_{k-m+2}^T)s_{k-m+1}s_{k-m+1}^T(\mathbf{V}_{k-m+2} \ldots \mathbf{V}_k) \\ &+ \ldots \\ &+ \rho_k s_k s_k^T \qquad k = m, m+1, \ldots \end{aligned} \tag{9.10}$$

Note that because of the criteria laid down by the line search ($s^T y > 0$), the QN matrices $\mathbf{H}$ retain are always positive definiteness.

9.4 Update condensation algorithm

9.4.1 Introduction

The update condensation algorithm offers an alternative approach to the limited storage quasi-Newton methods. The idea of this approach is to discard all updates when the available storage is filled, and to replace them by an 'artifical update' which contains condensed information of previous updates. This approach can be applied to any quasi-Newton method, but for the purpose of illustration, a rank two update such as BFGS is used here.

9.4.2 The method

In this limited storage approach, suppose that storage for m updates is available. All but one storages are available for the usual quasi-Newton updates in additive form, such as those in the VSCG algorithm, while one storage is reserved.

After $m-1$ iterations, when the evaluations of $x_{m+1} = x_m - \lambda_m \mathbf{H}_m g_m$ and g_{m+1} are being carried out, the reserved storage is filled by the update defined by

$$\mathbf{H}_m = \mathbf{H}_1 + \sum_{i=1}^{m-1} \mathbf{U}_i. \tag{9.11}$$

Before proceeding with the mth iteration, $\mathbf{H}_m$ is replaced by a restart matrix $\hat{\mathbf{H}}$ of the form

$$\hat{\boldsymbol{H}} = \delta \boldsymbol{H}_1 + \hat{\boldsymbol{U}} \tag{9.12}$$

where $\delta > 0$ is a scaling factor which is chosen to ensure that $\hat{\mathbf{H}}$ is positive definite, while $\hat{\mathbf{U}}$ is a rank two 'artifical update' constructed from the existing 'natural' updates $\mathbf{U}_1, \mathbf{U}_2, \ldots, \mathbf{U}_{m-1}$. This 'artifical update' is obtained by condensing the infomation held in the 'natural updates'. The information defining $\hat{\mathbf{U}}$ is placed in the reserved storage space, and all the natural updates are then deleted.

Subsequent 'natural' updates are constructed by the Broyden updating formula (9.6), but with $\mathbf{H}$ replacing $\mathbf{H}_m$ in the construction of $\mathbf{U}_m$, defined by the iteration

$$\mathbf{H}_{k+1} = \hat{\mathbf{H}} + \mathbf{U}_k, \qquad k = m, m+1, \ldots \tag{9.13}$$

it is then stored in the space thus freed. When this storage becomes full again, form a new condensation by (9.12), as before, delete the 'natural' updates, and repeat this prodedure. Thus, after every $m-1$ iterations, a condensation occurs and this cycle repeats.

In this algorithm, the restart matrix $\hat{\mathbf{H}}$ must satisfy the following equations:

$$\hat{\mathbf{H}} y_m = \mathbf{H}_m y_m \tag{9.14}$$

and

$$\hat{\mathbf{H}} g_{m+1} = \mathbf{H}_m g_{m+1}. \tag{9.15}$$

These relationships ensure that $\mathbf{U}_m(s_m, y_m, \mathbf{H}_m y_m) = \mathbf{U}_m(s_m, y_m, \hat{\mathbf{H}} y_m)$, and so following the condensation the search direction $\hat{p}_{m+1} = -\mathbf{H}_{m+1} g_{m+1}$ is the same as would

have been obtained from the full quasi-Newton method.

Further discussion of these conditions and a full account of this algorithm can be found in Reed (1997).

9.5 Application in the solution of finite element systems

Using an iterative method, the incremental residual load of a finite element system during the kth iteration in the nth load increment can be written in the general form

$$\Phi_k = \mathbf{K}_k \Delta u_k - \Delta F \tag{9.16}$$

where $\mathbf{K}_k$ is the nonlinear stiffness matrix defined either in the general form (4.35), or (6.38) for the beam element.

At the start of load increment, it is taken that

$$\Delta u_0 = 0 \qquad \text{and} \qquad \mathbf{K}_1 \Delta u_1 = \Delta F.$$

9.5.1 Quasi-Newton method

In a quasi-Newton method, the equation

$$\Phi(\Delta u) = 0$$

can be solved by defining the algorithm

$$\Delta u_n^{(k+1)} = \Delta u_n^{(k)} + \lambda_k p_k, \tag{9.17}$$

where the steplength λ_k may be determined by a line search, and the quasi-Newton method for the search vector p_k is given by

$$p_k = -\mathbf{H}_k \Phi_k, \tag{9.18}$$

where $\mathbf{H}_k$ is the matrix approximating the inverse Jacobian of Φ, and is formed from the successive updating relationship

$$\mathbf{H}_{k+1} = \mathbf{H}_k + \mathbf{U}(s_k, \mathbf{H}_k y_k). \tag{9.19}$$

In this application, the starting matrix $\mathbf{H}_1$ is taken as $\mathbf{K}_1^{-1}$, where $\mathbf{K}_1$ is the nonlinear stiffness matrix evaluated at the start of the current load increment.

As all computations are carried out at the nth load increment, the displacement term $u_n^{(k+1)}$ is denoted as u_{k+1} for convenience.

Let

$$s_k = \Delta u_{k+1} - \Delta u_k, \qquad y_k = \Phi_{k+1} - \Phi_k, \qquad \text{and} \qquad v_k = s_k - \mathbf{H}_k y_k,$$

then (9.5) and (9.8) give

$$\mathbf{H}_k = \mathbf{K}_1^{-1} + \sum_{i=0}^{k-1} \frac{1}{\alpha_i} v_i v_i^T \tag{9.20}$$

To avoid a line-search iterative algorithm, Φ_{k+1} may be approximated by the term $\mathbf{K}_k \Delta u_{k+1} - \Delta F$. Then this, (9.17) and the exact line-search condition $p_k^T \Phi_{k+1} = 0$ lead to the steplength

$$\lambda_k = \frac{-p_k^T \Phi_k}{p_k^T \mathbf{K}_k p_k}. \tag{9.21}$$

9.6 Performance comparison and discussion

In this section, the example described in section 3.7 is used as a sample test to compare the performance of the variants of quasi-Newton algorithms. The parameters are the same as before, but a coarse mesh is used to discretise the elastic block.

It has been observed that identical results have been obtained by all of these methods. The main aim of this exercise is to compare the efficiency in terms of computational time required. However, as the mesh is coarse, the computational time is very short and hence it is very difficult to detect the difference.

This exercise has been repeated by the use of some other simple models, and it has been found that all algorithms give rise to identical results, and the performance in terms of the required computational times is very similar. However, it must be point out that although these algorithms work well with sample models with coarse mesh, none of them can give convergent results for a model with a more complicated mesh which may include a combination of various types of element, or a finer mesh with a large number of elements. This may be caused by an inadequte convergence criterion, or becasue there are some problems with convergence within each increment, namely:

1. $\mathbf{K}_1$ may not be a good initial approximation;

2. the steplength λ_k is not evaluated accurately enough. It may require a line-search algorithm to evaluate;

3. it may require to re-start if p_k is not sufficiently 'downhill'.

However, from the examples that have been carried out, the signs are very positive, and it is hoped that with some modifications made to these quasi-Newton algorithms, this problems can be fully overcome in the near future.

Chapter 10

Applications

In this chapter, a wedge stability problem is presented as a model application. This problem can often lead to the more practical situation where rock slope stabilization is involved, and it also contributes to the stability problem of a cavern wall.

10.1 Wedge stability problem

The stability of a slope is one of the most frequent problems that a civil engineerer has to consider. The stabilty failure of this problem is mostly attributed to the weakness in the discontinuities between rock mass, when sliding, toppling, or a combination of these two phenomena occurs.

One of the most common solutions to this problem is to install appropriate rockbolts between discontinuities to increase the strength of support and thus the saftey factor. This is due to the fact that rockbolts are generally cheap, durable, and easy to install. In this application, untensioned grouted rockbolts are used as support to stabilize the sliding of the rock mass.

10.1.1 The problem

The two-dimensional wedge stability problem has been extensiveiy analysed by Marenče (1992), although his treatment of this problem has concentrated on the stiffness analysis, where the *bolt crossing joint* and the grout are treated as a sub-structure which is added to the stiffness of the rock, while the main objective of this exercise is to analyse the deformation of the rock. A comparison between these two algorithms in this problem can be found at the end of this chapter.

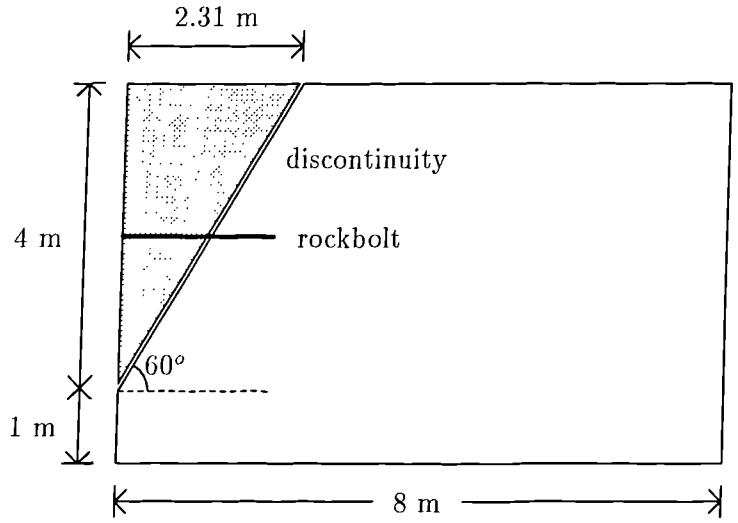

Figure 10.1: Geometry of the wedge problem

In this problem, a rectangular rock block is used as a model to test the stability of a vertical excavation or a cavern wall. The block is 5 m high and 8 m long. The 'slope' of the discontinuity, or the joint, is inclined at 60^o to the horizontal, and the wedge is at the top left hand corner of the block. The vertical edge of the wedge is of height 4 m.

A horizontal grouted rockbolt of length 4 m is placed through the wedge and the discontinuity, and is secured to the rock mass. It sits 2 m from the top end of the wedge, as shown in Figure 10.1, and the details of its finite element mesh are shown in Figure 10.2. The rockbolt is a standard untensioned grouted rockbolt, and is subject to deformation in a manner described in Chapter 7. Here, the problem is identified as a plane strain problem.

In this model, if the support of the rockbolt is removed from the wedge, the wedge is liable to slide along the slope of the discontinuity or penetrate into the surrounding rock, and the amount of deformation depends on the material property of the rock, the rockbolt, and the stiffness of the joint, which is defined by its tangential k_s and normal k_n components. To initiate deformation, a uniform surface traction is applied normally downwards along the top edge of the wedge.

All materials used here are taken to be perfectly elastic, and are assumed to be weightless, uniform, homogeneous and isotopic. The rock mass has an elasticity modulus of 10 GN/m^2 and a Poisson's ratio of 0.3, while the rockbolt has a dowel modulus of 10^8. The tangential and the normal stiffness of the joint are taken as $2 \times 10^5 N/m^2$ and 10^7 N/m^2

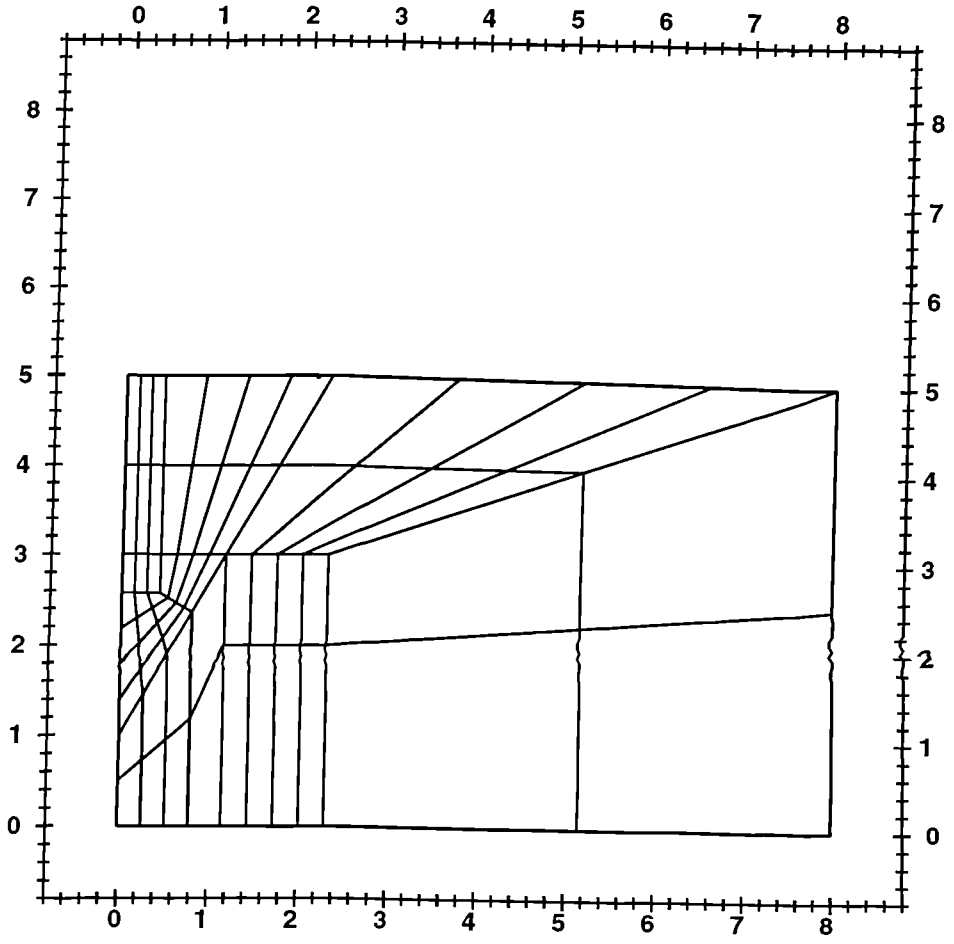

Figure 10.2: Mesh details of the wedge problem

respectively. Other parameters of the rockbolt used in this model are given in the following table.

	Elasticity modulus GN/m^2	Poisson's ratio	Shear modulus GN/m^2	Radius m
Bolt	210.00	0.30		0.013
Grout	20.00	0.30	8.33	0.020

Table 10.1: Material properties

For comparison, the wedge problem is repeated several times using large displacement formulation. The above set of parameters is referred to as the 'standard' set, and it will be

used as a base for testing the same model in the following section, and only modifications made to this set will be mentioned henceforth.

No exaggeration factor is used in all examples in this section, ie. deformed meshes shown are of their actual sizes.

10.2 Without the support of the rockbolt

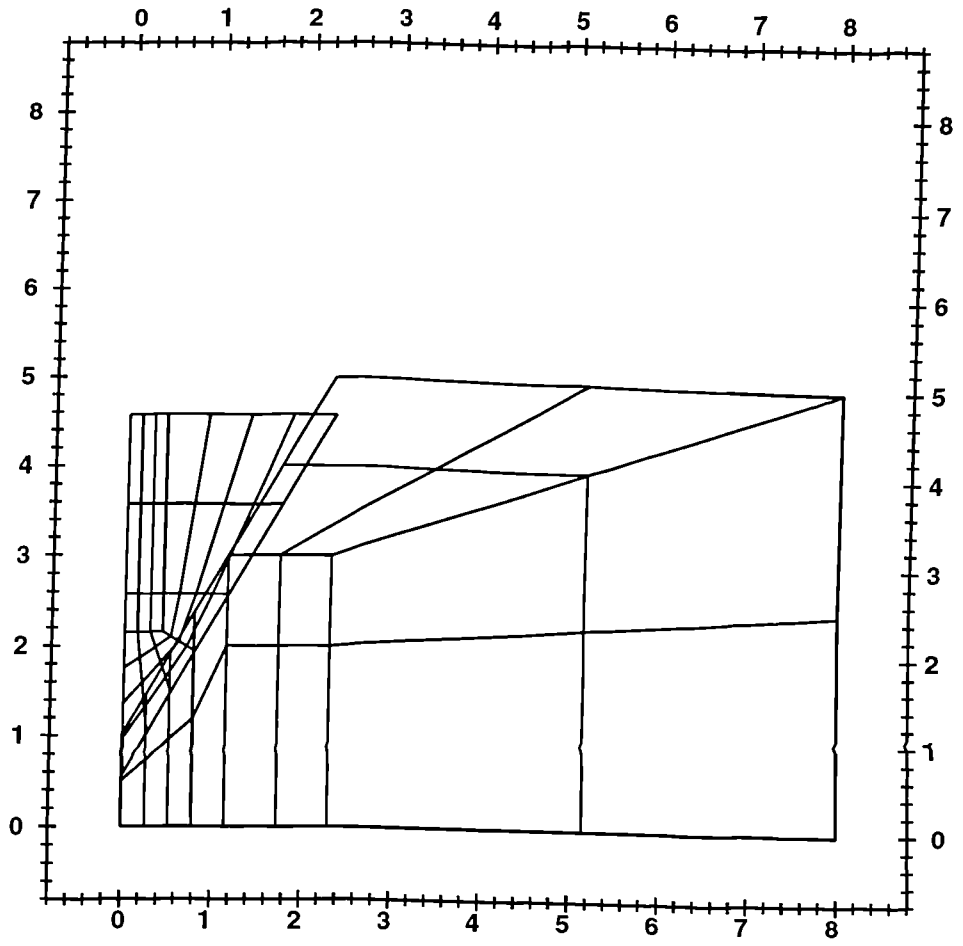

Figure 10.3: (a) Wedge problem without the rockbolt as a support

The following results are obtained with the standard set of parameters and with the rockbolt removed from the wedge problem. It can be seen in Figure 10.3(a) that the wedge penetrates directly into the rock mass, and the amount of penetration depends heavily on the stiffness of the joint.

In order to control the amount of penetration between the wedge and the rock mass, the tangential and the normal components of the stiffness of the joint have been increased to $2 \times 10^6 \mathrm{N/m^2}$ and $10^8 \mathrm{N/m^2}$ respectively. With this modification, the results are shown in Figure 10.3(b).

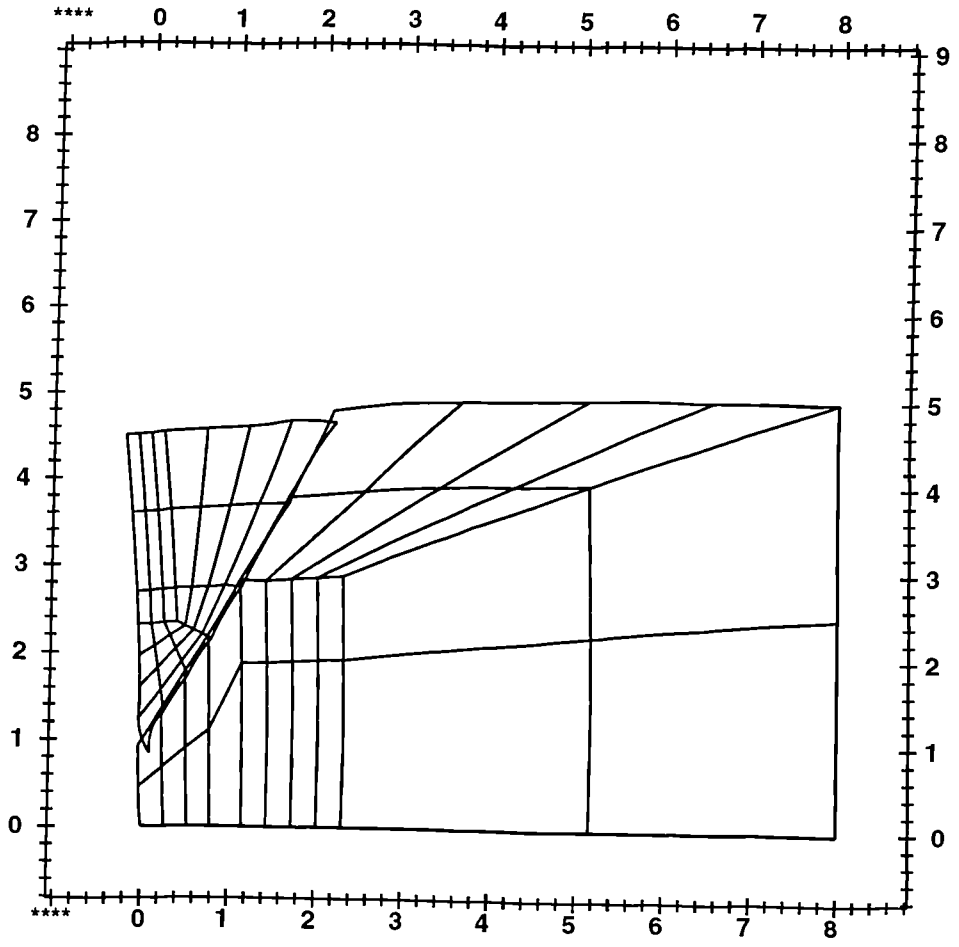

Figure 10.3(b): Wedge problem without the rockbolt, but with increased joint stiffness

Note that as the formulation governing the mechanics of the joint element is in linear form, it would be not be possible to find the critical load applied on the wedge before it collapses.

10.3 Bar element discretization

The following results are obtained when the rockbolt using bar element discretization of the steel bolt is used. The deformation theory of this test is based on the original idea of a rockbolt introduced by Aydan (1989).

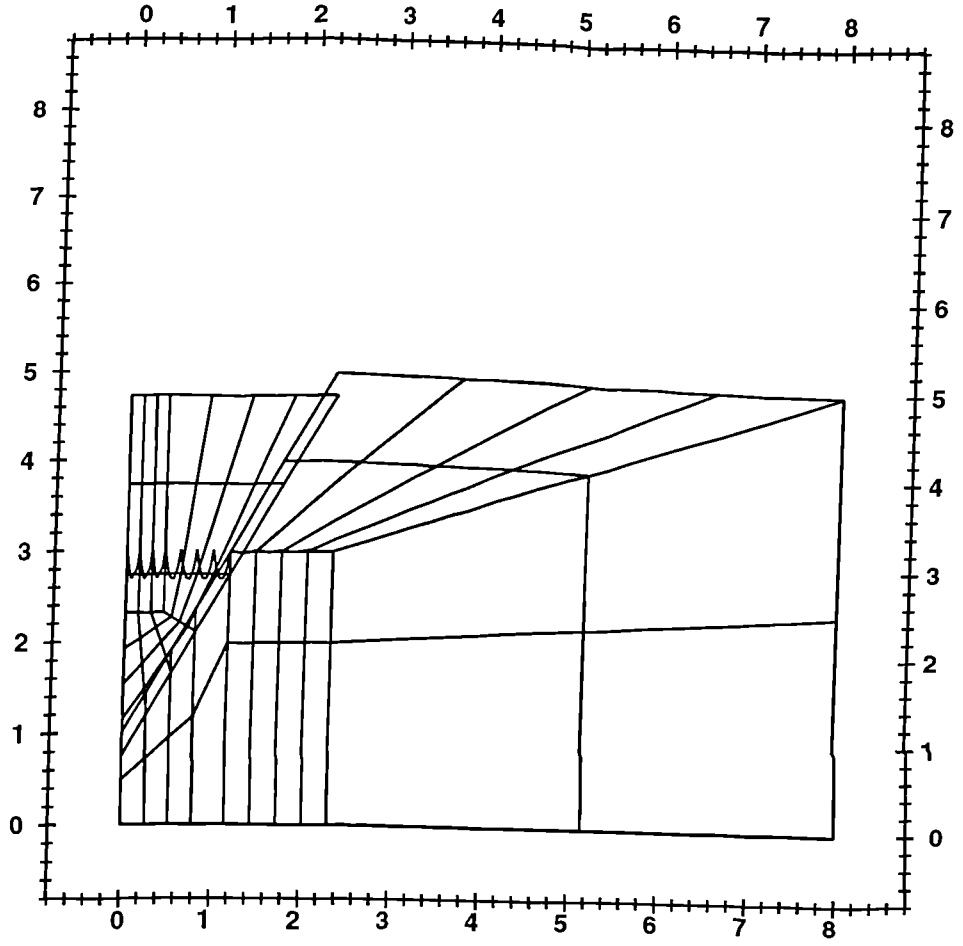

Figure 10.4: Bar element discretization of steel bolt

From the results, it can be seen that the rockbolt elements are discontinuous in slope at the ends nodes, and it reflects a similar type of problem encountered with the bar element discretization of a thin rod when the thin rod behaves like a strut. Further, the left hand end of the bolt is deformed in a 'parabolic shape'. This is perhaps caused by the two-point Gauss integration rule which is used to obtain the stiffness matrix of the bolt. Similar parabolic distributions are observed for stresses in quadratic elements in undrained con-

solidation or in nearly-incompressible materials (reference Reed (1984), Naylor (1974)). The same phenomenon is evident in Figure 8.12, for bar elements.

Higher order Gauss rule has been used, but it is noted that no improvement can be made.

10.4 Beam element discretization of steel bolt

In this section, the beam element discretization for the bolt, as described in Section 8.8, is used for all tests here.

10.4.1 Standard parameters

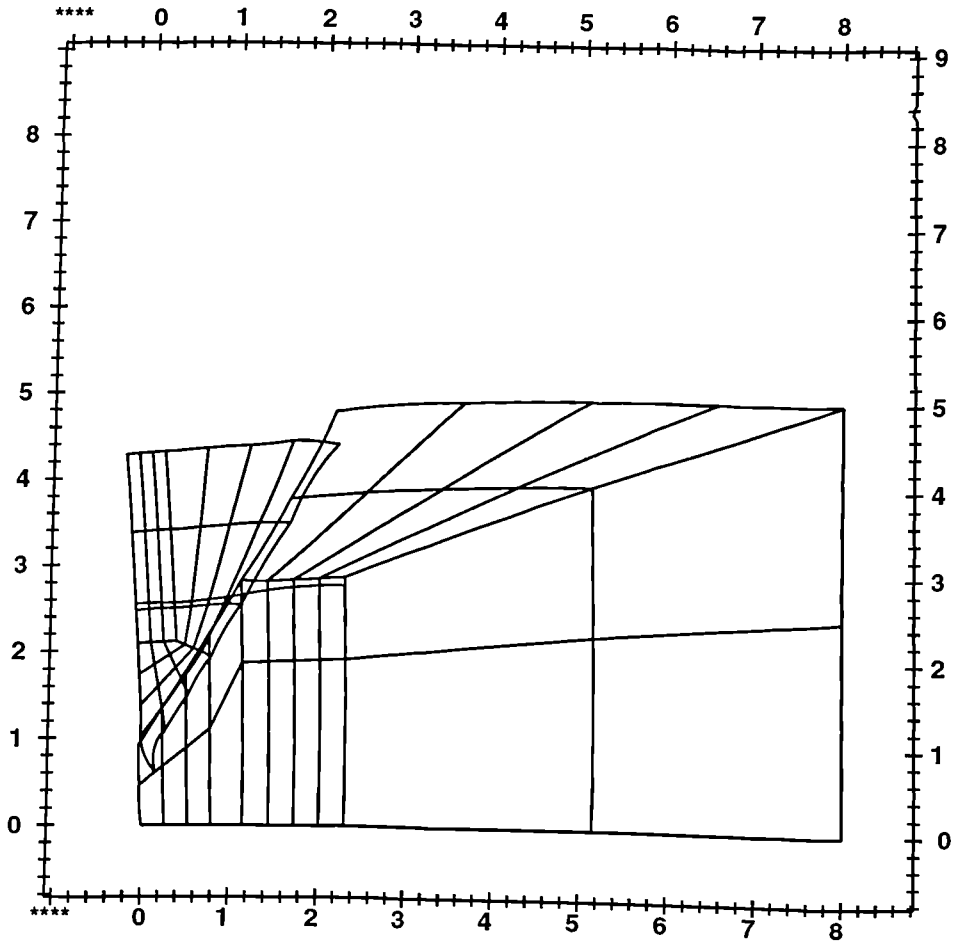

Figure 10.5: Wedge problem with the standard set of parameters

In this analysis, the small deformation theory of the joint element is mixed with the large deformation theories of other types of element, and hence in effect, the joint element deforms in a slightly different way. Therefore it is natural that in this test, the deformation at both ends of the joint along the wedge does not appear to be very smooth. To overcome this problem, a large deformation theory for the joint element is needed. The rockbolt itself, modelled by beam elements, deforms in a realistic manner, and limits the movement of the wedge along the joint.

It has also been found that this analysis fails when the left hand end of the bolt is modelled to be fixed to the rock in order to simulate a plate being attached at that point. This situation can be simulated when the bolt and the rock nodes are discretised to be the same node in the mesh.

10.4.2 Increasing the stiffness of the joint

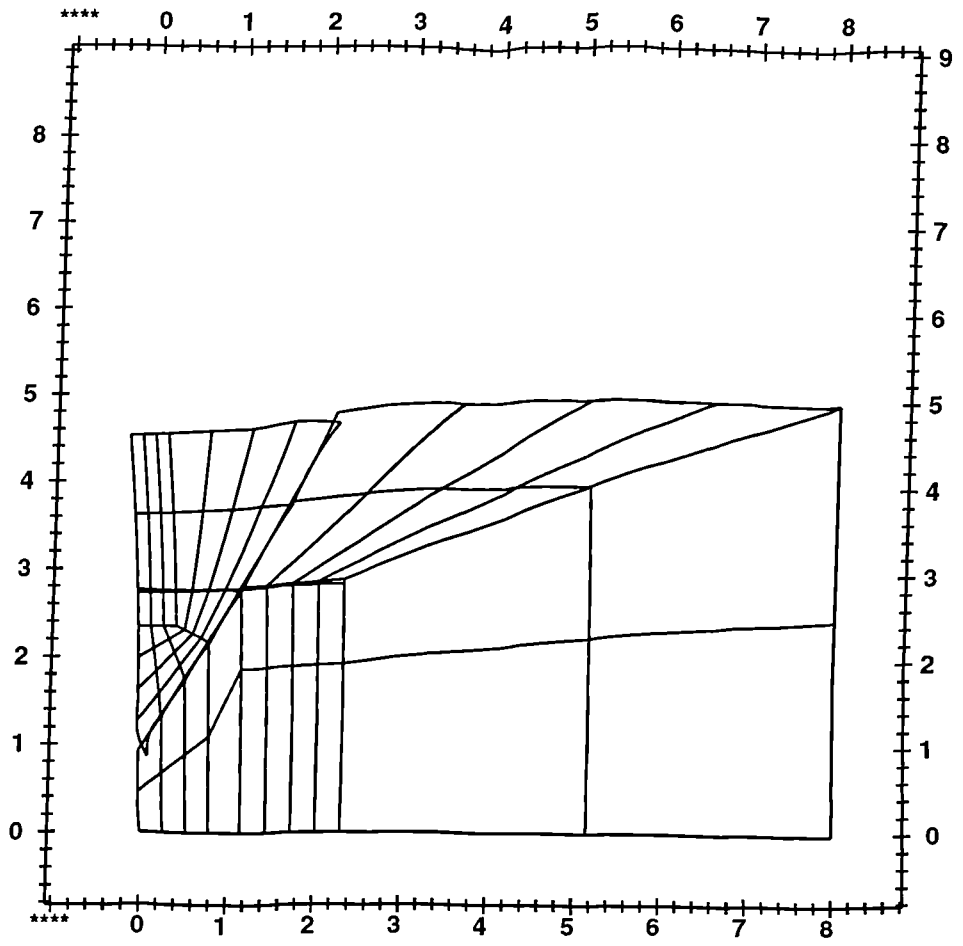

Figure 10.6: Wedge problem - joint with higher stiffness moduli

In this test, the normal and the tangential stiffness of the joint are taken to be $10^9 \mathrm{N/m^2}$ and $2 \times 10^7 \mathrm{N/m^2}$ respectively. Here, the wedge is successfully held in place by the rockbolt.

10.4.3 Modifying the parameters of the rockbolt

In this test, the radii of the bolt and the grout are increased to 0.05m and 0.08m respectively. Further, the Young's modulus of the bolt has also been increased to $300\mathrm{Gm/m^2}$.

It can be seen that with the increase of its stiffness, the rockbolt deforms less, and it can in general offer better support to the wedge. This in broad agreement with logical

expectation.

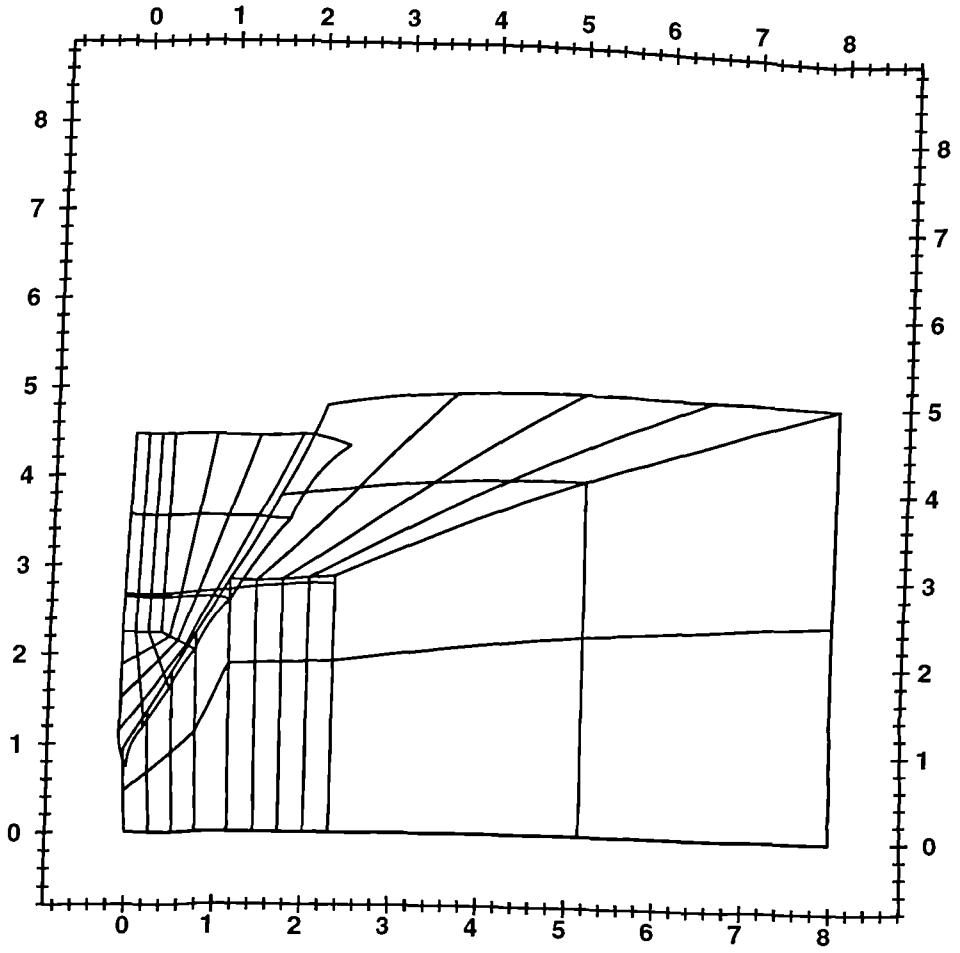

Figure 10.7: Wedge problem - rockbolt with increased stiffness and diameter

10.5 Comparison with Marenče and his associates' results

This wedge problem has also been investigated fully by Marenče and his associates at the Institut für Baustatik in the Universität Innsbruck. In their work, the rockbolt element used in the problem is based on the algorithm proposed by Swoboda & Marenče (1991, 1992, 1995) and Marenče (1992).

10.5.1 Bolt Crossing Joint

The *bolt crossing point* (BCJ) element has been designed to connect the bolt elements on both sides of the discontinuity. The element assumed two nodes, one on each side of the discontinuity, and they connected the bar nodes of the bolt element. In the grout-rock interface, the other nodes of the element were connected through an interface element representing the joint. Figure 10.8 shows details of this BCJ element.

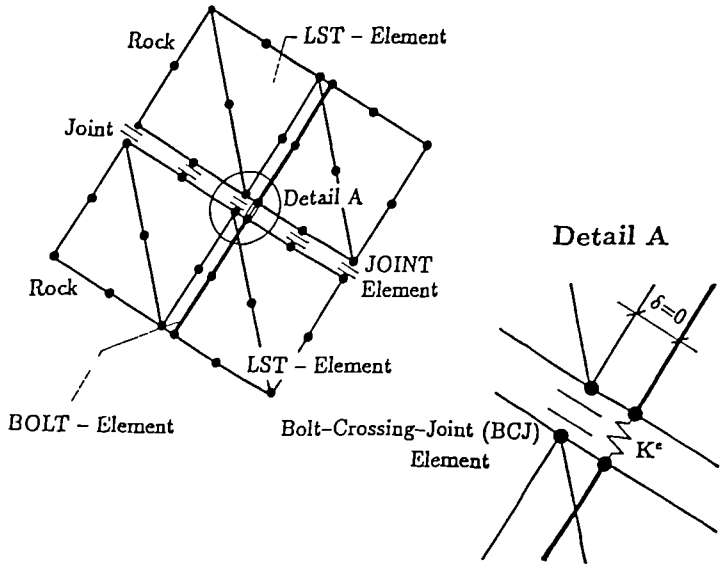

Figure 10.8: *Bolt crossing joint element* and conncetion with finite element mesh (from Swoboda & Marenče (1995).

The BCJ element was modelled as springs which describe the bolt resistance according to the movements on the joint. The stiffness marix of the BCJ can be written as

$$\mathbf{K}^e = \begin{bmatrix} k_{11} & k_{12}^* & -k_{11} & -k_{12}^* \\ k_{12}^* & k_{22} & -k_{12}^* & -k_{22} \\ -k_{11} & -k_{12}^* & k_{11} & k_{12}^* \\ -k_{12}^* & -k_{22} & k_{12}^* & k_{22} \end{bmatrix} \tag{10.1}$$

where k_{11} was a shear stiffness, k_{22} was a normal stiffness, and k_{12}^* was the mean of a connection between a shear displacement and a normal force k_{12}, and a connection between a normal displacement and a shear force k_{21}, ie $k_{12}^* = \dfrac{k_{12} + k_{21}}{2}$.

10.5.2 Wedge stability problem

In order to evaluate the performance of the new rockbolt element, parameters used in the example in Section 10.1 have been specifically chosen to match those used by Marenče and his associates at the Institut für Baustatik at the Universität Innsbruck as closely as possible. In particular, all material properties of the rock mass, the elasticity moduli, Poisson's ratios, shear moduli and the radii of the bolt and the grout, as listed in Table 10.1, are taken to be the same. However, in the BCJ element, the stiffness of the grout varies according to displacement. These values are shown in Table 10.2 and in Figure 10.9.

Direction	Stiffness (N/m^2)	Displacement (m)
transverse	$v_1 = 1.7028 \times 10^8$	$v_2 = 5 \times 10^{-6}$
	$v_3 = 1.1016 \times 10^8$	$v_4 = 6 \times 10^{-3}$
	$v_5 = 0$	$v_6 = 10^{-2}$
axial	$v_{12} = 0.4$	$v_9 = 10^{-3}$
	$v_7 = 1.3693 \times 10^4$	$v_{10} = 3 \times 10^{-3}$
	$v_8 = 5.477 \times 10^3$	$v_{11} = 10^{-2}$

Table 10.2: Grout stiffness

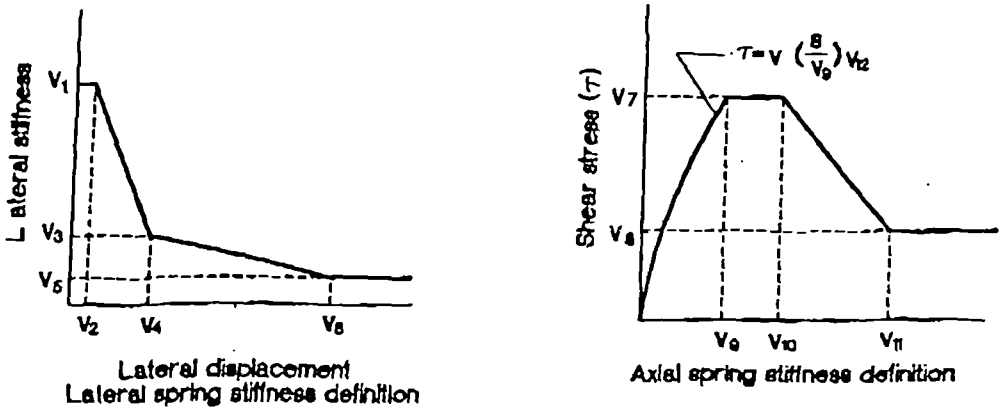

Figure 10.9: Variable grout stiffness for BCJ element

Figure 10.10 shows the results obtained by them when a set of closely matched parameters is used. It can be seen that the general shape of the deformed wedge is very similar, indicating that the two algorithms for modelling rockbolts give very similar results. However, due to the different emphasis of these two analyses, direct comparisons

between these two algorithms cannot be obtained.

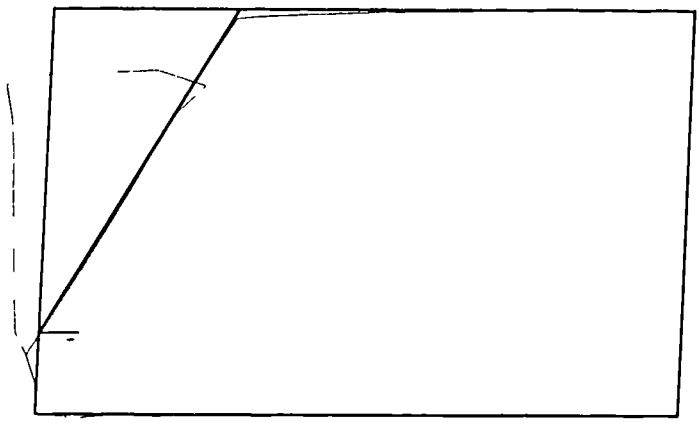

Figure 10.10: Wedge problem - results obtained at Universität Innsbruck

Chapter 11

Conclusions

11.1 A brief summary

Rockbolts have become one of the most fundamental support members of modern tunnelling technology in recent years. Because of their well-confirmed reinforcement effect in practice, their popularity is set to continue, and many researchers have conducted studies in the numerical simulation of rockbolt behaviour in the past and present.

11.1.1 The design philosophy

Before the development of a specialized rockbolt element, engineers used elastic bar or truss elements to represent the reinforcing effect of rockbolts. The design of some of the later generations of rockbolt model is based on the rockbolt element introduced by Aydan in 1989. This element in its coupled form could offer greater flexibility, and could more appropriately represent the mechanics of a rockbolt, so that the axial and shear loading can be accounted for by the steel bar, and the shear stress and the dowel effect by the interface and the grout annulus. The new rockbolt element proposed in this research is a modification of this original rockbolt element, when the beam element replaces the bar element in the discretization of the steel bolt.

In this study, a geometrically nonlinear finite element analysis is carried out to investigate the validity of a plane strain analysis in simulating the rockbolt as support in the two-dimensional tunnelling in rock mass. Further, linear material behaviour corresponding to perfectly elastic and isotropic materials has been assumed. As shown in much of the literature, plasticity or visco-plasticity might be considered as a better theory which can more realistically represent the material characteristics of the rock mass and rockbolt, but

because of the limitation of this research, this option has been omitted. It is, of course, possible to consider and implement this, and other types of nonlinear material, in the future.

The effects of using rockbolts as reinforcement within discontinuous rock mass depends not only on the design of the rockbolts, but also, to quite a large degree, on the rock strength, the stiffness of the joints, and the deformability of the rockbolts. The sensitivity of these factors can dramatically affect the behaviour of the rock mass and the efficiency of the rockbolts. This sensitivity is more evident when geometric nonlinearity is considered in the numerical model, because the nonlinear behaviour may cause collapse when the applied load exceeds the critical load. Therefore in the computer simulation of tunnelling problems, great care must be exercised in the use of these factors.

The finite element method has been one of the most commonly used numerical methods to analyse problems in tunnel excavation. To represent a structure of complicated shape and construction, it advocates the use of a finite element mesh which includes several different types of element. Because of the difference in geometry and mechanical responses, each type of element requires the use of a different nonlinear stiffness matrix in the small and the large displacement analysis.

The large displacement formulations of some elements, such as the eight-noded isoparametric element, have been well established in the past, and they have been documented and implemented by many researchers, while for others, such as the beam element and the proposed new rockbolt element, the algorithms have been established analytically in this research from the fundamental theories. To verify the validity of these formulae, some hypothetical examples are used to test these elements, so that evaluation of the performance of the algorithms can be made, and the results can be directly compared.

11.2 Main conclusions

At the end of each chapter, conclusion has been made so that the results could be summarized, and any features and/or shortcomings of the algorithms could be pointed out. This thesis has been organised in such a way that different types of element are presented in order so that the new rockbolt element can be readily constructed.

1. In the finite element approach to investigate a tunnelling problem, eight-node isoparametric elements are used to discretise the rock mass, and six-noded joint elements are used to discretise the discontinuities or the space between the rock mass. The small deformation theory of the joint element has been well developed by Beer (1985), for the cases of shell-shell, shell-solid, solid-solid contacts. In this thesis, the three-dimensional solid-solid contact theory was adopted to two-dimensional analysis.

2. The large displacement formulations for the bar and the beam element have been established and compared in some practical examples, and it has been concluded that when a structure, such as a uniform thin rod, is discretised by these elements under identical situations, the beam element gives more realistic results because it includes angular bending moments, ensuring continuity of curvature along the beam.

3. To simulate the effect of rockbolts as support in tunnel excavation, an Aydan type rockbolt element has been scrutinized. In the first instance, the steel bolt is discretised by a bar element, and in the second, a beam element is used for the same purpose, while the grout discretization remains the same throughout. Large displacement formulations of these two different forms are then established and compared, and it has been found that the superiority of the beam element found earlier in the deformation theory does carry forward to the rockbolt element, indicating that the new element attains a marked improvement over the original one.

11.3 Suggestions for possible further development

Limitations of the current studies have been discussed in previous chapters, and there are several areas in which the present research can be further developed. To improve on the efficiency and accuracy of the algorithm, and to enhance the generality of this research, the following suggestions are made.

1. **Material nonlinearity**

   The effect of modelling the rock mass and the rockbolt by nonlinear material has not been considered in this work. Elasto-plastic and visco-plastic models are generally considered to possess a more realistic behaviour than the perfectly elastic material. Further, the material is assumed to be homogeneous and isotropic. Therefore the effect of material nonlinearity and behaviours of different material could be investigated in the future. Of particular importance would be slip and debonding

mechanisms in the grout, and yield in the bolt.

2. **Three-dimensional analysis**

   Throughout this thesis, a two-dimensional plane strain analysis has been used. Aydan (1989) has shown that this analysis can be extended to three-dimensional, when the extra dimension of the new rockbolt element can be constructed in a similar manner. Although it would inevitably increase the size of the problem, and hence demand a longer computational time, it would allow the method to analyse more complex problems.

3. **Large displacement formulations for a joint element**

   The joint element used in this work is based on the small displacement analysis suggested by Beer (1985). A full account on how this linear behaviour can be combined with nonlinear behaviour of the other types of elements has been fully described in Chapter 7. For completeness and for a more realistic representation, it is necessary to develop a new large displacement formulation for the joint element.

4. **Rockbolt element with four or five nodes**

   By construction, the new rockbolt element is one-dimensional, with the steel bolt and the grout each represented by a sub-element with three nodes. In Chapter 6, the large deformation theories of a two-noded and a three-noded beam element have been established. It can be shown that, although a three-noded element exhibits a slightly more natural bending characteristics than its two-noded counterpart, the difference is not very significant. If this phenomenon holds in most other cases, it may be worthwhile to consider a similar rockbolt element with five nodes as an alternative, with two nodes representing the steel bolt and three representing the grout, or four nodes if two nodes can be used to join to linear rock elements. In either one of these representations, the accuracy of the results may be slightly reduced, but, as the number of degrees of freedom involved in each rockbolt element reduces, so does the overall size of the global stiffness matrix of the structure. Whence, the solution procedure will gain in faster computational time.

5. **Other supporting media**

   The rockbolt is the only supporting medium in tunnel excavation under consideration in this thesis. In Chapter 1, however, other common types of rock mass supporting media have been briefly described, and in general, if they can be combined, the

overall effiency of the support will be greatly increased. In particular, Marenče (1992) modelled the use of mylonit and crushed rock, shotcrete lining and pre-stressed bolts, as well as grouted rockbolts to simulate the excavation and stabilization problem of a cavern. Therefore, in the computer simulation of tunnelling problems, it would be useful if these and other media can be discretised by the use of other types of element or algorithms in the finite element analysis of the tunnel.

6. Residual load

In large displacement analysis, the assembly of nonlinear stiffness matrices of the elements involved in the mesh will give rise to a system of nonlinear algebraic equations. The solution procedure of this system using residual loads advocates the conversion of the nonlinear system into an approximate linear system of equations, whereby the results of this approximate system are refined by iterative methods. The iterative solution procedure has converged in the simple examples presented here (provided that the applied load does not cause collapse), but an analysis of convergence is lacking. Although this iterative method works well, and has proved to be fairly reliable and accurate, it is nevertheless too inefficient and time consuming. It will be interesting to investigate some better algorithms to deal with residual load in order to significantly increase the efficiency of the analysis as a whole.

7. Quasi-Newton methods

To provide a more efficient alternative to the iterative method used in this work, attempts have been made to incorporate limited storage quasi-Newton algorithms, where the solution of the nonlinear system of stiffness equations is solved directly by iterative methods, into the program. Although these methods work and can provide identical results, at present only structures with a simple mesh or a coarse mesh with only a small number of elements involved, can give convergent results. However, the signs are quite encouraging and it is clear that these quasi-Newton methods need further refinement so that they can be readily adapted to solve problems when structures with complex mesh are involved.

Appendix A

Instructions of the program ELAST

A.1 General descriptions

The program **ELAST** is coded in FORTRAN and has been compiled and run using the DOS version of FTN77 (Salford FORTRAN). It is designed to analyse two-dimensional plane stress/plane strain and axisysmmetric problems in elasticity, using finite element methods. This program is developed as an extension to the program package **FELIPE**, which has been principally developed and continuously updated by Dr. Martin Reed since 1985. In the solution procedure of the nonlinear equilibrium equation, **ELAST** also incorporates, as an option, some Quasi-Newton limited storage algorithms, which have been adapted from the theory and the program written by Dr. Reed in September 1997.

Relevant parts that deal with problems in elasticity using isoparametric elements have been lifted out from **FELIPE**, and they form the basis of **ELAST**. New algorithms have been incorporated according to the requirement of this thesis. These include the following additional features:

1. The large deformation theories for bar and beam elements (as well as for two-dimensional elements), using Lagrangian formulations to model the nonlinear geometric behaviour of objects modelled by these elements. A choice can be made for the conventional small deformation analysis or the large deformation analysis. Further, these elements can be discretised by 2 or 3 nodes, and they can be distinguished from the details of the mesh supplied from the data file.

2. The small deformation theory of joint element has been adapted from works published by Beer. This algorithm has been mixed with large displacement theories of other types of element.

3. A new rockbolt element which incorporates a beam element, instead of the bar element, to model the steel bolt has been introduced. Again, Lagrangian formulations have been used. This new rockbolt element can be compared directly with the original element, and the program of the latter is written in a sister program **ELAST1**.

4. A choice of solution procedures for the nonlinear equilibrium equation has been offered in the program. This allows the use of either the conventional iterative method that involves residual loads, or one of the variants of the limited storage Quasi-Newton minimization methods.

Figure A1.1 shows the flowchart of **ELAST**. It illustrates how the input procedure, the main program, the subroutines and the output procedure are linked in this program.

New routines are written and relevant subroutines are modified, and they are incorporated into the program **ELAST**. These include:

ELAST	the main program to control the new computing procedure;
POSITION	to establish the global displacement vector for the mesh;
STEPV1	to calculate and accumulate incremental strains and stresses in large displacement analysis, so that these values can be used in the next iteration/increment;
STEPV3	to calcuate residual loads;
BARB	to calculate stiffness matrix of beam element;
JNTB	to calculate stiffness matrix of joint element;
BLTB	to calculate stiffness matrix of rockbolt element;
SRF	to generate shape functions and their derivatives of various types of element.

A.2 Input from data file

A supplementary program **PREFEL** is used as a pre-processor of **ELAST**. This program generates the mesh and the loadings, and associates each element with its appropriate

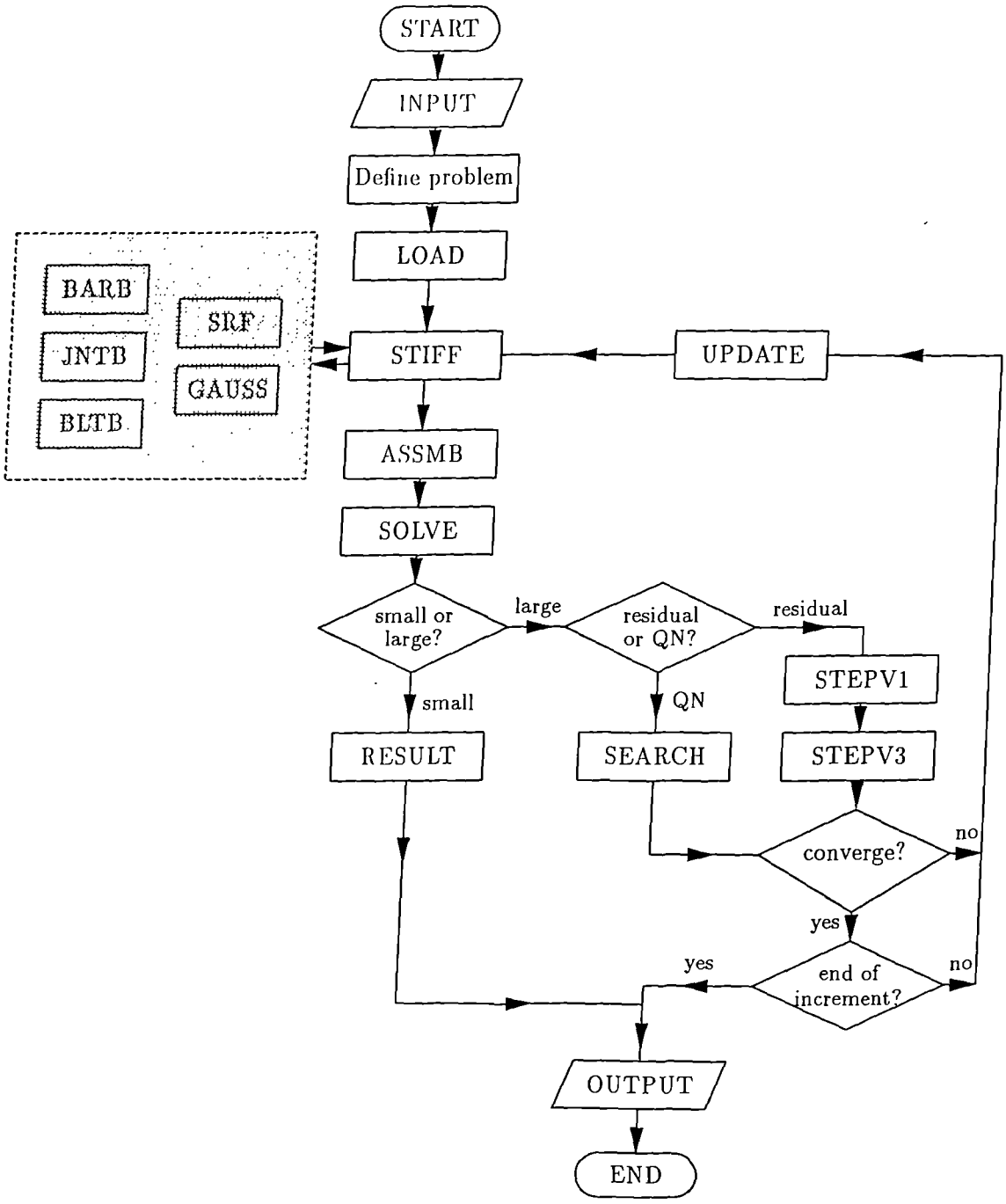

Figure A.1: Flowchart for the program **ELAST**

material property. It also assigns node number and element number to the mesh in order to minimize the overall size of the resulting global stiffness matrix. The details are then stored in a data file `*.dat`, and it can be retrieved before the analysis begins.

(1) Input data arrays from data file `*.dat`

INFILE	name of input data file
LNODN	number of node in an element
LNODS	global node numbers around element
LPROS	material property set number of a single element
LSIDN	number of side of an element
NELEM	total number of elements in mesh (max. = MELEM)
NKODE	fixity code of each node
NNODE	number of nodes in a single element (max. = MNODE):-
	2 or 3 - one-sided bar or beam element;
	4 or 6 - one-sided rockbolt element or two-sided joint element;
	8 - quadratic serendipity element;
NPOIN	total number of nodes in mesh (max. = MPOIN)
NPROS	number of material property sets
NTOTV	total number of degrees of freedom (max. = MTOTV)
NTYPS	element type
	1 - two sided joint element
	2 - one-sided rockbolt element
	3,4 - one sided bar or beam element
	9 - eight-noded isoparametric element
OUTFIL	name of output data file (`*.out`)
PROPS(LSET,1)	Young's modulus of material property set LSET
PROPS(LSET,2)	Poisson's ratio of material property set LSET
TITLE	title of the problem (maximum 80 characters)

(2) Input loadings from data file `*.dat`

FX	x-component of nodal load
FY	y-component of nodal load

ISET1	set-number of uniform surface traction
LCARD	a flag to indicate the status of the loading data:-
	0 - start of data
	1 - end of data
N1, N3	nodes along the edge where uniform surface traction is applied
NP	global node number at which point node is applied
PRESS(1,N1)	normal-component of surface traction
PRESS(2,N1)	tangential-component of surface traction

An example of the data file is shown below:

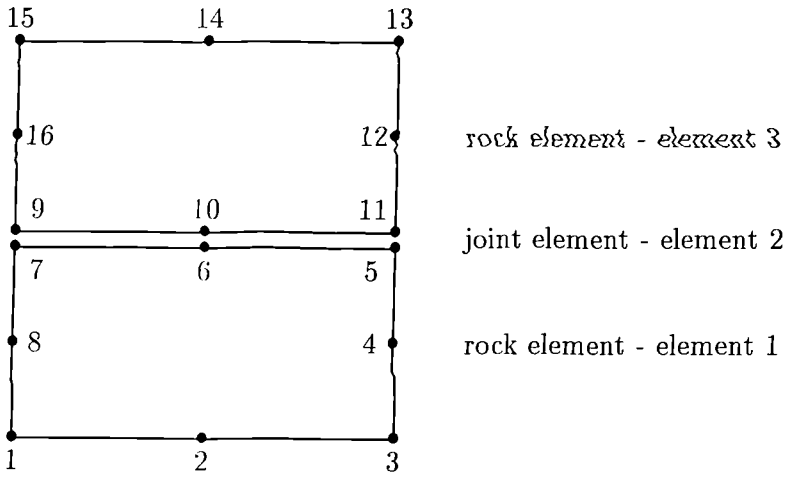

Figure A.2: Mesh details of an example

In the following example that investigates the effect of a joint between rock masses, a very simple mesh is shown in Figure A.2. Element 1 and 3 are the rock (eight-noded isoparametric) elements, while element 2 is the six-noded joint element. Point node with magnitude 0.2×10^3 in both the x- and y-directions are applied to node 15, together with an uniform surface traction of 0.1×10^5 applying normally at the top edge of the top rock element. In this analysis, four incremental loads of equal size are used.

The following is the details of the data file of this mesh:

```
An example of joint element
 npoin nelem mstyp npros
   16     3    10     1
  nside nset elt        nodes
0   4     1    1     1    2    3    4    5    6    7    8
0   2     1    2     9   10   11    7    6    5
1   4     1    3     9   10   11   12   13   14   15   16
  kode node  x-coord   y-coord
0  11    1   0.00000   0.00000
0  11    2   2.00000   0.00000
0  11    3   4.00000   0.00000
0  00    4   4.00000   1.00000
0  00    5   4.00000   2.00000
0  00    6   2.00000   2.00000
0  00    7   0.00000   2.00000
0  00    8   0.00000   1.00000
0  00    9   0.00000   2.00000
0  00   10   2.00000   2.00000
0  00   11   4.00000   2.00000
0  00   12   4.00000   3.00000
0  00   13   4.00000   4.00000
0  00   14   2.00000   4.00000
0  00   15   0.00000   4.00000
1  00   16   0.00000   3.00000
   set cmpnt        value
0   1    1          0.200E+06
0   1    2          0.300E+00
1
 nbset npset
    0    1
   ld  node x-cmpnt   y-cmpnt
0   1   15 0.200E+03 0.200E+03
1
    set  forces:     normal    tangential
```

```
1   1    1 2          0.100E+04 0.000E+00
  nnas elt  n set     n set
0   3    3 13 1      15 1
1
 nincs    increment sizes
    4 0.25 0.25 0.25 0.25
```

Note that:

1. node numbers of the loaded edge are listed in anti-clockwise sequence;
2. in a six-noded joint element, the first three nodes discretise the bottom edge of the top sub-element, while the last three discretise the top edge of the bottom sub-element; and the node numbers are listed in the direction from left to right;
3. in a six-noded rockbolt element, the first three nodes discretise the steel bolt, while the last three discretise the grout; the node numbers are listed in the direction from left to right;
4. the surface traction applied to the edge of an element is always assumed to be uniform, and its contribution to the nodes concerned is automatically computed by the program. Further, the element edges to be loaded can be arranged *in any order*;
5. variables such as NELEM, NNODE, NPOIN, NTOTV etc. are generated by **PREFEL**.

A.3 Input instructions for the program ELAST

Upon retrieving data from the data set, **ELAST** will carry out the computation, and some of the most important variable names or arrays used within the program are listed below:

(1) Input option

IMETH	Quasi-Newton method type :
	0 - initial;
	1 - VSCG;

	2 - update condensation;
	3 - L-BFGS;
	4 - tangential stiffness;
	5 - inexact Quasi-Newton
NINCS	number of increment steps used
NITER	maximum number of iterations allowed for calculating residuals
NLAPS	deformation type :-
	1 - small displacement theory;
	2 - large displacement theroy.
NPSTR	problem type :-
	1 - plane stress;
	2 - plane strain.
NUMUS	number of updates stored in limited storage QN algorithm
TOLLR	tolerance factor

(2) Node coordinates and shape functions

ASDIS	global displacement vector
ASLOD	global load vector
BMATX	element strain matrix
CARTD(1,I)	x-derivative of shape function in Cartesian coordinates x, y
CARTD(2,I)	y-derivative of shape function in Cartesian coordinates x, y
COORD(NP,1)	x coordinate of node NP
COORD(NP,2)	y coordinate of node NP
COORD(NP,3)	θ coordinate of node NP (for beam element or steel bolt only)
DERIV(1,I)	ξ derivative of shape function in local coordinates ξ, η
DERIV(2,I)	η derivative of shape function in local coordinates ξ, η
DMATX	element elasticity matrix
ESTIF	element stiffness matrix
GSTIF	global stiffness matrix in condensed form
RESLD	global residual vector
SHAPE	shape functions of an element in local coordinates ξ, η
STRSG	stress at Gauss points (in Cartesian coordinates)

(3) Other input details provided in **ELAST**

(a) in subroutine JNTB

STIKS	horizontal stiffness of joint
STIKN	vertical stiffness of joint

(b) in subroutine BLTB

D	dowel effect modulus of rockbolt
EBOLT	Young's modulus of steel bolt
GBOLT	shear modulus of steel bolt
GGROUT	shear modulus of grout
RBOLT	radius of rockbolt
RHOLE	radius of grout

(4) Gauss quadrature rule

GPEPS	Gauss point strain
GPSIG	Gauss point stress
GPWTS	Gauss weight
GPLOC	values of Gauss point local coordinates
NGTOT	order of Gauss quadrature for numerical integration

Note that:

1. the size of the increment step need not be equal, and the size value can be stored in the array FINCS;
2. the results for each incremental load are stored in the print file `*.prt`, so that they can be referred to if and when required;
3. when the stiffness matrix ESTIF for each element has been formed, it is written in a temporary scratch file.

   The sequence of subroutines in STIFF to obtain ESTIF is run for each element. Therefore, if there are NELEM number of elements in the body, the sequence will

be repeated NELEM times. when one element stiffness matrix will be created in a scratch file in each loop;

4. the order of Gauss quadrature is the minimum number of points required, and it is set automatically according to the type of each element.

A.4 Output

After the program is executed, the final results are prepared and stored in an output file `*.out`. A post-processor **FELVUE** has been specifically written to read data from this output file, and then plot the deformation or stress field graph accordingly. As a complete package, **PREFEL** and **FELVUE** form part of **FELIPE**.

In order to scrutinize the deformation graph more closely, a zoom facility is available, and an exaggeration factor can be used to magnify the amount of deformation. Postscript files of these graphs can also be prepared using this program, so that hardcopies can be readily available.

Note that except for the extension, the name of the output file is the same as the input file and the print file.

Bibliography

[1] Argyris, J.H., Kelsey, S., Kamel, H. (1964) Matrix methods of structural analysis. *AGARDograph,* Pergamon Press, No. 72.

[2] Aydan, Ö., Kyoya, T., Ichikawa, Y., Kawamoto, T., Ito, T., Shimizu, Y. (1988) Three-dimensional simulation of an advancing tunnel supported with forepoles, shotcrete, steel ribs and rockbolts. *In: Proc. 6th International Conference on Numerical Methods in Geomechanics,* Balkema, Rotterdam, pp. 1481-1486.

[3] Aydan, Ö. (1989) *The stabilisation of rock engineering structures by rockbolts.* Doctor of Engineering Thesis. Nagoya University, Nagoya, Japan.

[4] Aydan, Ö., Kawamoto, T. (1991) A comparative numerical study on the reinforcement effects of rockbolts and shotcrete support systems. *In: Computer Methods and Advances in Geomechanics,* 2, G. Beer, J.R. Booker, J.P. Carter (ed.), Balkema, Rotterdam, pp. 1443-1448.

[5] Banerjee, P.K., Raveendra, S.T. (1986) Advanced boundary element analysis of two- and three dimensional problems of elastoplasticity. *Int. J. Num. Meth. Eng.,* **23**, pp. 985-1002.

[6] Bathe, K.J., Ramn, E., Wilson, E.L. (1975) Finite element formulation for large deformation dynamic analysis. *Int. J. Num. Meth. Eng.,* **9**, pp. 353-386.

[7] Bathe, K.J., Ozdemir, H. (1976) Elastic-plastic large deformation static and dynamic analysis. *Int. J. Solids Struct.,* **6**, pp. 81-92.

[8] Bathe, K.J. (1996) *Finite Element Procedures in Engineering Analysis.* Prentice-Hall, New York.

[9] Beaver, P. (1972) *A History of Tunnels.* Peter Davis, London.

[10] Beer, G. (1985) An isoparametric joint interface element for finite element analysis. *Int. J. Num. Meth. Eng.,* **21**, pp. 585-600.

[11] Beer, G., Watson, J.O., Swoboda G (1987) Three-dimensional analysis of tunnels using infinite boundary elements. *Computers and Geomechanics,* **3**, pp. 37-58.

[12] Bjurström, S. (1974) Shear strength of hard rock joints reinforced by grouted untensioned bolts. *In: Proc. 3rd ISRM Congress,* Denver, pp. 1194-1199.

[13] Bowen, R. (1975) *Grouting in Engineering Practice.* Applied Science, London.

[14] Brady, B.G.H. Lorig, L.J., (1988) Analysis of rock reinforcement using finite difference methods. *Computers and Geotechnics,* **5**, pp. 123-149.

[15] Brebbia, C.A., Venturini, W.S. (ed.) (1987) *Boundary Element Techniques: Applications in Stress Analysis and Heat transfer.* Computational Mechanics Publications, Southampton.

[16] Brink, U. (1991) *Comparison of coupled finite element-boundary element and infinite element techniques* in elastostatics. MSc Dissertation, Brunel University, Department of Mathematics and Statistics.

[17] Brown, E.T., Bray, J.W., Ladanyi, B. Hoek, E., (1983) Characteristic line calculations for rock tunnels. *J. Geotech. Eng. Am. Soc. Civ. Eng.,* **109**, pp. 15-39.

[18] Brown, E.T. (ed.) (1987) *Analytical and Computational Methods in Engineering Rock Mechanics.* Allen & Unwin, London.

[19] Buckley, A., LeNir, A. (1983) QN-like variable storage conjugate gradients. *Mathematical Programming,* **27**, pp. 155-175.

[20] Buckley, A., LeNir, A. (1985) ALGORITHM 630: BBVSCG - A variable storage algorithm for function minimization. *ACM Transactions on Mathematical Software,* **11**, pp. 103-119.

[21] Carter, J.P., Booker, J.R., Davis, E.H. (1977) Finite deformation of an elasto-plastic soil. *Int. J. Numer. Anal. Methods Geomech.,* **1**, pp. 25-43.

[22] Chandra, A., Mukherjee, S. (1983) Application of the boundary element method to large strain large deflection problems of viscoplasticity. *J. of Strain Anal.,* **18**, pp. 261-270.

[23] Cheung, Y.K., Yeo, M.F. (1979) *A Practical Introduction to Finite Element Analysis.* Pitman, London.

[24] Coates, D.F., Yu, Y.S. (1970) Three dimensional stress distributions around a cylindrical hole and anchor. *In: Proc. 2nd ISRM Congress,* Belgrade, pp. 175-182.

[25] Cookson, R.A., El-Zafrany, A. (1987) State of the art review of the boundary element method. *Advances in the use of the Boundary Element Method for Stress Analysis,* Mechanical Engineering Publications, London, pp. 1-8.

[26] Coull, A., Dykes, A.R. (1972) *Fundamentals of Structural Theory.* McGraw-Hill, Maidenhead.

[27] Cruse, T.A. (1969) Numerical solutions in three-dimensional elastostatics. *Int. J. Solids Struct.,* **5**, pp. 1259-1274.

[28] David on, H.L., Chen, W.F. (1974) Elastic-plastic large deformation response of clay to footing loads. Report no. 355-18, Fritz Engng. Lab., Lehigh University, PA.

[29] Davie . A.J. (1980) *The Finite Element Method: A First Approach.* Oxford University Press.

[30] Day, R.A., Potts, D.M. (1991) Zero thickness interface - numerical stability and application. *Int. J. Numer. Anal. Methods Geomech.,* **18**, pp. 689-708.

[31] Dennis, J.E. Jr., Schnabel R.B. (1983) *Numerical Methods for Unconstrained Optimization and Nonlinear Equations.* Prentice-Hall, London.

[32] Desai, C.S., Phan, H.V. (1980) Three dimensional finite element analysis including material and geometrical non linearities. *Computer Methods in Nonlinear Mechanics,* J.T. Oden (ed.) North-Holland Publishing Co., 2nd ed., pp. 205-224.

[33] Eberhardsteiner, J., Mang, H.A., Torzicky B.G.H. (1991) Elastoplastic coupled BE-FE stress analysis of a tube of Vienna's underground line U3, considering sequences of driving and securing by shotcrete. *In: Computer Methods and Advances in Geomechanics,* **2**, G. Beer, J.R. Booker, J.P. Carter (ed.), Balkema, Rotterdam, pp. 1461-1466.

[34] Egger, P. (1973) Einfluss des Post-Failure - Verhaltens von Fels auf den Tunnelausbau unter besonderer Berücksichtigung des Ankerausbau. *Veröff. Inst. Böden und Felsmech.,* No. 57, Univ. Karlsruhe, Germany.

[35] Egger, P., Pellet, F. (1992) Numerical and experimental investigations of the behaviour of reinforced joint media. *In: Proc. International Conference on Fractured and Joint Rock Masses,* Lake Tahoe, USA.

[36] Fenner, R. (1938) *Untersuchungen zur Erkenntnis des Gebirgsdrucks.* Diss. T.U.Breslau.

[37] Fletcher, R. (1987) *Practical Methods of Optimization.* 2nd ed., J Wiley, Chichester.

[38] Florence, A.L., Schwer, L.E. 1978) Axisymmetric solution of a Mohr-Coulomb material around a circular hole. *Int. J. Numer. Anal. Methods Geomech.,* **2**, pp. 367-379.

[39] Gallagher, R.H., Padlog, J., Bijlaard, P.P. (1962) Stress analysis of heated complex shapes. *J. Am. Rocket Soc.,* **32**, pp. 700-707.

[40] Georgiou, P. (1981) *The coupling of the direct boundary element method with the finite element displacement technique in elastostatics.* PhD Thesis. Southampton University.

[41] Ghaboussi, J., Wilson, E.L., Isenberg, J. (1973) Finite element for rock joints and interfaces. *J. Soil Mech. & Found. Div., ASCE,* pp. 833-848.

[42] Goodman, R.E., Taylor, R.L., Brekke, T.L. (1968) A model for the mechanics of jointed rock. *J. Soil Mech. & Found. Div., ASCE,* **94**, pp. 637-659.

[43] Heuze, F.E., Goodman, R.E. (1973) Finite element and physical model studies of tunnel reinforcement in rock *In: Proc. 15th U.S. Symposium on Rock Mechanics,* pp. 37-67.

[44] Hinton, E. (ed.) (1992) *Introduction to Nonlinear Finite Element Analysis.* NAFEMS, Glasgow.

[45] Hinton, E., Owen, D.R.J. (1977) *Finite Element Programming.* Academic Press, London.

[46] Hobst, L., Zajíc, J. (1983) *Anchoring in Rock and Soil.* Developments in Geotechnical Engineering, Vol. 33, Elsevier. Amsterdam.

[47] Hoek, E., Brown, E.T. (1980) Underground excavations in rock. Institution of Mining and Metallurgy, London.

[48] Hohberg, J-M (1990) Short communication - A note on spurious oscillations in FEM joint elements. *Earthquake Engng. and Struc. Dynamics,* **19**, pp. 773-779.

[49] Hrennikoff, A. (1941) Solution of problems in elasticity by the framework method. *J. Appl. Meth.*, **8**, pp. 169-175.

[50] Irons, B., Ahmad, S. (1984) *Techniques of Finite Elements.* Ellis Horwood, Chichester.

[51] Jaeger, J.C., Cook, N.G.W. (1979) *Fundamentals of Rock Mechanics.* 3rd ed., Chapman and Hall, London.

[52] Kaiser, P.K. (1980) Effect of stress history on the deformation behaviuor of underground openings. *In: Underground Rock Engineering, Proc. 13th Canadian Rock Mechanics Symposium*, Montreal, pp. 113-140.

[53] Kellogg, O.D. (1929) *Foundations of Potential Theory.* Springer Verlag, New York.

[54] Labiouse, V. (1996) Ground response curves for rock excavations supported by ungrouted tensioned rockbolts. *Rock Mech. & Rock Eng.*, **29**, pp. 19-38.

[55] Lachat, J.C., Watson, J.O. (1976) Effective numerical treatment of boundary integral equations - a formulation for three-dimensional elastostatics. *Int. J. Num. Meth. Eng.*, **10**, pp. 991-1005.

[56] Lampe, D. (1963) *The Tunnel.* George G. Harrap, London.

[57] Lemos, J.V., Hart, R.D., Cundall, P.A. (1985) A generalised distinct element program for modelling jointed rock mass - A keynote lecture. *In: Proc. International Symposium on Fundamentals of Rock Joints.*, pp. 335-343.

[58] Liu, D.C., Nocedal, J. (1989) On the limited memory BFGS method for large scale optimization. *Mathematical Programming*, **45**, pp. 503-528.

[59] Lorig, L.J., Brady, B.G.H. (1984) A hybrid computational scheme for excavation and support design in jointed rock media. *ISRM Symposium*, Cambridge, British Geotech. Soc., pp. 105-112.

[60] Marence, M. (1992) *Numerical model for rockbolts under consideration of rock joint movements.* PhD Thesis. University of Innsbruck, Austria.

[61] Martin, H.C. (1965) On the derivation of stiffness matrices for the analysis of large deflection and stability problems. *In: Proc. of the Conference on Mathmatical Methods in Structural Mechanics*, Wright-Patterson Air Force Base, Ohio, USA, AFFDL-TR-66-80, pp. 697-715.

[62] Meek, J.L. (1971) *Matrix Structural Analysis.* McGraw-Hill, New York.

[63] Melosh, R.J. (1965) Basis for derivation of matrices for the direct stiffness method. *J.A.I.A.A.*, **1**, pp. 1631-1637.

[64] McHenry, D. (1943) A lattice analogy for the solution of plane stress problems. *J. Inst. Civ. Engng.*, **12**, pp. 59-82.

[65] Naylor, D.J. (1971) Stresses in nearly incompressible materials by finite elements with application to the calculation of excess pore pressures. *Int. J. Num. Meth. Eng.*, **8**, pp. 443-460.

[66] Nocedal, J. (1980) Updating quasi-Newton matrices with limited storage. *Mathematics of Computation,* **35**, pp. 773-782.

[67] Oden, J.T. (1969) Finite element applications in nonlinear structural analysis. *In: Proc. Symposium on the Application of FEM in Civil Engineering.,* Knoxville, TN, pp. 419-456.

[68] Pacher, F. (1973) Gebirgsklassifizierung für den Tunnelbau. *Ingenieurbüro für Geologie und Bauwesen,* Salzburg.

[69] Pan, X.D. (1988) *Numerical modelling of rock movements around mine openings.* PhD Thesis. University of London (Imperial College).

[70] Pellet, F. (1994) *Strength and deformability of jointed rock masses reinforced by rockbolts.* PhD Thesis. Swiss Federal Institute of Technology, Lausanne, Switzerland.

[71] Qu, R., Reed, M.B. (1992a) *The 3D version of the finite element program FESTER.* Brunel University, Department of Mathematics and Statistics. Technical report TR 05 92.

[72] Qu, R., Reed, M.B. (1992b) Mathematical modelling of bolts by finite element method in the program FESTER. *Unpublished.*

[73] Rabcewicz, L. (1964a) The New Austrian Tunnelling Method, Part I. *Water Power.*

[74] Rabcewicz, L. (1964b) The New Austrian Tunnelling Method, Part II. *Water Power.*

[75] Rabcewicz, L. (1965) The New Austrian Tunnelling Method, Part III. *Water Power.*

[76] Reed, M.B. (1984) An investigation of numerical errors in the analysis of consolidation by finite elements. *Int. J. Numer. Anal. Methods. Geomech.,* **8**, pp. 243-257.

[77] Reed, M.B. (1986) Stresses and displacements around a cylindrical cavity in soft rock. *IMA J. Appl. Math.,* **36**, pp. 223-245.

[78] Reed M.B. (1990) An iterative method for the solution of the implicit elasto-viscoplasticity equations. *In: The Mathmatics of Finite Elements and Applications VII,* J.R. Whiteman (ed.), Academic Press, London, pp. 301-312.

[79] Reed, M.B. (1997) *Update condensation - a new approach to quasi-Newton minimization with limited storage.* Brunel University, Department of Mathematics and Statistics. Technical report TR/16/97.

[80] Reed, M.B., Lavender, D.A. (1988) *FESTA - An elasto-viscoplastic finite-element program for geotechnical applications.* Brunel University, Department of Mathematics and Statistics. Technical report TR/14/88.

[81] Reed, M.B., Pan, X.D. (1990) *Development process of program FESTA.* Brunel University. Department of Mathematics and Statistics. Technical report TR/02/90.

[82] Ross, C.T.F. (1990) *Finite Element Methods in Engineering Science.* Ellis Horwood, Chichester.

[83] Roy, S., Rajagopalan (1997) Analysis of rockbolt reinforcement using beam-column theory. *Int. J. Numer. Anal. Methods Geomech.,* **21**, pp. 241-253.

[84] St. John, C.M., Van Dillen, D.E. (1983) Rockbolts: A new representation and its application in tunnel design. *In: Proc. 24th U.S. Symposium on Rock Mechanics,* pp. 13-25.

[85] Schäfer, H. (1975) A contribution to the solution of contact problems with the aid of bond elements. *Comp. Meths. Appl. Mech. Engng.,* **6**, pp. 335-354.

[86] Smith, G.D. (1978) *Numerical Solution of Partial Differential Equations: finite Difference methods.* Oxford University Press.

[87] Stjern, G., Myrvang, A. (1998) The influence of blasting on grouted rockbolts. *Tunnelling and Underground Space Tech.,* **13**, pp. 65-70.

[88] Swoboda, G., Mertz, W. (1987) Rheological analysis of tunnel excavations by means of coupled finite element (FEM)-boundary element (BEM) analyses. *Int. J. Numer. Anal. Methods Geomech.,* **11**, pp. 115-129.

[89] Swoboda, G., Ebner, H., Wang, S.J., Zhang, J.M. (1988) Application of the 'decoupled finite element analysis' in tunnelling. *In: Proc. 6th International Conference on Numerical Methods in Geomechanics.,* Balkema, Rotterdam, pp. 1465-1472.

[90] Swoboda, G., Marenče, M. (1991) FEM modelling of rock bolts. *In: Computer Methods and Advances in Geomechanics,* **2**, G. Beer, J.R. Booker, J.P. Carter (ed.), Balkema, Rotterdam, pp. 1515-1520.

[91] Swoboda, G., Marenče, M. (1992) Numerical modelling of rock bolts in intersection with fault system. *In: Proc. Numerical Models in Geomechanics,* NUMOG IV, Swansea, UK, pp. 729-738.

[92] Swoboda, G., Marenče, M. (1995) Numerical model for rock bolts with consideration of rock joint movements. *Rock Mech. Rock Engng.,* **28(3)**, pp. 145-165.

[93] Timoshenko, S., Goodier, J.N. (1951) *Theory of Elasticity.* 2nd ed., McGraw-Hill, New York.

[94] Turner, M.J., Clough, R.W., Martin, H.C., Topp, L.T. (1956) Stiffness and deflection analysis of complex structures. *J. Aero. Sci.,* **23**, pp. 805-823.

[95] Turner, M.J., Dill, E.H., Martin, H.C., Melosh, R.J. (1960) Large deflections of structures subjected to heating and external loads. *J. Aero. Sci.,* **27**, pp. 97-107.

[96] Turner, M.J., Martin, H.C., Weikel, R.C. (1964) Further development and applications of the stiffness method. *AGARDograph,* Pergamon Press, No. 72, pp. 203-266.

[97] West, G. (1988) *Innovation and the rise of the Tunnelling Industry.* Cambridge University Press.

[98] Wilson, A.H. (1980) A method of estimating the closure and strength of lining required in drivages surrounded by a yield zone. *Int. J. Rock Mech. Min. Sci. & Geomech. Abstr.,* **17**, pp. 349-355.

[99] Yamada, Y. (1972) Incremental formulation for problems with geometric and material nonlinearities. *In: Advances in Computational Methods in Structural Mechanics Design,* Univ. of Alabama Press, pp. 325-355.

[100] Zienkiewicz, O.C., Cheung, Y.K. (1965) Finite elements in the solution of field problems. *The Engineer,* **220**, pp. 507-510.

[101] Zienkiewicz, O.C. et al. (1970) Analysis of nonlinear problems in rock mechanics with particular reference to jointed rock systems. *In: Proc. 2nd ISRM Conference,* Belgrade, pp. 8-14.

[102] Zienkiewicz, O.C., Nayak, G.C. (1971) A general approach to problems of large deformation and plasticity using isoparametric elements. *In: Proc. 3rd Conference on Matrix Methods in Structural Mechanics,* Wright-Patterson A.F.B., OH, pp. 1-65.

[103] Zienkiewicz, O.C., Kelly, D.W., Bettess, P. (1977) The coupling of the finite element method and boundary solution procedures. *Int. J. Num. Meth. Eng.,* **11**, pp. 355-375.

[104] Zienkiewicz, O.C., Taylor, R.L. (1989) *The Finite Element Method.* 4th ed., Vol. 1, McGraw-Hill, London.

[105] Zienkiewicz, O.C., Taylor, R.L. (1991) *The Finite Element Method.* 4th ed., Vol. 2, McGraw-Hill, London.